

**THE GEOLOGY AND GEOCHEMISTRY OF  
GRANITOIDS IN THE CHILDARA REGION, WESTERN  
GAWLER CRATON, SOUTH AUSTRALIA:  
IMPLICATIONS FOR THE PROTEROZOIC TECTONIC  
HISTORY OF THE WESTERN GAWLER CRATON, AND  
DEVELOPMENT OF LODGE-STYLE GOLD  
MINERALISATION AT TUNKILLIA**

by

**Gary M Ferris**

*Gary Michael*

**Submitted in partial fulfilment of the requirements for  
Masters of Exploration Geology**



**University of Tasmania**

**December 2001**

This thesis contains no material which has been accepted for the award of any other degree or diploma in any institution and, to the best of my knowledge and belief, contains no copies or paraphrases of material previously published or written by other people, except where due references are made in the text of the thesis.

DATED 1-8-02

SIGNED 



<b>LIST OF FIGURES.....</b>	<b>iv</b>
<b>LIST OF PLATES.....</b>	<b>iv</b>
<b>LIST OF TABLES.....</b>	<b>viii</b>
<b>APPENDICES.....</b>	<b>ix</b>
<b>PLANS .....</b>	<b>ix</b>
<b>ABSTRACT .....</b>	<b>1</b>
<b>ACKNOWLEDGEMENTS.....</b>	<b>4</b>
<b>Chapter 1 Introduction .....</b>	<b>5</b>
1.1 Introduction .....	5
1.2 Project Aims .....	5
1.3 Background.....	6
1.3.1 Geology.....	6
1.3.2 Geophysics.....	7
1.4 Climate and Physiography.....	9
<b>Chapter 2 Stratigraphy .....</b>	<b>11</b>
2.1 Introduction .....	11
2.2 Stratigraphy of the Gawler Craton.....	11
2.2.1 Archaean .....	11
2.2.2 Palaeoproterozoic.....	12
2.2.3 Mesoproterozoic .....	14
2.3 Stratigraphy of CHILDARA .....	15
2.4 Archaean.....	15
2.4.1. Glenloth Granite (ALmg) .....	16
2.5 Palaeoproterozoic .....	16
2.5.1 Undifferentiated Palaeoproterozoic basement .....	16
2.6.1 Tunkillia Suite.....	17
2.5.1.1 Orthogneiss (L <sub>1</sub> ) .....	17
2.5.1.2 Granite (L <sub>2</sub> ).....	18
2.5.1.3 Mylonite (L <sub>3</sub> ).....	20
2.5.1.4 Mafic dykes (L <sub>4</sub> ).....	21
2.5.1.5 Rhyolite, rhyodacite dykes (L <sub>5</sub> ).....	21
2.5.1.6 Aplite Dykes (L <sub>6</sub> ) .....	22
2.5.2 St Peter Suite.....	23
2.6 MESOPROTEROZOIC .....	27
2.6.1 Gawler Range Volcanics .....	27
2.6.1.1 Childera Dacite (Myc).....	28
2.6.1.2 Mangaroongah Dacite (Mym) .....	30
2.6.1.3 Arburee Rhyolite (Mya) .....	31
2.6.1.4 Karkulta Rhyolite (Myk).....	31
2.6.1.5 Bunburn Dacite (Myb) .....	32
2.6.1.6 Baldry Rhyolite (Myl).....	34
2.6.1.7 Nuckulla Basalt (Myn) .....	34
2.6.1.8 Yantea Rhyodacite (Myy) .....	35
2.6.1.9 Whyeela Dacite (Myh) .....	36
2.6.1.10 Moonamby Dyke Suite (Myz).....	36
2.6.2 Hiltaba Suite (Mh) .....	37
2.6.2.1 Gabbro (Mh <sub>6</sub> ) .....	39
2.6.3 Munjeela Granite (M-u).....	40
2.6.4 Quartz Blows .....	41
<b>Chapter 3 Geochemistry .....</b>	<b>42</b>

<b>3.1 Introduction .....</b>	<b>42</b>
3.1.1 Constraints on the data.....	42
3.1.2 Granite classification .....	42
<b>3.2 Archaean/Early Palaeoproterozoic .....</b>	<b>44</b>
3.2.1 Glenloth Granite.....	44
3.2.1.1 Introduction and sampling.....	44
3.2.1.2 Chemical variation .....	45
<b>3.3 Palaeoproterozoic .....</b>	<b>47</b>
3.3.1 Tunkillia Suite and related Karraran Orogeny intrusives .....	48
3.3.1.1 Introduction and sampling.....	48
3.3.1.2 Chemical variation .....	48
3.3.2 St Peter Suite.....	54
3.3.2.1 Introduction and sampling.....	54
3.3.2.2 Chemical variation .....	55
<b>3.4 Mesoproterozoic.....</b>	<b>62</b>
3.4.1 Hiltaba Suite.....	62
3.4.1.1 Introduction and sampling.....	62
3.4.1.2 Chemical variation .....	63
3.4.2 Glyde Hill Volcanic Complex .....	70
3.4.2.1 Introduction and sampling.....	70
3.4.2.2 Chemical variation .....	70
3.4.3 Munjeela Granite .....	76
3.4.3.1 Introduction and sampling.....	76
3.4.3.2 Chemical variation .....	77
<b>3.5 Summary and Conclusions .....</b>	<b>79</b>
<b>Chapter 4 Regional Tectonics and Structural Geology .....</b>	<b>84</b>
4.1 Introduction .....	84
4.2 Tectonic Subdomains of the Gawler Craton.....	84
4.3 Tectonic/tectonothermal Events on the Gawler Craton .....	86
4.4 Shear Zones on the Western Gawler Craton .....	87
4.5 Regional tectonics of the CHILDARA Area .....	88
4.5.1 Description of rock units.....	89
4.6 Regional shear zones .....	90
4.6.1 Yarlbirinda Shear Zone .....	91
4.6.2 Yerda Shear Zone .....	98
4.6.3 Koonibba Fault Zone .....	98
4.7 Relative chronology and timing of deformation within the Yarlbirinda Shear Zone.....	99
<b>Chapter 5 Tectonic Development of the CHILDARA region, Western Gawler Craton.....</b>	<b>101</b>
5.1 Introduction .....	101
5.1.1 Problems with granite classification and discrimination diagrams.....	101
5.2 Palaeoproterozoic to Mesoproterozoic magmatism on CHILDARA .....	104
5.3 Petrogenesis of the St Peter Suite.....	105
5.4 Comparison of St Peter Suite with Australian Proterozoic granites and modern arc magmatism. ....	107
5.4.1 Comparative geochemistry .....	109
5.5 Tectonic/Tectonothermal Evolution of the CHILDARA Area, Western Gawler Craton .....	111
5.5.1 Sm-Nd isotope results for the St Peter Suite.....	111

5.5.2 Tectonic episode 1 .....	112
5.5.3 Tectonic episode 2 .....	113
5.5.4 Tectonic episode 3 .....	113
5.5.5 Tectonic episode 4 .....	114
5.5.6 Tectonic episode 5 .....	116
<b>5.6 Implications for the development of the Hiltaba Suite/Gawler Range</b>	
<b>Volcanics.....</b>	<b>116</b>
5.6.1 Glyde Hill Volcanic Complex – Silicic Lava or Ignimbrite? .....	119
<b>5.7 CONCLUSIONS.....</b>	<b>122</b>
<b>Chapter 6 Geology of Tunkillia Gold Prospect .....</b>	<b>124</b>
<b>6.1 Introduction .....</b>	<b>124</b>
6.1.1 Exploration History.....	124
<b>6.2 Rock Types .....</b>	<b>125</b>
6.2.1 Tunkillia Augen Gneiss (TAG) .....	126
6.2.2 Fuzzy Granitoid (FUG).....	126
6.2.3 Central Alteration Zone (CAZ).....	126
6.2.4 Phyllite/ultra-mylonite shear (PUS).....	127
6.2.5 Mafic Dyke (MAD) .....	127
6.2.6 Dacite/rhyolite Dyke (DAD).....	127
6.2.7 Other Minor Units.....	128
6.2.8 Summary .....	128
<b>6.3 Structural Geology of the Tunkillia Area.....</b>	<b>129</b>
<b>6.4 Alteration Assemblage .....</b>	<b>132</b>
6.4.1 K-Ar dating of sericite alteration .....	132
<b>6.5 Fluid Inclusions.....</b>	<b>133</b>
6.5.1 Methods.....	133
6.5.2 Fluid Inclusion Types .....	134
6.5.3 Microthermometric Results .....	135
<b>6.6 Sulphur Isotopes .....</b>	<b>138</b>
6.6.1 Analytical Techniques .....	139
6.6.2 Results.....	140
<b>6.7 Lead Isotopes.....</b>	<b>141</b>
6.7.1 Analytical Methods.....	141
6.7.2 Results.....	141
<b>6.8 DISCUSSION.....</b>	<b>142</b>
6.8.1 Comparisons to Moonta-Wallaroo (Au-Cu) Tarcoola (Au), Menninnee Dam (Pb-Zn) and Olympic Dam Cu-U-Au-Ag deposits .....	142
6.8.1.1 Physio-chemical conditions of ore fluids .....	143
6.8.1.2 Sulphur isotopes .....	148
6.8.1.3 Lead isotopes.....	149
6.8.1.4 Fluid chemistry.....	151
6.8.2 Tunkillia: Magmatic versus Metamorphic Fluid Source .....	152
<b>6.9 CONCLUSIONS.....</b>	<b>155</b>
<b>Chapter 7 Summary .....</b>	<b>157</b>
<b>REFERENCES.....</b>	<b>160</b>

## LIST OF FIGURES

Figure 1 Location of CHILDARA on the western Gawler Craton, South Australia. ....	6
Figure 2 General geology of the Gawler Craton (from Daly <i>et al.</i> , 1998).....	8
Figure 3 Total magnetic intensity (TMI) image of CHILDARA 1:250 000 map sheet showing main geologic features.....	9
Figure 4 Basement stratigraphy of the Gawler Craton (modified from Daly and Flint, 1998).....	13
Figure 5 Location and extent of Gawler Range Volcanics and Hiltaba Suite magmatism (Stewart, 1992).....	15
Figure 6 Mean standard weighted age for sample R389873 from northeast of Ceduna. ....	24
Figure 7 Mean standard weighted age for sample R444813.....	25
Figure 8 U-Pb concordia diagram of zircon analyses of sample R469578 from west of Kondoolka Batholith. ....	25
Figure 9 U-Pb concordia plot for sample from Kondoolka Batholith (see Appendix B for original data).....	38
Figure 10 TMI image showing location of Glenloth Granite samples used in this section. ....	45
Figure 11 Streckeisen plot for Archaean/Early Palaeoproterozoic Glenloth Granite samples .....	46
Figure 12 ASI plot for Glenloth Granite.....	46
Figure 13 Rb-Ba-Sr plot for Glenloth Granite.....	46
Figure 14 SiO <sub>2</sub> histogram and harker diagrams of major oxides for Glenloth Granite. Elements in wt%.....	47
Figure 15 Incompatible-compatible element plot for Glenloth Granite. ....	47
Figure 16 Chondrite normalised REE plot for Glenloth Granite. ....	47
Figure 17 TMI image showing location of Tunkillia Suite groups on CHILDARA .....	48
Figure 18 SiO <sub>2</sub> histogram for Tunkillia Suite and related Kararan Orogeny intrusives. ....	51
Figure 19 Streckeisen plot for Tunkillia Suite and related Kararan Orogeny intrusives. ....	51
Figure 20 Molecular Al/(Ca+Na+K) versus Al/(Na+K) plot after Maniar and Piccoli (1989). ....	51
Figure 21 Rb-Ba-Sr plot for the Tunkillia Suite and related Kararan Orogeny intrusives. Fields 1 diorites, 2 granodiorites, 3 anomalous granites, 4 normal granites, 5 strongly differentiated granites .....	51
Figure 22 Na/(Na+K) vs SiO <sub>2</sub> plot for the Tunkillia Suite and related Kararan Orogeny intrusives.....	51
Figure 23 Harker diagrams of major elements vs SiO <sub>2</sub> for Tunkillia Suite and related intrusives. Elements in wt %.....	52
Figure 24 Selected trace element vs SiO <sub>2</sub> plots for Tunkillia Suite and related intrusives.....	53
Figure 25 Ga/Al v Na <sub>2</sub> O+K <sub>2</sub> O and Ga/Al v Zr for Tunkillia Suite and related intrusives. ....	53
Figure 26 Mantle normalised incompatible-compatible plot of average values for Tunkillia Suite and related intrusives.....	53
Figure 27 Chondrite normalised REE plot of average values for Tunkillia Suite and related intrusives. .....	53
Figure 28 TMI image showing location of St Peter Suite samples.....	54
Figure 29 SiO <sub>2</sub> histogram for the St Peter Suite. ....	57
Figure 30 Streckeisen plot for St Peter Suite.....	57
Figure 31 Ca-Na-K plot for St Peter Suite.....	59
Figure 32 Rb-Ba-Sr plot for St Peter Suite.....	59
Figure 33 Na/(Na+K) vs SiO <sub>2</sub> plot for St Peter Suite. ....	59
Figure 34 Ga/Al v Zr and Na <sub>2</sub> O + K <sub>2</sub> O plots for St Peter Suite. ....	59
Figure 35 Harker diagrams of major elements vs SiO <sub>2</sub> for St Peter Suite. Elements in wt%.....	60
Figure 36 Harker diagrams of trace elements vs SiO <sub>2</sub> for St Peter Suite.....	61
Figure 37 Mantle normalised plot of average values for groups 2 and 7 of the St Peter Suite.....	61
Figure 38 Chondrite normalised REE plots of average values for groups 2 and 7 of the St Peter Suite.....	61
Figure 39 Chondrite normalised REE for Group 7 of the St Peter Suite. ....	62
Figure 40 TMI image showing location of seven Hiltaba Suite plutons on CHILDARA. ....	62
Figure 41 SiO <sub>2</sub> histogram for Hiltaba Suite.....	64
Figure 42 Streckeisen plot for Hiltaba Suite.....	65
Figure 43 ASI plot for Hiltaba Suite.....	65
Figure 44 Na/(Na + K) vs SiO <sub>2</sub> plot for the Hiltaba Suite samples on CHILDARA.....	65
Figure 45 Molecular Al/(Ca+Na+K) versus Al/(Na+K) plot for the Hiltaba Suite after Maniar and Piccoli (1989). ....	65
Figure 46 Rb-Ba-Sr plot for Hiltaba Suite.....	65

The geology and geochemistry of granitoids in the CHILDARA region, western Gawler Craton, South Australia: implications for the Proterozoic tectonic history of the western Gawler Craton and the development of lode-style gold mineralisation at Tunkillia.

Figure 47	Harker diagrams of major elements vs SiO <sub>2</sub> for Hiltaba Suite. Elements in wt %.....	66
Figure 48	Harker diagrams of trace elements vs SiO <sub>2</sub> for Hiltaba Suite. ....	67
Figure 49	Rb/Ba v SiO <sub>2</sub> plot for Hiltaba Suite. ....	67
Figure 50	Ga/Al vs Na +K and Zr plots for Hiltaba Suite. ....	67
Figure 51	Mantle normalised trace element plot of Hiltaba Suite. ....	68
Figure 52	Chondrite normalised REE plot of Hiltaba Suite. ....	68
Figure 53	TMI image showing location of Glyde Hill volcanic samples .....	70
Figure 54	SiO <sub>2</sub> histogram for Glyde Hill Volcanic Complex.....	73
Figure 55	Alkali-lime variation diagram for the Glyde Hill Volcanic Complex (fields from Le Bas <i>et al.</i> , 1986). ....	73
Figure 56	(Na <sub>2</sub> O + K <sub>2</sub> O) v SiO <sub>2</sub> diagram for Glyde Hill Volcanic Complex. ....	73
Figure 57	Harker plots of major elements vs SiO <sub>2</sub> for Glyde Hill Volcanic Complex.....	74
Figure 58	Harker plots of trace elements vs SiO <sub>2</sub> for Glyde Hill Volcanic Complex. ....	75
Figure 59	Primordial mantle normalised plot of trace elements for the Glyde Hill Volcanic Complex. ....	76
Figure 60	Chondrite normalised REE plot for Glyde Hill Volcanic Complex. ....	76
Figure 61	SiO <sub>2</sub> histograms of the Hiltaba Suite and Glyde Hill Volcanics. ....	76
Figure 62	K/Rb v SiO <sub>2</sub> plot for Hiltaba Suite and Glyde Hill Volcanics. ....	76
Figure 63	TMI image showing location of Munjeela Granite samples .....	77
Figure 64	SiO <sub>2</sub> histogram for Munjeela Granite.....	78
Figure 65	Streckeisen plot of Munjeela Granite.....	78
Figure 66	Rb-Ba-Sr plot for Munjeela Granite.....	78
Figure 67	ASI plot for Munjeela Granite. ....	78
Figure 68	Ga/Al v Na <sub>2</sub> O + K <sub>2</sub> O plot for Munjeela Granite. ....	78
Figure 69	Primordial mantle normalised plot for Munjeela Granite.....	78
Figure 70	Chondrite normalised plot for Munjeela Granite samples.....	78
Figure 71	Streckeisen plot of Tunkillia Suite, St Peter Suite and Hiltaba Suite samples on CHILDARA. ....	81
Figure 72	SiO <sub>2</sub> histogram of Tunkillia Suite, St Peter Suite and Hiltaba Suite samples on CHILDARA. ....	81
Figure 73	AFM plot for Tunkillia Suite, St Peter Suite and Hiltaba Suite samples on CHILDARA (fields from Irvine and Baragar, 1971). ....	81
Figure 74	SiO <sub>2</sub> v Al <sub>2</sub> O <sub>3</sub> of Tunkillia Suite, St Peter Suite and Hiltaba Suite samples on CHILDARA.....	82
Figure 75	Na <sub>2</sub> O v SiO <sub>2</sub> for Tunkillia Suite, St Peter Suite and Hiltaba Suite samples on CHILDARA. ....	82
Figure 76	SiO <sub>2</sub> v K <sub>2</sub> O for Tunkillia Suite, St Peter Suite and Hiltaba Suite samples on CHILDARA. ....	82
Figure 77	ASI v CaO plot for Tunkillia Suite, St Peter Suite and Hiltaba Suite samples on CHILDARA. ....	82
Figure 78	Ga/Al v Na <sub>2</sub> O + K <sub>2</sub> O for Tunkillia Suite, St Peter Suite and Hiltaba Suite samples on CHILDARA. ....	82
Figure 79	Primordial mantle normalised plot of average values for selected groups of Tunkillia Suite, St Peter Suite and Hiltaba Suite samples on CHILDARA.....	83
Figure 80	Chondrite mantle normalised plot of average values for selected groups of Tunkillia Suite, St Peter Suite and Hiltaba Suite samples on CHILDARA.....	83
Figure 81	Zr/Sm v Sr/Yb plot for Tunkillia Suite, St Peter Suite and Hiltaba Suite from CHILDARA.....	83
Figure 82	Tectonic Subdomains of the Gawler Craton (Parker, 1990). ....	85
Figure 83	Revised tectonic Subdomains of the Gawler Craton (modified from Teasdale, 1997). Inset box shows current study area.....	86
Figure 84	Shear Zones on the western Gawler Craton (modified from Teasdale, 1997). ....	88
Figure 85	Interpretation of the basement geology of CHILDARA (Fairclough and Daly, 1994). ....	89
Figure 86	TMI image showing major shear zones on CHILDARA. ....	91
Figure 87	Equal area stereoplot of poles to the regional foliation within the Yarlbirinda Shear Zone.....	92
Figure 88	Equal area stereoplot of stretching lineations for rocks within the Yarlbirinda and Yerda Shear Zones. ....	94
Figure 89	Location of outcrops within Yarlbirinda Shear Zone described in text over TMI image.....	97
Figure 90	Detailed TMI image of northern part of Yarlbirinda Shear Zone showing dominant fabrics and major features described within the text. ....	100
Figure 91	Diagram showing different geological environments of Phanerozoic granitic rocks (from Pitcher, 1987). ....	103

Figure 92 Rb-(Y+Nb) tectonic discrimination plot for Tunkillia Suite, St Peter Suite and Hiltaba Suite granitoids (after Pearce <i>et al.</i> , 1984).....	104
Figure 93 Plot of R1-R2 multicaticonic points for Tunkillia Suite, St Peter Suite and Hiltaba Suite samples on CHILDARA.....	104
Figure 94 SiO <sub>2</sub> histogram for the St Peter Suite (Hiltaba and Tunkillia Suites shown for comparison). .....	105
Figure 95 Plot of Al <sub>2</sub> O <sub>3</sub> v Yb (after Arth, 1976) for tonalites of the St Peter Suite.....	106
Figure 96 Plot of Y v Sc for tonalites of the St Peter Suite. ....	106
Figure 97 SiO <sub>2</sub> histogram for St Peter Suite, Mabel Downs Suite and Dougalls Suite showing restricted SiO <sub>2</sub> ranges for Mabel Downs and Dougalls suites. Data for Mabel Downs and Dougalls Suites from Sheppard <i>et al.</i> , (1997).....	108
Figure 98 Major oxide classification diagram of Group 2 St Peter Suite, CAT Group Arunta Inlier and modern Island arc granites (group symbols same as Figure ). (fields from AJR White, Pers. comm., 1988).....	109
Figure 99 SiO <sub>2</sub> histogram of St Peter Suite (Group 2 and mafic samples) and Arunta Inlier and modern island arc granites. ....	110
Figure 100 Tectonic discrimination diagram of Pearce <i>et al.</i> (1984) for Group 2 St Peter Suite, CAT Group from Arunta Inlier and modern island arc granites.....	110
Figure 101 Plot of SiO <sub>2</sub> v Sr for Group 2 St Peter Suite, CAT Group from Arunta Inlier and modern island arc granites. Included is HHP granites from Arunta Inlier for comparison.....	110
Figure 102 Plot of SiO <sub>2</sub> v Y for Group 2 St Peter Suite, CAT Group from Arunta Inlier and modern island arc granites. Included is HHP granites from Arunta Inlier for comparison.....	110
Figure 103 Chondrite normalised REE patterns for Average values of Group 2 St Peter Suite and CAT Group Arunta Inlier. ....	110
Figure 104 Chondrite normalised REE patterns for HHP Group Arunta Inlier and selected Tunkillia Suite and Hiltaba Suite groups from CHILDARA area.....	110
Figure 105 TMI image showing main Munjeela Granite pluton west of the Koonibba Fault Zone. Diagram also shows location of mafic dykes and mafic lithologies and Yumbarra magnetic anomaly and Kalanbi mafic units. ....	114
Figure 106 TMI image showing mostly E-W trending late-stage faults. Faults cut Hiltaba Suite plutons, and hence are younger than ~1585 Ma. ....	115
Figure 107 Summary of postulated relationships between the various rock units in the Lake Everard area (from Giles, 1980).....	117
Figure 108 Diagrammatic scheme for generation of the Gawler Range Volcanics and Hiltaba Suite granitoids (Flint, 1993 after Huppert and Sparks, 1988). ....	118
Figure 109 Nuckulla Basalt plotted on a discrimination diagram for the separation of subduction components from mantle components (after Pearce, 1983).....	119
Figure 110 TMI image of part of the western Gawler Craton showing possible movement of the Harris Greenstone belt by Mesoproterozoic tectonics. ....	123
Figure 111 Total magnetic intensity image showing location of calcrete anomalies at Tunkillia (Helix Resources NL website). ....	125
Figure 112 Generalised section of the Tunkillia prospect (Standish <i>et al.</i> , 1997). ....	128
Figure 113 Summary structural diagram of main structural orientations from diamond drill core from Area 223 (modified from Standish <i>et al.</i> , 1997). ....	129
Figure 114 (A) schematic diagram showing how large-scale crustal fault architecture controls fluid migration pattern. First order localisation of near-lithostatic pressured regimes can be controlled by major fluid focussing faults terminating below low permeability crustal regimes. (B) Variation of fluid pressure within depth profile A-B in (A) (from Cox <i>et al.</i> , 1991). ....	130
Figure 115 Schematic block diagram of structure within Tunkillia Region (Rankin, 1997b).....	131
Figure 116 Histogram of homogenisation temperatures.....	138
Figure 117 Tm (final melting temperature in °C) versus temperature of homogenisation for Tunkillia samples. ....	138
Figure 118 Graph showing sulphur isotope values from Tunkillia. ....	140
Figure 119 Plot of <sup>207</sup> Pb/ <sup>206</sup> Pb vs <sup>206</sup> Pb/ <sup>204</sup> Pb showing Tunkillia data and Stacey and Kramers (1975) growth curve (blue line). The data intersects the curve at 1556 Ma. ....	142
Figure 120 Stability fields of silver and gold thio and chloro complexes and K-Al-silicates with temperature and pH (from Cooke and Large, 1995).....	144
Figure 121 Variations in gold solubility with pH at 300° C (from Cooke and Large, 1995). ....	145
Figure 122 Variations in gold solubility with pH at 350° C (from Cooke and Large, 1995). ....	145

Figure 123 A temperature-salinity diagram, which models the relationships between fluid chemistry for various ore deposit types based on fluid inclusion data (the boxes) with zones of gold and copper deposition based on chloride complex and thio complex solubility data (from Cooke and Large, 1995).	146
Figure 124 Fields of gold transport and deposition in $fO_2$ – temperature space. The gold association is controlled by the stability of $AuCl_2^-$ complexes (high temperature and $fO_2$ ). The gold-pyrite-copper association is absent where gold transport is dominated by $Au(HS)_2^-$ , at lower temperatures and only in the pyrite field (calculated from data provided in Huston and Large, 1989: $a_{(Cs)} = 10^{-3}$ , $a_{(Cl)} = 10^{0.5}$ , pH = 4).	148
Figure 125 Plumbotectonics of Doe and Zartman (1979) with four growth curves that result from the evolution of three lead reservoirs: mantle, lower crustal and upper crustal and a fourth growth curve, the orogene curve, that results from mixing of the three curves.	150
Figure 126 Lead isotope determinations from Tunkillia, Menninnie Dam and Tarcoola samples. Most samples plot above the Stacey and Kramer (1975) average crustal growth curve shown in blue with figures in millions of years.	151
Figure 127 Redox plot of Champion and Heinemann (1994) showing Hiltaba Suite granites located near Olympic Dam, Menninnie Dam, the Yarlbirinda Shear Zone and Tarcoola areas.	151
Figure 128 Diagrammatic representation of chemical pumping process possibly accompanying fault-valve behaviour on major fault zones associated with mesothermal gold deposits (Hodgson, 1993).	154

## LIST OF PLATES

Plate 1 Aerial view showing topography of central CHILDARA area.	10
Plate 2 Outcrop of Glenloth Granite showing mafic schlieren	16
Plate 3 “Magic carpet” metasedimentary enclave within Munjeela Granite at Point Sinclair.	17
Plate 4 Hand specimen of pebbly meta-conglomerate and meta-siltstone enclave within Hiltaba Suite granite from the Kondoolka Batholith (width of view is 12 cm).	17
Plate 5 Outcrop of coarse grained, augen granite gneiss located at Lakeside.	18
Plate 6 Outcrop of granite south west of Childera Outstation showing narrow mylonite zone.	19
Plate 7 Hand specimen of Yarlbirinda Hill showing coarse grained, K-feldspar dominant granite, which has been deformed under ductile and brittle regimes.	19
Plate 8 Outcrop of pseudotachylite at Yarlbirinda Hill.	20
Plate 9 Outcrop of mylonite at Lakeside	21
Plate 10 Detailed view of deformed rhyolite dyke, southwest of Childera Outstation showing elongate, ribbon quartz grains and relatively undeformed feldspar grains.	22
Plate 11 Narrow aplite dykes north of Lakeside.	23
Plate 12 Magmatic banding at Point Brown within Lp3.	24
Plate 13 Complex mingling relationships of the St Peter Suite.	24
Plate 14 Thin section of leucocratic granite from near the former OTC station, north of Ceduna showing zone of garnet grains (field of view is 0.5 mm)	26
Plate 15 Hand specimen of Childera Dacite showing flow banding and the generally phenocryst poor nature.	28
Plate 16 Hand specimen of Childera Dacite showing fine flow banding and coarse lithic clasts.	28
Plate 17 Thin sediment layer showing block faulting around compaction and water escape structures. (width of view is 4 cm).	28
Plate 18 Thin section showing detail of poorly sorted, angular fragments from Plate 17.	28
Plate 19 Thin epiclastic unit within Childera Dacite showing prominent graded bedding.	29
Plate 20 Hand specimen of Mangaroongah Dacite showing characteristic red feldspar phenocrysts.	30
Plate 21 General view of outcrop of Mangaroongah Dacite containing blocky perperite and hyaloclastite.	31
Plate 22 Detailed view of hyaloclastite showing reddish dacite and purple sediments.	31
Plate 23 Outcrop of Karkulta Rhyolite showing monomict autoclastic breccia.	32
Plate 24 Detailed view of prominent layering within the Bunburn Dacite with patches of almost spherical perlite	33
Plate 25 Outcrop of weathered macro perlite.	33
Plate 26 Thin section showing perlitic fractures within basaltic andesite (Bunburn Dacite).	33
Plate 27 Detailed view of thin section showing large spherical perlite.	33
Plate 28 Outcrop along edge of Lake Everard showing prominent radial fractures within macro-perlitic Bunburn Dacite.	33

Plate 29 Specimen of Baldry Rhyolite showing prominent flow layering.....	34
Plate 30 Large lithophysae showing elongation due to flow .....	34
Plate 31 Large lithophysae ('thunder egg') with smaller lithophysae on the surface. ....	34
Plate 32 Hand specimen of Nuckulla Basalt showing phenocryst poor nature of this unit. ....	35
Plate 33 Thin sediment layer which occurs at top of Nuckulla Basalt.....	35
Plate 34 Prominent flow layering dipping to the west within the Yantea Rhyodacite.....	36
Plate 35 Spherulites within the Yantea Rhyodacite.....	36
Plate 36 Hand specimen of Moonamby Dyke Suite showing characteristic porphyritic nature .....	37
Plate 37 Hand specimen of porphyritic Hiltaba Suite granite.....	37
Plate 38 Hand specimen of coarse grained Hiltaba Suite granite. ....	37
Plate 39 Hand specimen of Hiltaba Suite microgranite .....	37
Plate 40 Large outcrop of Hiltaba Suite granite from the Kondoolka Batholith.....	37
Plate 41 Coarse grained Hiltaba Suite granite from Arcoordaby Rockhole. ....	39
Plate 42 General view of low, scattered outcrop of gabbro/anorthosite south of Childera Outstation. ...	39
Plate 43 Detailed view of gabbro from above outcrop. ....	40
Plate 44 General view of Munjeela Rockhole. ....	41
Plate 45 Detailed view showing coarse grained microcline crystal.....	41
Plate 46 Detailed view of rodded quartz from west of New Year Hill. ....	41
Plate 47 Deformed granodiorite south of Tunkillia prospect with coarse feldspar grain showing dextral sense of shear (outcrop 6 on Figure 84).....	93
Plate 48 Dextral sense of shear defined by rotated feldspar porphyroclast from outcrop near Childera airstrip (outcrop 8 on Figure 84).....	93
Plate 49 Rotated feldspar grain showing dextral sense of shear from a granodiorite located SW of Yarranna Hill. ....	93
Plate 50 Narrow mylonite band within deformed granite with coarse feldspar grain showing dextral sense of shear from SW of Childera Outstation.....	93
Plate 51 Vertical face showing subvertical lineation in a rhyolite dyke from outcrop southwest of Childera (outcrop 8 on Figure 84) with ribbon quartz. ....	94
Plate 52 Shallow plunging stretching lineations south of Yarlbirinda Hill (outcrop 12 on Figure 84)...	95
Plate 53 Shallow dipping stretching lineation within granites along vermin proof fence (outcrop 1 on Figure 84). ....	95
Plate 54 Steeply plunging stretching lineation at Lakeside (outcrop 7 on Figure 84) (black line represents horizontal plane and pencil is parallel to the stretching lineation). ....	95
Plate 55 Folded, thin quartz vein (below main vein shown above). Fold axis rotates from horizontal to parallel to the stretching lineation.....	96
Plate 56 Thin section view of flow banding within Childera Dacite wrapping around an altered feldspar phenocryst. The hand specimen (see Plate 16) has a pseudo-fiamme appearance, but the thin section shows diffuse flow banding with no fiamme present (field of view is 2.4 cm).....	121
Plate 57 Drill core specimen of TAG. ....	126
Plate 58 Drill core sample of CAZ showing intense sericite alteration. ....	127
Plate 59 Drill core sample of mafic dyke (MAD) from Tunkillia prospect.....	127
Plate 60 Drill core sample of undeformed dacite dyke from Tunkillia prospect.....	128
Plate 61 General view of quartz hosted fluid inclusions trapped within pyrite grain within quartz veins in hole LED 03. Width of view is 2.4 mm.....	133
Plate 62 Detailed view of type 1b fluid inclusion.....	134

## LIST OF TABLES

Table 1 Average geochemical values for Tunkillia Suite and related intrusives. ....	50
Table 2 Average geochemical values for St Peter Suite. ....	58
Table 3 Summary of major oxide and trace element characteristics for seven Hiltaba Suite groups. ....	64
Table 4 Average geochemical values for Hiltaba Suite.....	69
Table 5 Average geochemical values for Glyde Hill Volcanic Complex.....	72
Table 6 Petrological, mineralogical and major elements characteristics of granitoids on the western Gawler Craton. ....	79
Table 7 Trace element compositions of granitoids from western Gawler Craton. ....	80



Table 8 Comparison of average values for St Peter Suite and Peninsular Ranges Batholith and Archaean TTG rocks. ....	107
Table 9 Physical features of silicic ignimbrites and lavas (from Henry and Wolff, 1992).....	120
Table 10 Occurrence of extensive silicic volcanic rocks of controversial origin (from Henry and Wolff, 1992).....	122
Table 11 Summary K-Ar data for Tunkillia samples.....	132
Table 12 Fluid inclusion data for Tunkillia samples. ....	136
Table 13 Sulphur isotope analyses of pyrite from Tunkillia (values in per mil relative to Canon Diablo Troilite). (* laser samples).....	140
Table 14 Results for lead isotope determinations of galena samples from V1-generation veins from Area 223, Tunkillia.....	141
Table 15 Temperature-salinity conditions for selected hydrothermal ore deposit types (from Cooke and Large, 1995). ....	144
Table 16 Relationships between temperature and redox conditions for selected hydrothermal ore types (from Cooke and Large, 1995). ....	146
Table 17 Geologic features of mineral deposits discussed in text. ....	156

## APPENDICES

Appendix A Geochemical sample locations and full geochemical analyses

Appendix B Geochronology data tables

## PLANS

- 1 1:250 000 geology map of CHILDARA
- 2 1:250 000 scale solid geology interpretation of CHILDARA

## ABSTRACT

The western Gawler Craton comprises poorly outcropping basement units which has hampered the tectonic understanding of the area. Recent high-resolution aeromagnetic data has provided an insight into the basement composition and allowed preliminary tectonic interpretation. The Gawler Craton is here divided into tectonic subdomains based on structural/metamorphic and aeromagnetic signature, and records a dominantly Proterozoic structural history. Regional mapping on CHILDARA 1:250 000 and reconnaissance sampling on FOWLER, STREAKY BAY, and NUYTS, was designed to determine the geochemistry of the basement lithologies, and attempt to construct a geological history of the western Gawler Craton, building on recent geochronology and structural/metamorphic work within the Fowler Subdomain to the west. This understanding is further used to constrain the age and controls on gold and base-metal mineralising events. Previous solid geology interpretations of the western Gawler Craton showed an Archaean basement to much of the area, however, this study has shown no Archaean exists within the Nuyts Subdomain.

Four main periods of Proterozoic granitoid plutonism over a 130 My period (~1690 – 1560 Ma) are recognised on CHILDARA. Recent geochronology has shown that major structures post-date the Kimban Orogeny (1845 – 1695 Ma), hence deformation and associated magmatism on the western and northern Gawler Craton are now attributed to the Kararan Orogeny (1690 – 1540 Ma).

The 1690-1670 Ma Tunkillia Suite is restricted to the eastern Nuyts Subdomain and scattered plutons within the Christie, Fowler and Cleve Subdomains. The Tunkillia Suite is felsic (67 – 76.5 wt% SiO<sub>2</sub> values) with Na/K <1, has high Rb/Sr, variable HREE enrichment and moderate to strong negative Eu anomalies. On CHILDARA, the Tunkillia Suite crops out within the Yarlbrinda Shear Zone, and hosts the Tunkillia and Nuckulla Hill gold prospects.

The 1630-1608 Ma St Peter Suite is restricted to the Nuyts Subdomain. Within the Kalanbi and Rocky Point-Cape Beaufort areas, these rocks generally resemble magmatic arc-related batholiths. The St Peter Suite is characterised by an expanded SiO<sub>2</sub> range (47-76 wt%), is sodic (Na/K >1), shows high Sr, K/Rb and Sr/Y and relatively low K<sub>2</sub>O, Rb, Rb/Sr, Th, U (ie: low heat producing granites), REE, and Nb. The St Peter Suite is LREE enriched, HREE and Y-depleted, with little or no Eu anomaly. These geochemical characteristics are similar to modern magmatic arc rocks and are consistent with formation within a subduction related environment, with magmas produced from partial melting of hydrous basalt at depths within the garnet stability field. The St Peter Suite is considered to have formed by fractionation of arc-type magmas and/or partial melting of arc-related intrusions, or mafic under-plating within a subduction related continental margin setting.

The Hiltaba Suite (1595-1575 Ma) is an extensive suite of felsic granites (>70 wt % SiO<sub>2</sub>) characterised by low Na/K (<1), high Rb/Sr and variable HREE enrichment, with moderate to strong negative Eu anomalies. The comagmatic Glyde Hill Volcanics correlate with the Gawler Range Volcanics, and comprise a series of dominantly felsic lavas and ignimbrites. The Hiltaba Suite/Gawler Range Volcanics generally do not show an arc affinity. They record a major shift in tectonic

environment from a dominantly compressional environment during the St Peter Suite magmatic event, to an intracontinental extensional environment, but the initial source of heat may be related to earlier subduction (ie: back-arc extension origin).

The 1560 Ma S-type Munjeela Granite represents a late stage melt and is related to a period of extension and basin formation to the west of the Koonibba Fault Zone.

The most likely tectonic model that accounts for these geochemical features is as follows. Continental collision occurred between the Fowler Subdomain and the proto-Yilgarn Craton to the west, initiating southward dipping subduction to produce the arc related St Peter Suite magmatism. However, this change appears to have been unsustainable and subsequent intraplate extension, possibly together with basaltic underplating of the continental crust, produced the voluminous Hiltaba Suite/Gawler Ranges Volcanics.

These geological events produced lode gold-style mineralisation within the Yarlbirinda Shear Zone. The Yarlbirinda Shear Zone is a major north-south trending shear zone located on eastern CHILDARA, which hosts the Tunkillia and Nuckulla Hill gold prospects. The host granites are extensively altered, with mineralisation associated with zones of intense sericite alteration. K-Ar dating of sericite from Tunkillia recorded a cooling age of ~1600 Ma, suggesting a relationship to the Hiltaba Suite/Gawler Range Volcanic magmatic event. Two main vein generations are defined at Tunkillia, with mineralisation located within narrow quartz veins (V1). V1 veins comprise quartz and sulphides and combine to form steeply dipping lenses ranging in thickness from cm-scale up to 1 m, which are sub-continuous along strike. Pyrite is the main sulphide with accessory galena and chalcopyrite. V2 veins comprise late, crosscutting calcite veins, which are barren.

Primary fluid inclusions hosted by V1 veins are typically two-phase at room temperature containing an aqueous phase and vapour. Preliminary fluid inclusion data suggests that gold deposition took place over a temperature range of 200° - 300° C from a low salinity fluid ( $\leq 4$  wt% NaCl equivalent). Sulphur isotope analysis shows the source of sulphur is magmatic (-2.23 to 3.19), and lead isotope data indicate that mineralisation is consistent with an origin by fluid release from Hiltaba Suite granites, however, the Pb-isotopic composition of other granitoid suites has not been characterised.

The Yarlbirinda Shear Zone shows evidence for an early phase of dextral strike-slip deformation, which is expressed by a regional foliation and shallow plunging stretching lineations. Kinematic indicators including S-C fabrics and rotated porphyroclasts show a dextral sense of shear. Later deformation comprised dip-slip movement, which produced steeply plunging stretching lineations and rotated porphyroclasts, showing a west-side-up sense of movement. Mineralisation at Tunkillia appears to be localised at the junction of the regional foliation and steeply plunging lineations, and is interpreted as late in the structural history. Late stage brittle structures related to the locking up of the Yarlbirinda and Yerda Shear Zones crosscut the shear zone and are unrelated to mineralisation. The Yarlbirinda Shear Zone is part of a large-scale west-directed transpressional duplex that developed on a regional restraining bend of the shear system.

---

U-Pb zircon geochronology shows that deformation within the Yerda Shear Zone was taking place at ~1592 Ma, but deformation within the Yarlbirinda Shear Zone must have ceased by ~1580 Ma when the Kondoolka Batholith was intruded. The extent of sericite alteration requires a voluminous influx of low pH fluids, with the Hiltaba Suite the most likely source. This fluid mixed with low salinity metamorphic fluids which leached Pb and S from the granites at depth.

---

## ACKNOWLEDGEMENTS

Firstly I would like to thank my supervisors at CODES, Dr Ron Berry and Dr Garry Davidson for their support and encouragement for me to continue after a lengthy intermission. Garry was especially helpful in convincing me to finish the project. Thank you to the various laboratory technicians who prepared fluid inclusion mounts etc.

This study was initiated by discussions with Acacia Resources after a visit to Tunkillia, so I am grateful to Dave Borton for the support. A big thank you to the former employees of Acacia Resources, Andrew Beckwith, Tony Standish and Richard Hill for your hospitality on site and continued support and ideas. Many thanks to Dr John Parker and Equinox Resources NL for allowing me to stay at Childera Outstation during field work on Lake Everard Station. Thanks to Simon, Tina, Sophie and William at Kondoolka Station, and to Graeme and Jeanette at Lake Everard Station for your hospitality. Cheers to Zurg for field assistance.

Thanks to Sue Daly at PIRSA for discussions on geology and the meaning of life, your support and friendship is most appreciated. Thanks to other workmates including Mike (Patsy), Liz and a special mention to Mike Pate from the PIRSA Core Library for cutting and labelling countless samples. Cheers to Alan Mauger who helped resurrect my thesis when MS Word crashed. Thanks to Neville Alley, Director of Minerals, PIRSA for the support he provides staff and the research opportunities available to staff. Cheers to Martin (muffy) Fairclough for reading various drafts and all the jokes. A big thank you to Annette and Sylvia who helped with printing and binding.

Thanks to my parents and parents in-laws for their support. A big thank you to Anne for supporting my wife during the last few months, it certainly made life easier. Thanks to James for looking after Henry when required.

Finally, my wife Shirley deserves a medal for the support she has given me over the course of this thesis. She was always there with advice, support and cheered me up during the times when my computer would crash or things were not going according to plan. This thesis is dedicated to my son Henry who must have wondered why dad did not come home some nights.

## Chapter 1 Introduction

### 1.1 Introduction

The geology of the western Gawler Craton, South Australia, has previously received scant attention due to poor geological exposure. Basement outcrop represents <10% of surface exposure, with vast sheets of sand blanketing underlying basement rocks. The recent acquisition of high-resolution aeromagnetic imagery, flown as part of the South Australian Exploration Initiative (SAEI) in 1993, has greatly improved our ability to determine the geology and tectonic history of the western Gawler Craton.

Due to poor exposure of basement rocks and limited geochronological data, little is known of the age of the basement, and the age of major structures on the western Gawler Craton. As a result, much of the western Gawler Craton was interpreted as Archaean with younger intrusives of the Lincoln Complex, St Peter Suite and Hiltaba Suite (Fairclough and Daly, 1994). However, recent data suggests that the western Gawler Craton contains only minor Archaean basement, with most crustal material produced in the Palaeoproterozoic, during periods of continental collision and subsequent crustal extension.

Previous descriptions of the geology of the western Gawler Craton has suffered from extrapolation of geological units and deformation history, defined from the better exposed southern Gawler Craton.

### 1.2 Project Aims

The main aim of this thesis is to revise the basement geology, determine the tectonic history for the CHILDARA area, and determine the source and timing of mineralisation at Tunkillia. This thesis comprises two parts. Part one discusses the geology of CHILDARA, with information derived through:

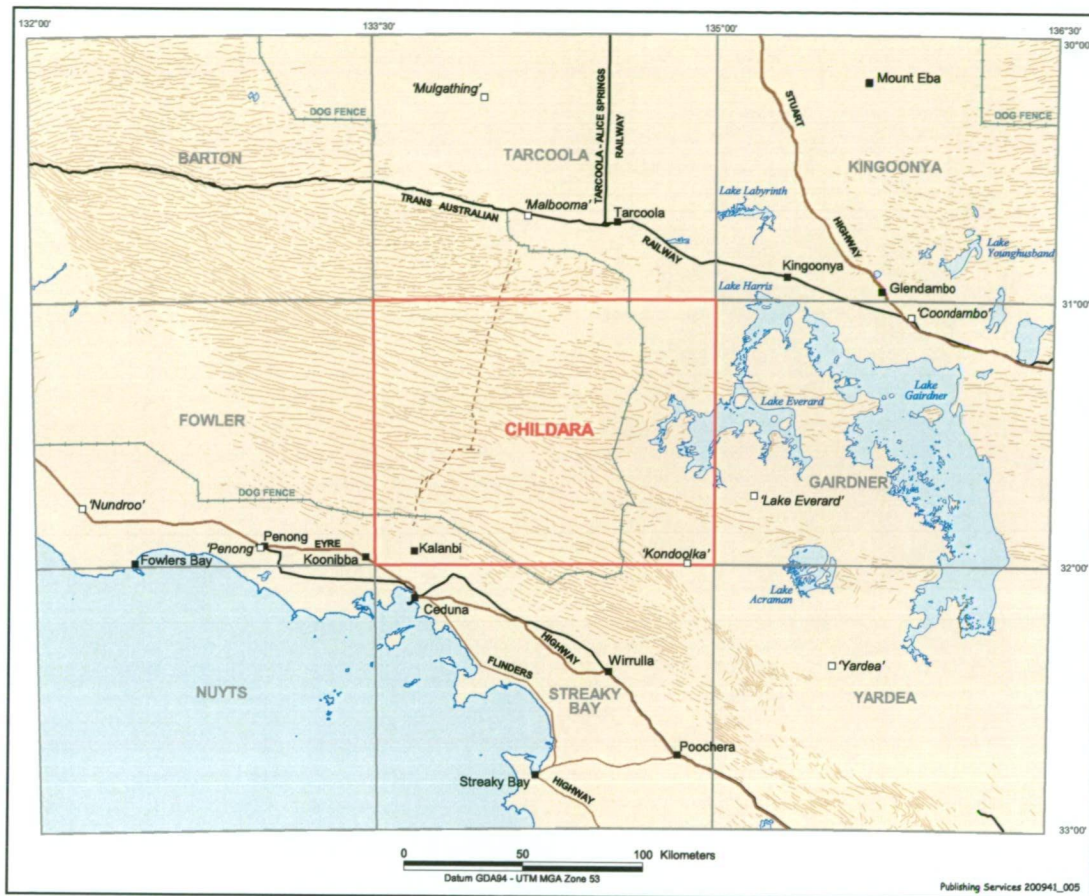
- regional mapping of CHILDARA 1:250 000 map sheet and preliminary reconnaissance sampling of the surrounding map areas;
- interpretation of the structural and tectonic history of the area;
- geochemical analysis of granitoids and associated rocks (Appendix A); and
- geochronological analysis of selected rocks. 5 new zircon U-Pb ages and 1 monazite age were carried out as part of this project (Appendix B).

Part two investigates gold mineralisation at Tunkillia within the Yarlbirinda Shear Zone. Methods used include:

- geochronology of the host granite at Tunkillia;
- K-Ar dating of sericite alteration associated with mineralisation;
- sulphur isotope analysis of pyrite samples from quartz veins to determine source of sulphur;
- lead isotope analysis of galena from quartz veins to determine the date and source of mineralisation; and
- fluid inclusion analysis of vein quartz to identify physio-chemical conditions of mineralisation.

### 1.3 Background

The CHILDARA 1:250 000 map area is located on the western Gawler Craton (Figure 1), an ancient crystalline shield comprising Palaeoproterozoic to Mesoproterozoic metasediments, volcanics and granites (Figure 2), which has been tectonically stable since 1450 Ma (Thomson, 1975; Parker, 1993). Basement outcrop is poor and is restricted to scattered, low sheets of granite and inselbergs over much of the area. Brown (1885), during an expedition from Ceduna to Mount Finke, commented on granite inselbergs in northwestern CHILDARA.



**Figure 1** Location of CHILDARA on the western Gawler Craton, South Australia.

#### 1.3.1 Geology

Bennett (1968) produced a preliminary geological map of part of CHILDARA. Blissett and Vitols (1974) carried out a helicopter survey to collect samples and map basement outcrops on the western Gawler Craton. This survey was the basis for the 1:250 000 geological mapping (Blissett, 1977, 1980). Samples were assayed for a range of elements including base metals and gold; see Figure 3 in Blissett and Vitols (1974) for sample locations and assay values. Company mineral exploration has been restricted to the more accessible areas along the eastern and southwestern sections of the map area (Figure 1).

During 1996, calcrete sampling by Helix Resources NL and Equinox Resources NL delineated gold anomalies at Tunkillia and Nuckulla Hill respectively within the Yarlbirinda Shear Zone. The Tunkillia prospect is located at the northern end of the



Yarlbrinda Shear Zone, where the north-south trending shear zone curves into the northwest striking Yerda Shear Zone. Martin (1996) reported that mineralisation at Tunkillia is hosted by variably deformed granite, which has been extensively haematite and/or silica-sericite-chlorite altered. Areas 223 and 191 are located within demagnetised zones along the margins of the shear zone, with gold mineralisation associated with steeply dipping, high-grade veins within an envelope of essentially barren, but highly altered granite. At Area 223, mineralisation occurs over a strike length of 500 m and is between 10 and 120 m wide, with a high-grade zone 10-25 m in width.

Within the central part of the Yarlbrinda Shear Zone, Equinox Resources NL delineated gold mineralisation at Myall, Sheoak and Bimba, collectively called the Nuckulla Hill prospect. Rock types range from brecciated granite to syenogranite, quartz diorite, adamellite and mylonitic gneisses, which have undergone amphibolite-facies metamorphism (Parker, 1996). Post-peak metamorphic sericitisation and quartz veining were followed by calc-silicate±epidote veining ±chlorite±adularia±quartz±fluorite or calcite (Parker, 1996). Gold grades range from 7 m at 3.1 g/t including 3 m at 6.2 g/t within drillhole NHAC 26 at Sheoak, to 3 m at 1.67 g/t (NHAC 150) and 5 m at 1.71 g/t (NHAC 152) at the Bimba prospect (Daly *et al.*, 1998).

### 1.3.2 Geophysics

The first geophysical study of the area was carried out by the Bureau of Mineral Resources Geology and Geophysics (BMR) in 1961 in the search for iron ore deposits using reconnaissance airborne magnetic and radiometric surveys over most of CHILDARA (Quilty, 1962). BMR also conducted a regional gravity survey by helicopter, which included CHILDARA during 1970 (Pettifer and Fraser, 1974).

High-resolution aeromagnetic data flown by World Geoscience Corporation, Geoterrex and Kevron during 1992-95 has greatly enhanced the exploration potential of the western Gawler Craton. Major structures have been delineated, including the Yarlbrinda Shear Zone which extends for ~170 km and trends north-south along the western margin of the Gawler Range Volcanics, but is reorientated to the northwest where it intersects the Koonibba Fault and the Yerda Shear Zones (Figure 3).

Regional mapping of CHILDARA was based on Department of Lands colour aerial photographs at a scale of 1:86 950 (Surveys 3327 and 3334). Geological boundaries were transferred to topographic bases prepared by the Spatial Information Services Branch of PIRSA at aerial photograph scale.



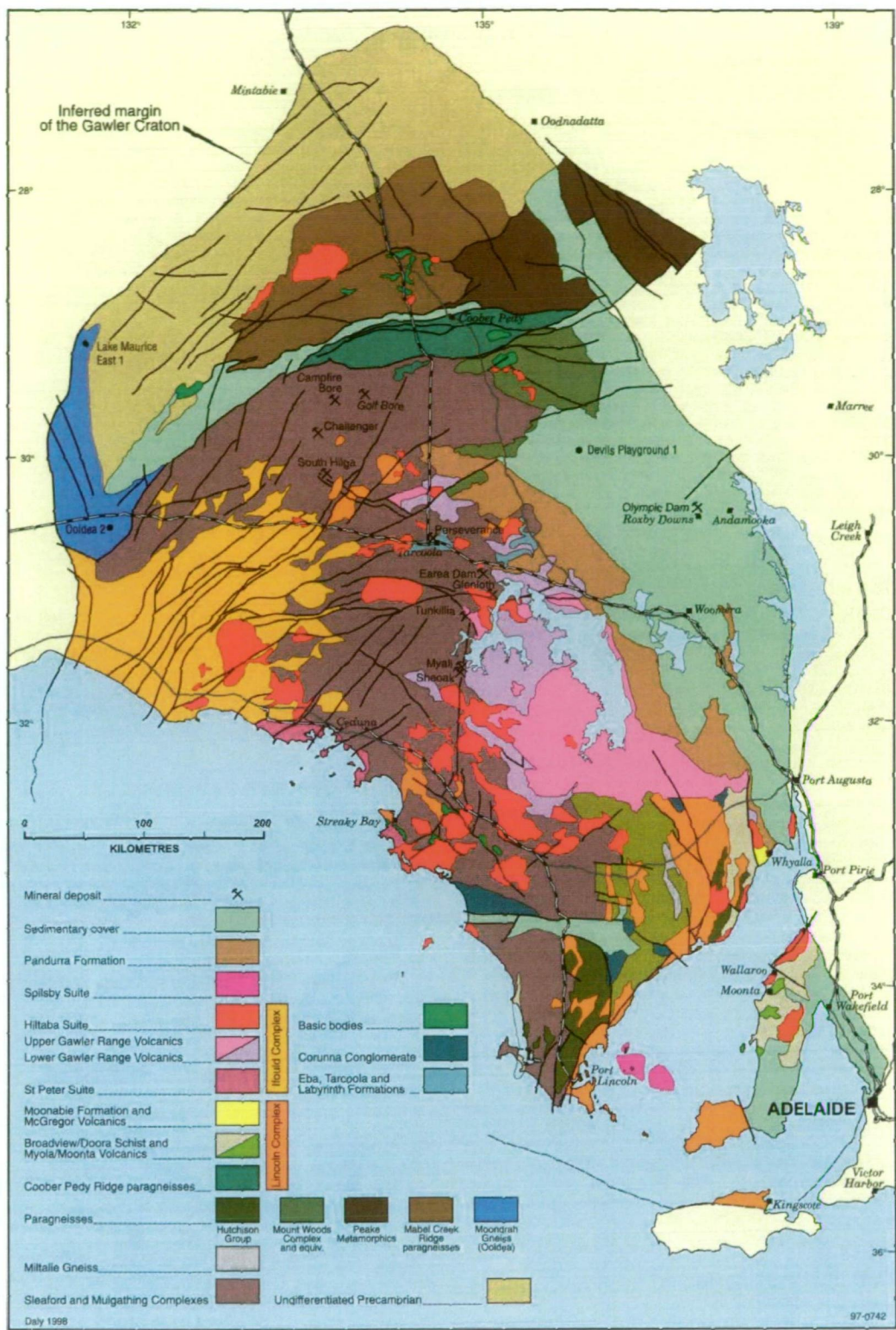
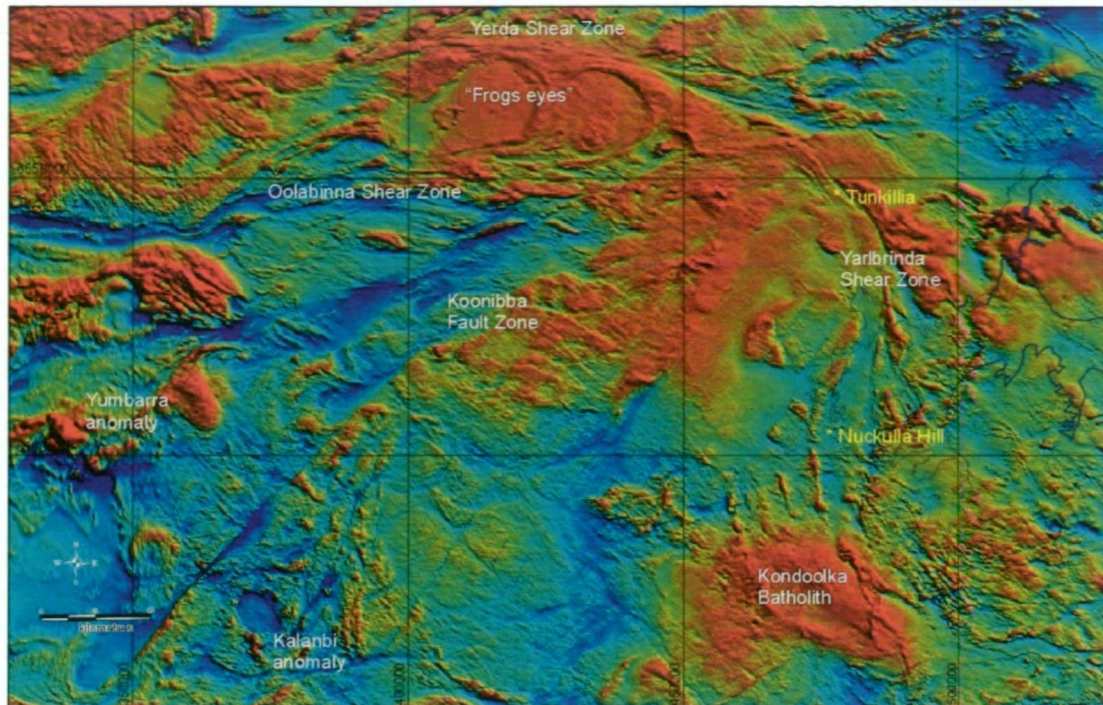


Figure 2 General geology of the Gawler Craton (from Daly *et al.*, 1998).





**Figure 3** Total magnetic intensity (TMI) image of CHILDARA 1:250 000 map sheet showing main geologic features.

#### 1.4 Climate and Physiography

CHILDARA lies between latitudes 31°00' and 32°00' south and longitudes 133°30' and 135°00' east (Figure 1). The eastern part of the map area comprises the large sheep grazing pastoral leases of North Well, Lake Everard and Kondoolka, with access via station tracks from the main graded dirt road from Wirrulla to Kingoonya. The Kalanbi area in southwest of CHILDARA comprises smaller land holdings used for cereal growing. The majority of the map area falls within the Yellabinnia Regional Reserve (Figure 1) with public access tracks located along the Vermin Proof Fence (VPF), and Googs Track, which traverses the park from Kalanbi Gate northwards to Malbooma rail siding west of Tarcoola.

CHILDARA has a semi-arid climate with long, hot summers during which the temperature commonly exceeds 35°C, and short cool winters. Rainfall ranges from 330 mm on the coast at Ceduna to <170 mm at Kingoonya in the north. Rainfall is variable, with long periods of drought common. Good rains occasionally occur during thunderstorm activity.

The topography of CHILDARA is dominated by sand dunes of the Great Victoria Desert (Plate 1) which generally rise 100–150 m above sea level. The Gawler Range Volcanics in the Lake Everard area and Hiltaba Suite granite outcrops in the Kondoolka area form long ridges and isolated hills, which rise up to 75 m above the surrounding plains. Within the volcanics, dacitic units form prominent hills whilst the rhyolites are more subdued. Granite in other parts of the map area generally crop out as low isolated sheets within areas of scrub. A series of playa lakes occupying topographic depressions and usually associated with areas of parabolic or network dunes occur across central CHILDARA.



**Plate 1** Aerial view showing topography of cental CHILDARA area.



## Chapter 2 Stratigraphy

### 2.1 Introduction

CHILDARA is located on the western Gawler Craton, an ancient crystalline shield comprising Palaeoproterozoic to Mesoproterozoic metasediments, volcanics and granites, which have been tectonically stable, with the exception of minor epeirogenic movements since ~1450 Ma (Parker, 1990, 1993). Due to poor basement outcrop, the geology of the western Gawler Craton is poorly constrained, compared to other cratonic areas within Australia. This chapter summarises the basement stratigraphy of the Gawler Craton and focuses on the stratigraphy of CHILDARA.

### 2.2 Stratigraphy of the Gawler Craton

The stratigraphy presented in this section is summarised from recent literature (Drexel *et al.*, 1993; Daly 1996; Daly *et al.*, 1998) and is necessary to provide the geological framework for the following stratigraphical review of CHILDARA. Due to recent mapping, the stratigraphy of the Gawler Craton is constantly being revised. Recent U-Pb SHRIMP dating has defined new units and provided constraints on the timing of deformation of major structures on the Gawler Craton (Teasdale, 1997; Fanning, 1997). The basement stratigraphy of the Gawler Craton is shown in Figure 4 and the interpretative basement geology shown in Figure 2.

#### 2.2.1 Archaean

Archaean Sleaford Complex and Mulgathing Complex, form the basement rocks to the much of the Gawler Craton (Figure 2). The Sleaford and Mulgathing Complexes are lithologically similar and comprise orthogneisses and paragneisses, mafic volcanics and syn-tectonic granitoids (Daly and Fanning, 1993).

The Sleaford Complex is confined to the southern Gawler Craton where it crops out along the west coast of Eyre Peninsula. The Sleaford Complex is divided into four units (Daly and Fanning, 1993):

- Dutton Suite granitoids;
- Unnamed Gneiss;
- Wangary Gneiss; and
- Carnot Gneiss.

The Mulgathing Complex occurs on the central and northern Gawler Craton and comprises ten rock units (Daly, 1986; Daly and Fanning, 1993):

- Metasedimentary Christie Gneiss;
- Meta-igneous or metasedimentary Kenella Gneiss;
- Hopeful Hill Basalt;
- South Lake Gabbro;
- Lake Harris Komatiite;
- Blackfellow Hill Pyroxenite;

The geology and geochemistry of granitoids in the CHILDARA region, western Gawler Craton, South Australia: implications for the Proterozoic tectonic history of the western Gawler Craton and the development of lode-style gold mineralisation at Tunkillia.

- Aristarchus Peridotite;
- Mobella Tonalite and associated synorogenic granitoids;
- Unnamed calc-alkaline volcanics; and
- late-orogenic Glenloth Granite.

The Sleaford and Mulgathing Complexes have undergone regional deformation and metamorphism during the Sleaford Orogeny. This deformation will be discussed in Chapter 4.

### 2.2.2 Palaeoproterozoic

Palaeoproterozoic rocks are widespread on the Gawler Craton (Figure 2), and comprise crystalline metasediments, metavolcanics and granitoids, which have been variably deformed and metamorphosed (Parker, 1993). The main stratigraphic units are shown in Figure 4.

The Miltalie Gneiss (Parker *et al.*, 1981; Parker and Lemon, 1982) is a grey, migmatitic granite gneiss, which has a U-Pb zircon crystallisation age of  $2014 \pm 28$  Ma (Fanning *et al.*, 1988). The Miltalie Gneiss was intruded into the Sleaford Complex and together they form the base of the Hutchinson Group (Parker and Lemon, 1982). The Hutchinson Group and other Palaeoproterozoic metasediments reflect a period of relative tectonic stability and basin development.

The Hutchinson Group is an extensive sequence of shallow clastic and chemical marine sediments, with minor acid and mafic volcanics (Parker, 1993). The true thickness of the Hutchinson Group is uncertain, but Daly (1996) estimated a total thickness of 3 500 m. Parker (1980) subdivided the Hutchinson Group into three main sequences:

- a basal quartzite sequence (Warrow Quartzite);
- a mixed chemical and clastic sequence (Middleback Subgroup); and
- upper pelitic Yadnarie Schist.

On the northern and western Gawler Craton, depocentres for Palaeoproterozoic sedimentation include:

- Tarcoola-Kingoonya area (Wilgena Hill Jaspilite and overlying clastic sequence and interbedded volcanics of the Labyrinth Formation);
- Peake and Denison Inlier (Tidnamurkuna Volcanics and overlying Baltucoodna Quartzite);
- the Mount Woods Inlier;
- The Coober Pedy and Mabel Creek Ridges; and
- the Ooldea area (Figure 4).

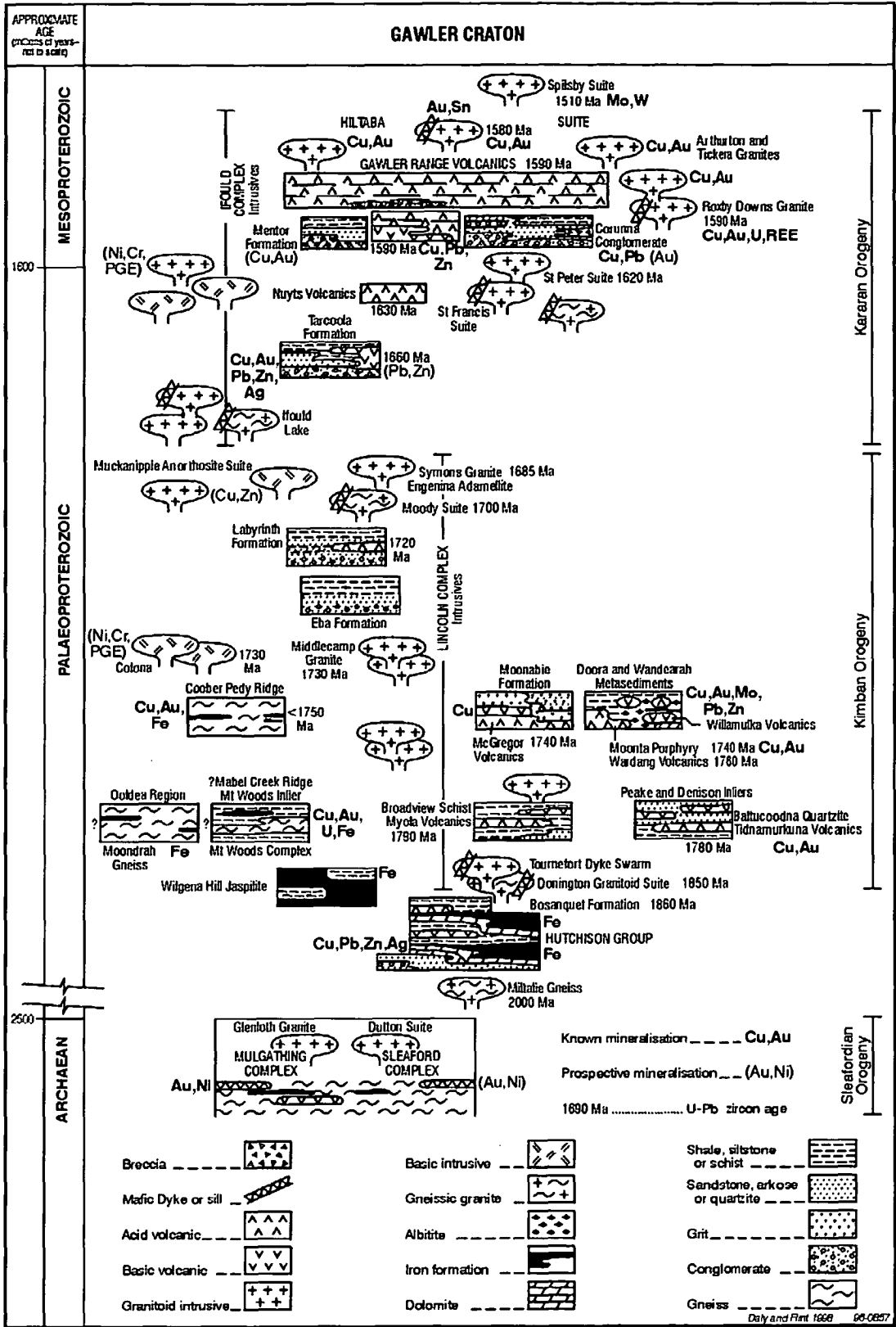


Figure 4 Basement stratigraphy of the Gawler Craton (modified from Daly and Flint, 1998).

The geology and geochemistry of granitoids in the CHILDARA region, western Gawler Craton, South Australia: implications for the Proterozoic tectonic history of the western Gawler Craton and the development of lode-style gold mineralisation at Tunkillia.

Following the deposition of the above units, the Gawler Craton underwent a period of orogenic activity and associated magmatism. On the southern Gawler Craton, the Kimban Orogeny was defined as three distinct events: KD<sub>1</sub> from 1845-1795 Ma, KD<sub>2</sub> from 1795-1745 Ma and KD<sub>3</sub> from 1745-?1695 Ma (Parker, 1993; Daly, 1996).

Voluminous, syntectonic magmatism accompanied each deformation event outlined above. During KD<sub>1</sub>, the Donnington Granitoid Suite, Tournefort Dyke Suite and Minbrie Gneiss were intruded. The Middle Camp and Carpa Granites were intruded during KD<sub>2</sub>, and the Moody Suite represent KD<sub>3</sub> intrusives (Figure 4).

On the northern and western Gawler Craton, intrusion of Symons Granite, Engenina Adamellite and Muckanippie Anorthosite Complex were formerly correlated with the Kimban Orogeny. However, these units are related to the Kararan Orogeny (Daly *et al.*, 1998). This will be discussed further in Chapter 4.

During the late Palaeoproterozoic, relatively large volumes of bimodal, but dominantly felsic intrusives, termed the St Peter Suite were intruded on the western Gawler Craton (Figures 2 and 4).

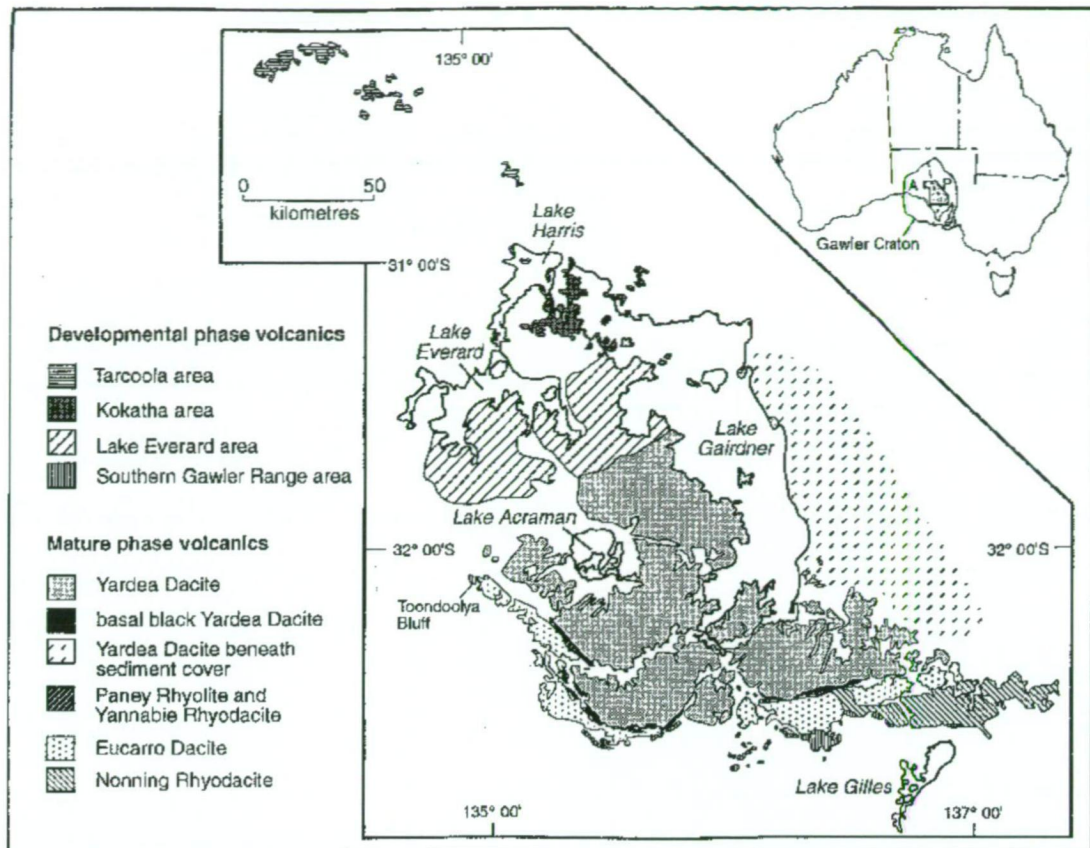
### 2.2.3 Mesoproterozoic

During the Mesoproterozoic, the Gawler Craton underwent extensive felsic, anorogenic magmatism producing the Gawler Range Volcanics and Hiltaba Suite granite (Figure 2). The Gawler Range Volcanics cover an area of approximately 25 000 km<sup>2</sup> and are the dominant Proterozoic outcropping unit on the Gawler Craton (Figures 2 & 5). The Gawler Range Volcanics are a series of dominantly felsic lavas and ignimbrites, with minor mafic lavas.

The Hiltaba Suite intrudes the Gawler Range Volcanics and are a suite of mostly oxidised, K-feldspar dominant granite. The discovery of the Olympic Dam Cu-U-Au ore body, hosted within the Roxby Downs Granite, a member of the Hiltaba Suite, has greatly increased the prospectivity of the Gawler Craton.

Since the Gawler Range Volcanics/Hiltaba Suite granite magmatism, the craton has been relatively stable with minor magmatism recorded at 1520 Ma (Spilsby Suite) and deposition of the Corunna Conglomerate on eastern Eyre Peninsula.

This outline of the stratigraphy of the Gawler Craton is not exhaustive and readers are referred to Drexel *et al.* (1993), Daly (1996) and Daly *et al.* (1998) for more comprehensive descriptions.



**Figure 5** Location and extent of Gawler Range Volcanics and Hiltaba Suite magmatism (Stewart, 1992).

Previous solid geology interpretations (Parker, 1987; Fairclough and Daly, 1994) show that the basement on CHILDARA is dominantly Archaean, intruded by Palaeoproterozoic and Mesoproterozoic intrusives. However, recent mapping and Sm–Nd isotope analysis, indicate no known Archaean basement within the Nuyts Subdomain.

### 2.3 Stratigraphy of CHILDARA

The stratigraphy of CHILDARA is presented in Blissett (1980). Giles (1977, 1980) presented detailed stratigraphy for the Glyde Hill Volcanic Complex. This section is based on regional mapping of the CHILDARA 1:250 000 sheet.

Five main periods of magmatism are recorded on CHILDARA:

1. Archaean Mulgathing Complex;
2. 1690–1670 Ma Tunkillia Suite;
3. 1630–1608 Ma St Peter Suite;
4. 1595–1575 Ma Gawler Range Volcanics and Hiltaba Suite Granite; and
5. ~1560 Ma Munjeela Granite.

### 2.4 Archaean

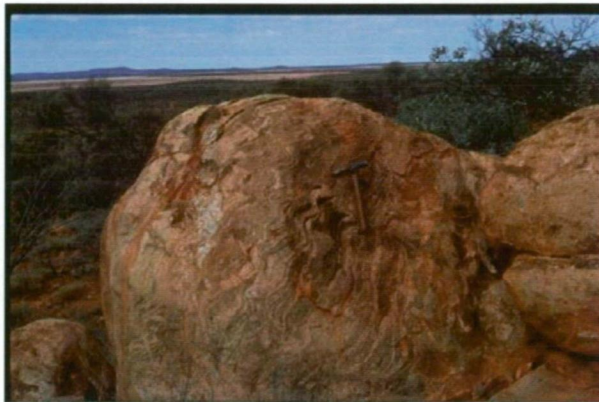
Archaean rocks on the western Gawler Craton belong to the Mulgathing Complex (Daly *et al.*, 1979; Daly 1985, 1986). Only the Glenloth Granite crops out on CHILDARA. Daly and Fanning (1990) report a preliminary U–Pb crystallisation age of 2440 Ma for the Glenloth Granite.

The geology and geochemistry of granitoids in the CHILDARA region, western Gawler Craton, South Australia: implications for the Proterozoic tectonic history of the western Gawler Craton and the development of lode-style gold mineralisation at Tunkillia.



### **2.4.1. Glenloth Granite (ALmg)**

The Glenloth Granite varies from granite to granodiorite in composition, is poorly to well foliated, medium to coarse grained, and varies from pinkish brown to grey in colour. It consists predominantly of quartz, microcline with subordinate plagioclase, and contains angular remnants of layered quartz–feldspar–biotite–hornblende gneiss, and convoluted biotite and hornblende-rich schlieren (Plate 2).



**Plate 2 Outcrop of Glenloth Granite showing mafic schlieren**

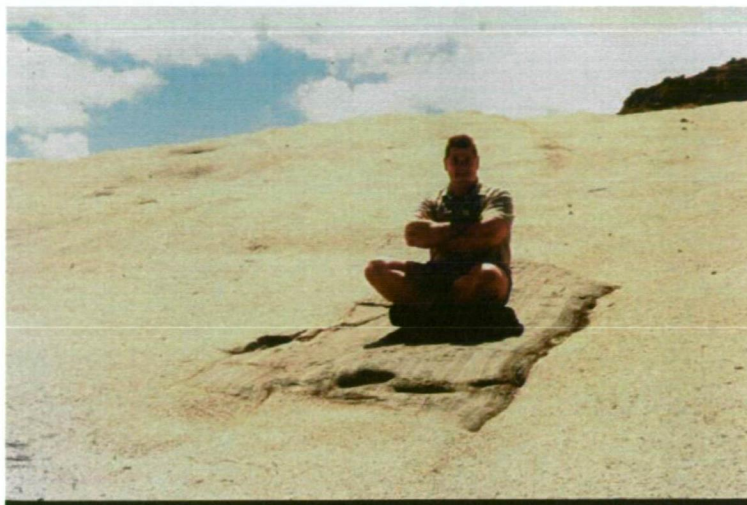
On northeastern CHILDARA, quartz–feldspar–biotite granite, interpreted to be Glenloth Granite crops out in the New Year Hill area. Extensive areas of kaolinised granite, capped by silcrete, crops out on northeastern CHILDARA, and these are interpreted to represent weathered Glenloth Granite.

## **2.5 Palaeoproterozoic**

### **2.5.1 Undifferentiated Palaeoproterozoic basement**

Within the CHILDARA area, interpreted Palaeoproterozoic units including metasediments and orthogneisses occur as enclaves in younger rocks. At Rocky Point on STREAKY BAY, Palaeoproterozoic St Peter Suite granite intrudes quartzofeldspathic orthogneiss that possibly represent Palaeoproterozoic basement. At Point Sinclair, enclaves of well-foliated, quartz–feldspar–biotite–garnet schist occur within Mesoproterozoic Munjeela Granite (Plate 3). On CHILDARA, rafts of metasedimentary enclaves are present in Hiltaba Suite granite within the Kondoolka Batholith (Plate 4). West of Childera Outstation, enclaves of andalusite–biotite hornfels occur within Tunkillia Suite granite. These metasediments represent undifferentiated basement rocks.

Mylonite from an outcrop west of the Vermin Proof Fence (VPF), comprises thinly laminated, alternating pink and brown to grey layers, similar in appearance to mylonite from south of Yarlbirinda Hill. Mason (1998) reported that the precursor was possibly a fine-grained, feldspathic silty sediment.



**Plate 3** “Magic carpet” metasedimentary enclave within Munjeela Granite at Point Sinclair.



**Plate 4** Hand specimen of pebbly meta-conglomerate and meta-siltstone enclave within Hiltaba Suite granite from the Kondoolka Batholith (width of view is 12 cm).

### 2.6.1 Tunkillia Suite

Rocks within the Yarlbirinda Shear Zone belong to the Tunkillia Suite (new name). The Tunkillia Suite represent a suite of comagmatic late Palaeoproterozoic (1690-1670 Ma), I-type intrusives and rhyolite, mafic and aplite dykes.

Multigrain analyses of zircons from foliated granite from the Tunkillia prospect (hole LED 10 155-157 m) gave an upper intercept age of  $1680 \pm 5$  Ma (Appendix B), which represents crystallisation age. This is similar to the date obtained for a foliated, rhyolite dyke, intruded into foliated granite southwest of Childera Outstation, which recorded a magmatic age of  $1679 \pm 12$  Ma (A.J. Parker, Geosurveys, pers. comm., 1997).

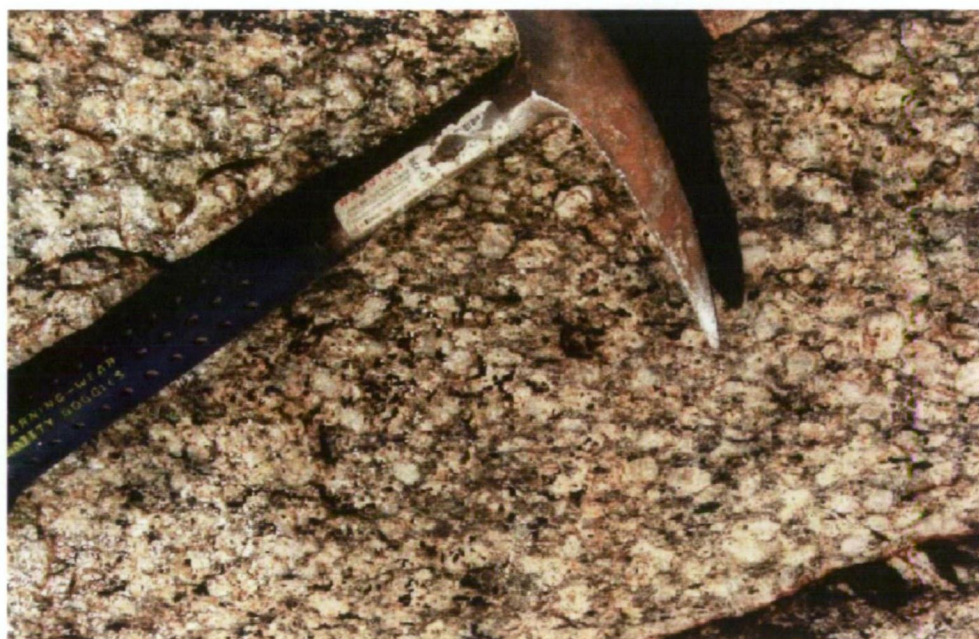
Based on the regional mapping, six main lithologies were delineated, L<sub>1-6</sub>.

#### 2.5.1.1 Orthogneiss (L<sub>1</sub>)

This unit includes a variety of coarse-grained, megacrystic granites to augen gneisses ranging in composition from granite (K-feldspar dominant) to quartz syenite. These rocks are altered, partly recrystallised and variably deformed.



The main exposures occur along the edges of lakes north of Fyne Dam, in an area Equinox Resources NL called Lakeside. The rocks comprise a series of comagmatic, coarse-grained augen gneiss, with some coarse orthoclase augen up to 15 mm in diameter, but averaging 1–5 mm (Plate 5). Quartz content varies from 15–40% and is extensively recrystallised to fine-grained (0.5–1 mm) grains; rare elongated grains up to 4 mm in length occur. Plagioclase content varies from 10 to 20%, with grains up to 8 mm in length, but averaging <1 mm and is commonly altered to sericite and albite. Biotite is present as an accessory phase and is mostly recrystallised and altered to leucoxene. Minor outcrops of coarse grained, augen granite gneiss are located south and southwest of Childara Outstation.



**Plate 5 Outcrop of coarse grained, augen granite gneiss located at Lakeside.**

#### 2.5.1.2 Granite ( $L_2$ )

This unit comprises variably deformed, grey to pink, medium to coarse-grained, adamellite, quartz syenite to granodiorite. K-feldspar and plagioclase are common, with both occurring as blocky euhedral crystals and smaller anhedral grains. The coarser grains represent better-preserved primary igneous grains, whereas the smaller grains show the effects of dynamic regional deformation and metamorphism. There are no diagnostic metamorphic minerals available to positively identify the grade of metamorphism, but the style of deformation is consistent with upper greenschist to amphibolite facies.

At Lakeside, medium to coarse grained granite crops out as low discontinuous sheets and tors. The granite contains sub-equal amounts of coarse K-feldspar grains up to 15 mm in length, with finer grained plagioclase and quartz.

West of Childera Outstation, medium grained, foliated granite crops out. The original texture of the rock has been extensively altered by regional deformation producing a granoblastic mosaic of K-feldspar, plagioclase (albite), quartz and minor biotite.



South west of Childera Outstation, granite crops out as a prominent linear ridge. The rock ranges from slightly deformed with only quartz being recrystallised producing a foliation to narrow, mylonite zones, in which all minerals are completely recrystallised (Plate 6).



**Plate 6 Outcrop of granite south west of Childera Outstation showing narrow mylonite zone.**



**Plate 7 Hand specimen of Yarlbrinda Hill showing coarse grained, K-feldspar dominant granite, which has been deformed under ductile and brittle regimes.**

South of Tunkillia base camp, granite crops out as low sheets and rounded tors. Rock type ranges from granodiorite to biotite monzogranite to adamellite gneiss. Alkali feldspar and plagioclase are present in nearly equal amounts with minor primary biotite. Alkali feldspar is present as large, blocky crystal up to 12 mm in

The geology and geochemistry of granitoids in the CHILDARA region, western Gawler Craton, South Australia: implications for the Proterozoic tectonic history of the western Gawler Craton and the development of lode-style gold mineralisation at Tunkillia.



length. Plagioclase is much finer grained up to 4 mm in length and commonly altered to sericite. Quartz is moderately abundant and has been completely recrystallised. Biotite is randomly scattered throughout the rocks and has been extensively replaced by chlorite. Minor fine grained, recrystallised biotite occurs in thin anastomosing lamellae which suggests a S-C fabric (Purvis, 1998a).

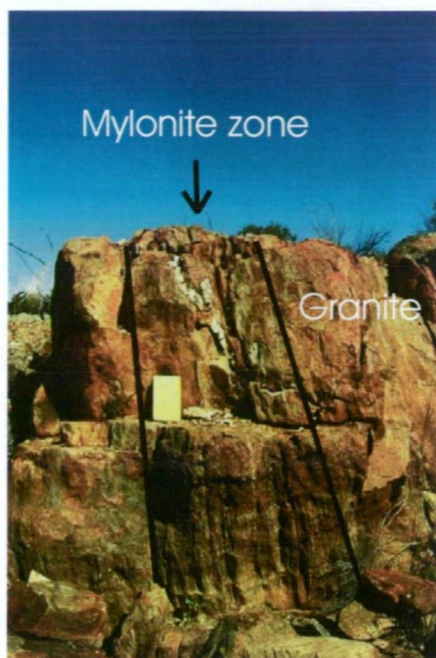
Webb (1978) obtained a tentative Rb–Sr age of 1640 Ma for two samples from Yarlbrinda Hill, which formed the basis of assignment to the Glenloth Granite (Blissett 1980); it is now assigned to the Tunkillia Suite. Yarlbrinda Hill comprises predominantly protomylonitic granitoid gneiss, with coarse-grained lenticular red K-feldspar (up to 30 x 8 mm) and finer grained cream to red lenticular plagioclase grains (Plate 7). Petrological examination shows that the original rock comprised a medium- to coarse-grained potassic granite, which was subsequently deformed under ductile conditions, producing lenticular feldspar augen and prominent foliation development (Purvis, 1997). Later, more pervasive brittle deformation produced microfracturing of coarse feldspar grains and recrystallisation of original quartz into irregular lenses and incipient veins. Yarlbrinda Hill also contains abundant pseudotachylite development (Plate 8).



**Plate 8 Outcrop of pseudotachylite at Yarlbrinda Hill.**

#### *2.5.1.3 Mylonite ( $L_3$ )*

At several localities, narrow (up to 3 m wide) mylonite zones are observed, derived from precursor granitoids, aplite and rhyolite dykes. North of Fyne Dam, two narrow mylonite zones occur within megacrystic gneisses of  $L_1$  and granite of  $L_2$ . The most prominent mylonite zone is approximately 3 m wide (Plate 9) and crops out approximately 50 m to the east of a narrow (~20 cm wide) mylonite zone.



**Plate 9 Outcrop of mylonite at Lakeside**

#### 2.5.1.4 Mafic dykes ( $L_4$ )

Thin (<10 m wide) dykes of fine to coarse-grained amphibolite intrude units  $L_1$  and  $L_2$ . These dykes do not crop out well, and are present as scattered float, which generally define the trend of the dykes. The rock has a characteristic dark green crystalline appearance, which in thin section displays a relict igneous texture, modified by regional metamorphism and deformation. This has resulted in the recrystallisation of precursor minerals, and the development of foliation. Mason (1998) reported that the original rock were dolerites, comprising phenocrysts of plagioclase, ?pyroxene and ?Fe-Ti oxides, within a finer groundmass, which suffered regional lower amphibolite facies metamorphism, producing the assemblage plagioclase, hornblende and opaques.

#### 2.5.1.5 Rhyolite, rhyodacite dykes ( $L_5$ )

Deformed, porphyritic rhyolite dykes intrude granite gneiss ( $L_2$ ) southwest of Childera Outstation (Plate 10). The dyke has chilled margins. The dykes similar in appearance to dykes of the Moonamby Dyke Suite ( $Ma_5$ ) which intrude the Gawler Range Volcanics, but are deformed. SHRIMP dating of zircons recorded a magmatic age of  $1679 \pm 12$  Ma (A.J. Parker, Geosurveys, pers. comm., 1997). This date provides a minimum age for the host granite and also a maximum age for deformation within the Yarlbirinda Shear Zone.





**Plate 10** Detailed view of deformed rhyolite dyke, southwest of Childera Outstation showing elongate, ribbon quartz grains and relatively undeformed feldspar grains.

South of Childera Outstation near the airstrip, a brick-red, fine-grained, spherulitic rhyolite intrudes granite and augen gneiss. The rock is not foliated and its stratigraphic position is uncertain. As it does not appear similar to nearby volcanic units of the younger Glyde Hill Volcanic Complex, it has been placed within the Tunkillia Suite.

#### *2.5.1.6 Aplite Dykes ( $L_6$ )*

North of Fyne Dam, narrow (up to 0.2 m wide) aplite dykes intrude coarse-grained augen gneiss and granite ( $L_1$  and  $L_2$ ) (Plate 11). These dykes trend north-south and dip  $73^\circ$  to the east. Approximately 1 km to the south along an east-west track and within a nearby creek, off-white, felsic crystalline rock with a moderately strong foliation occurs as scattered float. The rock comprises quartz and feldspar with minor muscovite, which defines a foliation. The fine grained nature of the rock suggests that it originated as an aplite, which was subsequently deformed and recrystallised.



**Plate 11** Narrow aplite dykes north of Lakeside.

### 2.5.2 St Peter Suite

The St Peter Suite (Flint *et al.*, 1990), defines a suite of comagmatic granitoids which crop out along the coast from Streaky Bay to Rocky Point, west of Ceduna. Flint *et al.* (1990) defined five units Lp<sub>1</sub>, Lp<sub>2</sub>, Lp<sub>3</sub>, Lp<sub>5</sub> and Lp<sub>6</sub>:

Lp<sub>1</sub> comprises pink, fine to medium-grained granite, and adamellite, grading to a medium to coarse-grained, pink to red, granite which varies from weakly to moderately well foliated.

Lp<sub>2</sub> is a series of dolerite, diorite, amphibolite and lamprophyre dykes, which intrude Lp<sub>1</sub>, Lp<sub>3</sub> and Lp<sub>5</sub>. In the Kalanbi area, a suite of ultramafic to intermediate rocks, were drilled in the search for nickel sulphides. Rock types include troctolite, olivine hypersthene gabbro, olivine gabbro and amphibolites. Purvis (1983) divided these ultramafic units into three groups;

1. cumulate metagabbros, locally rich in magnetite±apatite derived from a relatively fractionated magma (ie: tholeiitic basalt);
2. troctolite, olivine hypersthene gabbro and olivine gabbro of cumulus origin, but from a less fractionated magma than group 1; and
3. chloritic metaperidotite or metapyroxenite.

These rocks are correlated with Lp<sub>2</sub> based on similar geochemistry.

Lp<sub>3</sub> is a suite of fine to medium-grained adamellite to granodiorite dykes, which intrude Lp<sub>1</sub>. At Point Brown and Smooth Pool, some dykes show magmatic banding (Plate 12) along the margins (Berry and Flint, 1988) and other areas show zones of complex mingling between units (Plate 13). Knight (1997) reported trondhjemite at Point James, and tonalite at Cape Beaufort and Rocky Point, which are correlated with Lp<sub>3</sub> and Streaky Bay granodiorite of Dove (1997).





Plate 12 Magmatic banding at Point Brown within Lp3.



Plate 13 Complex mingling relationships of the St Peter Suite.

Lp<sub>5</sub> is a suite comprising medium-grained, porphyritic adamellite to granodiorite. Lp<sub>6</sub> intrudes all other units and comprises pink, medium-grained, porphyritic granite containing pale pink microcline phenocrysts up to 15 mm.

A sample from a granodiorite dyke from Point Brown (Lp<sub>3</sub>) was dated using single and multi-grain IDTIMS analyses of zircons (Fanning, 1997). Five of the six zircon grains analysed yielded discordant U–Pb analyses, which produced an upper concordia intercept age of 1619±15 Ma. However, one zircon grain yielded a concordant <sup>207</sup>Pb/<sup>206</sup>Pb age of 1620±4 Ma, interpreted to represent the crystallisation age of the St Peter Suite (Rankin and Flint, 1991). Knight (1997) dated a tonalite (Lp<sub>3</sub>) from Cape Beaufort using the Kobar technique and recorded a Pb–Pb zircon crystallisation age of 1608 ±8 Ma. Previous mapping on CHILDARA did not record any occurrences of St Peter Suite age rocks. However, regional mapping and geochronology during the present study has shown that the St Peter Suite is more widely distributed than previously thought.

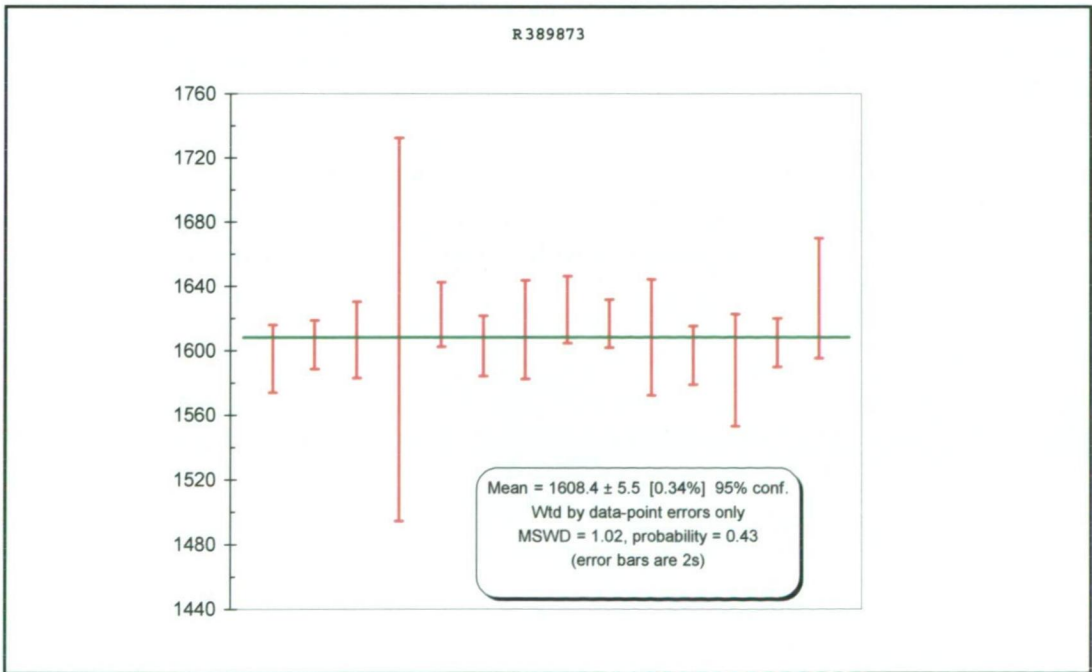


Figure 6 Mean standard weighted age for sample R389873 from northeast of Ceduna.

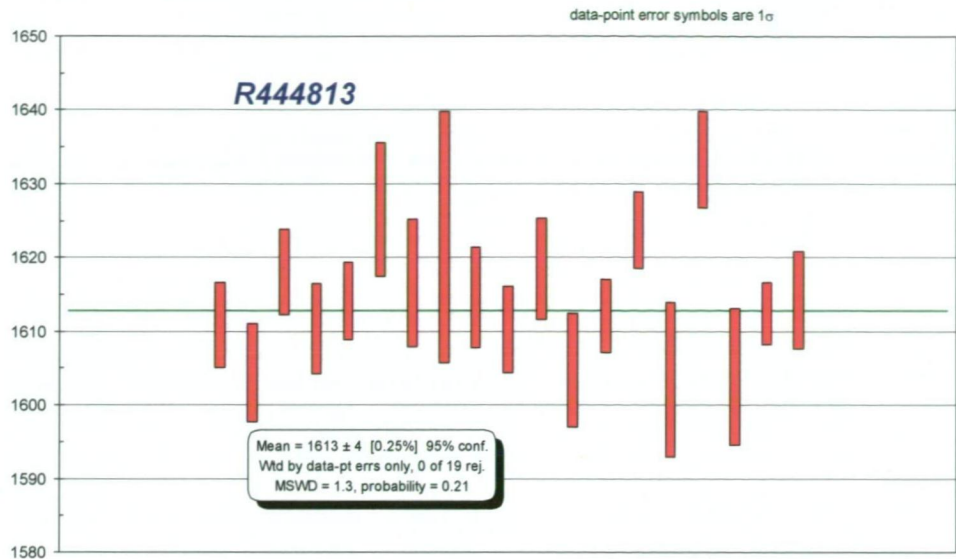


Figure 7 Mean standard weighted age for sample R444813.

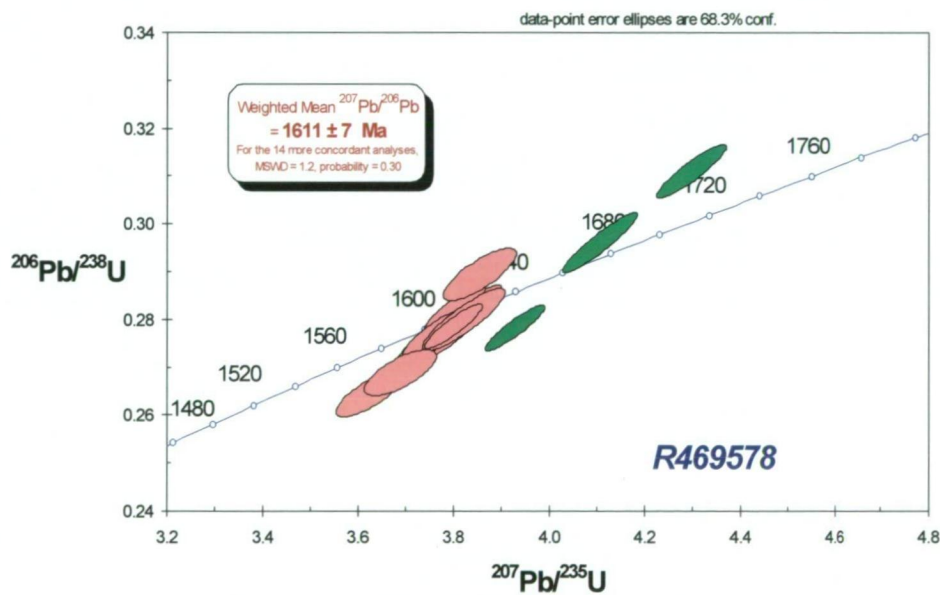
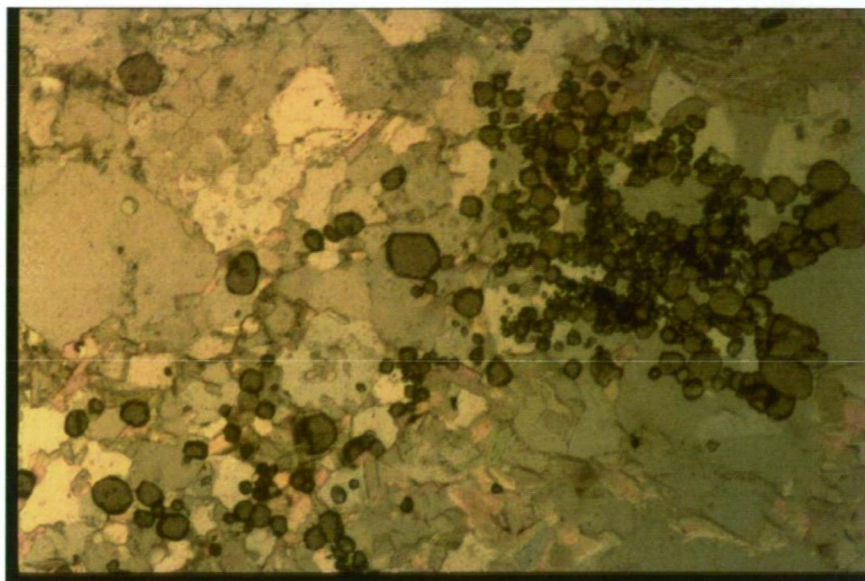


Figure 8 U-Pb concordia diagram of zircon analyses of sample R469578 from west of Kondoolka Batholith.

Northeast of Ceduna, several outcrops of fine to medium-grained, pink to pale orange adamellite to granodiorite were mapped (Lp<sub>7</sub>). Outcrops are generally poor, comprising low, isolated sheets. Sample R389873 comprised a weakly foliated hornblende–biotite granodiorite with distinctive small aggregates of magnetite–sphene–zircon–apatite, which suggest an I-type affinity (Purvis, 1998b). Multigrain analysis of zircon using SHRIMP gave a mean standard weighted age of 1608±5.5 Ma (Figure 6; Appendix B), an age similar to that reported by Knight (1997) for a tonalite from Cape Beaufort. An outcrop of deformed granodiorite from northern CHILDARA (R444813) gave a mean standard weighted age of 1613±4 Ma (Figure 7; Appendix B).



Outcrops of leucocratic granite to adamellite, containing minor Ca-rich garnet (Plate 14) were mapped near the former OTC Station northeast of Ceduna (Lp<sub>8</sub>). These rocks are strongly foliated, trending 020°, with a strong quartz fabric in which the quartz c-axes are roughly parallel to the foliation (Purvis, 1998b).



**Plate 14 Thin section of leucocratic granite from near the former OTC station, north of Ceduna showing zone of garnet grains (field of view is 0.5 mm)**

The presence of garnet suggests a possible S-type affinity, but the presence of sphene indicates sufficient activity of CaO within the melt to produce a Ca-rich garnet, which indicates an A-type affinity. The presence of rare fluorite enclosed in biotite also supports an A-type affinity (Purvis, 1998b).

Southwest of Yarlbirinda Hill, a small rockhole of pink to pale orange, medium-grained mylonitic granite gneiss (Lp<sub>9</sub>), comprising K-feldspar (45–55%), quartz (~30%), plagioclase (10%) and minor biotite was mapped. In thin section, feldspar augen are totally recrystallised and the groundmass is rich in fine-grained K-feldspar with a strong fabric. Multigrain analyses using SHRIMP gave a weighted mean  $^{207}\text{Pb}/^{206}\text{Pb}$  age of  $1611 \pm 7$  Ma, which is thought to represent the crystallisation age (Figure 8). This outcrop is part of a pluton to the southwest of the Kondoolka Batholith, which suggests that the entire pluton is part of the tectonothermal event that produced the St Peter Suite to the west. South of Yarlbirinda Hill, two low outcrops of foliated, gneissic adamellite occur. These rocks comprise porphyroblastic, K-feldspar and finer grained plagioclase crystals within a fine-grained quartzofeldspathic matrix. Webb (1978) obtained a tentative Rb–Sr date of 1640 Ma, similar to that obtained for Yarlbirinda Hill. Based on geochemistry, these are interpreted as part of the St Peter Suite.

St Francis Granite is a pale grey to pink, massive, medium grained equigranular to locally porphyritic leucogranite (Parker, 1993). The St Francis Granite is interpreted as a low-volume, high-level intrusive associated with the Nuyts Volcanics. Rankin and Flint (1989) report the St Francis Granite is highly differentiated with elevated Rb, Zr, and  $\text{Na}_2\text{O} + \text{K}_2\text{O}$ , and low  $\text{Al}_2\text{O}_3$ , CaO, Sr, P and  $\text{TiO}_2$ .

The Nuyts Volcanics are a suite of felsic volcanics, which crop out within the Nuyts Archipelago. They comprise dark grey to pink porphyritic rhyodacite to rhyolite which gave a U-Pb crystallisation ages of  $1631 \pm 3$  Ma (Cooper *et al.*, 1985) and  $1627 \pm 2$  Ma (Rankin *et al.*, 1990).

## 2.6 MESOPROTEROZOIC

### 2.6.1 Gawler Range Volcanics

The Mesoproterozoic Gawler Range Volcanics (GRV) (Thomson, 1966) are a sequence of bimodal volcanics, which crop out over an area of 25 000 km<sup>2</sup> within the central Gawler Craton (Figures 2 & 5). They comprise subaerial felsic volcanics, dominantly as lava flows, domes and dykes, with minor ashflow and ignimbrite layers.

The GRV was divided into two broad groups, the upper and lower sequences, based on structural differences (Blissett, 1986). Blissett (1986) and Blissett *et al.* (1993) defined the lower sequence as a series of moderate to steeply dipping ignimbritic dacite–rhyodacite–rhyolite units, with minor breccia and lava flows, that were erupted from localised vents within the Kokatha (Chitanilga Volcanic Complex, Branch, 1978), Lake Everard (Glyde Hill Volcanic Complex) and Paney areas. Blissett (1986) and Blissett *et al.* (1993) defined the upper sequence as a voluminous series of flat-lying to slightly dipping, porphyritic, ignimbritic, rhyodacite to dacite sheets, including the extensive Yardea Dacite.

Flint (1993) reported that the felsic units of the upper and lower sequences have similar chondritic trace-element patterns, and U–Pb zircon ages  $1591 \pm 3$  and  $1592 \pm 3$  Ma, respectively (Fanning *et al.*, 1988). This indicates that the break between the upper and lower units was geologically short and did not reflect any significant geochemical difference.

Stewart (1992) divided the GRV into a developmental phase and a mature phase, based upon geochemical and isotopic differences. The developmental phase comprises basalts to high silica rhyolites, erupted from localised centres including Lake Everard, Kokatha, Tarcoola and Toondoolya Bluff (Stewart, 1992). The mature phase is chemically and isotopically more homogeneous than the developmental phase, and comprises the voluminous Yardea Dacite, Eucarro Dacite and Nonning Rhyodacite (Stewart, 1992).

Blissett (1975) defined the Glyde Hill Complex as a separate volcanic package located near Lake Everard and centred near Glyde Hill Outstation. The Glyde Hill Volcanic Complex comprises a series of dacite, rhyodacite and rhyolite units erupted from a volcanic centre not related to the Chitanilga Volcanic Complex (Branch, 1978) to the north or the main Yardea Dacite unit to the east. Giles (1977) reported that the volcanic pile in the Lake Everard area comprises a sequence of conformable, strongly welded crystal and/or vitric and/or lithic tuffs of ashflow origin, lava dome, localised lava flows and shallow intrusives in the form of plugs and dykes. The volcanics are entirely subaerial and there is evidence for at least one major period of erosion. The Yantea Rhyodacite, in places occupies palaeo-valleys within older units (Giles, 1980).

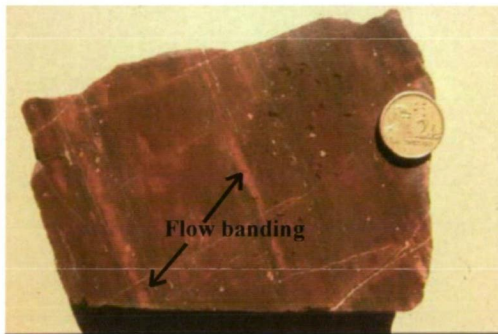


The Glyde Hill Volcanic Complex represents a sequence of volcanics erupted from a discrete centre located in the Lake Everard area, but geochemical studies suggest that the Glyde Hill Volcanic Complex, together with the Chitanilga Volcanic Complex, and the Toondulya Bluff sequence to the south, have a common petrogenesis (Flint, 1993).

Giles (1977) defined eleven units, which comprise the Glyde Hill Volcanic Complex; these unit names will be used to describe the stratigraphy of the Lake Everard area.

#### 2.6.1.1 Childera Dacite (Myc)

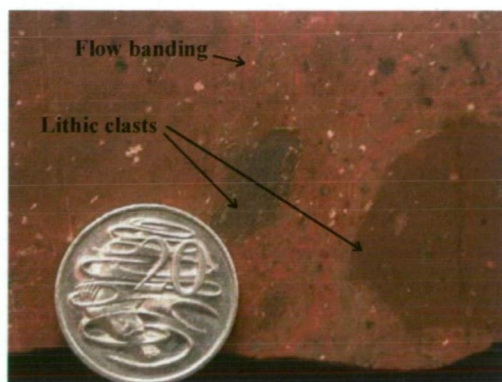
The base of the Glyde Hill sequence is the Childera Dacite (Giles, 1977) which is at least 200 m thick; the base is covered by alluvium. The basal section comprises a dark grey basaltic andesite, which crops out north of Childera Outstation and grades into a massive, purplish red to red-brown dacite.



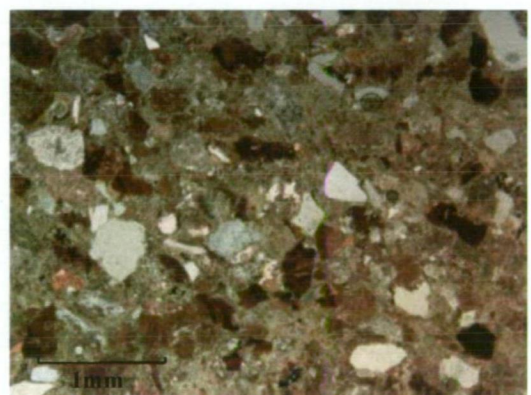
**Plate 15** Hand specimen of Childera Dacite showing flow banding and the generally phenocryst poor nature.



**Plate 17** Thin sediment layer showing block faulting around compaction and water escape structures. (width of view is 4 cm).



**Plate 16** Hand specimen of Childera Dacite showing fine flow banding and coarse lithic clasts.



**Plate 18** Thin section showing detail of poorly sorted, angular fragments from Plate 17.





**Plate 19 Thin epiclastic unit within Childera Dacite showing prominent graded bedding.**

The Childera Dacite is characteristically phenocryst poor (~2–10%) with phenocrysts of plagioclase and less commonly clinopyroxene and pyroxene (Plate 15). The Childera Dacite is aphyric, massive to partly flow banded (Plate 16), comprising a series of lava flows, separated by localised epiclastic layers (Plates 17–19). The basal basaltic andesite is massive, dark grey to black, comprising a fine-grained mosaic of plagioclase microlites with rare opaques and chlorite (Giles, 1980). This grades into the more widespread red-brown dacite unit.

At one location, the Childera Dacite contains coarse lithic clasts (Plate 16) and fine wispy layering (pseudo-fiamme texture). In thin section, this is observed as flow layering with no evidence of fiamme. The coarse lithic fragments most likely represent accidental lithics, hence suggesting the Childera Dacite is a lava flow.

Thin epiclastic layers deposited in water are found separating lava flows (Plates 17–19). These sediments comprise alternating layers of alkali-feldspar-poor and alkali feldspar ± plagioclase-rich sediments with abundant pumice fragments. These layers are generally thin (~20–30 cm), but one layer is ~1–1.5 m thick and shows pronounced slump structures including box-folds (Plate 17). Plate 17 shows a prominent water escape structure and is characterised by poorly sorted, angular grains (Plate 18), indicating deposition from a high-energy source, most likely a fluvial system depositing sediments due to decrease in flow. The angularity of these sediments, suggest they have not travelled far from source. The dip of these layers varies from moderate (35° to the south) to shallow (10° to the south). The difference in dip may reflect a varied pre-existing topography. These sediments are localised and are evidence for intermittent reworking of volcanoclastic material including pumice within small lakes and river systems during a hiatus in volcanic activity.

The basal dacite above the sediment layers is generally highly vesicular, hence the lava was gas rich. Vesicles are infilled with quartz and chlorite. In thin section, the Childera Dacite shows irregular flow layering with clay present in some layers. The groundmass comprises microcrystalline, red, K-feldspar with minor, subhedral to euhedral phenocrysts of albite to sericite altered plagioclase grains up to 4 mm in length. Rare ferromagnesian phenocrysts, possibly originally hornblende, are present, but are altered to chlorite, epidote and sericite. Rounded and resorbed quartz phenocrysts up to 1 mm in diameter are rare.

Giles (1977, 1980) reported the Childera Dacite represents several ash-flow tuff sheets erupted relatively rapidly. However, the presence of patchy flow layering, rarity of lithic fragments, lack of broken phenocrysts, and homogeneity of the unit over large distance, indicate that the Childera Dacite is most likely a high temperature, low

The geology and geochemistry of granitoids in the CHILDARA region, western Gawler Craton, South Australia: implications for the Proterozoic tectonic history of the western Gawler Craton and the development of lode-style gold mineralisation at Tunkillia.



viscosity lava. Sediment layers, representing breaks in lava flows comprise a variety of reworked volcanoclastic particles including pumice. The presence of pumice suggests an air-fall component, but the source of the pumice is unknown and is interpreted to be located some distance away. Textures including slump structures and water escape structures (Plate 17) indicate deposition within water, most probably small lakes and rivers developed between flows.

#### 2.6.1.2 Mangaroongah Dacite (Mym)

Conformably overlying the Childera Dacite is the Mangaroongah Dacite. The Mangaroongah Dacite ranges in composition from basaltic andesite (56.7 wt% SiO<sub>2</sub>) to porphyritic red-brown dacite (69.2 wt % SiO<sub>2</sub>).



**Plate 20** Hand specimen of Mangaroongah Dacite showing characteristic red feldspar phenocrysts.

The Mangaroongah Dacite comprises a mixed phenocryst population including fine to coarse-grained K-feldspar, unaltered plagioclase locally rimmed by K-feldspar, reddish albite to sericite altered euhedral plagioclase phenocrysts and extremely resorbed plagioclase phenocrysts (Plate 20). The groundmass comprises randomly oriented albitised plagioclase microlites within a mass of microcrystalline, reddened, K-feldspar with minor chlorite and magnetite. The upper zones of flows are vesicular, with vesicles infilled with chlorite, epidote and quartz.

Rare outcrops contain elongated vesicles, which represent flow directions. Northeast of Childera Outstation, vesicles strike 150-160° and dip 45° to the east. This outcrop also contains blocky peperite and hyaloclasite (Plate 21 & 22), which indicates contemporaneous volcanism and sedimentation (Busby-Spera and White, 1987; Hanson and Schweickert, 1982). Sediments were possibly deposited within a restricted lacustrine environment.

The Mangaroongah Dacite is clearly distinguishable from the Childera Dacite in hand sample by increase in phenocryst abundance (up to 15-20%). Giles (1977, 1980) reported the Mangaroongah Dacite is a strongly welded, crystal-vitric tuff of ash flow origin, comprising several restricted cooling units. However, the presence of flow aligned elongated vesicles, peperite and the absence of lithic clasts indicate that the Mangaroongah Dacite is most likely a silicic lava.





**Plate 21** General view of outcrop of Mangaroongah Dacite containing blocky peperite and hyaloclastite.



**Plate 22** Detailed view of hyaloclastite showing reddish dacite and purple sediments.

#### 2.6.1.3 Arburee Rhyolite (*Mya*)

The Arburee Rhyolite conformably overlies and intrudes the Mangaroongah Dacite, and comprises porphyritic rhyolite, which is easily recognisable in the field by its characteristic orange weathering colour. Unweathered samples are purple – grey in colour, and contain coarse-grained, euhedral K-feldspar, medium-grained quartz phenocrysts, altered plagioclase and minor pyroxene.

Blissett (1975, 1977, 1980, 1985) included the Arburee Rhyolite within the Wheepool Rhyolite, which crops out north of Lake Everard Homestead. However, Giles (1977, 1980) demonstrated that geochemically, petrographically and stratigraphically, the Arburee Rhyolite is a localised rhyolitic flow and not related to the Wheepool Rhyolite.

Giles (1977, 1980) interpreted the Arburee Rhyolite as a lava dome produced by a series of lava flows. The linear nature of outcrop, and the viscosity of acid lavas indicate that the Arburee Rhyolite was possibly erupted from a linear, eastwest trending fissure (Giles, 1977).

#### 2.6.1.4 Karkulta Rhyolite (*Myk*)

Conformably overlying the Mangaroongah Dacite, is a small/areally limited porphyritic rhyolite, flow banded rhyolite and rhyolitic breccia referred to by Giles (1977) as the Karkulta Rhyolite. Giles (1980) reports that the Karkulta Rhyolite occurs at the same stratigraphic level as the Arburee Rhyolite, but contains biotite associated with plagioclase phenocrysts. Giles (1980) suggests the rhyolite breccia represents a site of erosion of a former lava dome, but field evidence including the monomict nature of clasts and the apparent jigsaw fit of the clasts suggest an autoclastic breccia (Plate 23). The Southern margin of this unit is located within a creek and shows evidence of later sedimentation to produce a volcanoclastic breccia.





**Plate 23 Outcrop of Karkulta Rhyolite showing monomict autoclastic breccia.**

#### *2.6.1.5 Bunburn Dacite (Myb)*

The Bunburn Dacite (Giles, 1977) is a laterally extensive unit, trending roughly eastwest. The Bunburn Dacite is between 30-100 m thick and ranges in composition from basaltic andesite (58.8 wt %  $\text{SiO}_2$ ) to rhyodacite (69 wt %  $\text{SiO}_2$ ). The Bunburn Dacite is characteristically phenocryst poor, with rare, fine to medium-grained, K-feldspar phenocrysts, within a devitrified groundmass, with microlitic to microlitic-spherulitic texture defined by feldspar microlites (Giles, 1977, 1980).

The Bunburn Dacite shows localised layering from millimetre to centimetre scale. A outcrop along southern Lake Everard shows layering dipping steeply ( $62^\circ$ ) to the south-southeast. The steepness of the dip may indicate proximity to a vent buried under lake sediments or a possible ramp structure.

The Bunburn Dacite contains prominent perlite which range in size from <1 cm diameter (Plate 25) up to 50 cm diameter (Plate 26) which are termed macro-perlite. The perlite indicates that the Bunburn Dacite was a glass rich lava. In thin section, the Bunburn Dacite shows prominent perlitic textures (Plates 26 & 27); the groundmass now comprises well oriented microlites of alkali feldspar. Some parts of the outcrop show prominent radial fractures (Plate 28).

Yamagishi and Goto (1992) report macro-perlite from subaqueous rhyolite lavas from Southern Hokkaido, Japan, up to 6 cm in diameter which they called macro-perlite. Yamagishi and Goto (1992) suggest the macro-perlite resulted from thermal stress fracturing due to primary quenching of water and not hydration. The size range of perlitic fractures seen at the outcrop along the edge of Lake Everard may be the result of initial joint spacing within the rock produced by hydration of original glass, with macro-perlite formed in zones of widely spaced joints. Macro-perlite was only observed at this one outcrop, with finer perlite (generally <1 cm in diameter) observed at other outcrops. This may suggest that the glassy lava cooled more rapidly at this location due to the presence of surface water.

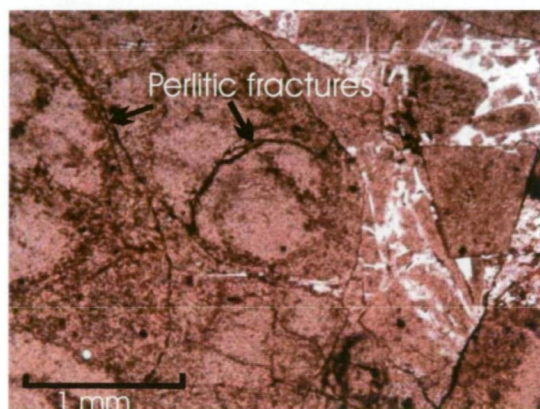




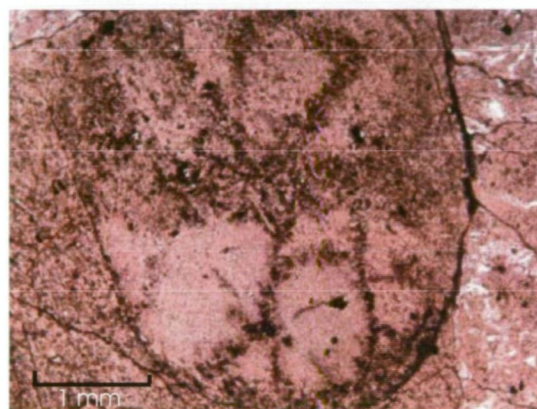
**Plate 24** Detailed view of prominent layering within the Bunburn Dacite with patches of almost spherical perlite



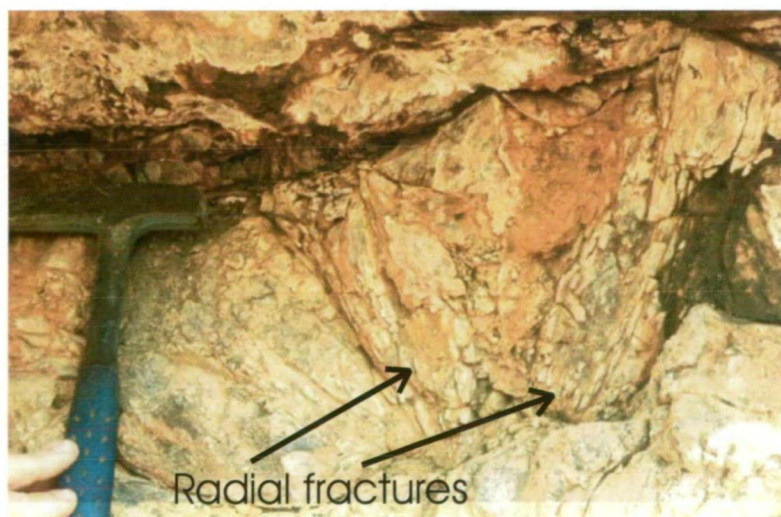
**Plate 25** Outcrop of weathered macro perlite.



**Plate 26** Thin section showing perlitic fractures within basaltic andesite (Bunburn Dacite)



**Plate 27** Detailed view of thin section showing large spherical perlite.



**Plate 28** Outcrop along edge of Lake Everard showing prominent radial fractures within macro-perlitic Bunburn Dacite.

Giles (1980) interpreted the Bunburn Dacite as a simple cooling unit of ash-flow origin, with zones of autobrecciation near the top due to the effects of gas streaming.

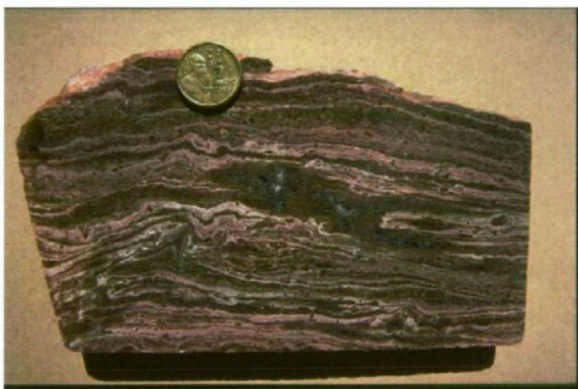


However, the presence of prominent layering, macro-perlite and absence of lithic fragments favour a silicic lava origin.

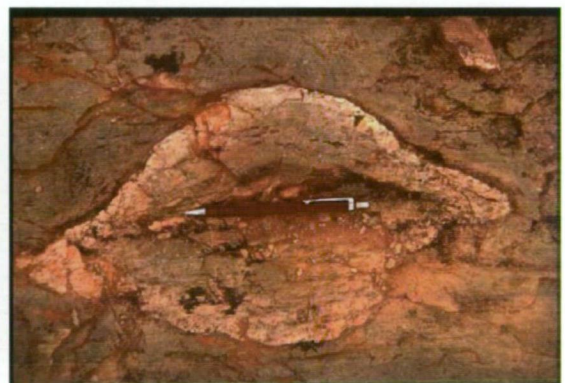
#### 2.6.1.6 Baldry Rhyolite (Myl)

The Baldry Rhyolite outcrops predominantly on GAIRDNER and was included within the Wheepool Rhyolite by Blissett (1980). However, Giles (1977, 1980) interpreted the Baldry Rhyolite as a local rhyolite unit, which overlies the Bunburn Dacite.

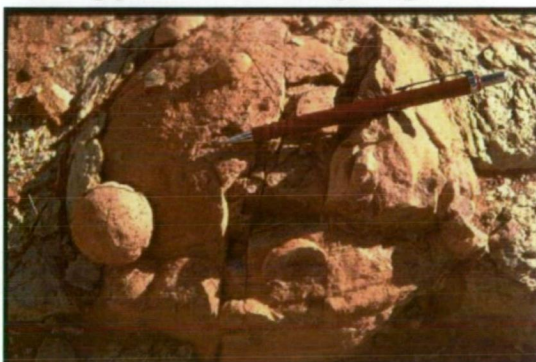
The Baldry Rhyolite comprises white to off-white, rhyolite containing medium-grained quartz phenocrysts (Plate 29) with flattened lithic and pumice fragments and abundant spherulites and lithophysae. Giles (1980) reported the Baldry Rhyolite retains the original vitroclastic texture, which indicates a pyroclastic origin. Giles (1977) called this unit a rheoignimbrite due to the semi-continuous flow banding indicative of flowage during welding. Outcrops along the edge of a lake east of Apostles Tank contain numerous spherulites and lithophysae, within a densely welded rhyolitic ignimbrite (Plates 30 & 31).



**Plate 29 Specimen of Baldry Rhyolite showing prominent flow layering.**



**Plate 30 Large lithophysae showing elongation due to flow**



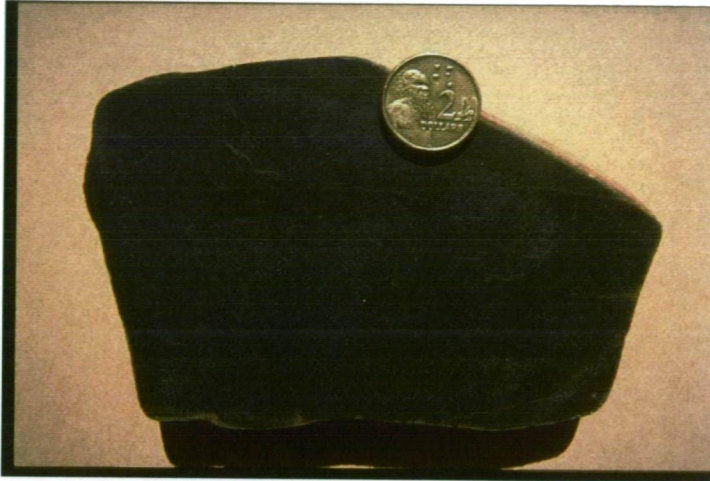
**Plate 31 Large lithophysae ('thunder egg') with smaller lithophysae on the surface.**

#### 2.6.1.7 Nuckulla Basalt (Myn)

The Nuckulla Basalt (Giles, 1977), is a massive, dark green to grey, fine-grained basaltic lava flow which crops out over a limited area near Nuckulla Well and Dam. The Nuckulla Basalt conformably overlies the Bunburn Dacite, but the contact is marked by approximately 3 m of sediment. The basalt is plagioclase-rich with albite to



sericite altered plagioclase laths to 0.3 mm in length with minor, fine-grained (<0.1 mm) clinopyroxene (Plate 32).



**Plate 32** Hand specimen of Nuckulla Basalt showing phenocryst poor nature of this unit.



**Plate 33** Thin sediment layer which occurs at top of Nuckulla Basalt.

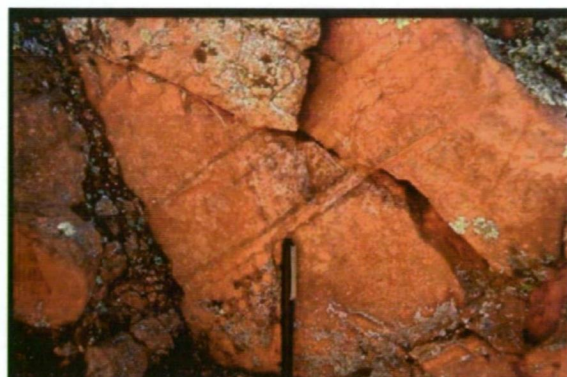
West of Nuckulla Tank, a thin sediment layer overlies the Nuckulla Basalt (Plate 33). Giles (1980) interpreted this layer as an air-fall tuff, but a volcanoclastic origin is favoured.

#### 2.6.1.8 Yantea Rhyodacite (Myy)

The Yantea Rhyodacite (Giles, 1977) disconformably overlies several older volcanic units and comprises massive, brick red, porphyritic rhyodacite grading to dacite, containing coarse-grained phenocrysts of K-feldspar and chlorite (after clinopyroxene) within a devitrified matrix (Giles, 1977, 1980). The brick red colour is due to limonite staining within the groundmass (Giles, 1977).



Prominent flow layering was observed (Plate 34) with moderate dips to the west, and several layers up to 3 m thick of spherulites were observed throughout the Yantea Rhyodacite (Plate 35).



**Plate 34** Prominent flow layering dipping to the west within the Yantea Rhyodacite.



**Plate 35** Spherulites within the Yantea Rhyodacite.

Giles (1980) reported the Yantea Rhyodacite is up to 150 m thick, and composed of at least four, simple cooling units comprising welded ash-flow tuffs separated by thin non-welded tuffs and lapilli tuffs. However, the lack of lithic fragments, presence of flow banding and the homogeneous porphyritic nature of the rock suggest a silicic lava origin.

#### *2.6.1.9 Whyeela Dacite (Myh)*

The Whyeela Dacite is the youngest extrusive unit in the Glyde Hill Volcanic Complex (Giles, 1977), and conformably overlies the Yantea Rhyodacite. The Whyeela Dacite is up to 100 m thick and is confined to a semicircular structure ~8 km across located on GAIRDNER.

#### *2.6.1.10 Moonamby Dyke Suite (Myz)*

The Moonamby Dyke Suite (Giles, 1977) are a series of red, highly porphyritic rhyolite and rhyodacite dykes (Plate 36) up to 100 m wide and up to 18 km long, which intrude the Glyde Hill Volcanic Complex. The dykes trend north to northeast, branching and become thinner northwards. They all have chilled margins. The Moonamby Dyke Suite are possibly related to intrusion of the Hiltaba Suite, as several dykes contain plugs of granite similar in appearance to nearby outcrops of Hiltaba Suite granite. The dykes only occur along the western margin of the Lake Everard Volcanic Complex.

The dykes are slightly variable but have a porphyritic appearance and are easily recognisable in the field by their characteristic rounded “tor” appearance, compared to the highly jointed, “blocky” volcanics.

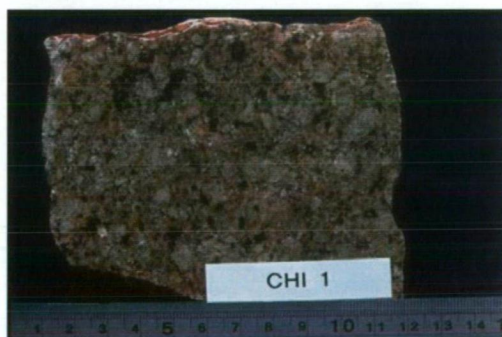




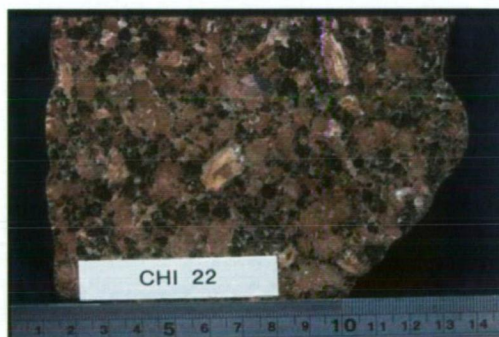
**Plate 36** Hand specimen of Moonamby Dyke Suite showing characteristic porphyritic nature

### 2.6.2 Hiltaba Suite (Mh)

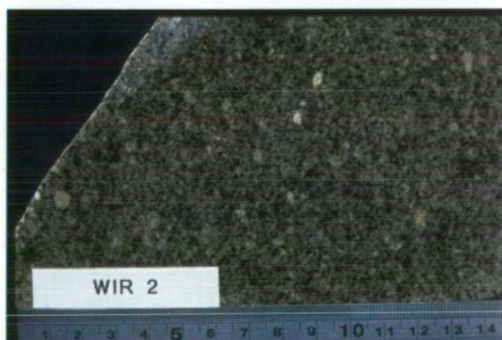
The Hiltaba Suite is a variable suite of massive, granitoids found on the Gawler Craton, which range in composition from granite to granodiorite. Texturally, the Hiltaba Suite is variable, ranging from high-level, sub-volcanic, porphyritic granite (Plate 37), equigranular, medium- to coarse-grained granite (Plate 38) to microgranite (Plate 39). On CHILDARA, there are no observable contacts between the Hiltaba Suite and the Gawler Range Volcanics, but the intrusive nature is observed on YARDEA, GAIRDER and STREAKY BAY. Hiltaba Suite granite crops out on eastern CHILDARA, and is characteristically a red-pink, fine to coarse grained, massive, K-feldspar dominant granite. In the Kondoolka area, the Hiltaba Suite outcrops as large inselbergs (Plate 40). The Kondoolka Batholith is a large zoned, composite intrusive, which shows considerable textural and geochemical variation.



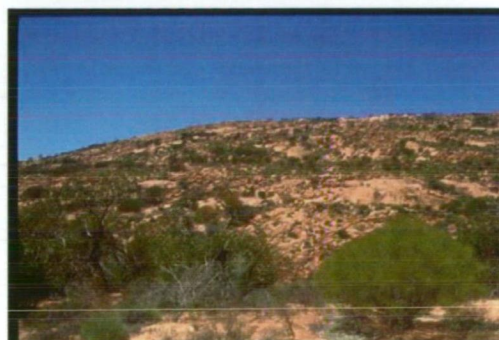
**Plate 37** Hand specimen of porphyritic Hiltaba Suite granite.



**Plate 38** Hand specimen of coarse grained Hiltaba Suite granite.

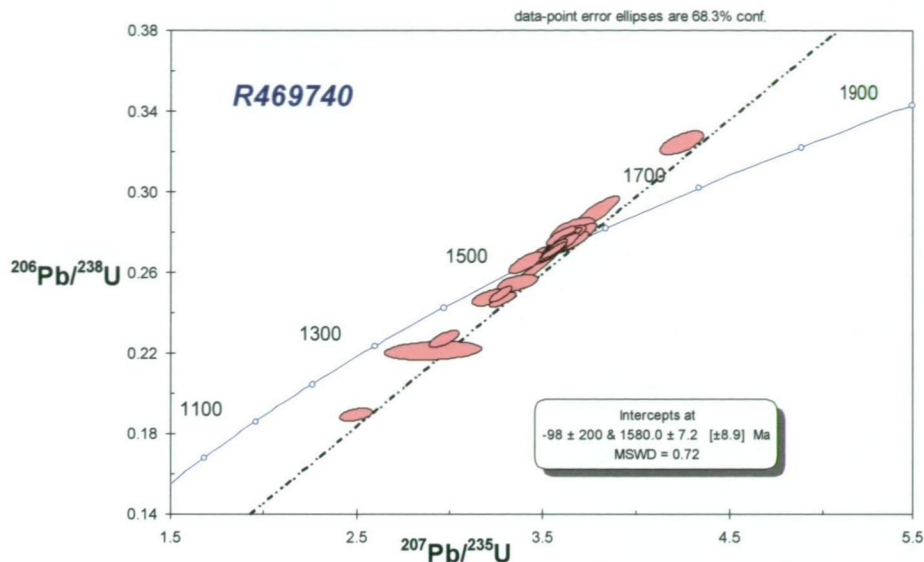


**Plate 39** Hand specimen of Hiltaba Suite microgranite



**Plate 40** Large outcrop of Hiltaba Suite granite from the Kondoolka Batholith.

The geology and geochemistry of granitoids in the CHILDARA region, western Gawler Craton, South Australia: implications for the Proterozoic tectonic history of the western Gawler Craton and the development of lode-style gold mineralisation at Tunkillia.



**Figure 9** U-Pb concordia plot for sample from Kondoolka Batholith (see Appendix B for original data).

Multigrain zircon analysis of massive, coarse grained granite within the Kondoolka Batholith gave a crystallisation age of  $1580 \pm 7$  Ma (Figure 9; Appendix B), which helps to constrain the deformation within the Yarlbrinda Shear Zone.

On Lake Everard Pastoral Lease, numerous outcrops of Hiltaba Suite granite are located west of Childera Outstation. Several outcrops previously mapped as Hiltaba Suite have been incorporated within the Tunkillia Suite based on structure and limited geochronology. Outcrops in the Meelera Rockhole area contain coarse grained, equigranular and porphyritic granite phases, which suggests that these are two slightly immiscible variants of the same magma.

The Hiltaba Suite is generally massive with little or no evidence of deformation. Multigrain zircon analysis of a grey, foliated plagioclase–quartz–K-feldspar–biotite granodiorite on northern CHILDARA, gave an age of  $1592 \pm 11$  Ma, with some inheritance of older zircons at  $1714 \pm 12$  Ma. The  $1592 \pm 11$  Ma age is interpreted as the represent crystallisation age, which implies that foliation development was either syn–emplacement or post–emplacement. This granodiorite is located within the Yerda Shear Zone, hence helps to constrain the timing of deformation.

Granite at Arcoordaby Rockhole is coarse grained with K-feldspar grains up to 25 mm in length and has a prominent foliation trending  $087^\circ$  defined by biotite and mafic enclaves (Plate 41). A sample from Arcoordaby Rockhole was dated at  $1578 \pm 12$  Ma using the Kober Pb-Pb method (Stewart and Foden, 2001).





**Plate 41** Coarse grained Hiltaba Suite granite from Arcoordaby Rockhole.

The Kondoolka Batholith crosscuts the Yarlbrinda Shear Zone, but shows no evidence of witnessing the foliation development on northern CHILDARA. The accepted time range for the Hiltaba Suite is 1595-1575 Ma and this suggests that deformation occurred within that interval, but post emplacement of the Kondoolka Batholith at ~1580 Ma.

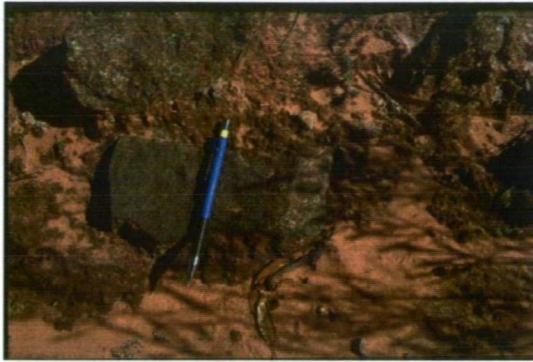
#### 2.6.2.1 Gabbro ( $Mh_6$ )

South of Childera Outstation, dark green to grey, coarse-grained anorthosite to gabbroic anorthosite crops out (Plate 42). The rock contains coarse-grained, grey, plagioclase, which ranges in size from 1-7 mm in length, and dark green patches of chlorite, possibly after hornblende or pyroxene (Plate 43). A weak layering is evident in outcrop, but no tectonic foliation was observed which suggests that the rock was intruded post shearing within the Yarlbrinda Shear Zone.



**Plate 42** General view of low, scattered outcrop of gabbro/anorthosite south of Childera Outstation.





**Plate 43 Detailed view of gabbro from above outcrop.**

The gabbro/anorthosite body forms a prominent magnetic feature on the northern margin of the Kondoolka Batholith. However, the rock contains accessory magnetite and has a low magnetic susceptibility, which suggests the magnetic source is located below the surface expression, and may represent a layered complex.

Rankin and Flint (1991) report that gabbroic plugs on St Peter Island differ geochemically from diorite/amphibolite dykes of the St Peter Suite and field relationships suggest that these gabbroic plugs are younger than the Nuyts Volcanics. The gabbroic plugs on St Peter Island are possibly similar to gabbros drilled by Mines and Energy on STREAKY BAY (Whitten, 1963). The latter comprise plagioclase, pyroxene and olivine with minor magnetite, pyrite, ilmenite and apatite (Rankin and Flint, 1991) with no evidence of deformation.

### 2.6.3 Munjeela Granite (M-u)

The Munjeela Granite (new name) comprises medium- to coarse-grained grey, equigranular, muscovite–biotite±garnet granite. The Munjeela Granite does not crop out on CHILDARA and is defined from exposures on FOWLER (Munjeela Rockhole) and NUYTS (Point Bell and Point Sinclair). Granite at Munjeela Rockhole (Plate 44) comprises massive, muscovite–biotite syenogranite to adamellite with some very coarse microcline crystals (Plate 45) and coarse muscovite to 8 mm in grain size. Part of the outcrop contains accessory garnet up to 2 mm in diameter.

Granite from Point Sinclair is similar to Munjeela Rockhole, but granite at Point Bell is foliated with feldspar augen elongate parallel to the foliation, which strikes 030°–060°. The presence of muscovite and garnet suggests an S-type granite. Granite from Munjeela Rockhole has an Sm–Nd depleted mantle model age of ~2120 Ma (K Stewart, University of Adelaide, pers. comm., 1998). SHRIMP dating of zircons was attempted, but the zircon grains are ragged and 3 analyses produced a range of discordant results between 1560 Ma and 1900 Ma.

Electron microprobe dating of monazite grains was undertaken at CODES using the technique reported in Montel *et al.* (1996). Seventeen spots were analysed, and fourteen gave a weighted mean age of  $1562 \pm 15$  Ma (Appendix B). The 3 remaining grains produced a range of ages between 1145 to 1457 Ma, which Berry (CODES, pers. comm., 2001) interprets as reflecting variable resetting to an age possibly about 1200 Ma. Berry (CODES, pers. comm., 2001) reports these 3 grains have lower Y and HREE and higher MREE than the main group supporting a different origin.





**Plate 44** General view of Munjeela Rockhole.



**Plate 45** Detailed view showing coarse grained microcline crystal.

Rb-Sr analyses of five samples from Point Bell (5533 RS 65-69) produced an isochron age of  $1507 \pm 29$  Ma (Webb *et al.*, 1986). Rb-Sr analyses of one sample from Point Sinclair produced an age of 1535 Ma assuming an initial  $^{87}\text{Sr}/^{86}\text{Sr}$  ratio of 0.705 (Webb *et al.*, 1986).

The Munjeela Granite has a characteristic smooth, low magnetic intensity appearance on regional aeromagnetic data and two small plutons are interpreted to have intruded along the Koonibba Fault on CHILDARA (see Plan 2).

#### **2.6.4 Quartz Blows**

On northern CHILDARA, massive quartz blows which form a prominent topographic high, crop out at New Year Hill. The quartz blows are up to 300 m in length and up to 100 m wide, but are mostly narrow, linear ridges of milky white quartz, which are oriented predominantly north-south. The quartz blows are subvertical to vertical, but west of New Year Hill quartz is folded and sheared (Plate 46). The quartz blows indicate possible eastwest extension and may be related to movement on the Yerda Shear Zone to the south.



**Plate 46** Detailed view of rodded quartz from west of New Year Hill.

## Chapter 3 Geochemistry

### 3.1 Introduction

Basement geology on CHILDARA is dominated by granitoids, which range in composition from granodiorite, monzogranite, syenogranite, tonalite, S-type two mica-garnet granite to granite (*senso stricto*). Regional mapping and limited U-Pb geochronology has outlined five periods of granite magmatism:

1. Archaean to early Palaeoproterozoic Glenloth Granite (2440 Ma);
2. Tunkillia Suite and equivalents (1690-1670 Ma);
3. St Peter Suite (1630-1608 Ma);
4. Gawler Range Volcanics (1592 Ma)/Hiltaba Suite granite (1595-1575 Ma); and
5. S-type, two mica  $\pm$  garnet granite - Munjeela Granite (~1560 Ma).

This chapter will present geochemical data for samples collected during field mapping, combined with historical data for the five groups outlined above. As granite represents the most voluminous component of the western Gawler Craton, any tectonic model must consider the granite geochemical evidence.

#### 3.1.1 Constraints on the data

All samples collected during regional mapping were assayed for a standard suite of oxides and elements, including trace elements and rare earth elements (REE), at Amdel Laboratories, Adelaide. Whole rock analyses of major oxides were by IC4E (Induction Coupled Plasma) and trace elements assayed using IC4M. REE were assayed using IC4R. Au, Pt and Pd were assayed by fire assay (FA3) and measured by atomic absorption analyses. Some samples gave erratic REE patterns due to analyses being below detection limits, these data were discarded.

Unfortunately, most of the samples from the PIRSA western Gawler Craton data set do not contain a full range of whole rock, trace and rare earth element data. Selected sample analyses from Dove (1997) and Knight (1997) were incorporated in the data set for the St Peter Suite.

Geochemical analyses for all samples are presented in Appendix A.

#### 3.1.2 Granite classification

Numerous classification schemes for granitoids exist within the literature, and the reader is referred to Pitcher (1987) and Barbarin (1990) for further detail. This chapter will focus on the geochemistry of granitoids from the western Gawler Craton, using major, trace and rare earth elements.

Chappell and White (1974) categorised granites from the Lachlan Fold Belt as S-types (sedimentary protoliths) or I-types (igneous protoliths). These terms were further modified to S-(supracrustal) and I-(intracrustal) types (Chappell and White, 1983).

Collins *et al.* (1982) further subdivided S- and I-types to include A-types, which are derived from source areas which already had a granite melt removed. Whalen *et al.* (1987) report that A-type granites are characterised by high  $\text{SiO}_2$ ,  $\text{Na}_2\text{O} + \text{K}_2\text{O}$ ,  $\text{Fe/Mg}$ ,  $\text{F}$ ,  $\text{Zr}$ ,  $\text{Nb}$ ,  $\text{Ga}$ ,  $\text{Sn}$ ,  $\text{Y}$  and REE (except  $\text{Eu}$ ) contents, and low  $\text{CaO}$ ,  $\text{Ba}$  and  $\text{Sr}$ . Whalen *et al.* (1987) suggested that plotting  $\text{Ga/Al}$  versus specific major and trace elements clearly distinguishes A-type granites from S- and I-types. Wyborn (2001) reports that discriminant diagrams developed by Eby (1990) for Phanerozoic granites do not work for Proterozoic granites, because they are enriched in  $\text{Zr}$ ,  $\text{Nb}$ ,  $\text{La}$ ,  $\text{Ce}$  and  $\text{Y}$  relative to Phanerozoic granites.  $\text{Ga/Al}$  plots will be used only to show relative differences between granitoid units on CHILDARA.

White (1979) and Pitcher (1982) defined M-type granites as those derived from melting of subducted oceanic crust or overlying mantle. Chappell and Stephens (1988) further refined the definition of M-types to consist of mafic diorite, quartz diorites and gabbros, which have similar geochemistry to andesitic magmas (Wyborn, 2001). Chappell and Stephens (1988) further subdivided I-type granites into I-(tonalitic) types and I-(granodioritic) types.

Zen (1986) proposed using the alumina saturation index (ASI) to differentiate the more mafic granites into S- and I-types. ASI is  $(\text{mol. Al}_2\text{O}_3/\text{CaO} - 3.3 \text{ P}_2\text{O}_5 + \text{K}_2\text{O} + \text{Na}_2\text{O})$ , with more mafic I-type granites recording values  $<1.1$ . However, ASI has problems with altered samples, and mafic magnetite and hornblende bearing I-type granites, which become more peraluminous with increasing  $\text{SiO}_2$  content (Wyborn, 1993). Wyborn (1993) reports that ASI is unreliable for S-type granites derived from immature sediments, which produce ASI values  $<1.1$ .

El Bouseily and El Sokkary (1975) used elements  $\text{Rb}$ ,  $\text{Ba}$  and  $\text{Sr}$  to trace differentiation trends in granites from quartz diorites, granodiorites, normal granites, strongly differentiated granites and a group of anomalous granites. The basis for the ternary plot is that the  $\text{Ba/Sr}$  ratio increases with differentiation and the  $\text{Ba/Rb}$  ratio decreases with differentiation (El Bouseily and El Sokkary, 1975).

O'Connor (1965) used molecular normative  $\text{Ab-An-Or}$  ternary plots to classify felsic granitoids, based on major element chemistry. The  $\text{Ab-An-Or}$  plot and fields, was further modified by Barker (1979).

Wyborn *et al.* (1992) subdivided Australian Proterozoic granites into 5 groups based on  $\text{Sr}$  and  $\text{Y}$  contents:

1. I-type,  $\text{Sr}$ -depleted,  $\text{Y}$ -undepleted, restite dominated;
2. I-type,  $\text{Sr}$ -depleted,  $\text{Y}$ -undepleted, fractionated, low in incompatible elements;
3. I-type,  $\text{Sr}$ -depleted,  $\text{Y}$ -undepleted, enriched in incompatible elements;
4. I-type,  $\text{Sr}$ -undepleted,  $\text{Y}$ -depleted; and
5. S-type,  $\text{Sr}$ -depleted,  $\text{Y}$ -undepleted.

The  $\text{Sr}$ -depleted,  $\text{Y}$ -undepleted patterns are thought to indicate source regions that contained plagioclase, but not garnet. This is used to infer the depth of source, with garnet source rocks being indicative of depths  $>45$  km (Wyborn *et al.*, 1992).

Diagrams used in this section include;

- Harker diagrams of major and trace elements versus SiO<sub>2</sub>;
- Streckeisen (1976) modal granite classification;
- Molar CaO-Na<sub>2</sub>O-K<sub>2</sub>O diagrams (Barker, 1979);
- Aluminium Saturation Index (Zen, 1986);
- Rb-Ba-Sr ternary plot (El Bouseily and El Sökkary, 1975);
- Ga/Al plots (Whalen *et al.*, 1987; Eby, 1990);
- Multi-element primordial mantle normalised spidergrams (primordial mantle abundances are from Sun and McDonough, 1989); and
- Chondrite normalised REE spidergrams (chondritic normalising values are from Nakamura, 1974 and Evensen *et al.*, 1978).

These diagrams are used to classify the five main granitoid phases within the CHILDARA region. The tectonic significance of each group is then discussed.

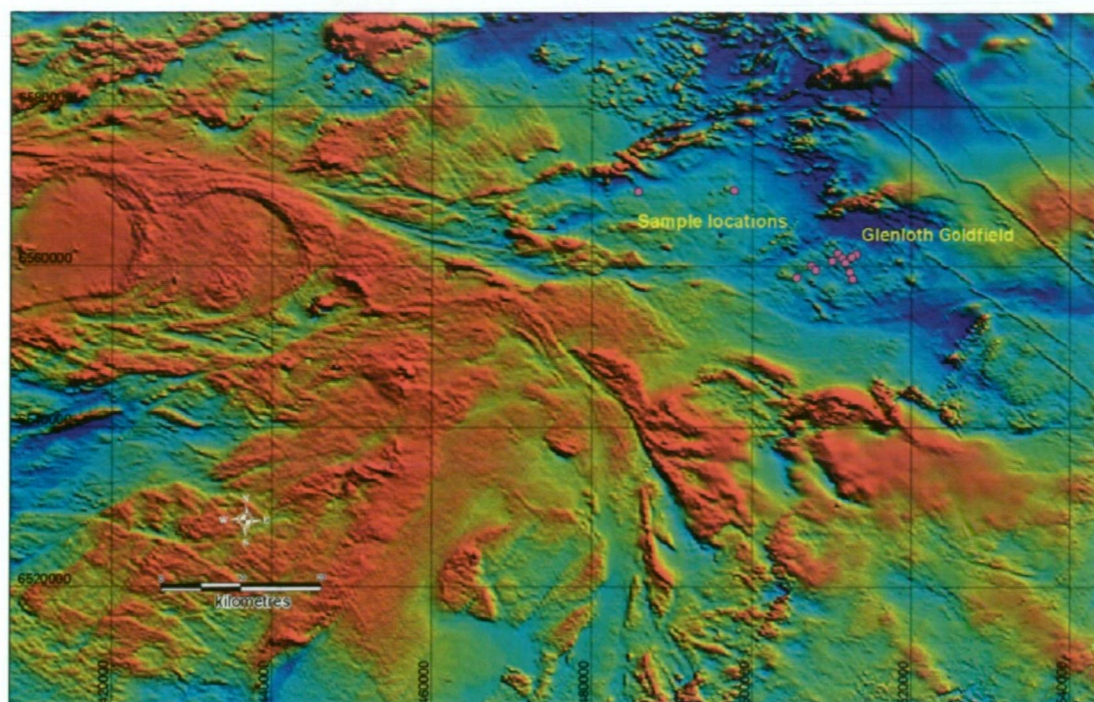
### **3.2 Archaean/Early Palaeoproterozoic**

#### **3.2.1 Glenloth Granite**

##### **3.2.1.1 Introduction and sampling**

The Glenloth Granite is a quartz-K-feldspar-plagioclase ± biotite and biotite or hornblende rich schlieren-bearing gneissic granite. Daly and Fanning (1990) report a preliminary U-Pb crystallisation age of 2440 Ma. Glenloth Granite crops out on the northeastern corner of CHILDARA at New Year Hill. The Glenloth Granite comprises a minor part of the igneous basement for the area, hence will not be discussed in great detail. Data used in this section, comprise three outcrop samples collected on northeastern CHILDARA, and data from the PIRSA western Gawler Craton data package (Appendix A). Sample locations are shown in Figure 10. Due to lack of high quality data, no trace element or Ga/Al plots are presented.





**Figure 10** TMI image showing location of Glenloth Granite samples used in this section.

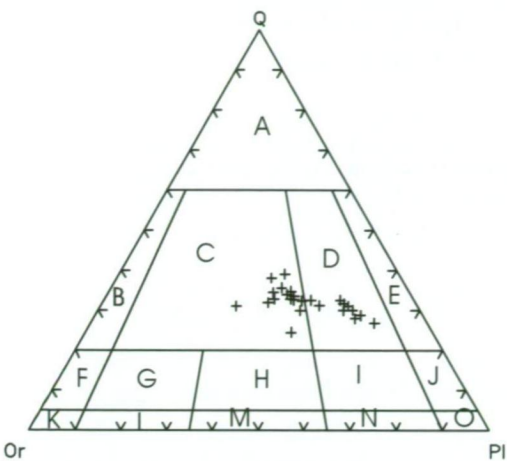
#### 3.2.1.2 Chemical variation

All samples plot within the granite and granodiorite fields on a Streckeisen (1976) plot (Figure 11). All samples, except two, plot within the I-type field on a ASI diagram, and generally define an I-type trend (Figure 12). On a Rb-Ba-Sr diagram (Figure 13), Glenloth Granite ranges from 'anomalous granite' via 'granite' to 'strongly differentiated granite', hence, the Glenloth Granite is not strongly fractionated.

SiO<sub>2</sub> ranges from 67 to 75 wt % (Figure 14A) and Harker diagrams of major oxides versus SiO<sub>2</sub> show negative correlations with the exception of Na<sub>2</sub>O + K<sub>2</sub>O and P<sub>2</sub>O<sub>5</sub> (Figure 14). Trace element data is inconclusive, due to lack of data, but Ba, Sr, U and Th show no correlation with increasing SiO<sub>2</sub> content (not shown).

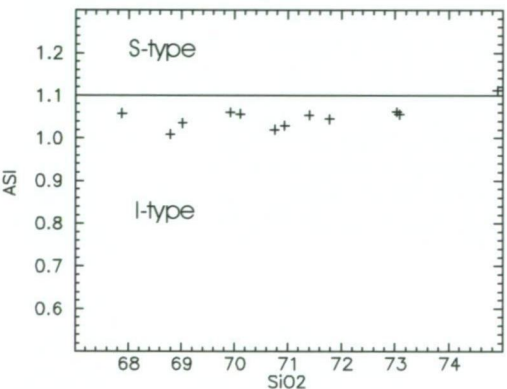
The Glenloth Granite is strongly depleted in Nb, Sr, Ti and strongly enriched in Th (Figure 15). The Glenloth Granite has steep, positively sloping LREE patterns with a small positive Eu anomaly and steep HREE patterns (Figure 16).



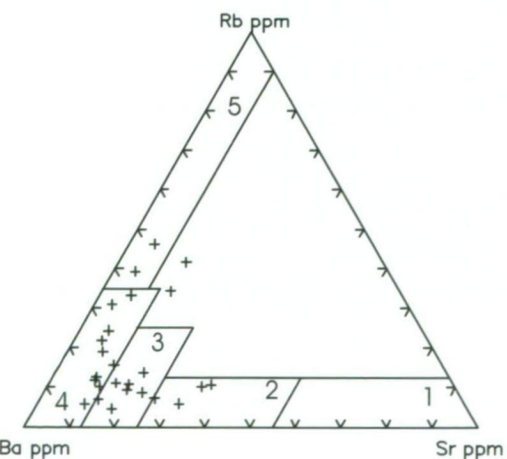


**Figure 11** Streckeisen plot for Archean/Early Palaeoproterozoic Glenloth Granite samples

(Legend: A = quartz-rich granitoids, B = alkali-feldspar granite, C = granite, D = granodiorite, E = tonalite, F = alkali-feldspar quartz syenite, G = quartz syenite, H = quartz monzonite, I = quartz monzodiorite/quartz monzogabbro, J = quartz diorite/quartz gabbro/quartz anorthosite, K = alkali-feldspar syenite, L = syenite, M = monzonite, N = monzodiorite/monzogabbro, O = diorite/gabbro/anorthosite.

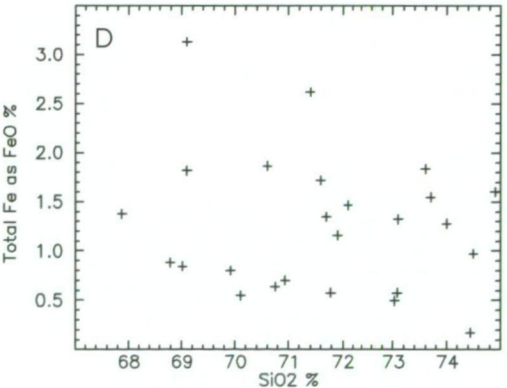
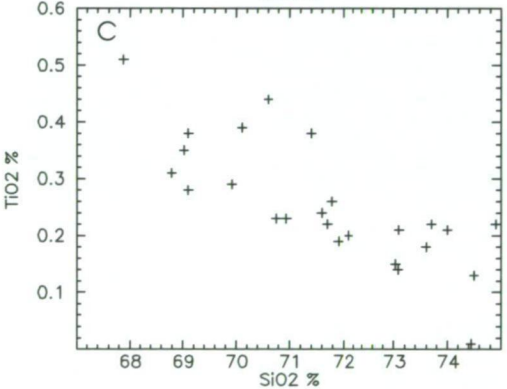
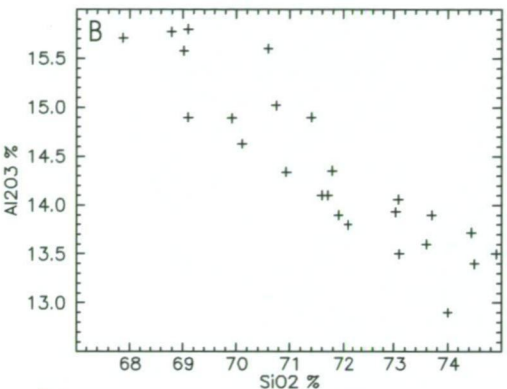
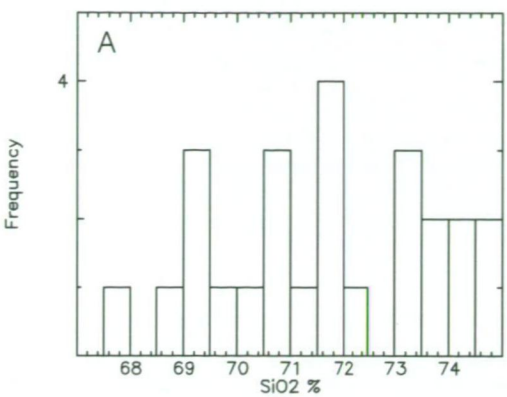


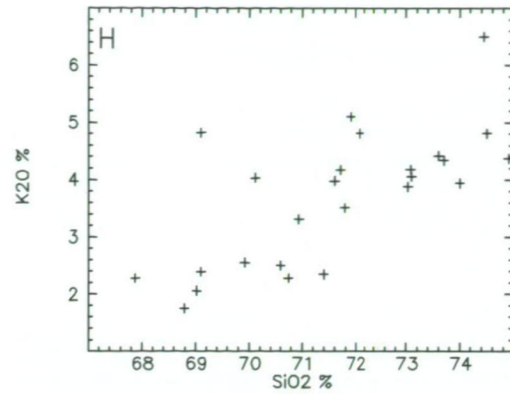
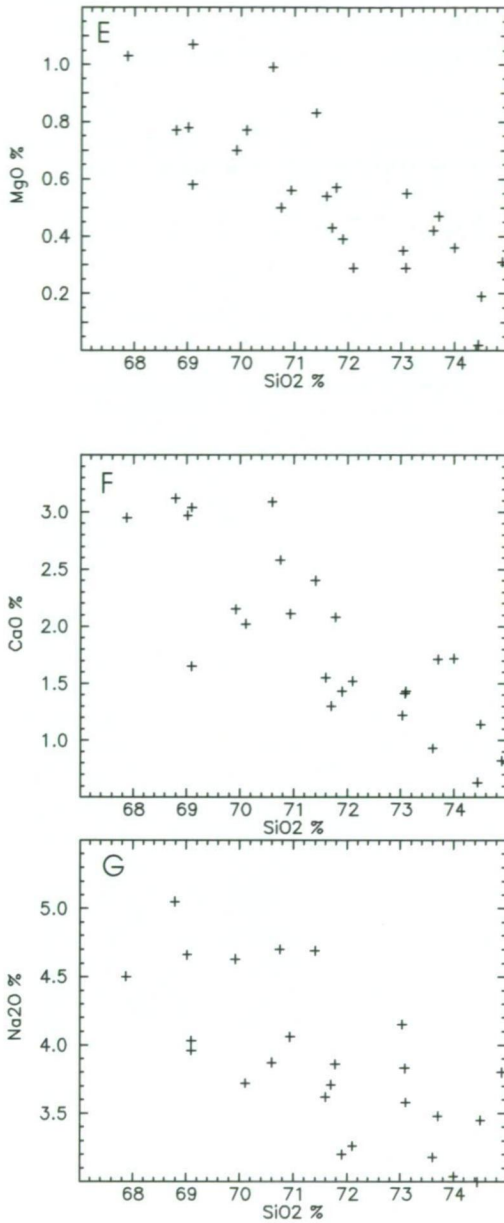
**Figure 12** ASI plot for Glenloth Granite.



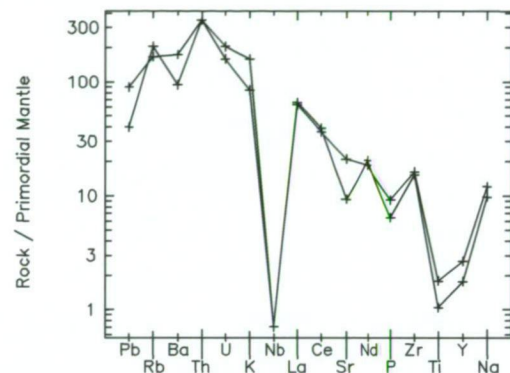
**Figure 13** Rb-Ba-Sr plot for Glenloth Granite.

Fields 1 diorites, 2 granodiorites, 3 anomalous granites, 4 normal granites, 5 strongly differentiated granites.

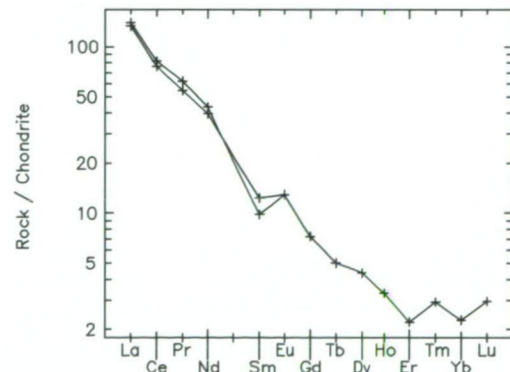




**Figure 14** SiO<sub>2</sub> histogram and harker diagrams of major oxides for Glenloth Granite. Elements in wt%.



**Figure 15** Incompatible-compatible element plot for Glenloth Granite.



**Figure 16** Chondrite normalised REE plot for Glenloth Granite.

### 3.3 Palaeoproterozoic

Daly *et al.* (1998) used the term Ifould Complex to encompass deformed multiphase plutons intruded during the Kararan Orogeny (~1650 – 1540 Ma). The Kararan Orogeny postdates the Kimban Orogeny and Daly *et al.* (1998) proposed that the Kararan Orogeny was related to continental collision between the eastern proto-Yilgarn Craton, in the northwest, and the central Gawler Craton-East Antarctic Craton in the south.

The geology and geochemistry of granitoids in the CHILDARA region, western Gawler Craton, South Australia: implications for the Proterozoic tectonic history of the western Gawler Craton and the development of lode-style gold mineralisation at Tunkillia.



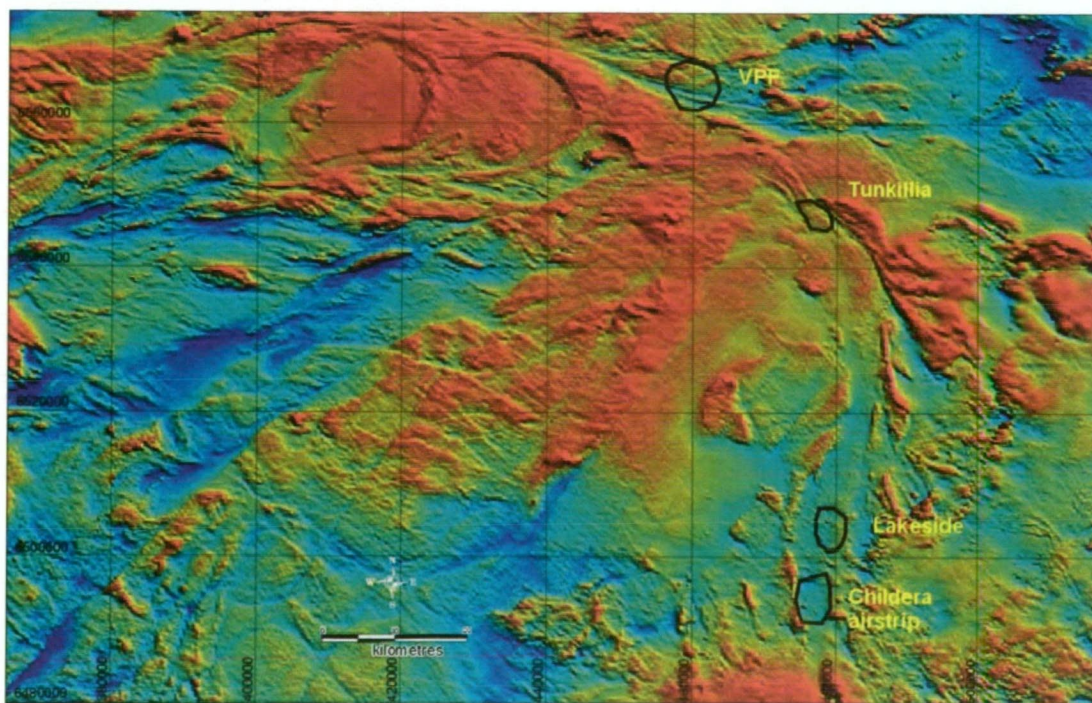
Teasdale (1997) defined the term Ifould Complex, for variably deformed, comagmatic, I-type granitoids and mafics, from the Lake Ifould area on FOWLER. The term Ifould Complex will not be used due to the conflicting definitions.

### 3.3.1 Tunkillia Suite and related Karraran Orogeny intrusives

#### 3.3.1.1 Introduction and sampling

The Tunkillia Suite (new name), crops out predominantly within the Yarlbrinda Shear Zone, and is interpreted to represent a significant part of the basement geology on CHILDARA (Plan 2). Six mappable units were described in the previous chapter, but the units are comagmatic, hence, samples have been divided into four groups (Childera Airstrip, Lakeside, VPF and Tunkillia) based on geographical location (Figure 17). Samples of known 1670 Ma granite including Barton South, Lake Ifould, Mulgathing Rocks, Little Pinbong, Lake Tallacootra and Wynbring Rocks are included. Table 1 shows average geochemical values for each group.

Forty outcrop samples were collected during regional mapping, and drill core from the Tunkillia prospect was supplied by Acacia Resources Ltd. Sample locations and geochemical analyses are presented in Appendix A.



**Figure 17 TMI image showing location of Tunkillia Suite groups on CHILDARA**

#### 3.3.1.2 Chemical variation

The Tunkillia Suite and related Karraran Orogeny intrusives are dominantly felsic, and range in composition from diorite, granodiorite, syenite to granite.  $\text{SiO}_2$  content

The geology and geochemistry of granitoids in the CHILDARA region, western Gawler Craton, South Australia: implications for the Proterozoic tectonic history of the western Gawler Craton and the development of lode-style gold mineralisation at Tunkillia.

ranges from 62.9 % to 77.3 % (Figure 18) and they plot mostly within the granite field on a Streckeisen (1976) diagram (Figure 19).

The Tunkillia Suite and related Kararan Orogeny intrusives are peraluminous (Figure 20) and plot within the anomalous to strongly differentiated granite fields on a Rb-Ba-Sr plot (Figure 21). The Tunkillia Suite and related Kararan Orogeny intrusives plot predominantly within the potassic field on a silica versus alkali plot (Figure 22).

Major elements including  $\text{Al}_2\text{O}_3$ ,  $\text{TiO}_2$ ,  $\text{FeO}$ ,  $\text{MgO}$ ,  $\text{CaO}$  and  $\text{P}_2\text{O}_5$  all show an inverse relationship to increasing  $\text{SiO}_2$  content (Figure 23). VPF samples show higher  $\text{Al}_2\text{O}_3$  content for similar  $\text{SiO}_2$  contents than other groups with the exception of Barton South (Figure 23A).  $\text{K}_2\text{O}$  shows a slight increase, while  $\text{Na}_2\text{O}$  shows scatter with increasing  $\text{SiO}_2$  (Figure 23).

Trace elements generally show a scatter of the data with few trends observed (Figure 24). Ba shows a increase up to ~70 wt%  $\text{SiO}_2$ , then decreases with increasing  $\text{SiO}_2$  content. Ba shows a broad range of values from 55-4900 ppm. The highest Ba value comes from a biotite-hornblende monzogranite (sample R368573) located on Meelera 1:100 000. This rock has been strongly deformed and possibly enriched in Ba by hydrothermal alteration. Three samples from Childara Airstrip group show Ba values ranging from 2350-2750 ppm and are also possibly affected by localised alteration. Zr values show a decreasing trend with increasing  $\text{SiO}_2$ , but VPF samples show a significantly lower Zr content compared to the other group (Figure 24B).

The Tunkillia Suite and related intrusives plot predominantly within the A-type granite field on Ga/Al (Whalen *et al.*, 1987) plots (Figure 25).

The Tunkillia Suite and related intrusives are typically low in Sr, Nb, Rb, and Ti (Figure 26), and are classified as Sr-depleted and Y-undepleted (Group 3 of Wyborn *et al.* 1992). The Tunkillia Suite and related intrusives are moderately enriched in LREE, with chondrite normalised La values ~30-400 (Figure 27). The Tunkillia Suite shows a significant negative Eu anomaly, and HREE traces are relatively flat (Figure 24). Average Eu/Eu\* values range from 0.30-1.09 (Table 1).



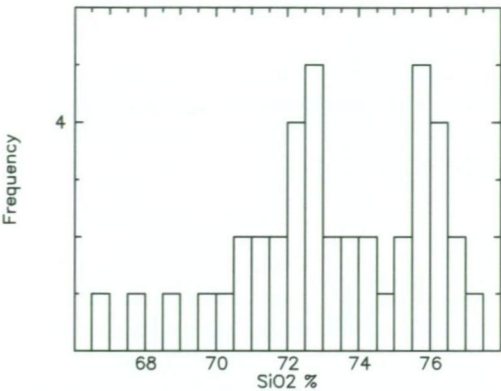
**Table 1 Average geochemical values for Tunkillia Suite and related intrusives.**

UNIT	Average Airstrip (n=12)	Average Lakeside (n=8)	Average VPF (n=10)	387449 Tunkillia (n=1)	444825 Barton (n=1)	Average Lake Ifould (n=4)	444835 Mulgathing (n=1)	444824 Pinbong (n=1)	Average Tallacootra (n=3)	444826 Wynbring (n=1)
Major elements (wt%)										
SiO <sub>2</sub>	72.91	74.23	74.11	66.70	72.03	71.74	76.46	72.83	72.30	73.16
Al <sub>2</sub> O <sub>3</sub>	13.28	13.00	13.77	14.60	15.31	15.08	12.10	12.86	13.90	13.41
CaO	0.96	0.72	1.44	2.58	2.02	2.29	0.79	1.05	1.31	1.31
Fe <sub>2</sub> O <sub>3</sub>	2.13	2.57	1.29	4.14	1.94	2.35	1.59	2.76	2.58	1.89
K <sub>2</sub> O	5.43	5.66	4.68	4.98	4.06	3.40	5.38	6.52	4.98	5.53
MgO	0.38	0.30	0.22	0.95	0.78	0.67	0.31	0.59	0.47	0.41
MnO	0.06	0.04	0.03	0.14	0.02	0.03	0.04	0.06	0.04	0.03
Na <sub>2</sub> O	3.06	2.78	3.39	1.96	3.48	3.93	2.88	2.07	3.56	3.10
P <sub>2</sub> O <sub>5</sub>	0.08	0.04	0.08	0.14	0.03	0.06	0.03	0.05	0.10	0.05
TiO <sub>2</sub>	0.23	0.23	0.12	0.51	0.20	0.32	0.27	0.40	0.35	0.29
Na <sub>2</sub> O/K <sub>2</sub> O	0.56	0.49	0.72	0.39	0.86	1.16	0.54	0.32	0.72	0.56
Trace elements (ppm)										
Ba	1194.17	510.63	1328.00	1250.00	1422.00	1360.00	289.00	766.00	875.67	986.00
Cr	14.17	96.25	24.00	40.00	17.00	13.25	9.00	8.00	7.33	6.00
Ga	22.17	20.63	18.70	22.00	15.20	16.60	14.90	15.00	16.93	16.10
Hf	3.75	4.00	2.40	3.00	3.40	4.25	6.30	8.60	6.77	5.30
Nb	9.79	24.38	3.40	0.50	5.20	7.90	21.70	16.40	11.53	12.10
Rb	176.50	266.25	133.50	210.00	93.90	84.40	289.10	327.20	59.93	156.90
Sc	2.71	4.06	2.50	10.00	4.00	3.75	5.00	6.00	3.00	4.00
Sr	177.92	82.50	349.00	250.00	385.90	502.53	58.20	79.60	198.83	157.00
Ta	3.67	8.00	4.00	1.00	0.50	0.50	1.90	1.50	0.73	0.90
Th	15.00	24.00	14.65	25.50	11.70	21.75	35.90	41.30	5.63	18.00
U	3.06	4.69	1.78	2.00	1.51	1.16	6.56	4.64	0.83	2.45
V	11.67	31.25	12.00	40.00	31.00	26.75	14.00	16.00	16.00	17.00
Y	26.42	24.88	7.30	17.00	14.20	13.98	42.00	41.90	29.77	19.60
Zr	201.67	162.50	93.00	250.00	122.00	177.75	203.00	306.00	276.67	197.00
Rare earth elements (ppm)										
Ce	82.58	94.13	37.50	115.00	66.71	128.19	137.80	144.80	142.04	125.40
Dy	4.92	4.38	1.43	4.00	2.76	3.10	5.96	6.69	5.04	2.97
Er	2.75	2.50	0.55	2.00	1.15	0.99	4.04	3.93	2.77	1.78
Eu	0.58	0.47	0.33	1.50	1.02	1.02	0.71	0.81	1.35	1.03
Gd	5.25	4.13	1.70	6.00	4.05	6.25	6.37	7.59	6.82	4.30
Ho	0.92	0.81	0.25	0.50	0.46	0.48	1.29	1.39	1.02	0.63
La	45.00	50.63	24.10	63.00	34.35	60.69	65.77	69.74	72.54	629.50
Lu	0.40	0.38	0.25	0.25	0.12	0.12	0.60	0.50	0.32	0.28
Nd	31.83	20.63	14.55	44.50	25.62	43.24	48.71	50.88	54.32	42.10
Pr	9.17	7.50	4.15	13.00	7.10	12.74	14.45	15.00	15.19	12.73
Sm	3.71	3.81	0.55	7.50	4.44	7.79	8.16	8.87	8.70	6.09
Tb	0.65	0.50	0.25	0.50	0.63	0.81	1.11	1.26	1.02	0.64
Tm	0.54	0.50	0.50	0.50						
Yb	2.92	2.50	0.55	2.00	0.77	0.77	4.12	3.46	2.29	1.64
Eu/Eu*	0.4	0.36	0.94	0.66	0.73	1.09	0.29	0.30	0.56	0.58
Ce <sub>N</sub>	102.2	116.5	46.4	142.3	82.56	158.64	170.54	179.21	175.79	155.20
La <sub>N</sub> /Lu <sub>N</sub>	11.81	14.02	10.01	26.18	29.73	50.52	11.39	14.49	24.92	233.52

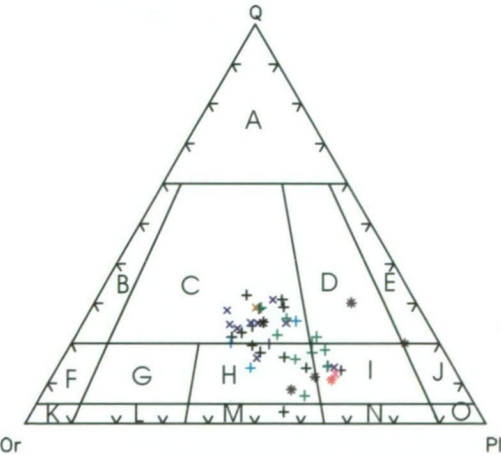
Eu/Eu\* - a measure of the Eu anomaly relative to the concentrations of Sm and Gd on a REE plot

Ce<sub>N</sub> - normalised value of Ce (Ce ppm/.808) (normalising value from Boynton, 1984)

La<sub>N</sub>/Lu<sub>N</sub> - (La ppm/.31)/(Lu ppm/.209) (normalising value from Boynton, 1984)

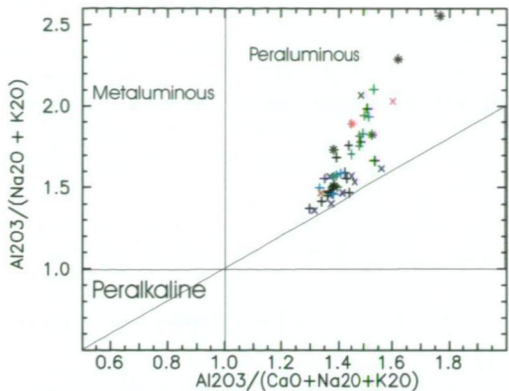


**Figure 18** SiO<sub>2</sub> histogram for Tunkillia Suite and related Kararan Orogeny intrusives.

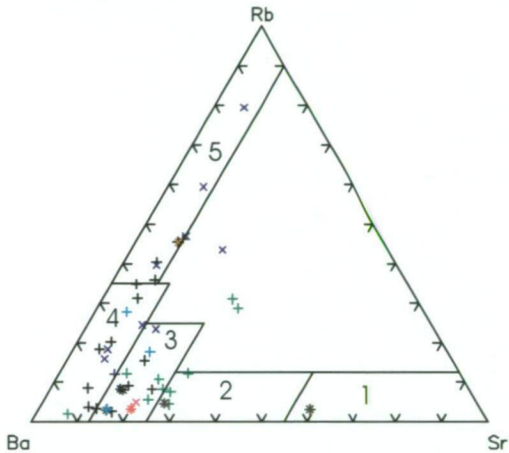


**Figure 19** Streckeisen plot for Tunkillia Suite and related Kararan Orogeny intrusives.

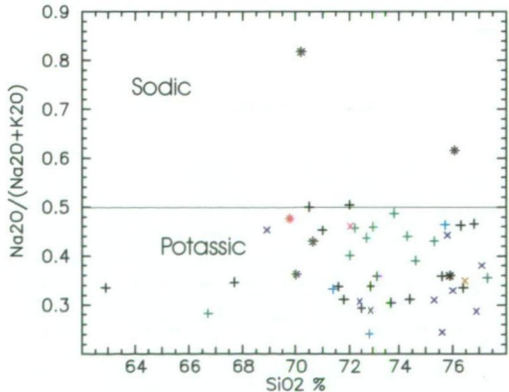
(Legend: A = quartz-rich granitoids, B = alkali-feldspar granite, C = granite, D = granodiorite, E = tonalite, F = alkali-feldspar quartz syenite, G = quartz syenite, H = quartz monzonite, I = quartz monzodiorite/quartz monzogabbro, J = quartz diorite/quartz gabbro/quartz anorthosite, K = alkali-feldspar syenite, L = syenite, M = monzonite, N = monzodiorite/monzogabbro, O = diorite/gabbro/anorthosite.



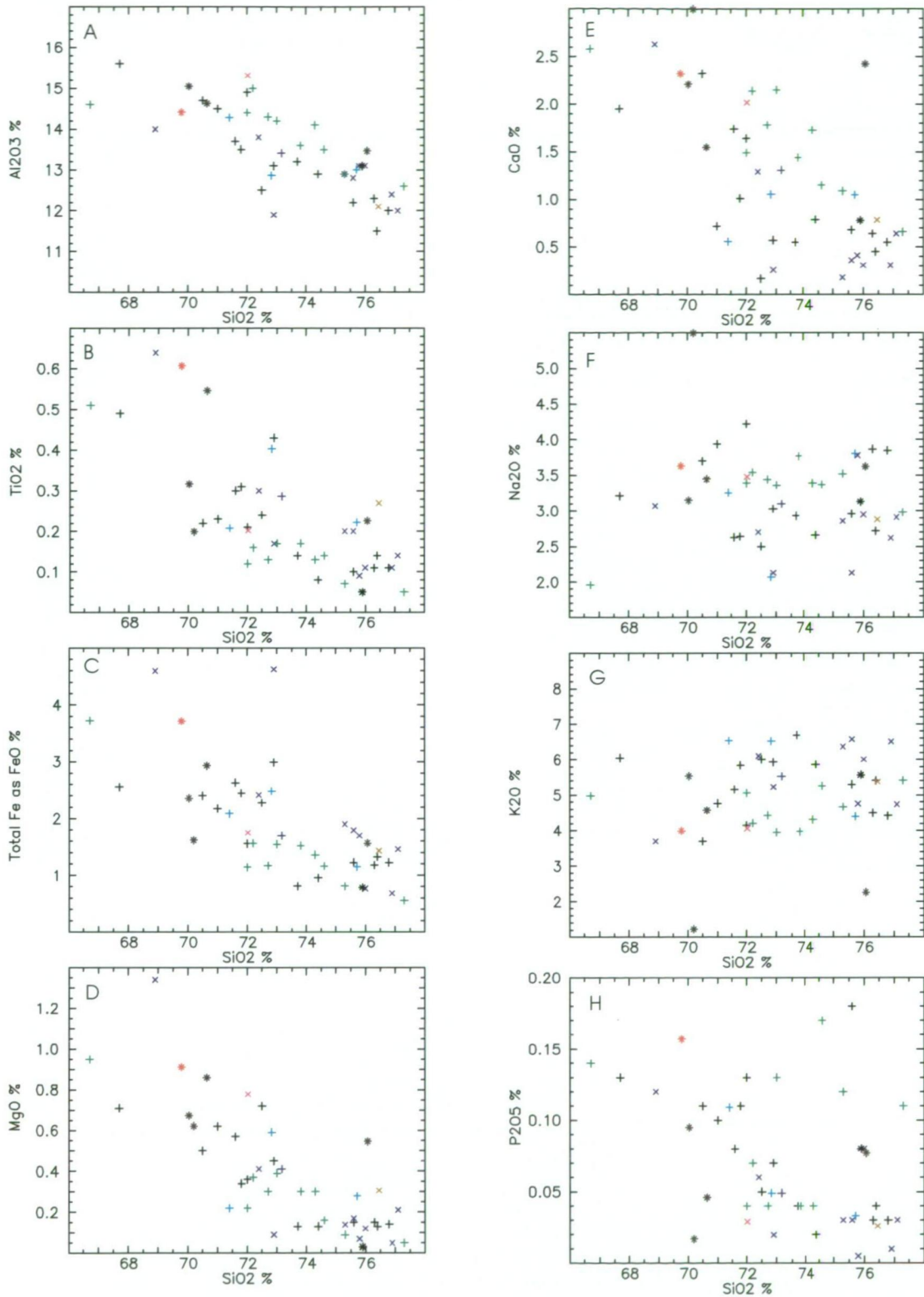
**Figure 20** Molecular Al/(Ca+Na+K) versus Al/(Na+K) plot after Maniar and Piccoli (1989).



**Figure 21** Rb-Ba-Sr plot for the Tunkillia Suite and related Kararan Orogeny intrusives. Fields 1 diorites, 2 granodiorites, 3 anomalous granites, 4 normal granites, 5 strongly differentiated granites



**Figure 22** Na/(Na+K) vs SiO<sub>2</sub> plot for the Tunkillia Suite and related Kararan Orogeny intrusives.



**Figure 23** Harker diagrams of major elements vs  $\text{SiO}_2$  for Tunkillia Suite and related intrusives. Elements in wt %.



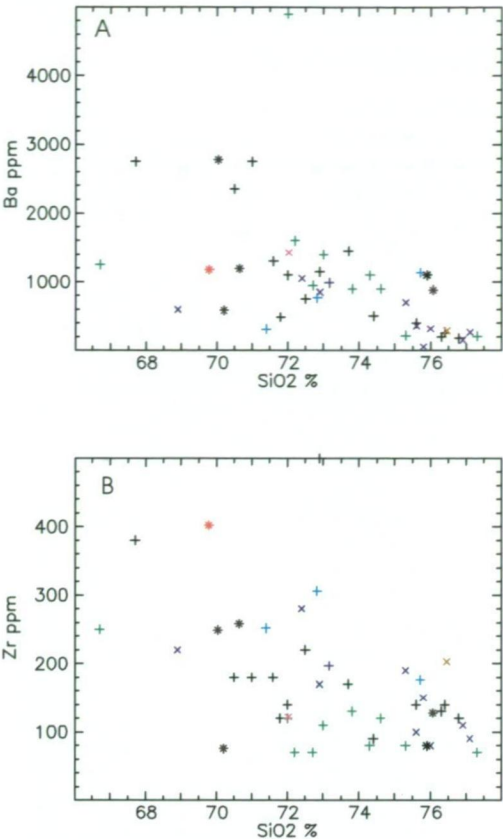


Figure 24 Selected trace element vs  $\text{SiO}_2$  plots for Tunkillia Suite and related intrusives.

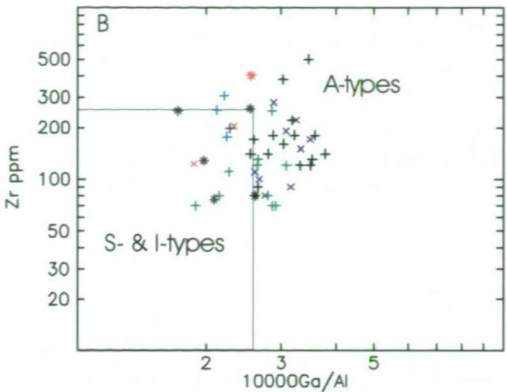
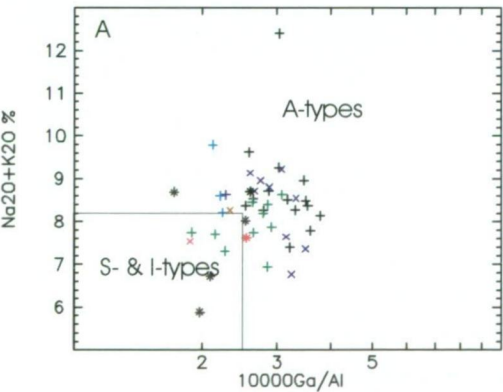


Figure 25  $\text{Ga}/\text{Al}$  v  $\text{Na}_2\text{O}+\text{K}_2\text{O}$  and  $\text{Ga}/\text{Al}$  v Zr for Tunkillia Suite and related intrusives.

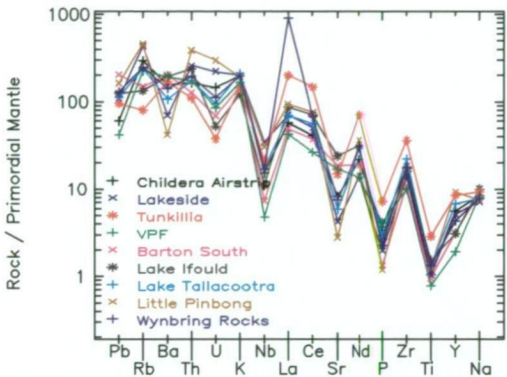


Figure 26 Mantle normalised incompatible-compatible plot of average values for Tunkillia Suite and related intrusives.

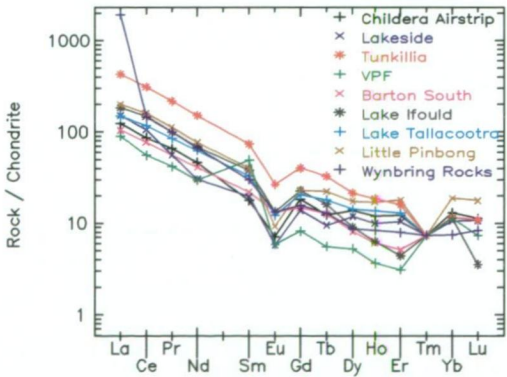
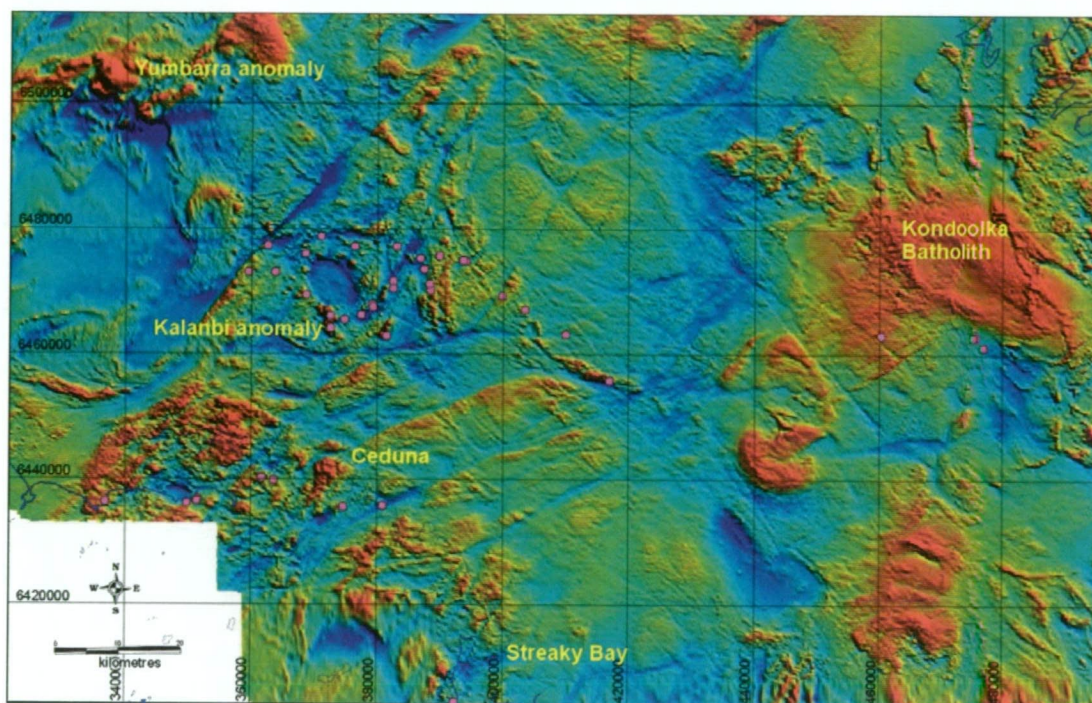


Figure 27 Chondrite normalised REE plot of average values for Tunkillia Suite and related intrusives.

### 3.3.2 St Peter Suite

#### 3.3.2.1 Introduction and sampling

The St Peter Suite comprises deformed, comagmatic, intrusive rocks which include granite, adamellite, trondhjemite, tonalite, granodiorite, diorite, and dolerite. The St Peter Suite is characterised by complex contact relationships between various units. Description of geological units is presented in section 2.4.2. Location of samples is shown in Figure 28.



**Figure 28** TMI image showing location of St Peter Suite samples.

The St Peter Suite has been divided into seven groups based on petrographic, geochemical and magnetic characteristics. Table 2 shows average geochemical values for the seven groups. Group 1 represents the St Francis Granite.

Group 2 comprises a complex group of lithologies ranging in composition from quartz diorite, tonalite, granodiorite, trondhjemite to adamellite (Lp3 and Lp8). Flint *et al.* (1990) defined Lp3 from the Point Brown area, but drilling in the Kalanbi area intersected a suite of rocks with similar geochemical characteristics. Garnet bearing granite from near the OTC tower, north of Ceduna, is included due to similar geochemical characteristics. Group 2 samples were further subdivided on SiO<sub>2</sub> content into 3 groups.

Group 3 represents unit Lp1, pink, fine to medium grained granite and adamellite from Point Westall and Smooth Pool on STREAKY BAY. The geochemical data is from Dove (1997), but does not contain a full suite of trace elements, hence only whole rock and minimal trace element data is discussed.

Group 4 comprises a suite of rocks ranging in composition from adamellite to granodiorite (some analyses of Lp3 and Lp7).

Group 5 comprises massive, late monzo- to syenogranite (Lp10). All samples were collected from drill holes within a large, ovoid north-northwest trending batholith. U-Pb dating of granite from drill hole CED 22 gave an upper intercept age of 1620 Ma.

Group 6 comprises mildly deformed to sheared granodiorite to adamellite, located within the vicinity of the Kondoolka Batholith (Lp9). Group 7 comprises mafic lithologies with high magnetic signature, ranging in composition from quartz diorite, diorite, metapyroxenite to gabbro.

Sample locations are shown on Figure 28. Sample groupings and geochemical analyses are presented in Appendix A.

### 3.3.2.2 Chemical variation

The St Peter Suite is dominantly intermediate to felsic with  $\text{SiO}_2$  contents ranging from 47.8 to 79 wt %, with an average  $\text{SiO}_2$  content of 71.63 wt % (Figure 29). All units of the St Peter Suite, with the exception of Groups 2 and 7, plot within the granite field on a Streckeisen (1976) diagram (Figure 30). Group 2 plots predominantly within the quartz monzodiorite/quartz monzogabbro fields, and group 7 plots in the monzodiorite/monzogabbro fields. A similar trend is evident on a CaO-Na<sub>2</sub>O-K<sub>2</sub>O diagram (Figure 31).

On a Rb-Ba-Sr diagram, mafic samples plot within the diorite to granodiorite fields, whereas felsic samples plot in the anomalous granite to strongly differentiated granite fields (Figure 32). The St Francis Granite (Group 1) is the most strongly differentiated (Figure 32). The St Peter Suite is sodic at low  $\text{SiO}_2$  values, and becomes more potassic with differentiation, mainly encompassing group 4 (Figure 33).

ASI values for the St Peter Suite are predominantly <1.1 and reflect an I-type trend (Table 2). The majority of the St Peter Suite plot within the I-type field on Ga/Al plots (Fig. 34)

With increasing fractionation,  $\text{TiO}_2$ ,  $\text{Fe}_2\text{O}_3$ , MgO, CaO and  $\text{P}_2\text{O}_5$  show a negative correlation (Figure 35). Na<sub>2</sub>O and K<sub>2</sub>O show enrichment with increasing  $\text{SiO}_2$  content (Figure 35).  $\text{Al}_2\text{O}_3$  shows an enrichment up to ~68 wt %  $\text{SiO}_2$  followed by a depletion (Figure 35A). Group 7 shows two trends in relation to MgO, with one group of samples recording an increase in MgO content with increasing  $\text{SiO}_2$ , the other group decreasing with increasing  $\text{SiO}_2$  (Figure 35D).

$\text{TiO}_2$  content at 50%  $\text{SiO}_2$  suggests three distinct endmembers (Figure 35B). Samples from holes CED 40 and 45 show low  $\text{TiO}_2$  due to low biotite and hornblende content. CED 40 contains a desilicated gabbro where original olivine and plagioclase have been replaced by pargasite and spinel during metamorphism (Purvis, 2000). This reaction probably also produced alteration of biotite to chlorite



and reduced the original  $\text{TiO}_2$  content. CED 45 contains anorthosite with no biotite, hence has low  $\text{TiO}_2$ .

Trace element plots show that Ba, Ce, Rb and Y exhibit enrichments up to ~70 wt %  $\text{SiO}_2$ , then become depleted at higher  $\text{SiO}_2$  levels (Figure 36). Sr increases to ~64 wt %  $\text{SiO}_2$  then decreases (Figure 36D). Zr data show a slight enrichment up to ~66 wt %  $\text{SiO}_2$ , followed by a rapid depletion (Figure 36E). A mafic dyke from Point Westall (1096-20) contains very high Ba, Ce, Ga and Sr (Fig 36). Two samples of Group 7 are enriched in  $\text{P}_2\text{O}_5$  due to accessory apatite.

Mantle normalised spidergrams for felsic units of the St Peter Suite (Groups 1, 3, 4, 5 and 6) show depleted Sr, Ti, Nb and P (Figure 37). The St Francis Granite (Group 1) is the most fractionated granite and shows extreme depletion in the above elements relative to the other groups (Figure 37). Groups 2 and 7 are depleted in Nb, P and Ti (Figure 38). Group 2 samples >70 wt%  $\text{SiO}_2$  are depleted in Sr, whereas samples <70 wt%  $\text{SiO}_2$  and Group 7 samples are enriched in Sr (Figure 38). Groups 1,3,4,5,6 and samples >70 wt%  $\text{SiO}_2$  from Group 2 are Sr-depleted, Y-undepleted granites (group 1 of Wyborn *et al.*, 1992). Group 2 samples <70 wt%  $\text{SiO}_2$  and Group 7 samples are Sr-undepleted and Y-undepleted (group 3 of Wyborn *et al.*, 1992).

Groups 4, 5 and 6 show similar trends on a chondrite normalised REE plot with steeply sloping LREE patterns, negligible Eu anomalies and relatively flat HREE patterns (Figure 37). Groups 2 and 7 also show similar trends with slightly enriched LREE, no Eu anomaly and flat HREE patterns (Figure 38).

However, samples from hole CED 45 within the main mafic intrusive at Kalanbi, exhibit primitive (5 times chondrite) patterns and a positive Eu anomaly (Figure 39). These rocks are anorthosites and represent cumulates. This magma possibly represents a composition close to the original parent magma for much of Group 7 mafic lithologies. Surrounding mafic rocks show evidence of crustal contamination and magma mingling. Sample R432909 from hole CED 46 (44.15-44.2m) shows a folded contact between a leucocratic tonalite and a foliated diorite to quartz diorite body, with amoeboid hornblende lenses, in a biotite-quartz microdiorite host (Purvis, 2000).

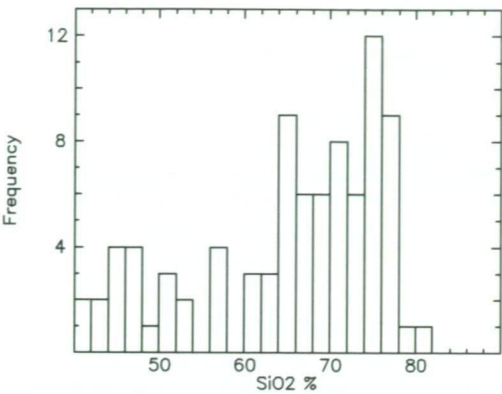


Figure 29 SiO<sub>2</sub> histogram for the St Peter Suite.

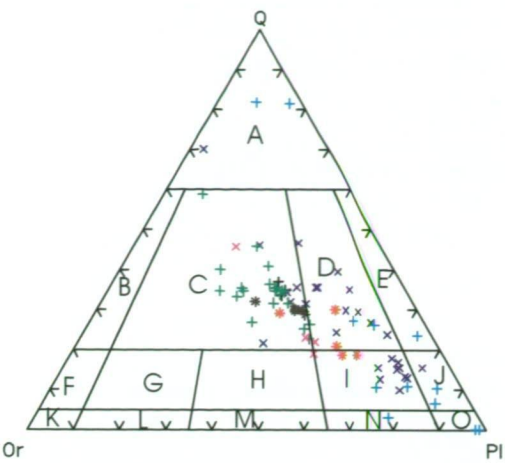


Figure 30 Streckeisen plot for St Peter Suite.

(Legend: A = quartz-rich granitoids, B = alkali-feldspar granite, C = granite, D = granodiorite, E = tonalite, F = alkali-feldspar quartz syenite, G = quartz syenite, H = quartz monzonite, I = quartz monzodiorite/quartz monzogabbro, J = quartz diorite/quartz gabbro/quartz anorthosite, K = alkali-feldspar syenite, L = syenite, M = monzonite, N = monzodiorite/monzogabbro, O = diorite/gabbro/anorthosite.

Table 2 Average geochemical values for St Peter Suite.

	St Peter Average Group 1 (n=4)	St Peter Average Group 2 <64% SiO <sub>2</sub> (n=9)	St Peter Average Group 2 64-70% SiO <sub>2</sub> (n=11)	St Peter Average Group 2 >70% SiO <sub>2</sub> (n=9)	St Peter Average Group 3 (n= 12)	St Peter Average Group 4 (n=21)	St Peter Average Group 5 (n=4)	St Peter Average Group 6 (n=5)	St Peter Average Group 7 (n=19)
Major elements (wt%)									
SiO <sub>2</sub>	77.04	60.25	66.30	75.13	64.59	73.87	67.48	71.38	47.37
Al <sub>2</sub> O <sub>3</sub>	12.43	18.01	17.96	14.00	16.78	13.84	15.95	14.34	23.00
CaO	0.18	4.71	2.08	0.48	0.18	0.93	2.45	1.89	9.57
Fe <sub>2</sub> O <sub>3</sub>	0.89	6.80	4.21	1.50	0.89	1.81	4.36	2.00	9.92
K <sub>2</sub> O	4.50	1.71	2.53	4.00	2.46	4.99	4.38	4.46	0.98
MgO	0.12	2.44	0.93	0.21	1.51	0.34	1.02	0.41	5.01
MnO	0.7	0.19	0.07	0.05	0.13	0.07	0.09	0.06	0.13
Na <sub>2</sub> O	4.26	4.39	4.93	3.72	5.16	3.32	3.43	3.69	1.66
P <sub>2</sub> O <sub>5</sub>	0.01	0.27	0.14	0.05	0.21	0.08	0.16	0.14	0.23
TiO <sub>2</sub>	0.11	0.66	0.46	0.21	0.11	0.23	0.55	0.23	0.87
Na <sub>2</sub> O/K <sub>2</sub> O	0.95	2.57	1.94	0.93	2.1	0.67	0.78	0.83	1.69
Trace elements (ppm)									
Ba	66	1052.44	1376.45	590.56	1421	728.38	1350.00	990.00	333.42
Cr	1.7	64.72	78.94	156.44	3.5	77.56	45.00	24.00	109.47
Ga	19.93	23.07	20.65	16.73	20.05	16.56	23.25	18.20	22.34
Hf		3.80	5.75	3.76		6.31	4.25	4.00	1.63
Nb	19.5	8.54	12.00	12.81	10.21	11.20	18.75	2.40	5.53
Rb	237	63.20	85.75	149.73	106.87	194.32	153.75	163.00	54.32
Sc	3.87	17.49	9.87	5.51	11.2	4.34	8.13	3.00	32.50
Sr	6.06	653.30	623.25	123.97	615.35	151.34	257.50	385.00	476.32
Ta		1.60	6.75	2.14		1.48	1.50	3.20	1.00
Th	17.3	6.06	12.43	15.28	16.83	17.23	15.00	14.20	3.43
U	2.2	1.36	2.60	2.65	1.88	3.25	3.55	2.60	1.20
V	7.7	93.11	48.73	17.67	61.92	16.86	40.00	12.00	202.63
Y	61.5	26.11	15.53	26.22	26.48	33.38	32.38	18.20	20.69
Zr	167	179.66	252.22	116.77	232.1	191.55	265.00	156.00	69.47
Rare earth elements (ppm)									
Ce	48.33	63.06	76.45	56.01	111.58	77.25	66.50	62.60	30.05
Dy		2.76	2.15	3.55		7.30	4.63	3.20	2.82
Er		1.48	1.16	1.90		4.21	2.74	1.70	1.57
Eu		1.43	1.33	0.93		1.14	1.66	0.55	1.18
Gd		3.46	2.71	3.78		7.50	5.43	3.60	3.14
Ho		0.54	0.41	0.65		1.56	0.98	0.55	0.57
La	20.33	31.94	42.64	25.11	57.33	42.45	39.13	38.20	15.36
Lu		0.23	0.20	0.27		0.69	0.46	0.30	0.26
Nd	23	31.61	30.59	21.50	37.5	29.60	45.63	27.30	19.09
Pr		5.92	6.75	7.30		11.60	9.63	7.00	3.92
Sm		4.96	4.81	5.02		7.14	7.25	2.00	3.87
Tb		0.44	0.36	0.63		0.94	0.73	0.55	0.43
Tm		0.23	0.19	0.32		0.70	0.44	0.50	0.25
Yb		1.50	1.23	2.83		4.16	2.95	1.90	1.55
Eu/Eu*		1.02	1.01	0.77		0.76	0.78	0.73	1.22
CeN		78.04	94.62	69.32		95.61	82.30	77.48	37.19
La <sub>N</sub> /Lu <sub>N</sub>		10.72	19.09	16.10		10.98	9.12	12.42	8.37
ASI		1.06	1.26	1.25		1.12	1.10	1.02	1.11



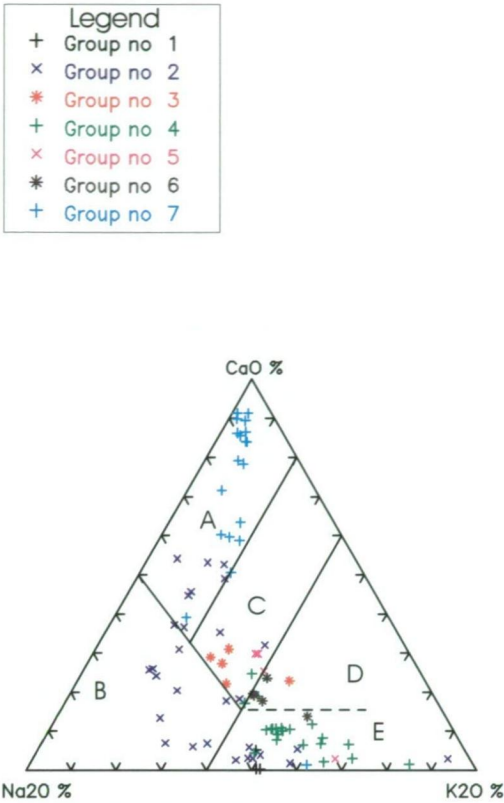


Figure 31 Ca-Na-K plot for St Peter Suite.

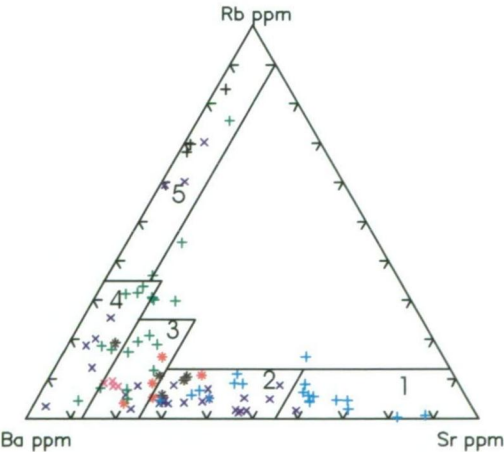


Figure 32 Rb-Ba-Sr plot for St Peter Suite.

Fields 1 diorites, 2 granodiorites, 3 anomalous granites, 4 normal granites, 5 strongly differentiated granites

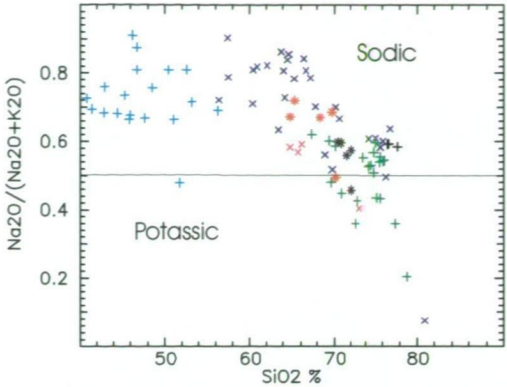


Figure 33 Na/(Na+K) vs SiO<sub>2</sub> plot for St Peter Suite.

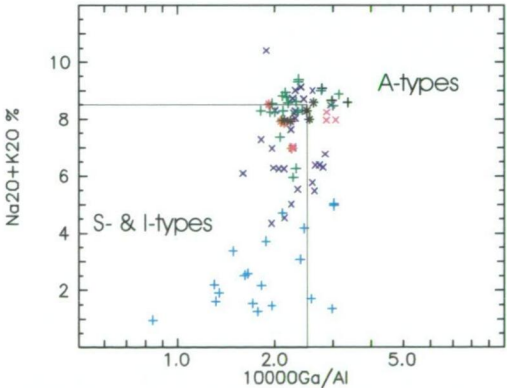
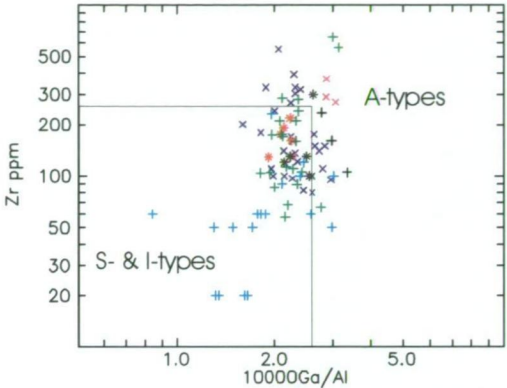
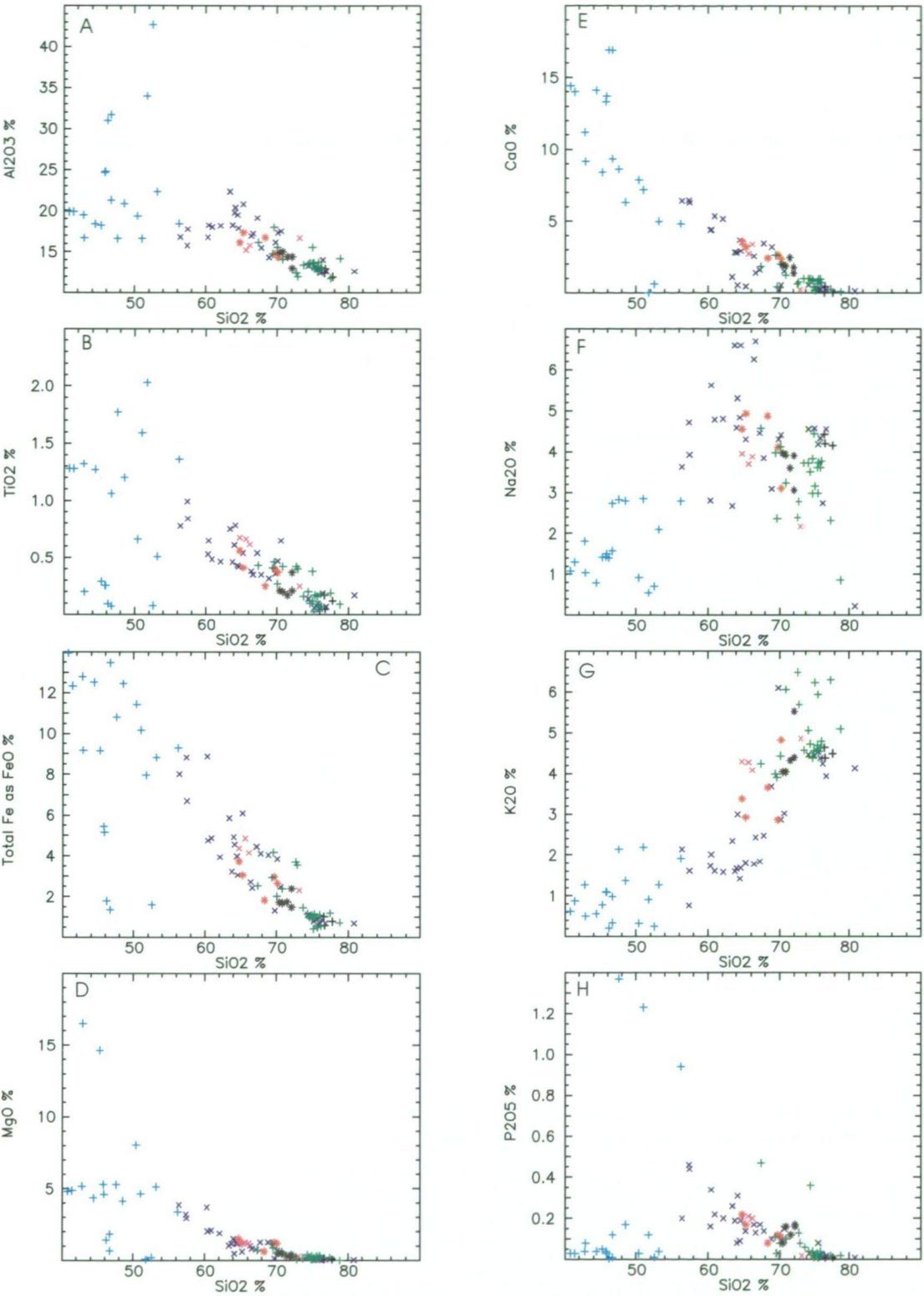


Figure 34 Ga/Al v Zr and Na<sub>2</sub>O + K<sub>2</sub>O plots for St Peter Suite.



**Figure 35 Harker diagrams of major elements vs SiO<sub>2</sub> for St Peter Suite. Elements in wt%.**

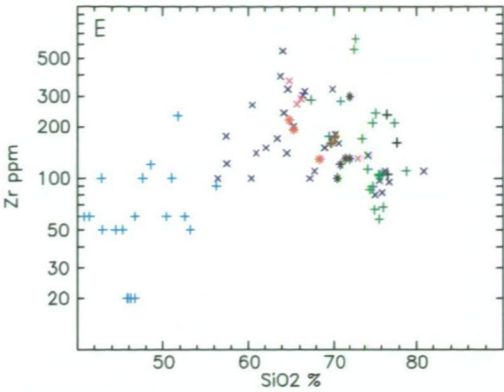
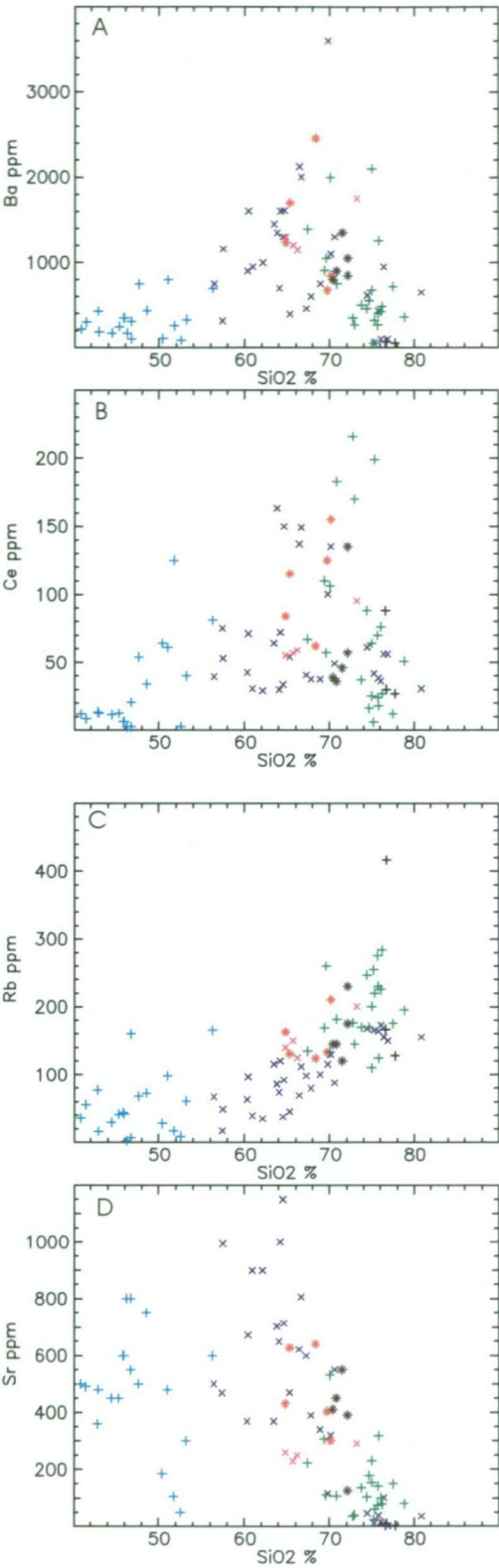


Figure 36 Harker diagrams of trace elements vs SiO<sub>2</sub> for St Peter Suite.

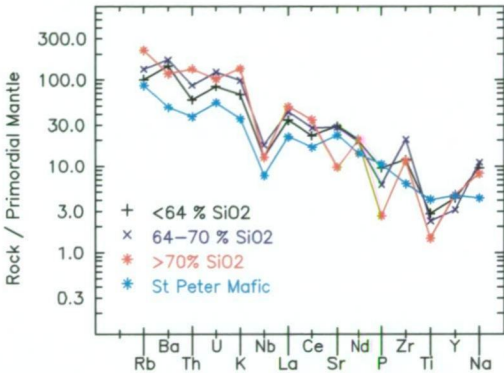


Figure 37 Mantle normalised plot of average values for groups 2 and 7 of the St Peter Suite.

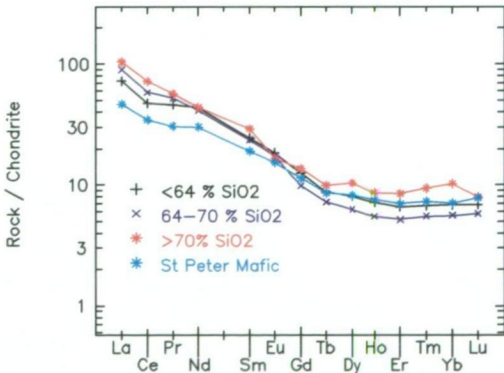


Figure 38 Chondrite normalised REE plots of average values for groups 2 and 7 of the St Peter Suite.



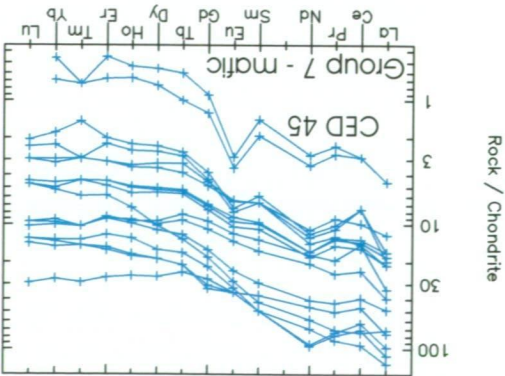


Figure 39 Chondrite normalised REE for Group 7 of the St Peter Suite.

3.4 Mesoproterozoic

3.4.1 Hiltaba Suite

3.4.1.1 Introduction and sampling

The Hiltaba Suite is the most common outcropping granitoid unit on CHILDIRA. Location of mapping samples and geochemical analyses are presented in Appendix A. Geochemical analyses were grouped into seven individual plutons defined from regional aeromagnetics (Figure 40).

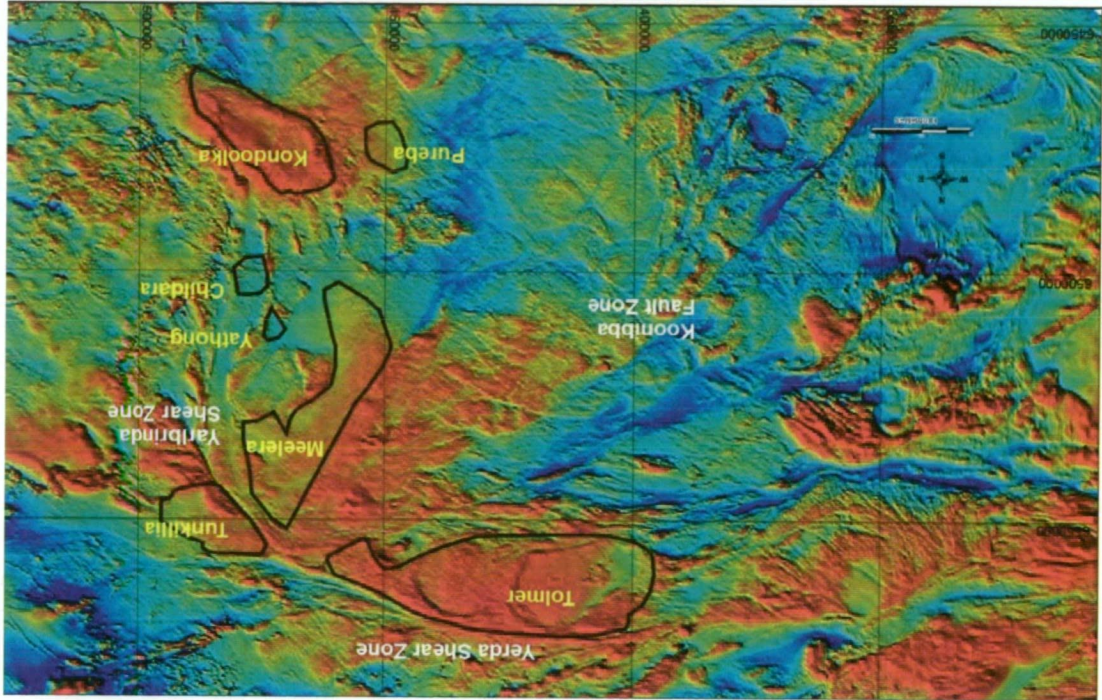


Figure 40 TMI image showing location of seven Hiltaba Suite plutons on CHILDIRA.

The Kondoolka group contains thirty six samples collected within the Kondoolka Batholith. The Kondoolka Batholith is a northwest trending batholith, which crosscuts the Yarbrinda Shear Zone on southeastern CHILDIRA (Figure 40). Granite from the Kondoolka Batholith is undeformed and ranges in texture from coarse grained, equigranular to porphyritic, high-level granite. A summary of major element and trace element characteristic for each group are shown in Table 3, and

The geology and geochemistry of granitoids in the CHILDIRA region, western Gawler Craton, South Australia: implications for the Proterozoic tectonic history of the western Gawler Craton and the development of lode-style gold mineralisation at Tunkilla.

average geochemical values for major elements and selected trace elements are presented in Table 4. Full geochemical data is presented in Appendix A.

The Childara group is located west of Childera Outstation and the Yarlbirinda Shear Zone, and comprise a homogenous group of massive, coarse grained granites. Six samples were collected and average geochemical values are presented in Table 4.

The Tunkillia group is located on the eastern side of the Yarlbirinda Shear Zone (Figure 40) and comprises foliated to massive granite. Five samples were collected and average geochemical values are presented in Table 4.

The Meelera group comprises six samples from west of the vermin proof fence and within the vicinity of Meelera Rockhole (Figure 40). Granite varies from massive, coarse grained homogeneous to porphyritic varieties.

The Tolmer group defines a prominent magnetic feature on northern CHILDARA (Figure 40), and is characterised by poor outcrop. Five samples were collected from scattered outcrops and range from massive coarse grained granite to foliated granodiorite within the Yerda Shear Zone.

One sample of porphyritic granite was collected to the west of the Kondoolka Batholith from Pureba Rockhole (Figure 40). Two samples of brick red, felsic granite were collected along the edge of a lake near Yathong Tank (Figure 40).

#### 3.4.1.2 Chemical variation

The Hiltaba Suite is a suite of predominantly massive granites.  $\text{SiO}_2$  content ranges from 67.6 to 79.8 wt% (Figure 41) and samples plot almost exclusively within the granite field on a Streckeisen (1976) diagram (Figure 42). and  $\text{Na}_2\text{O} + \text{K}_2\text{O}$  values are generally  $>8$  wt % (average – 8.15). ASI values are  $>1.1$  (Figure 43). The Hiltaba Suite is dominantly felsic, but some samples plot within the sodic field on a  $\text{Na}/(\text{Na} + \text{K})$  versus  $\text{SiO}_2$  diagram (Figure 44). The Hiltaba Suite is peraluminous (Figure 45) and has a high degree of differentiation on a Rb-Ba-Sr plot (Figure 46).

Major element plots show calc-alkaline trends with decreasing  $\text{Al}_2\text{O}_3$ ,  $\text{Fe}_2\text{O}_3$ ,  $\text{TiO}_2$ ,  $\text{MgO}$ ,  $\text{CaO}$  and  $\text{P}_2\text{O}_5$  with increasing  $\text{SiO}_2$  (Figure 47).  $\text{K}_2\text{O}$  and  $\text{Na}_2\text{O}$  show a general increase with increasing  $\text{SiO}_2$  (Figure 47). The Hiltaba Suite is enriched in Rb, Y, Zr, Th and U and depleted in Ba and Sr (Figure 48). Stewart and Foden (2001) report increasing Rb/Ba ratios with increasing  $\text{SiO}_2$  indicate fractionation of K-feldspar (Figure 49). The Hiltaba Suite plots predominantly within the A-type field on Ga/Al plots (Figure 50).

Stewart and Foden (2001) reports the Hiltaba Suite contains abundant large ion lithophile elements (eg: Rb, Ba, Eu, Pb and Cs). Data collected during this study show the Hiltaba Suite to be depleted in Ba and Pb. The Hiltaba Suite also shows strong zircon removal from melt at higher  $\text{SiO}_2$ .

Table 3 summarises the major oxide and trace element characteristics for each group, and Table 4 summarises the average chemical composition of the seven groups.



Mantle and chondrite normalised spidergrams show the Hiltaba Suite is geochemically homogeneous (Figs 51 and 52), hence chemistry alone is a poor discriminator of individual plutons. The Hiltaba Suite is depleted in Ba, Nb, P, Sr and Ti and enriched in Rb and Zr (Figure 51). Generally Rb/Sr values are >1 (Appendix A), however samples from the Yarranna Hill area on the western margin of the Kondoolka Batholith have high Sr (440-750 ppm). This is possibly due to contamination with metasediments. The Hiltaba Suite is classified as Sr-depleted and Y-undepleted (group 3 of Wyborn *et al.* 1992).

A chondrite normalised REE plot show that each pluton possesses similar REE patterns; steep LREE patterns, significant negative Eu anomalies and relatively flat HREE patterns prevail (Figure 52).

Table 3 Summary of major oxide and trace element characteristics for seven Hiltaba Suite groups.

Pluton	Major oxide characteristics	Trace element characteristics
Kondoolka	Broad compositional range which excluding mafic dykes and diorite enclave range from 67-79% SiO <sub>2</sub> . Pluton shows inverse relationship with decreasing Fe <sub>2</sub> O <sub>3</sub> , TiO <sub>2</sub> , MgO and CaO with increasing SiO <sub>2</sub> . Pluton is dominantly felsic (Na <sub>2</sub> O = K <sub>2</sub> O average = 8.27%). Plot within adamellite-granite field on a CaO-Na <sub>2</sub> O- K <sub>2</sub> O diagram.	Some very high Ba values (2620 ppm) but generally low to moderate Ba values, some high Rb (772 ppm), Sr (700 ppm) and Zr (712 ppm) values.
Childara	Limited compositional range 72-77.9% SiO <sub>2</sub> . Relatively low Al <sub>2</sub> O <sub>3</sub> , Fe <sub>2</sub> O <sub>3</sub> , MgO, CaO, P <sub>2</sub> O <sub>5</sub> . Na <sub>2</sub> O + K <sub>2</sub> O = 8.45. Plot within adamellite-granite fields on a CaO- Na <sub>2</sub> O - K <sub>2</sub> O diagram.	Low V, moderate Ba, Nb, Rb. Low Sr. High Th, U and W.
Meelera	Limited compositional range 70.2-77.2% SiO <sub>2</sub> . Al <sub>2</sub> O <sub>3</sub> varies from 11.3-15.2%. Major oxides including Fe <sub>2</sub> O <sub>3</sub> , CaO, and MgO show inverse relationship with increasing SiO <sub>2</sub> content. Na <sub>2</sub> O + K <sub>2</sub> O = 8.08. Plot within adamellite-granite fields on a CaO- Na <sub>2</sub> O - K <sub>2</sub> O diagram.	Low V and Nb. Moderate to high Ba, moderate Rb, Y and Zr. High Sr, Th and U.
Tolmer	Moderate compositional range – 68.6-75.7% SiO <sub>2</sub> (only 3 samples). Major oxides Fe <sub>2</sub> O <sub>3</sub> , TiO <sub>2</sub> and MgO show inverse relationship with increasing SiO <sub>2</sub> . Na <sub>2</sub> O + K <sub>2</sub> O = 8.09. Plot within granodiorite-adamellite-granite fields on a CaO- Na <sub>2</sub> O - K <sub>2</sub> O diagram.	Low Nb, moderate Ba, Rb, Sr, Th, U and Zr.
Tunkillia	Broad compositional range – 66.7-77.3% SiO <sub>2</sub> . Major oxides Fe <sub>2</sub> O <sub>3</sub> , TiO <sub>2</sub> and MgO show inverse relationship with increasing SiO <sub>2</sub> . Na <sub>2</sub> O + K <sub>2</sub> O = 8.39. Plot within adamellite-granite fields on a CaO- Na <sub>2</sub> O - K <sub>2</sub> O diagram.	Low Nb. Moderate Rb, Sr, Th, U and Zr.
Pureba	Relatively low SiO <sub>2</sub> relative to other plutons. Major oxides Fe <sub>2</sub> O <sub>3</sub> , TiO <sub>2</sub> and MgO show inverse relationship with increasing SiO <sub>2</sub> . Na <sub>2</sub> O + K <sub>2</sub> O = 8.48. Plot within adamellite-granite fields on a CaO- Na <sub>2</sub> O - K <sub>2</sub> O diagram	Relatively high Ba (950 ppm) and Zr (380 ppm) relative to other plutons.
Yathong	High SiO <sub>2</sub> content (av. 76.45 wt%). Major oxides Fe <sub>2</sub> O <sub>3</sub> , TiO <sub>2</sub> and MgO show inverse relationship with increasing SiO <sub>2</sub> . Na <sub>2</sub> O + K <sub>2</sub> O = 8.73. Plot within adamellite-granite fields on a CaO- Na <sub>2</sub> O - K <sub>2</sub> O diagram	Moderate Ba. Low Sr (52.5 ppm)

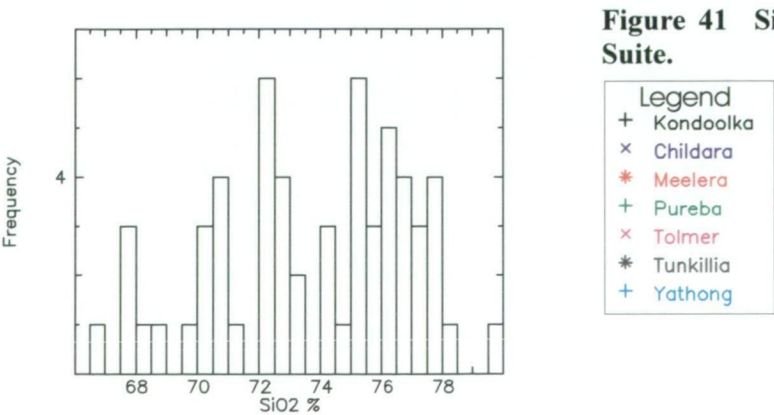
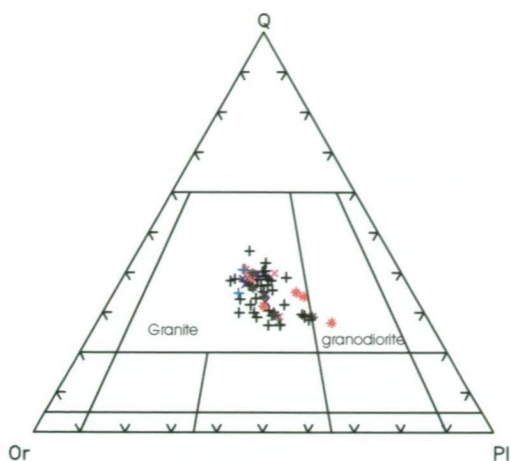


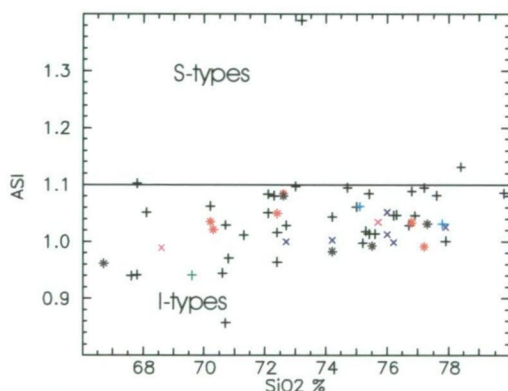
Figure 41 SiO<sub>2</sub> histogram for Hiltaba Suite.



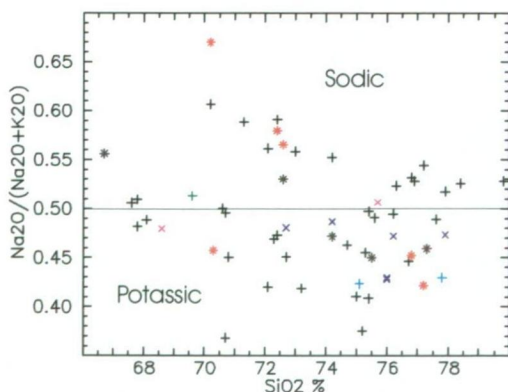


**Figure 42** Streckeisen plot for Hiltaba Suite.

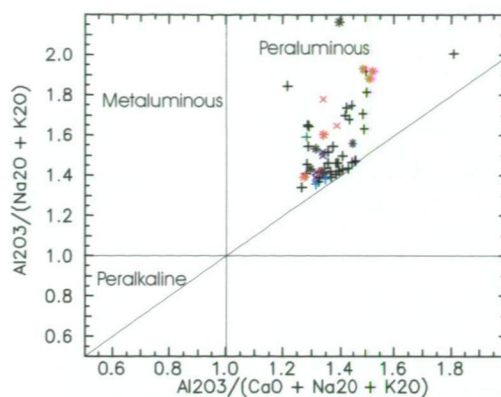
(Legend: A = quartz-rich granitoids, B = alkali-feldspar granite, C = granite, D = granodiorite, E = tonalite, F = alkali-feldspar quartz syenite, G = quartz syenite, H = quartz monzonite, I = quartz monzodiorite/quartz monzogabbro, J = quartz diorite/quartz gabbro/quartz anorthosite, K = alkali-feldspar syenite, L = syenite, M = monzonite, N = monzodiorite/monzogabbro, O = diorite/gabbro/anorthosite.



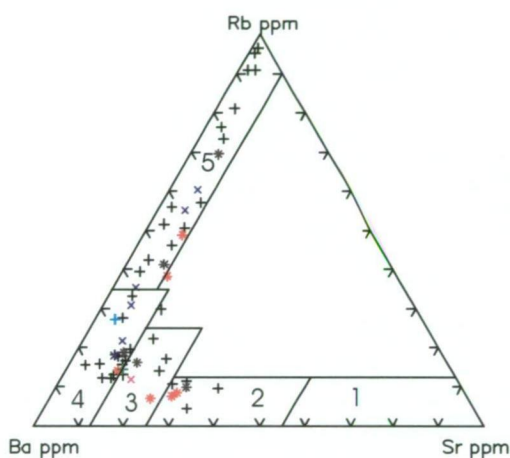
**Figure 43** ASI plot for Hiltaba Suite.



**Figure 44** Na/(Na + K) vs SiO<sub>2</sub> plot for the Hiltaba Suite samples on CHILDARA.

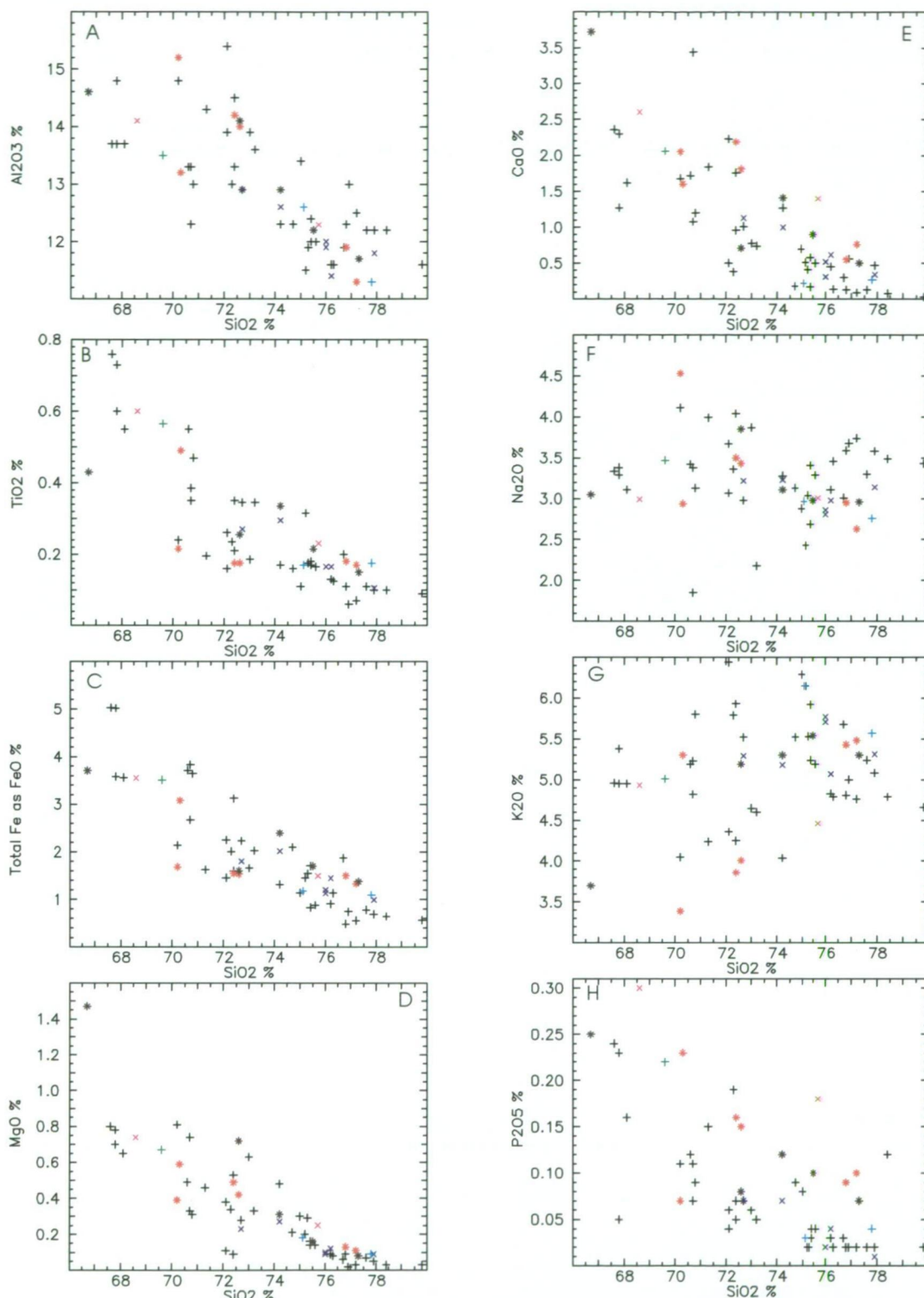


**Figure 45** Molecular Al/(Ca+Na+K) versus Al/(Na+K) plot for the Hiltaba Suite after Maniar and Piccoli (1989).



**Figure 46** Rb-Ba-Sr plot for Hiltaba Suite.

Fields 1 diorites, 2 granodiorites, 3 anomalous granites, 4 normal granites, 5 strongly differentiated granites



**Figure 47 Harker diagrams of major elements vs  $\text{SiO}_2$  for Hiltaba Suite. Elements in wt %.**

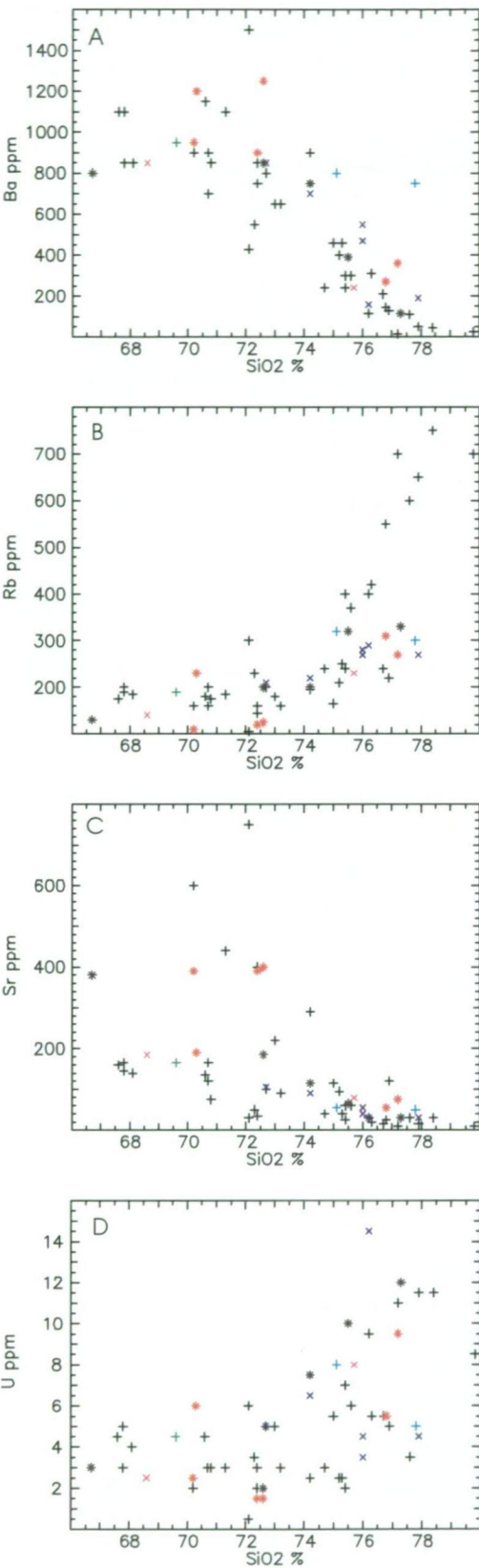


Figure 48 Harker diagrams of trace elements vs SiO<sub>2</sub> for Hiltaba Suite.

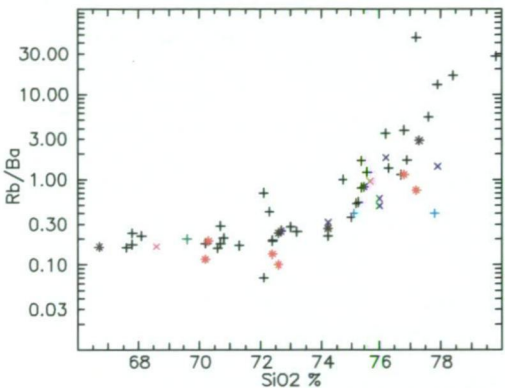


Figure 49 Rb/Ba v SiO<sub>2</sub> plot for Hiltaba Suite.

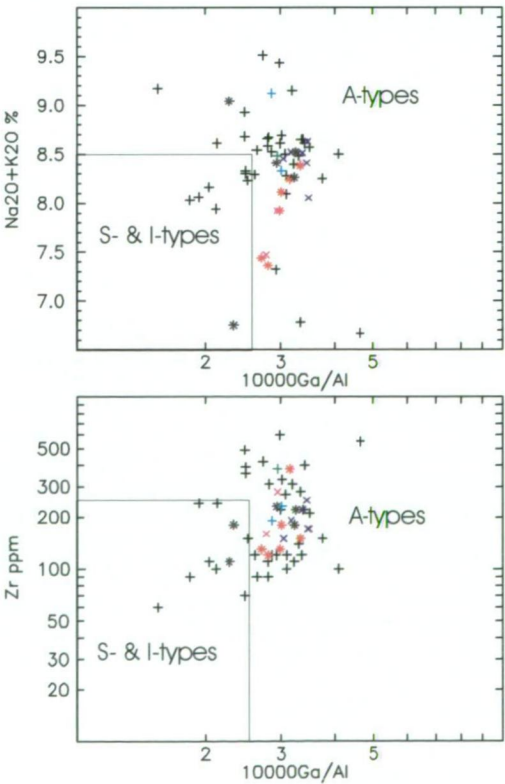


Figure 50 Ga/Al vs Na +K and Zr plots for Hiltaba Suite.

The geology and geochemistry of granitoids in the CHILDARA region, western Gawler Craton, South Australia: implications for the Proterozoic tectonic history of the western Gawler Craton and the development of lode-style gold mineralisation at Tunkillia.



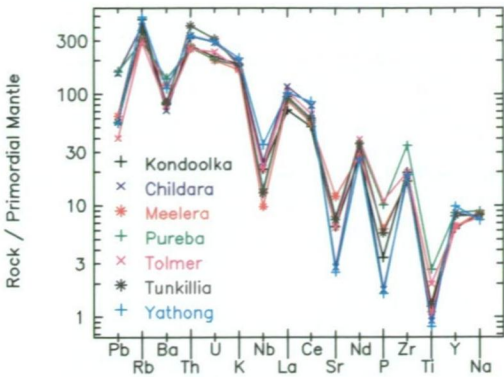


Figure 51 Mantle normalised trace element plot of Hiltaba Suite.

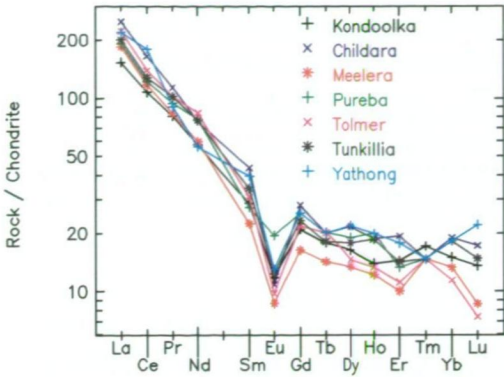


Figure 52 Chondrite normalised REE plot of Hiltaba Suite.

Table 4 Average geochemical values for Hiltaba Suite

	Hiltaba average	Hiltaba average	Hiltaba average	Hiltaba average	Hiltaba average	Hiltaba average	Hiltaba average
Group	Childara (n=6)	Kondoolka (n=36)	Meelera (n=6)	Pureba (n=1)	Tolmer (n=5)	Tunkillia (n=5)	Yathong (n=2)
Major elements (wt%)							
SiO <sub>2</sub>	75.50	73.62	77.8	69.60	72.15	73.26	76.45
Al <sub>2</sub> O <sub>3</sub>	12.10	12.95	11.3	13.50	13.20	13.10	11.95
CaO	0.65	0.93	0.27	2.06	2.00	1.45	0.25
Fe <sub>2</sub> O <sub>3</sub>	1.59	2.18	1.22	3.90	2.81	2.40	1.26
K <sub>2</sub> O	5.39	5.13	5.57	5.01	4.69	5.01	5.86
MgO	0.15	0.31	0.09	0.67	0.50	0.55	0.14
MnO	0.03	0.06	0.02	0.08	0.08	0.05	0.02
Na <sub>2</sub> O	3.04	3.28	2.76	3.47	3.00	3.19	2.87
P <sub>2</sub> O <sub>5</sub>	0.04	0.07	0.04	0.22	0.24	0.12	0.03
TiO <sub>2</sub>	0.19	0.26	0.18	0.56	0.42	0.28	0.17
Na <sub>2</sub> O/K <sub>2</sub> O	0.56	0.64	0.50	0.69	0.64	0.64	0.49
Trace elements (ppm)							
Ba	486.67	559.31	750	950.00	545.00	581.00	775.00
Cr	10.00	17.78	170	30.00	35.00	30.00	90.00
Ga	21.33	19.56	18.00	21.00	20.00	19.20	18.50
Hf	3.83	5.03	5	9.00	6.00	5.20	5.00
Nb	17.50	15.10	25	10.00	15.00	9.20	25.00
Rb	256.67	294.17	300	190.00	185.00	236.00	310.00
Sc	2.50	4.10	2.5	10.00	6.25	4.00	2.50
Sr	58.33	134.72	50.00	165.00	132.50	155.00	52.50
Ta	5.83	1.53	6.0	4.00	7.50	3.80	6.50
Th	30.67	25.03	30.5	24.00	23.25	37.90	30.75
U	6.42	4.75	5	4.50	5.25	6.90	6.50
V	10.00	13.61	10.00	20.00	15.00	16.00	10.00
Y	38.50	28.08	46	39.00	29.50	36.40	44.50
Zr	191.67	219.72	230	380.00	220.00	184.00	210.00
Rare earth elements (ppm)							
Ce	142.50	92.56	155	105.00	120.00	110.40	155.00
Dy	7.42	5.59	7.5	6.50	5.00	6.10	7.50
Er	4.33	3.24	4	3.00	2.50	3.20	4.00
Eu	0.83	0.91	1	1.50	0.75	0.95	1.00
Gd	7.67	5.76	7	7.00	6.00	6.40	7.00
Ho	1.42	1.05	1.5	1.50	1.00	1.40	1.50
La	81.67	50.36	67	63.00	73.00	66.20	72.00
Lu	0.58	0.46	1	0.50	0.25	0.50	0.75
Nd	47.92	36.15	30.50	49.00	52.75	48.30	35.25
Pr	14.50	10.32	10	12.00	13.00	13.00	11.50
Sm	8.83	5.78	7.5	5.50	6.25	6.90	8.00
Tb	1.00	0.89	1	1.00	1.00	0.90	1.00
Tm	0.50	0.58	0.50	0.50	0.50	0.50	0.50
Yb	4.17	3.31	4	4.00	2.50	4.00	4.00
Eu/Eu*	0.29	0.69	0.71	0.74	0.37	0.47	0.40
LaN/Lu <sub>N</sub>	15.29	13.26	21.40	13.09	30.33	16.58	11.48

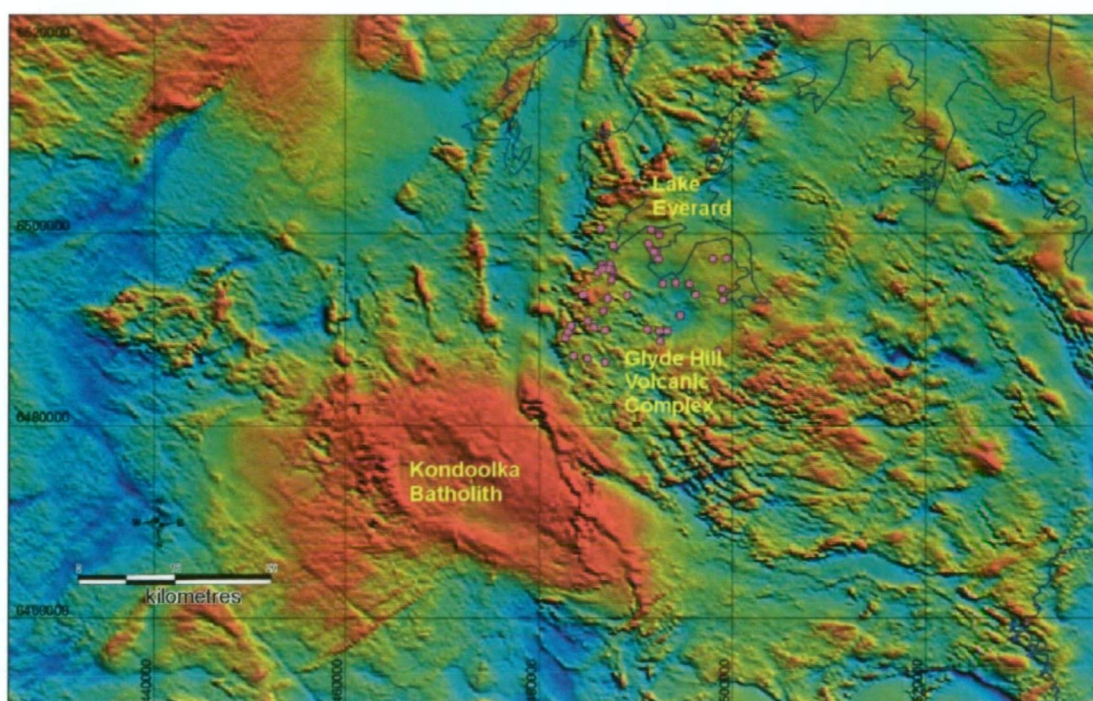
The geology and geochemistry of granitoids in the CHILDARA region, western Gawler Craton, South Australia: implications for the Proterozoic tectonic history of the western Gawler Craton and the development of lode-style gold mineralisation at Tunkillia.

### 3.4.2 Glyde Hill Volcanic Complex

#### 3.4.2.1 Introduction and sampling

The Glyde Hill Volcanic Complex (GHVC) on CHILDARA comprises nine main lithological units shown below, including a sequence of subaerial, dominantly felsic volcanics erupted from a discrete centre located in the Lake Everard area. Table 5 shows average geochemical values for units of the Glyde Hill Volcanic Complex.

Fifty rock chip samples and one drill hole (water well) sample were collected and analysed (see Figure 53 for sample location and Appendix A for geochemical analyses). Selected geochemical analyses from Stewart (1992) and Giles (1980) have been included.



**Figure 53** TMI image showing location of Glyde Hill volcanic samples

#### 3.4.2.2 Chemical variation

SiO<sub>2</sub> content for the GHVC ranges from 50.65 to 80.90 wt. %, with two prominent peaks at 64-65 and 69-71 wt. % (Figure 54). The GHVC plot within the rhyolite, quartz latite, dacite and andesite/basalt fields on a Alkali-lime index plot (Figure 55).

The GHVC plots predominantly within the alkaline field on a SiO<sub>2</sub> versus total alkali plot (Figure 56), whereas the Nuckulla Basalt, Bunburn Dacite and basaltic andesite from the Childera Dacite are sub-alkaline (Figure 56).

Giles (1980) showed the GHVC displayed major element trends broadly comparable to calc-alkaline volcanics, such as decreasing Al<sub>2</sub>O<sub>3</sub>, total Fe, MgO, CaO, TiO<sub>2</sub> and



P<sub>2</sub>O<sub>5</sub>, and increasing K<sub>2</sub>O with fractionation (Fig 58). These trends reflect fractionation of plagioclase, clinopyroxene, magnetite and apatite.

Trace elements including Ba, Ce, Y and Zr show scatter in the data, whereas, Sr and V show a decrease with fractionation (Fig 58). Rb and Th increase with fractionation (Figure 58).

Primordial mantle normalised plot shows the GHVC is depleted in Nb, Sr and Ti and enriched in Rb, Nd and Zr (Figure 59). The Childera and Mangaroongah Dacite are enriched in Ba relative to the other units due to plagioclase fractionation.

The Childera Dacite and Mangaroongah Dacite show similar geochemistry despite having different physical appearance and phenocryst populations. They show similar trends for major elements with the exception of P<sub>2</sub>O<sub>5</sub>. The Childera Dacite shows higher levels of P<sub>2</sub>O<sub>5</sub> at similar SiO<sub>2</sub> content (Figure 57H). Conversely, the Mangaroongah Dacite shows higher Al<sub>2</sub>O<sub>3</sub> content at similar SiO<sub>2</sub> content (Figure 57A).

Chondrite normalised plots show similar trends between units. All units with the exception of the Nuckulla Basalt, are enriched in LREE and show negative Eu anomalies and relatively flat HREE curves (Figure 60).

Giles (1980) reported that the Glyde Hill Volcanic Complex shows evidence for two distinct origins:

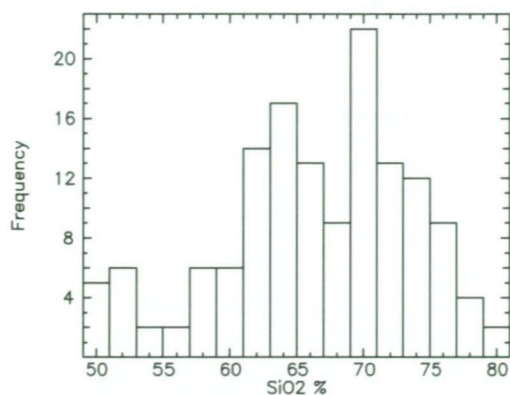
1. Nuckulla Basalt is most likely derived from relatively shallow (<60 km) hydrous melting of a LIL element enriched mantle source; and
2. Felsic units including Childera, Mangaroongah, Bunburn and Whyeela Dacites are derived from melting of a lower crustal, sialic residue of basaltic composition.

The Glyde Hill Volcanics should show similar geochemical trends to the Hiltaba Suite within the surrounding areas due to similar interpreted origins (ie: basaltic underplating of the crust model proposed by Giles, 1988). A SiO<sub>2</sub> histogram of the Glyde Hill Volcanics and Hiltaba Suite show the restricted SiO<sub>2</sub> range of the Hiltaba Suite relative to the Glyde Hill Volcanics (Figure 61). K/Rb ratios show two different trends between the volcanics and granites. The Hiltaba Suite shows decreasing K/Rb ratio with fractionation which indicates K-feldspar accumulation, however, K-feldspar was not an important crystallising phase within the Glyde Hill Volcanics (Figure 62). The origin of the Hiltaba Suite and Gawler Range Volcanics is not the object of this thesis and is the basis of ongoing study. Hence it will only be discussed briefly with reference to the tectonic model put forward in Chapter 5.

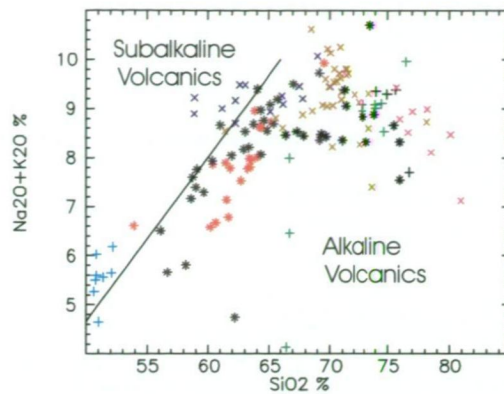
Table 5 Average geochemical values for Glyde Hill Volcanic Complex.

UNIT	Mya Arburee Rhyolite	Myb Bunburn Dacite	Myc Childera Dacite	Mye Wheepool Rhyolite	Myl Baldry Rhyolite	Mym Mangaroongah Dacite	Myn Nuckulla Basalt	Myy Yantea Rhyodacite	Myz Moonamby Dykes
Major elements (wt%)									
SiO <sub>2</sub>	75.36	64.31	62.53	67.36	75.66	62.60	50.90	71.21	71.82
Al <sub>2</sub> O <sub>3</sub>	12.41	16.30	13.90	13.70	12.70	14.53	17.05	13.61	13.05
CaO	0.17	1.04	1.78	1.55	0.42	1.72	6.45	0.46	0.66
Fe <sub>2</sub> O <sub>3</sub>	1.88	4.46	6.03	3.02	1.48	6.25	10.30	3.45	3.02
K <sub>2</sub> O	5.91	4.66	5.46	5.15	5.83	4.91	1.80	6.47	5.64
MgO	0.30	1.78	2.28	1.59	0.25	2.00	5.47	0.57	0.60
MnO	0.03	0.14	0.14	0.09	0.05	0.12	0.17	0.08	0.06
Na <sub>2</sub> O	3.02	4.58	2.70	2.45	2.98	3.52	3.32	2.61	2.92
P <sub>2</sub> O <sub>5</sub>	0.04	0.32	0.50	0.16	0.04	0.42	0.23	0.07	0.08
TiO <sub>2</sub>	0.31	0.76	1.02	0.66	0.17	1.05	1.17	0.41	0.39
Trace elements (ppm)									
Ba	1343.00	1824.25	1991.67		1116.25	3391.67	700.00	1522.22	1460.77
Cr		1.61	16.67	52.78	11.25	10.00	70.00	21.11	13.85
Ga		23.50	24.00		15.00	21.33	25.50	22.00	21.54
Hf		15.00	8.50		5.75	11.17	5.00	12.78	8.92
Nb	23.50	17.55	23.33		25.63	22.50	15.00	29.44	26.54
Rb	171.00	150.82	152.17	204.57	185.38	128.17	57.75	200.56	226.69
Sc	5.50	6.42	14.17		2.50	15.83	25.00	8.33	5.38
Sr	88.75	433.73	227.50	73.86	120.00	282.50	550.00	87.78	121.15
Th		3.54	18.08	19.33	18.06	15.33	6.75	24.56	28.15
U		3.17	2.58	2.94	2.31	2.33	1.00	4.22	4.12
V		23.71	93.33	22.92	13.75	88.33	200.00	15.56	26.15
Y	54.25	40.00	43.50	48.33	27.00	41.00	25.00	45.33	40.54
Zr	294.50	361.64	398.33	367.57	225.00	548.33	220.00	671.11	406.92
Rare earth elements (ppm)									
Ce	125.67	134.00	148.33	125.00	98.13	152.50	64.50	177.22	160.69
Dy	9.30	7.40	8.17	6.10	5.19	8.33	5.00	8.56	7.38
Er		4.00	4.00		2.50	4.17	3.00	4.22	4.00
Eu	1.10	2.25	2.17	1.00	0.47	2.08	1.50	1.83	1.31
Gd		8.20	8.83	6.70	4.88	9.50	5.00	8.89	7.38
Ho		1.50	1.58		1.00	1.50	1.00	1.56	1.50
La	47.00	67.00	72.00	53.50	51.50	76.33	31.50	87.00	83.08
Lu		1.00	0.46		0.31	0.50	0.25	0.61	0.58
Nd	46.67	56.14	53.42	46.00	30.44	57.25	26.50	55.89	47.62
Pr		15.00	12.83		8.50	14.33	6.00	14.67	12.62
Sm	8.10	9.30	3.88	8.20	2.56		2.00	7.89	5.58
Tb			1.42		0.69	1.42	1.00	1.44	1.23
Tm			0.50		0.50	0.50	0.50	0.50	0.50
Yb	4.80	4.02	4.00	3.50	2.50	3.67	2.00	4.22	4.08

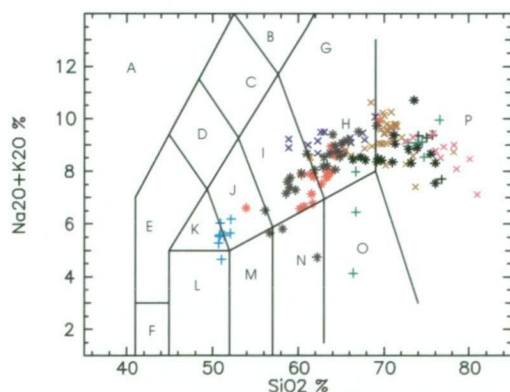
UNIVERSITY OF TADULAKA



**Figure 54**  $\text{SiO}_2$  histogram for Glyde Hill Volcanic Complex.



**Figure 56**  $(\text{Na}_2\text{O} + \text{K}_2\text{O})$  v  $\text{SiO}_2$  diagram for Glyde Hill Volcanic Complex.

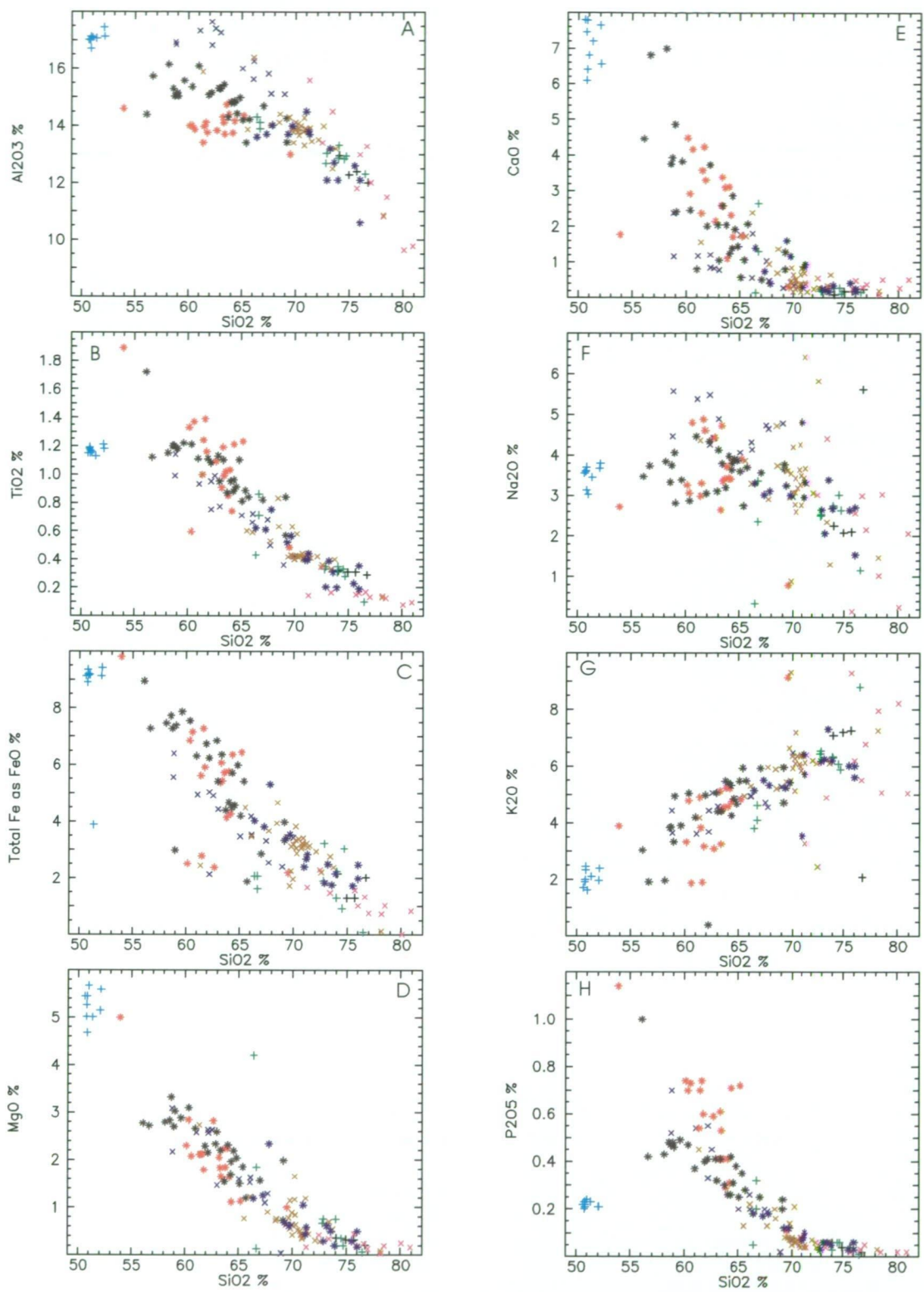


**Figure 55** Alkali-lime variation diagram for the Glyde Hill Volcanic Complex (fields from Le Bas *et al.*, 1986).

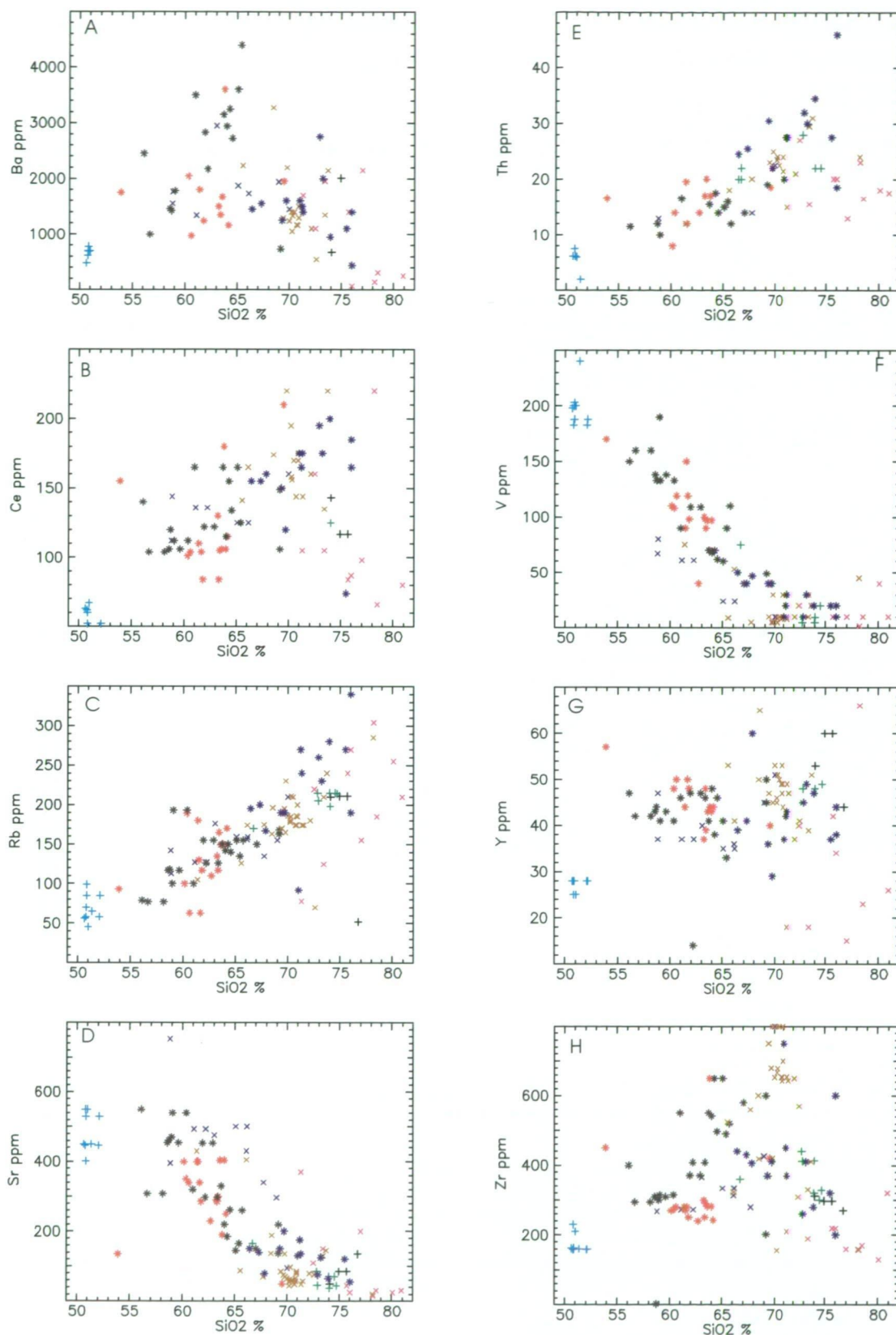
#### Fields

A – foidite, B – phonolite, C – tephriphonolite, D – phonotephrite, E – tephrite, F – picrobasalt, G – trachyte, H – trachydacite, I – trachyandesite, J – basaltic trachyandesite, L – basalt, M – basaltic andesite, N – andesite, O – dacite, P – rhyolite.

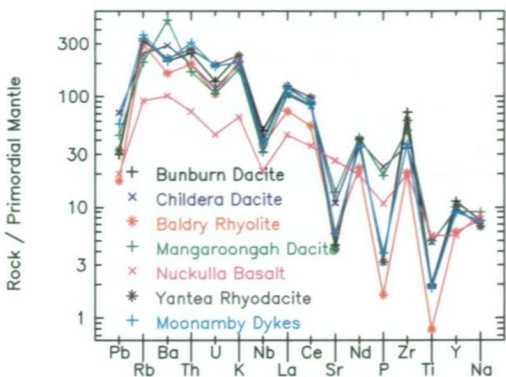




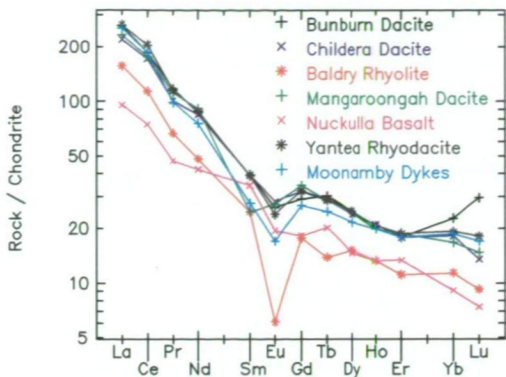
**Figure 57 Harker plots of major elements vs SiO<sub>2</sub> for Glyde Hill Volcanic Complex.**



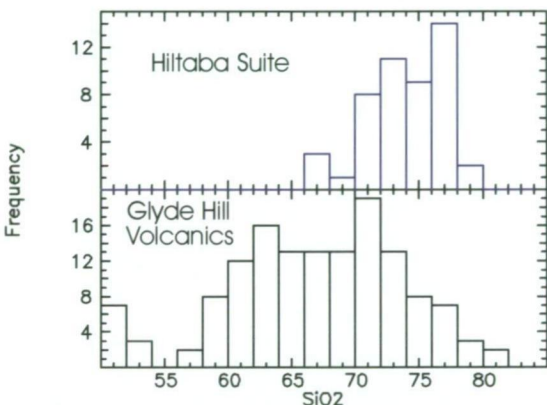
**Figure 58** Harker plots of trace elements vs  $\text{SiO}_2$  for Glyde Hill Volcanic Complex.



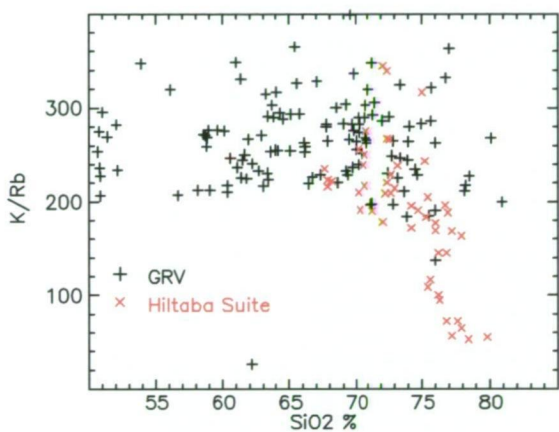
**Figure 59** Primordial mantle normalised plot of trace elements for the Glyde Hill Volcanic Complex.



**Figure 60** Chondrite normalised REE plot for Glyde Hill Volcanic Complex.



**Figure 61** SiO<sub>2</sub> histograms of the Hiltaba Suite and Glyde Hill Volcanics.



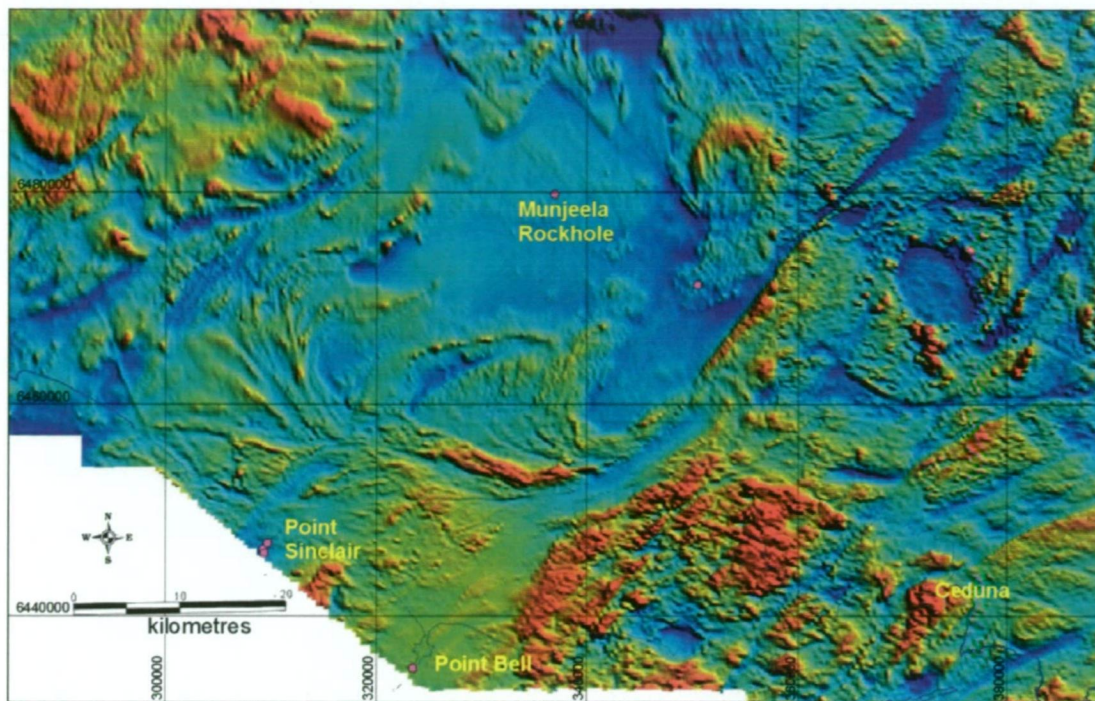
**Figure 62** K/Rb v SiO<sub>2</sub> plot for Hiltaba Suite and Glyde Hill Volcanics.

3.4.3 Munjeela Granite

3.4.3.1 Introduction and sampling

The Munjeela Granite comprises medium to coarse-grained, biotite-muscovite±garnet granite, which crops out at Munjeela Rockhole, Point Bell and Point Sinclair (Figure 63).





**Figure 63** TMI image showing location of Munjeela Granite samples

#### 3.4.3.2 Chemical variation

The Munjeela Granite is enriched in  $\text{SiO}_2$  ranging from 70.4 – 74.5 wt % (Figure 64);  $\text{K}_2\text{O} + \text{Na}_2\text{O}$  values range from 7.87 to 9.06 wt%. The Munjeela Granite plots within the granite field on a Streckeisen (1976) plot (Figure 65) and plots within the strongly differentiated field on a Rb-Ba-Sr diagram (Figure 66). The Munjeela Granite is metaluminous, with all but one sample having ASI values  $>1.1$  (Figure 67). The Munjeela Granite plot, predominantly within the combined S- I-type field on a Ga v Y plot (Whalen *et al.*, 1987)(Figure 68).

Major elements show a decrease with fractionation, except for  $\text{Al}_2\text{O}_3$  and  $\text{K}_2\text{O}$ , which show a scatter of data (not shown). The Munjeela Granite is strongly depleted in Ba, Sr, P, Ti, and is enriched in Rb (Figure 69); it falls within the Sr-depleted and Y-undepleted group 5 of Wyborn *et al.* (1992). The Munjeela Granite is steeply LREE enriched, with relatively flat HREE pattern, and a significant negative Eu anomaly (Figure 70). Depletion of Eu and Sr suggest extensive feldspar fractionation.

The Munjeela Granite is moderately potassic but no alteration is observed. The Munjeela Granite is an, unfractionated, restite rich, S-type granite. It has limited potential to produce metal rich fluids, hence has limited mineralisation potential.

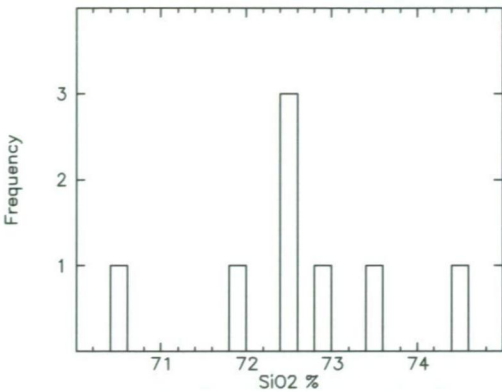


Figure 64 SiO<sub>2</sub> histogram for Munjeela Granite.

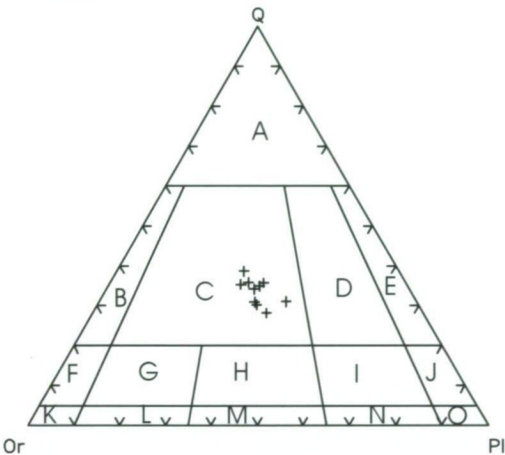


Figure 65 Streckeisen plot of Munjeela Granite.

(Legend: A = quartz-rich granitoids, B = alkali-feldspar granite, C = granite, D = granodiorite, E = tonalite, F = alkali-feldspar quartz syenite, G = quartz syenite, H = quartz monzonite, I = quartz monzodiorite/quartz monzogabbro, J = quartz diorite/quartz gabbro/quartz anorthosite, K = alkali-feldspar syenite, L = syenite, M = monzonite, N = monzodiorite/monzogabbro, O = diorite/gabbro/anorthosite.

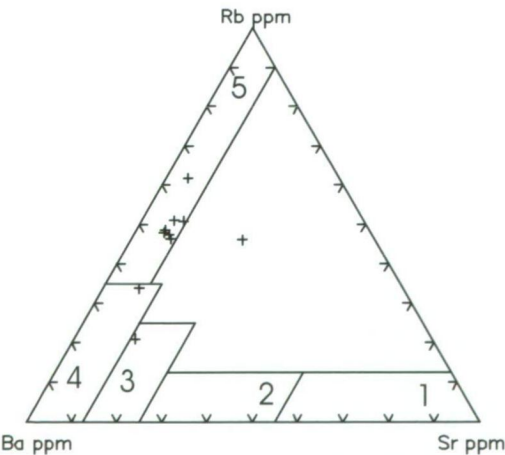


Figure 66 Rb-Ba-Sr plot for Munjeela Granite.

Fields 1 diorites, 2 granodiorites, 3 anomalous granites, 4 normal granites, 5 strongly differentiated granites

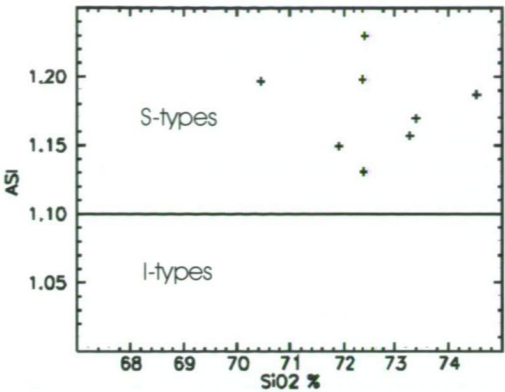


Figure 67 ASI plot for Munjeela Granite.

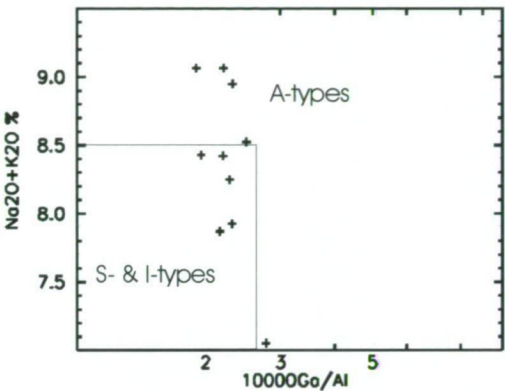


Figure 68 Ga/Al v Na<sub>2</sub>O + K<sub>2</sub>O plot for Munjeela Granite.

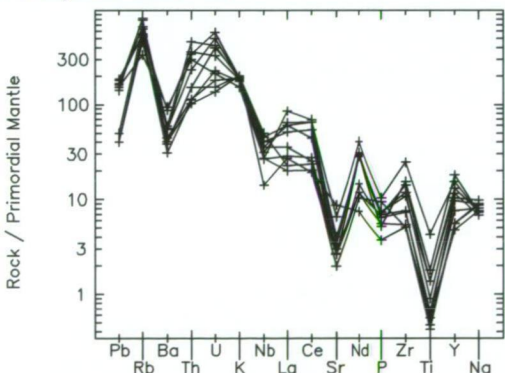


Figure 69 Primordial mantle normalised plot for Munjeela Granite.

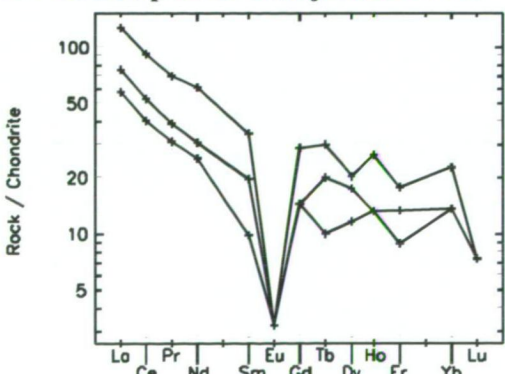


Figure 70 Chondrite normalised plot for Munjeela Granite samples.

The geology and geochemistry of granitoids in the CHILDARA region, western Gawler Craton, South Australia: implications for the Proterozoic tectonic history of the western Gawler Craton and the development of lode-style gold mineralisation at Tunkillia.

### 3.5 Summary and Conclusions

The magmatic evolution of the CHILDARA area can be divided into five main periods;

1. Archaean – early Palaeoproterozoic felsic magmatism (Glenloth Granite at ~2440 Ma);
2. Tunkillia Suite and related intrusives (~1690-1670 Ma);
3. St Peter Suite (~1630-1608 Ma);
4. Hiltaba Suite/Gawler Range Volcanics (~1595-1575 Ma); and
5. S-type Munjeela Granite (~1560 Ma).

The Glenloth Granite crops out north of the Yerda Shear Zone, on northeastern CHILDARA, and does not represent a major component of the basement of CHILDARA. Table 6 summarises the petrological, mineralogical and major element characteristics, and Table 7 summarises the trace element characteristics of each group.

Palaeoproterozoic magmatism on CHILDARA provides a record of crustal evolution spanning approximately 130 million years. During this period, igneous activity was not continuous, but occurred in three distinct phases, and each period contains a unique geochemical signature, enabling discrimination of granitoids based on major, trace and rare earth element chemistry. Prior to this project, limited, poor quality geochemical data existed for the CHILDARA area and western Gawler Craton, with the exception of the Glyde Hill Volcanic Complex (Giles, 1980).

The geochemistry presented in this chapter together with regional tectonics and structural observations presented in Chapter 4, will form the basis for discussing the tectonic framework for the CHILDARA region (Chapter 5).

**Table 6 Petrological, mineralogical and major elements characteristics of granitoids on the western Gawler Craton.**

Group	Rock types	Fe-Mg minerals	Accessory minerals	Other common characteristics	A/CKN	K/Na
Glenloth Granite	Granite, granodiorite	Biotite, hornblende		Contains mafic schlieren	1.05-1.11	0.5-1.15
Tunkillia Suite	Granodiorite, monzogranite, granite, syenite	Biotite, hornblende	Epidote, Apatite, Ilmenite, zircon	Variably deformed,	1.10-1.24	0.6-3.1
St Peter Suite	trondhjemite, tonalite, granodiorite, diorite, gabbro, anorthosite, monzogranite	Clino-pyroxene, biotite, hornblende	Magnetite, sphene, apatite, allanite, zircon, epidote	Show magma mingling textures, variably deformed	0.67->2	0.15-2.7
Hiltaba Suite	Granite, granodiorite, adamellite	Biotite, hornblende	Zircon, fluorite	Variable textures from microgranite to coarse grained, homogeneous to porphyritic	0.86-1.39	1 – 2.6
Munjeela Granite	granite	biotite	Muscovite, garnet, monazite	Mostly undeformed except Point Bell which is within Koonibba Fault Zone, contains mod. abundant metasedimentary enclaves	1.02-1.23	0.8-1.98

The geology and geochemistry of granitoids in the CHILDARA region, western Gawler Craton, South Australia: implications for the Proterozoic tectonic history of the western Gawler Craton and the development of lode-style gold mineralisation at Tunkillia.



**Table 7 Trace element compositions of granitoids from western Gawler Craton.**

Group	REE	HFSE	Rb & Th	LILE	Transition elements
Glenloth Granite	ΣREE 151-161 Ce <sub>N</sub> = 82-88 Yb <sub>N</sub> = 2.4 (Ce/Yb) <sub>N</sub> = 34-37	Nb = <1 Zr = 170 - 180 Y = 8 - 12	Rb = 105-130 Th = 32	Sr = 195-440 Ba = 650-1200	Ni = 5-9 Cr = 20-30
Tunkillia Suite	ΣREE 31-401 Ce <sub>N</sub> = 7-331 Yb <sub>N</sub> = 4-23 (Ce/Yb) <sub>N</sub> = 1.5-30	Nb = <1 - 25 Zr = 70 - 500 Y = 3 - 42	Rb = 44 - 350 Th = 2 - 67	Sr = 25 - 914 Ba = 55 - 4900	Ni = <1 - 11 Cr = 10 - 300
St Peter Suite	ΣREE 26-408 Ce <sub>N</sub> = 3-267 Yb <sub>N</sub> = 0.5 - 55 (Ce/Yb) <sub>N</sub> = 1 - 37	Nb = <1 - 38 Zr = 20 - 650 Y = 2 - 130	Rb = 3 - 417 Th = <1 - 40	Sr = 3 - 1150 Ba = 58 3600	Ni = <1 - 340 Cr = <1 - 600
Hiltaba Suite	ΣREE 39-848 Ce <sub>N</sub> = 23-508 Yb <sub>N</sub> = 5-52 (Ce/Yb) <sub>N</sub> = 4-33	Nb = <1 - 40 Zr = 60 - 600 Y = 3 - 93	Rb = 105 - 750 Th = 3 - 54	Sr = 10 - 750 Ba =	Ni = <1 - 13 Cr = 10 - 170
Munjeela Granite	ΣREE 67-262 Ce <sub>N</sub> = 54-145 Yb <sub>N</sub> = 10-29 (Ce/Yb) <sub>N</sub> = 2-8.5	Nb = 10-42 Zr = 38 - 272 Y = 8 - 81	Rb = 211 - 519 Th = 1 - 42	Sr = 8 - 182 Ba = 100 - 656	Ni = 1 - 11 Cr = 1

The Tunkillia and Hiltaba Suites are high SiO<sub>2</sub> granites and plot within the granite field on a Streckeisen plot (Figure 71). The St Peter Suite exhibits a much wider range of SiO<sub>2</sub> values and plots within the granite, granodiorite to quartz diorite/gabbro fields (Figure 71). Petrologically, the St Peter Suite ranges in composition from gabbro, diorite, tonalite, granodiorite to adamellite. The St Peter Suite shows a much broader compositional range (Figure 72) with SiO<sub>2</sub> values and is similar to the silica distribution observed for the west and central Peninsular Ranges Batholith, of southern and Baja California (Hill *et al.*, 1992). The Tunkillia and Hiltaba Suites show much less compositional variation, from granodiorite to adamellite. The Hiltaba and Tunkillia Suites do contain mafic lithologies, but they are considered a minor component compared to the St Peter Suite.

The St Peter Suite shows tholeiitic characteristics whereas the Tunkillia Suite and Hiltaba Suite plot within the calc-alkaline field on a AFM diagram Irvine and Baragar, 1971; Figure 73). The St Peter Suite is enriched in Al<sub>2</sub>O<sub>3</sub> compared to the Tunkillia and Hiltaba Suites at similar SiO<sub>2</sub> values (Figure 74). The St Peter Suite is also more sodic (Figure 75) and conversely less potassic than the Tunkillia and Hiltaba Suites (Figure 76).

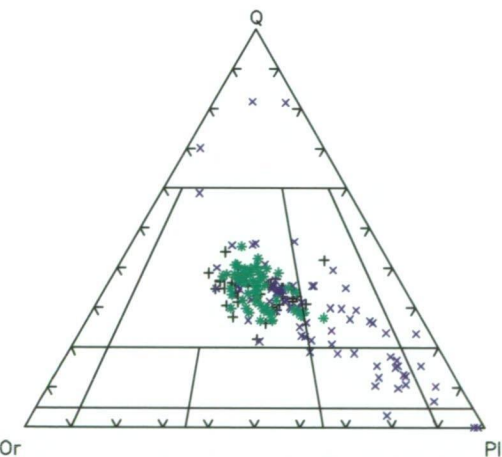
The St Peter Suite shows a considerable range in CaO values plotted against ASI values (Figure 77), whereas the Tunkillia and Hiltaba Suite show a more limited range (Figure 77). The St Peter Suite plots predominantly within the S- and I-type field on a Ga/Al versus total alkali plot; the Tunkillia and Hiltaba Suites plot predominantly within the A-type field (Figure 78).

On mantle normalised trace element plots, the Hiltaba Suite is depleted in Ba, Sr, Ti and enriched in Rb, Th, U and Y, relative to St Peter Suite which is relatively enriched in Sr and depleted in Th (Figure 79). The Hiltaba Suite and Tunkillia Suite are classified as Sr-depleted, Y-undepleted (Group 3 of Wyborn *et al.*, 1992), and the

St Peter Suite is classified as Sr-undepleted to Y-undepleted to Y-depleted (Groups 1 and 2 of Wyborn *et al.*, 1992).

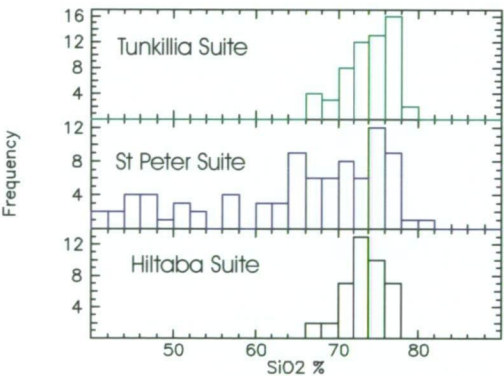
On chondrite normalised REE plots, the Tunkillia and Hiltaba Suites show prominent negative Eu anomalies (Figure 80), whereas the St Peter Suite show no Eu anomaly (Figure 80). The St Peter Suite is also depleted in REE compared to the Hiltaba and Tunkillia Suites. The significance of these geochemical differences will be discussed in more detail in Chapter 5.

Drummond *et al.* (1997) report the Sr/Yb ratio in tonalite magmas correlates with the garnet/plagioclase ratio in the restite, and can be used as a crude barometer for the site of partial melting. Drummond and Defant (1990) reported melting experiments showed that partial melts of basalts result in garnet amphibolite to eclogite restite, and will produce trondhjemitic melts with high Sr/Yb, with Yb efficiently removed by garnet. The resulting melt will become Sr enriched. Zr/Sm is sensitive to the proportion of hornblende, and high Zr/Sm indicates a high proportion of hornblende in the melt (Drummond *et al.*, 1997). The St Peter Suite ranges from low Zr/Sm and high Sr/Yb, suggesting melting of a garnet rich source (Figure 81). The Hiltaba Suite shows low Sr/Yb and variable Zr/Sm, which suggest melting of a basaltic source free of garnet.

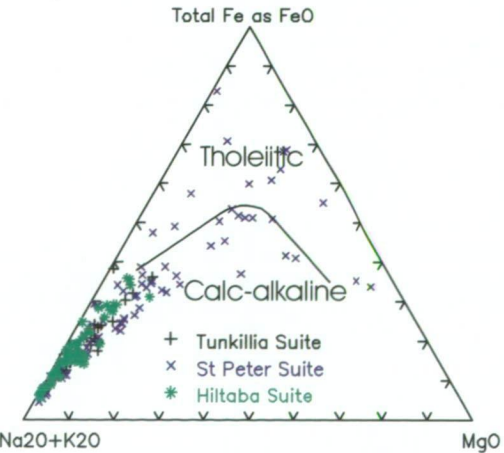


**Figure 71** Streckeisen plot of Tunkillia Suite, St Peter Suite and Hiltaba Suite samples on CHILDARA.

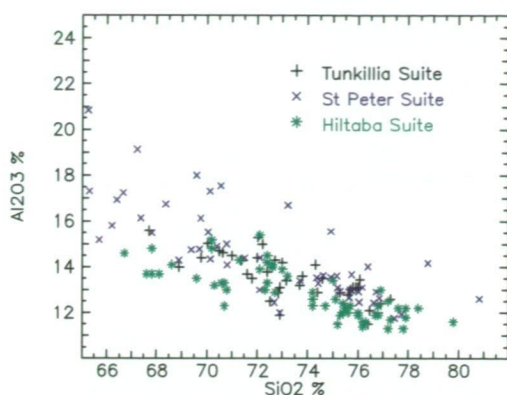
(Legend: A = quartz-rich granitoids, B = alkali-feldspar granite, C = granite, D = granodiorite, E = tonalite, F = alkali-feldspar quartz syenite, G = quartz syenite, H = quartz monzonite, I = quartz monzodiorite/quartz monzogabbro, J = quartz diorite/quartz gabbro/quartz anorthosite, K = alkali-feldspar syenite, L = syenite, M = monzonite, N = monzodiorite/monzogabbro, O = diorite/gabbro/anorthosite.



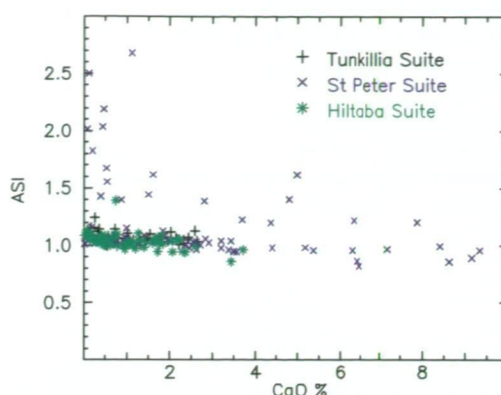
**Figure 72** SiO<sub>2</sub> histogram of Tunkillia Suite, St Peter Suite and Hiltaba Suite samples on CHILDARA.



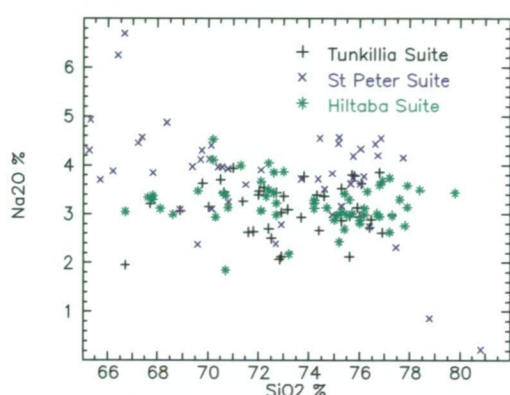
**Figure 73** AFM plot for Tunkillia Suite, St Peter Suite and Hiltaba Suite samples on CHILDARA (fields from Irvine and Baragar, 1971).



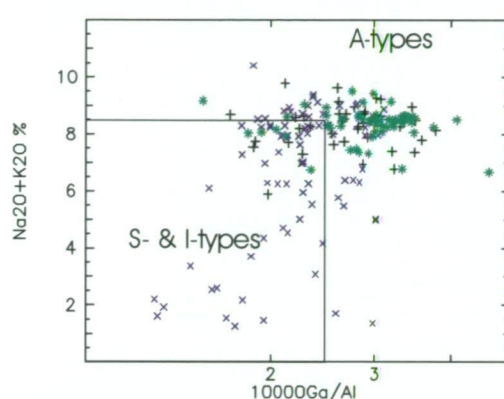
**Figure 74**  $\text{SiO}_2$  v  $\text{Al}_2\text{O}_3$  of Tunkillia Suite, St Peter Suite and Hiltaba Suite samples on CHILDARA.



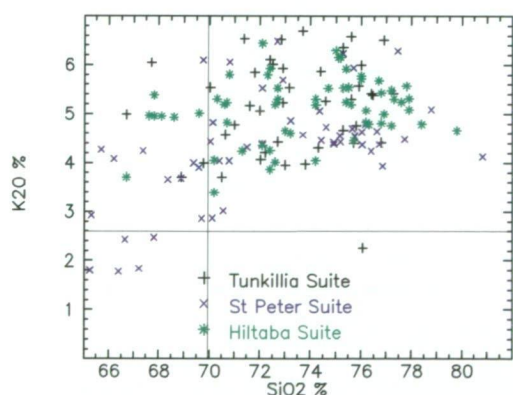
**Figure 77** ASI v CaO plot for Tunkillia Suite, St Peter Suite and Hiltaba Suite samples on CHILDARA.



**Figure 75**  $\text{Na}_2\text{O}$  v  $\text{SiO}_2$  for Tunkillia Suite, St Peter Suite and Hiltaba Suite samples on CHILDARA.



**Figure 78**  $\text{Ga}/\text{Al}$  v  $\text{Na}_2\text{O} + \text{K}_2\text{O}$  for Tunkillia Suite, St Peter Suite and Hiltaba Suite samples on CHILDARA.

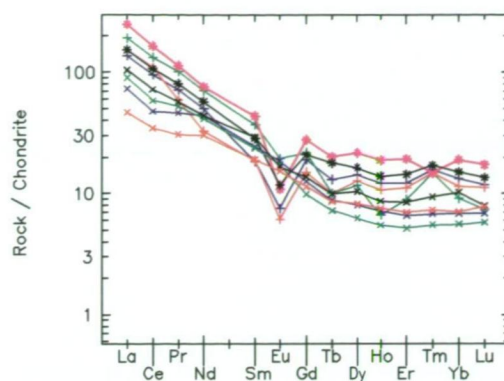


**Figure 76**  $\text{SiO}_2$  v  $\text{K}_2\text{O}$  for Tunkillia Suite, St Peter Suite and Hiltaba Suite samples on CHILDARA.

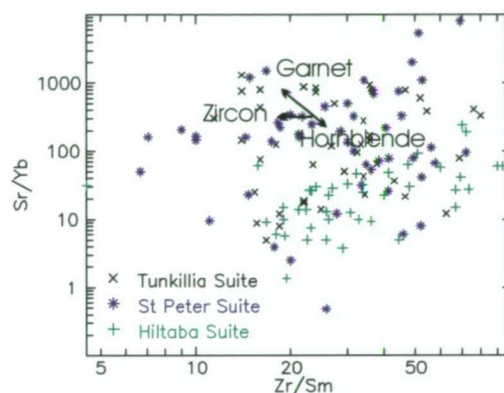




**Figure 79** Primordial mantle normalised plot of average values for selected groups of Tunkillia Suite, St Peter Suite and Hiltaba Suite samples on CHILDRAR.



**Figure 80 Chondrite mantle normalised plot of average values for selected groups of Tunkillia Suite, St Peter Suite and Hiltaba Suite samples on CHILARA.**



**Figure 81 Zr/Sm v Sr/Yb plot for Tunkillia Suite, St Peter Suite and Hiltaba Suite from CHILDARA.**

## Chapter 4 Regional Tectonics and Structural Geology

### 4.1 Introduction

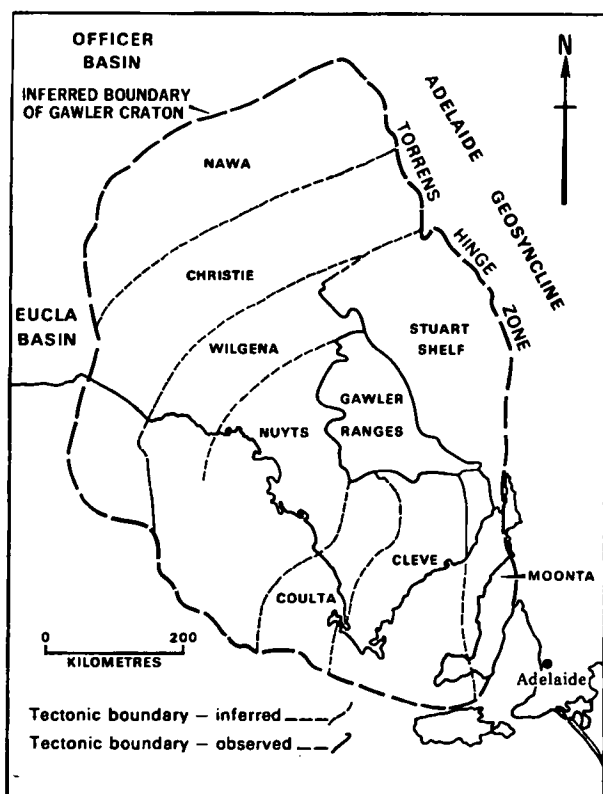
This chapter outlines the regional tectonic framework and present structural data collected during regional mapping in order to determine the timing of deformational events. Chapter 5 discusses the tectonic development specifically of the CHILDARA area, incorporating the granite geochemistry presented in Chapter 3 and structural data presented in this chapter.

### 4.2 Tectonic Subdomains of the Gawler Craton

Thomson (1980) and Parker (1990) divided the Gawler Craton into tectonic subdomains based on structural, metamorphic and stratigraphic characteristics (Figure 82). Teasdale (1997) defined three new subdomains, the Fowler, Coober Pedy and Lincoln Subdomains (Figure 83). The major geological features of each Subdomain are outlined below;

- Christie Subdomain – Archaean to Palaeoproterozoic rocks which comprise the original protolith, on which other units were deposited/incorporated (Parker, 1993; Teasdale, 1997). Major rock units include low magnetic intensity Mulgathing Complex granitoid units, linear highly magnetic zones of banded iron formation and ultramafic rocks, including peridotite, and highly magnetic ~1690-1670 Ma intrusives. The western boundary is the Karari Fault Zone and the eastern boundary is the Coorabie and Tallacootra Shear zones (Figure 83);
- Wilgena Subdomain – originally defined by Parker (1990) as a large northeast trending zone (Figure 82). Teasdale (1997) subdivided the Wilgena and part of the Christie Subdomains into the Christie, Fowler and Coober Pedy Subdomains (Figure 83), based on different metamorphic histories. The Wilgena Subdomain comprises high magnetic intensity metasediments, including banded iron formation, intruded by large elliptical Hiltaba Suite plutons. Boundaries are the Coorabie Shear Zone to the north and west, Yerda Shear Zone to the south and the Stuart Shelf to the east (Figure 83);
- Coober Pedy Subdomain – comprises sinuous, high magnetic intensity, iron-rich metasedimentary granulites. The northern boundary is the Karari Fault Zone and the southern boundary is the Tallacootra and Coorabie Shear Zones (Figure 83);
- Fowler Subdomain – comprises a northeast trending sinuous high magnetic intensity belt of Palaeoproterozoic igneous and metamorphic rocks. Boundaries are the Karari Fault Zone to the west and the Coorabie Shear Zone to the east (Figure 83). The Fowler Subdomain was previously termed the Fowler Suture Zone (Daly *et al.*, 1995), but is more recently described as the Fowler Orogenic Belt (Daly *et al.*, 1998);
- Nuyts Subdomain – comprises possible Palaeoproterozoic, ductile deformed metasediments or meta-igneous rocks into which variably magnetic, Palaeoproterozoic to Mesoproterozoic granitoid units were emplaced. It is bound to the north by the Yerda Shear Zone, and the west by the Coorabie Shear Zone. The overlying Gawler Range Volcanics obscure the eastern boundary (Figure 83);
- Cleve Subdomain – comprises basinal sediments of the Hutchinson Group, deformed during the Kimban Orogeny, also associated with significant granite

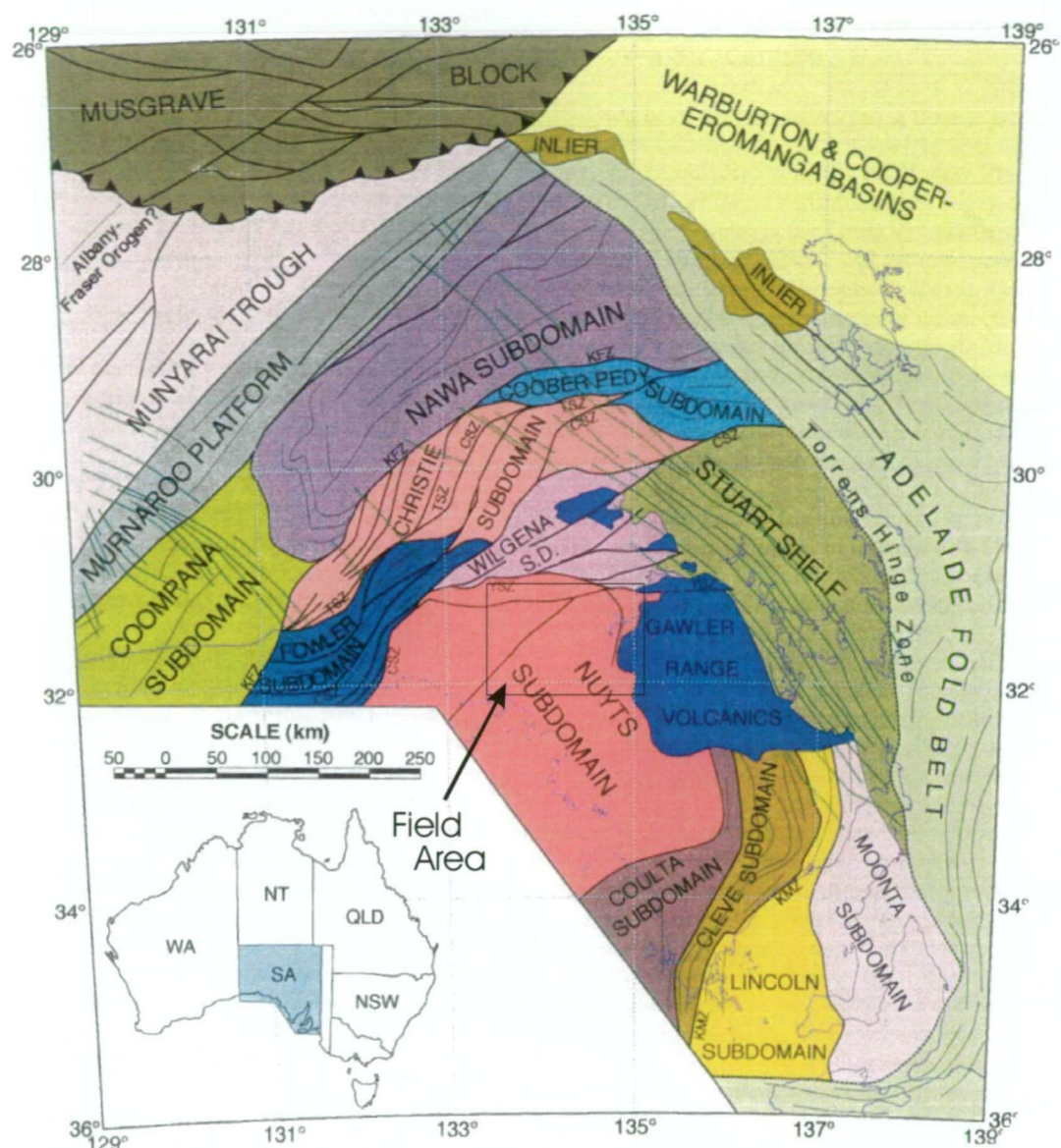
- magmatism (Lincoln Complex). The Cleve Subdomain is separated from the Coultas Subdomain by a major northeast trending shear zone (Figure 83);
- Coultas Subdomain – consists of Archaean to Palaeoproterozoic rocks, which comprise the original protolith on which younger units of the southern Gawler Craton were imposed (Teasdale, 1997). Dominated by Sleaford Complex and Dutton Suite intrusives. The northern boundary is inferred to be an east-west trending shear zone stitched by Hiltaba Suite plutons;
  - Moonta Subdomain – comprises high magnetic intensity Palaeoproterozoic metasediments and volcanics, and Mesoproterozoic Hiltaba Suite granite. Separated from the Lincoln Subdomain by an interpreted shear zone stitched by Hiltaba Suite plutons (Figure 83);
  - Lincoln Subdomain – comprises irregularly shaped Donnington Suite granitoids, separated from the Cleve Subdomain by the Kalinjala Mylonite Zone (Figure 83);
  - Nawa Subdomain – comprises a massive crustal block which appears unaffected by major shear zones. Bound to the northwest by the Murnaroo Platform, the Karari Fault Zone to the south and the Torrens Hinge Zone to the northeast. The Nawa Subdomain is separated from the Coompana Subdomain by an inferred shear zone (Figure 83);
  - Coompana Subdomain – comprises complex, heterogeneous magnetic anomalies.
  - Stuart Shelf – comprises a thick sequence of Mesoproterozoic to Neoproterozoic sediments which overlie interpreted Hiltaba Suite plutons (Figure 76);
  - Gawler Ranges Volcanics – large area of dominantly felsic volcanics which are relatively undeformed (Figure 83); and
  - Murnaroo Platform and Munyari Trough may form part of the Gawler Craton but are deeply buried by Officer Basin sediments (Figure 83).



**Figure 82 Tectonic Subdomains of the Gawler Craton (Parker, 1990).**

The geology and geochemistry of granitoids in the CHILDARA region, western Gawler Craton, South Australia: implications for the Proterozoic tectonic history of the western Gawler Craton and the development of lode-style gold mineralisation at Tunkillia.





**Figure 83** Revised tectonic Subdomains of the Gawler Craton (modified from Teasdale, 1997). Inset box shows current study area.

#### 4.3 Tectonic/tectonothermal Events on the Gawler Craton

Three major megacycles or tectonic events have been outlined for the formation of the Gawler Craton (Fanning *et al.*, 1988):

1. 2700 - 2300 Ma - Late Archaean sedimentation and volcanism followed by early Palaeoproterozoic plutonism and metamorphism (Sleaford Orogeny);
2. 2000 - 1700 Ma - initial basin/platform sedimentation followed by widespread plutonism, metamorphism and deformation (Kimban Orogeny) with local volcanism and continental sedimentation; and
3. 1650 - 1450 Ma - anorogenic acid magmatism including extensive felsic volcanism, high level granite plutonism and local intracontinental clastic sedimentation.

The geology and geochemistry of granitoids in the CHILDARA region, western Gawler Craton, South Australia: implications for the Proterozoic tectonic history of the western Gawler Craton and the development of lode-style gold mineralisation at Tunkillia.

Teasdale (1997) outlined five major tectonothermal cycles specifically for the western Gawler Craton:

1. late Archaean – early Proterozoic (~3.0 – 2.4 Ga) cycle involving sedimentation, complex ductile deformation and granulite facies metamorphism (Sleaford Orogeny);
2. magmatism, high-grade metamorphism and deformation during a late Palaeoproterozoic orogeny (1.74 – 1.65 Ma);
3. massive anorogenic, felsic magmatism at 1.63 – 1.58 Ga;
4. high-grade metamorphism and deformation during a compressional orogeny at 1.54 – 1.49 Ma; and
5. the amalgamation and reworking of the western Gawler Craton along major shear zones at 1.2 – 1.1 Ga.

The last tectonothermal cycle outlined by Teasdale (1997) is based on Kober and SHRIMP zircon dating of late-kinematic aplite dykes in the Lake Tallacootra area. Zircons yielded a Kober Pb-Pb age of  $1175 \pm 17$  Ma and a concordant SHRIMP U-Pb age of ~1180 Ma. Some coarser grained zircons recorded ages of ~1550-1600 Ma, ~1810 Ma, ~2100 Ma and ~2440 Ma, which are interpreted to be inherited components (Teasdale, 1997). Teasdale (1997) suggests that the Gawler Craton was “cratonised” at ~1100 Ma. Teasdale (1997) further suggests that no northwestern boundary exists for the Gawler Craton, with continuous basement rocks extending northwards, and including the Musgrave Block and the Albany Fraser Province, thereby suggesting that the notion “that the Gawler is a craton is somewhat flawed” (Teasdale, 1997; p130), even though they have different tectonic histories.

Fanning (PRISE, pers. comm., 2000) suggested the zircons dated by Teasdale may not have been magmatic zircons and appear to have been reworked or extensively corroded. Ar-Ar dating of biotite grown within the fabric at Lake Tallacootra gave preliminary results of ~1450 Ma (G. Fraser, AGSO, pers. comm., 2001; C.M. Fanning, PRISE, pers. comm., 2001), with no 1100 Ma data.

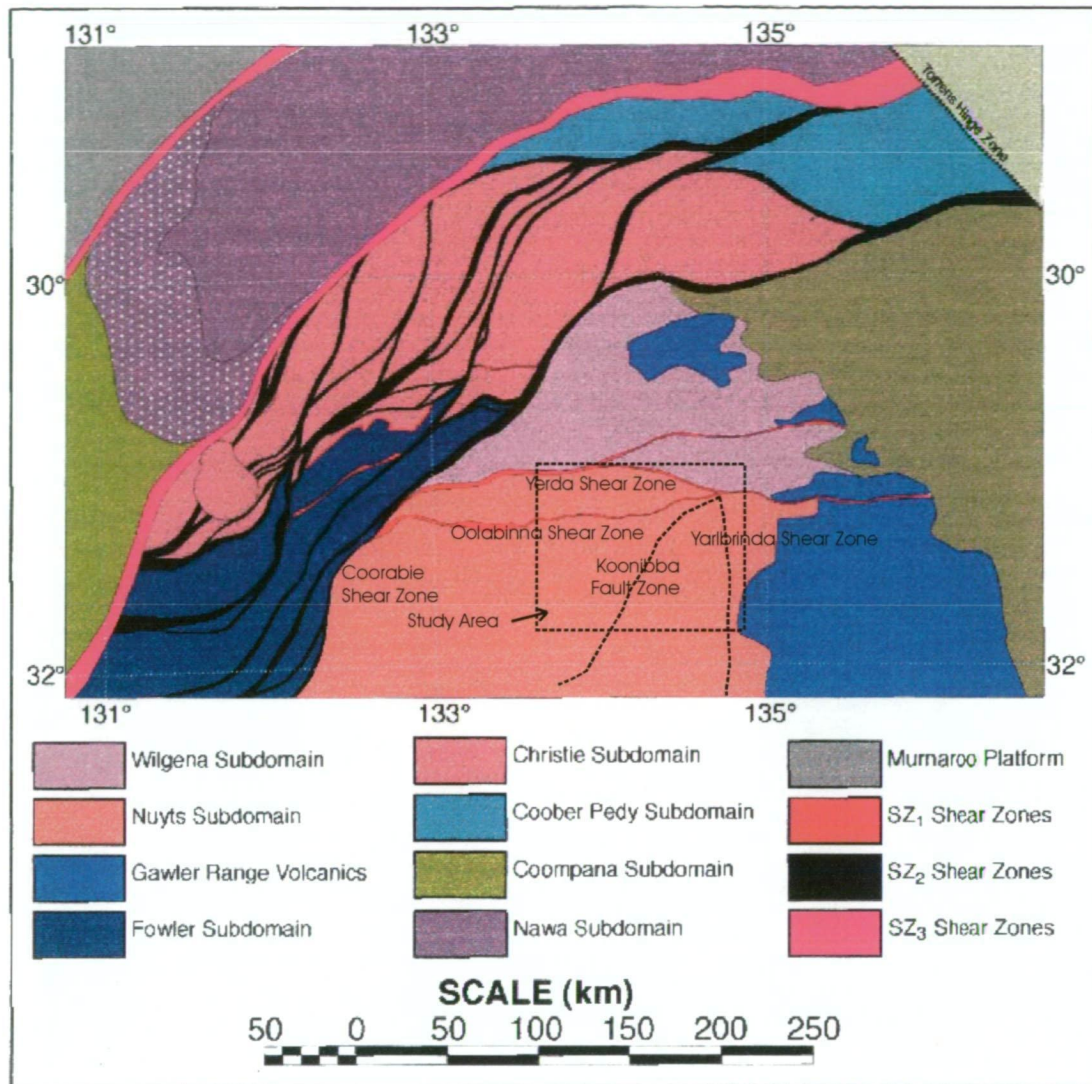
Based on this study, the Gawler Craton was “cratonised” during the Mesoproterozoic and was syn-tectonic with the emplacement of the early Hiltaba Suite granites. Daly *et al.* (1998) report deformed Hiltaba Suite granite from the Fowler Orogenic Belt and U-Pb dating has shown deformed Hiltaba Suite within the Yerda Shear Zone (this study).

#### 4.4 Shear Zones on the Western Gawler Craton

Teasdale (1997) delineated three generations of major craton-scale shear zones, which form the tectonic framework for the western Gawler Craton (Figure 84):

1. SZ<sub>1</sub> – early east-west trending shear zones;
2. SZ<sub>2</sub> – dominant set of northeast trending shear zones; and
3. SZ<sub>3</sub> - Karari Fault Zone.





**Figure 84** Shear Zones on the western Gawler Craton (modified from Teasdale, 1997).

The relative timing for each set of shear zones can be determined via crosscutting relationships and include;

- **SZ<sub>1</sub>** shear zones were active during the early stages of the Hiltaba Suite/Gawler Range Volcanic magmatic event. Magmatic zircons from a granodiorite within the east-west trending Yorda Shear Zone gave an interpreted crystallisation age of  $1592 \pm 11$  Ma.
- **SZ<sub>2</sub>** shear zones postdate:
  - ~1670 Ma Tunkillia Suite,
  - ~1590 Ma Hiltaba Suite granite,
  - SZ<sub>1</sub> east-west shear zones,
- **SZ<sub>3</sub>** (Karari Fault Zone) postdates the northeast trending SZ<sub>2</sub> shear zones,
- Both SZ<sub>2</sub> and SZ<sub>3</sub> shear zones predate the ~800 Ma Gairdner Dyke Swarm (Teasdale, 1997).

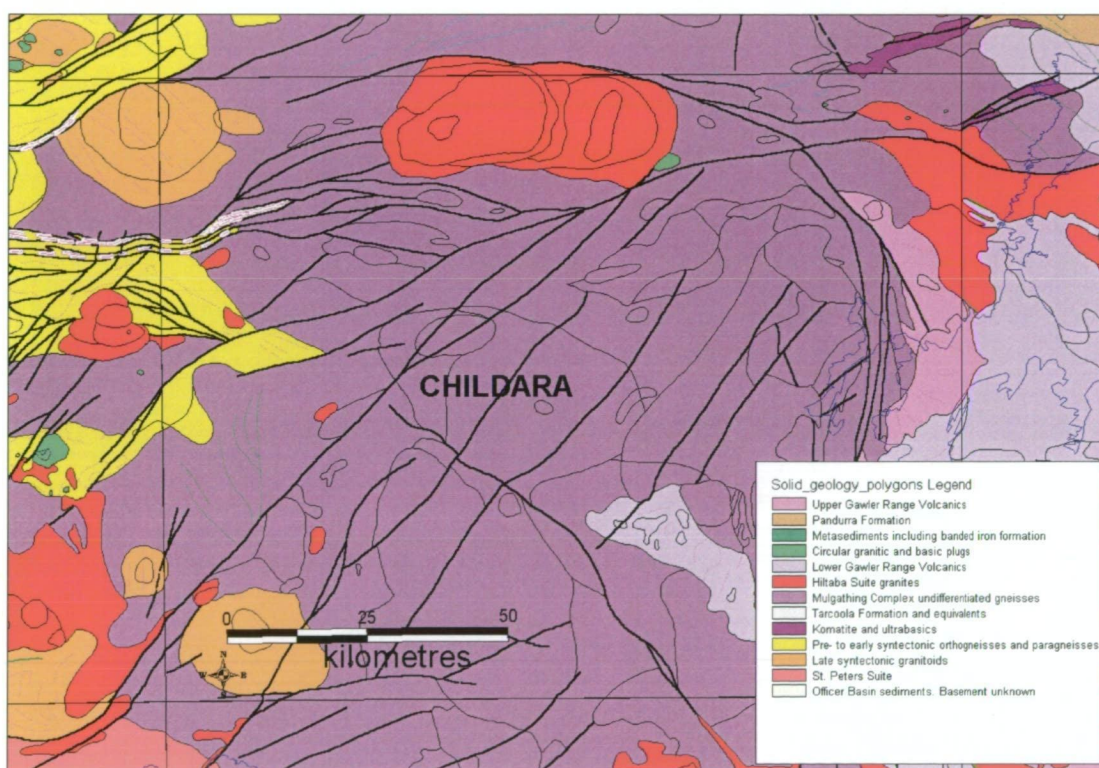
#### 4.5 Regional tectonics of the CHILDARA Area

An interpretation of basement geology for CHILDARA from the PIRSA, western Gawler Craton data set is shown in Figure 85 (Fairclough and Daly, 1994). An

The geology and geochemistry of granitoids in the CHILDARA region, western Gawler Craton, South Australia: implications for the Proterozoic tectonic history of the western Gawler Craton and the development of lode-style gold mineralisation at Tunkillia.



updated interpretation was produced as part of this project and is presented as Plan 2. The northeastern portion of the map sheet area lies within the Wilgena Subdomain, with the remainder being assigned to the Nuyts Subdomain. Parker (1990) defined the Koonibba Fault as the boundary between the Nuyts Subdomain and the Wilgena Subdomain to the west, but Teasdale (1997) interpreted the Coorabie Shear Zone as the boundary between the Nuyts and Fowler Subdomains. Based on regional mapping, the latter interpretation is favoured here due to the presence of St Peter Suite to the west of the Koonibba Fault and interpreted similar tectonic histories. The Fowler Subdomain was originally placed within the Christie Subdomain (Parker, 1990), but Teasdale (1997) showed the Christie, Wilgena and Fowler Subdomains have undergone different structural and metamorphic histories. Prominent mafic intrusives are seen on the aeromagnetics to the west of the Koonibba Fault Zone, and are thought to be part of the St Peter Suite. Hence the Koonibba Fault Zone does not represent a major crustal-scale fault or terrain boundary, but was an important structure during Mesoproterozoic terrain amalgamation.



**Figure 85 Interpretation of the basement geology of CHILDARA (Fairclough and Daly, 1994).**

#### 4.5.1 Description of rock units

The oldest basement for the Nuyts Subdomain is interpreted to be Palaeoproterozoic, ductily deformed metasediments and meta-igneous rocks. These do not outcrop, but are found as enclaves within younger rocks. These rocks are probably more extensive than is interpreted, but the dominant rock type of the Nuyts Subdomain appears to be granitoid intrusives. An east-west trending zone of low magnetic intensity, ductily deformed rocks are interpreted to represent these older metasediments (Plan 2).

West of Childara Outstation, an outcrop of relatively massive Tunkillia Suite granite, contains enclaves of andalusite-biotite hornfels, which suggests that the granite has stopped out high aluminium wall rocks, most probably metasediments, during emplacement. The western end of the Kondoolka Pluton contains a large enclave of meta-siltstone and meta-conglomerate (see Plate 4). Granite at Point Sinclair contains numerous enclaves of interpreted metasediments. The most conspicuous is the “magic carpet”, a rectangular enclave of metasedimentary quartz-feldspar-biotite-garnet schist (see Plate 3). St Peter Suite granite intrudes highly deformed metasediments at Rocky Point (Teasdale, 1997).

The Tunkillia Suite comprises variably magnetic I-type igneous intrusives. However, granite within the Yarlbirinda Shear Zone characteristically exhibits low magnetic intensity, which is interpreted to be the result of high strain and hydrothermal alteration (demagnetisation) of magnetite to haematite (Martin, 1996).

The St Peter Suite includes:

- very high magnetic intensity mafic/ultramafics near Kalanbi;
- high magnetic intensity, complexly mingled granite and mafics along the coast (ie: Rocky Point and Kalanbi area);
- low to moderate magnetic intensity granite;
- low magnetic intensity granite.

U-Pb dating suggests that the St Peter Suite magmatism is more widespread than previously thought and represents a major magmatic event on the western Gawler Craton.

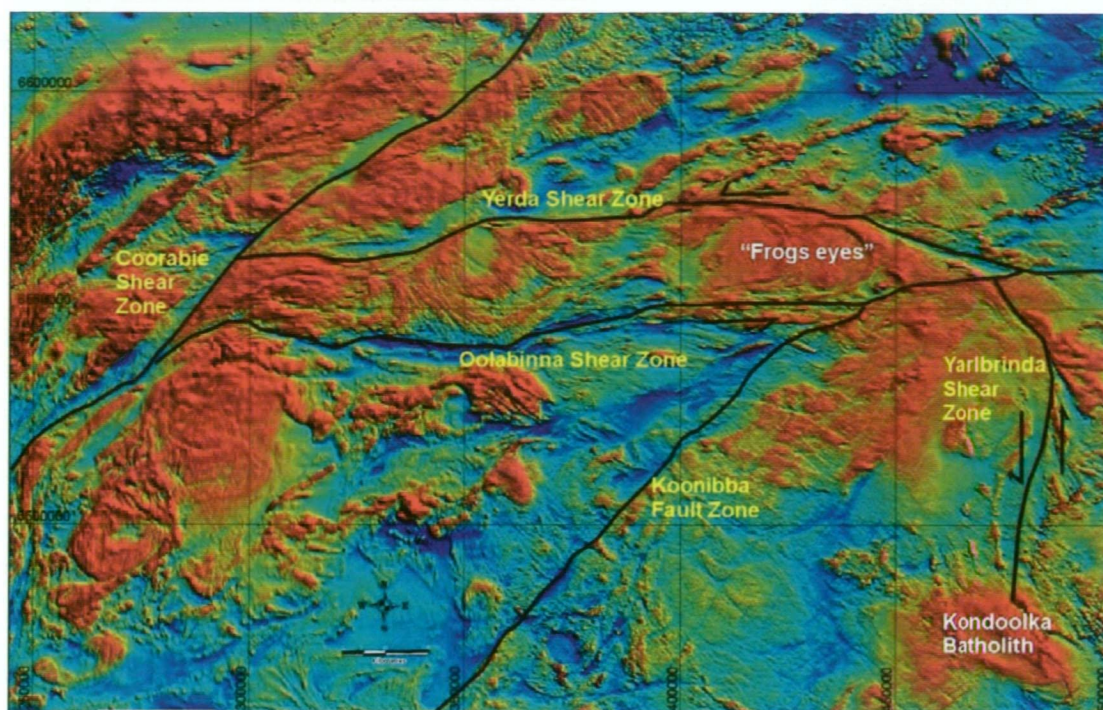
Granitoids of the Hiltaba Suite range from narrow zones of very high magnetic intensity along pluton margins to cores of low magnetic intensity.

The Munjeela Granite forms large regional plutons of low magnetic intensity on FOWLER. On CHILDARA, the Munjeela Suite forms two small plutons related to movement on the Koonibba Fault Zone, which are characterised by low magnetic intensity dilatational zones (Plan 2).

#### 4.6 Regional shear zones

Regional shear zones are prominent features on aeromagnetic images of the western Gawler Craton, with some representing tectonic subdomain boundaries. Within the study area, the Yarlbirinda and Yerda Shear Zones and the Koonibba Fault Zone are the major shear zones (Figure 86). The Oolabinna Shear Zone (new name) is a newly defined shear zone to the south of the Yerda Shear Zone (Figure 86) which is associated with the Yerda Shear Zone. The Yerda Shear Zone is interpreted to represent a major crustal scale shear zone, which separates the Nuyts and Wilgena Subdomains separating Archaean rocks within the Wilgena Subdomain from Palaeo- to Mesoproterozoic rocks within the Nuyts Subdomain. The Yarlbirinda Shear Zone and Koonibba Fault Zone are interpreted as shallower zones of deformation. Many of the shear zones show areas of intense alteration/ demagnetisation, which are now areas of low magnetic intensity.





**Figure 86** TMI image showing major shear zones on CHILDARA.

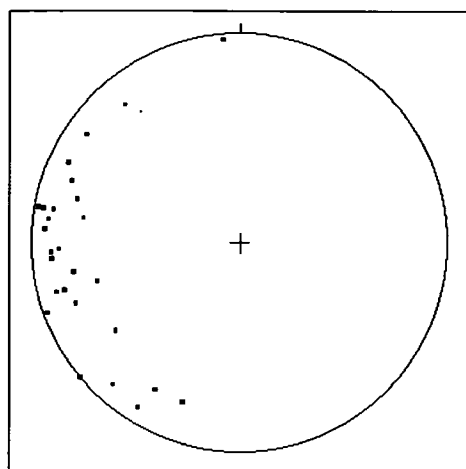
#### **4.6.1 Yarlbirinda Shear Zone**

The Yarlbirinda Shear Zone is approximately 150 km in length and up to 12 km wide at the widest point, but is generally ~4 km wide (Figure 86). The Yarlbirinda Shear Zone is a brittle-ductile fault zone, which separates the western edge of the Gawler Range Volcanics from Tunkillia Suite and St Peter Suite granitoids. The Yarlbirinda Shear Zone trends roughly north–south, but curves to the northwest on northern CHILDARA, and intersects the Koonibba Fault and Yerda Shear Zones (Figure 86).

The Yarlbirinda Shear Zone consists of a foliated and lineated zone of deformation striking N-S to NNW-SSE. Foliations within the Yarlbirinda Shear Zone are shown in Figure 87. Throughout the shear zone the foliation is subvertical, and S-C fabrics and rotated porphyroclasts show that the shear zone records a dextral sense of shear (Simpson and Schmid, 1983; Passchier and Simpson, 1986; Hanmer and Passchier, 1991). Plates 47 to 50 show rotated porphyroclasts showing dextral sense of shear from outcrops within the Yarlbirinda Shear Zone.

Within the Yarlbirinda Shear Zone, the style of deformation varies along strike. The dominant foliation within the granitoids is defined by the orientation of deformed/recrystallised quartz and aligned biotite flakes. Feldspar grains are generally well preserved. Plagioclase often shows evidence of sericite alteration, but K-feldspar grains are less deformed and form prominent augen up to 20 mm in length. At Yarlbirinda Hill (Location 11 on Figure 89), feldspar grains are extensively fractured within a brittle deformation regime which crosscuts the mylonitic foliation.





**Figure 87 Equal area stereoplots of poles to the regional foliation within the Yarlbirinda Shear Zone.**

At Tunkillia, K-feldspar grains within protomylonitic rocks are present as coarse augen that are mostly unaltered, whereas, plagioclase grains are commonly extensively sericitised. Within the Yarlbirinda Shear Zone, all types of mylonite are seen from protomylonite to ultramylonite, with narrow zones of phyllonite present at Tunkillia.

Outcrops near Childera airstrip and Lakeside (Figure 89) show a moderately well developed S-C foliation (Lister and Snoke, 1984). At Lakeside, the foliation strikes  $340^{\circ} - 010^{\circ}$  and dips steeply to the west. Asymmetric porphyroclast tails show the fault zone had a dextral sense of shear. The medium-grained granite at Lakeside is not as well foliated as the orthogneiss, and in places shows evidence of west side-up dip-slip movement. Rhyolite dykes within one outcrop near Childera airstrip show evidence of dip-slip deformation, with a west side-up sense of movement.

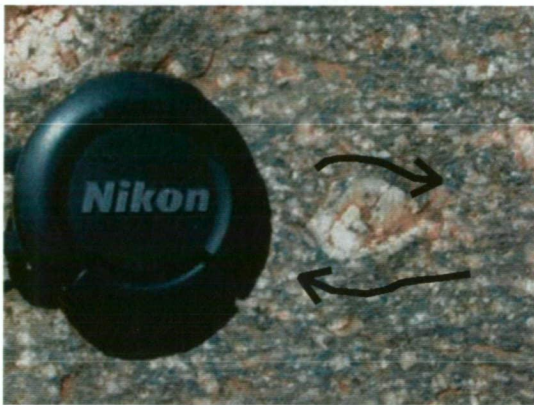
Mylonite zones at Lakeside (Plate 9), VPF, south of Yarlbirinda Hill (Plate 54) and west of the VPF (see Figure 89) represent narrow zones of high strain. Mylonites vary from several cm up to 3 m wide and appear to have been formed preferentially within aplite dykes (Lakeside), rhyolite dykes (west of Childera Outstation) or metasedimentary units (west of VPF). The mylonite zones slightly crosscut the regional foliation, which indicate the mylonites are slightly younger, but formed within the same north-south stress regime. At Lakeside, the mylonitic foliation strikes  $030^{\circ}$  and dips  $82^{\circ}$  to the west; foliation within the host granite strikes  $350^{\circ} - 010^{\circ}$  and dips  $80^{\circ}$  to the west. The mylonite contains a thin folded quartz vein in which the fold axis rotates from horizontal to parallel to the steeply dipping stretching lineation (Plate 57).



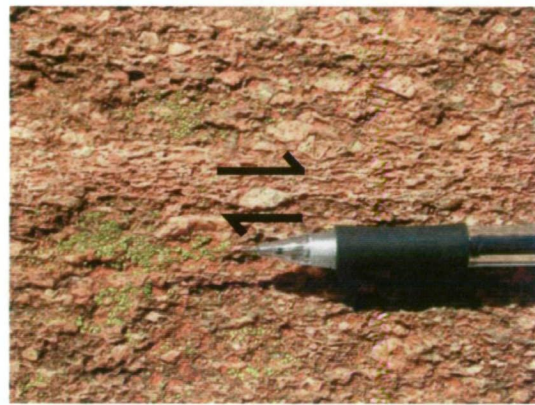
**Plate 47** Deformed granodiorite south of Tunkillia prospect with coarse feldspar grain showing dextral sense of shear (outcrop 6 on Figure 84).



**Plate 48** Dextral sense of shear defined by rotated feldspar porphyroclast from outcrop near Childera airstrip (outcrop 8 on Figure 84).



**Plate 49** Rotated feldspar grain showing dextral sense of shear from a granodiorite located SW of Yarranna Hill.



**Plate 50** Narrow mylonite band within deformed granite with coarse feldspar grain showing dextral sense of shear from SW of Childera Outstation.

Mylonite from west of VPF (outcrop 10 on Figure 89) is developed within possible metasediments. Mylonitic foliation strikes  $010^\circ$  and dips  $70^\circ$  to the west. In thin section, the foliation is crenulated, which suggests a later period of deformation in which the regional stress was reoriented. Outcrops within the northern part of the Yarlbrinda Shear Zone (outcrop 1 on Figure 89) are extensively foliated (mylonitic in part). The main foliation strikes  $290^\circ - 315^\circ$  and dips  $70^\circ - 80^\circ$  to the southwest. Localised, brittle structures trending  $045^\circ$  with minor alteration were observed.

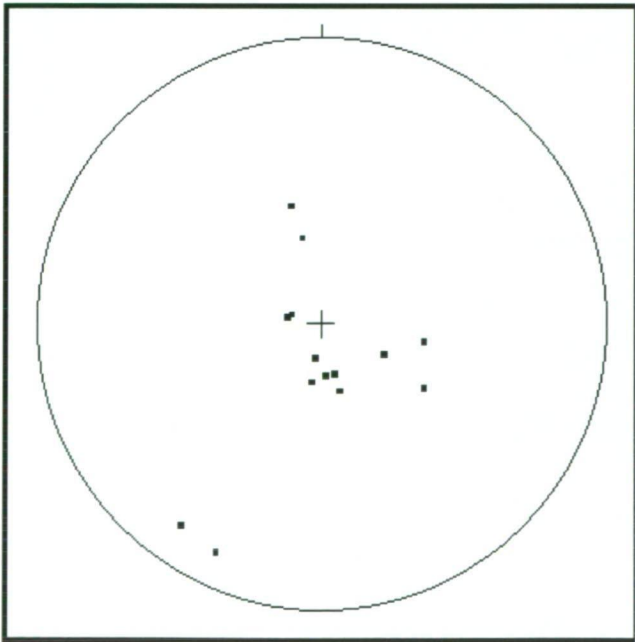
Stretching lineations defined by mineral alignment are generally shallow plunging  $10^\circ - 20^\circ$  to the north to northwest (Plate 51 and 52), but at Lakeside, stretching lineations are steep, plunging  $70^\circ - 80^\circ$  to the south (Plate 53)(Figure 88). The stretching lineation at Lakeside is a L-S tectonite produced by the combination of steeply plunging lineation and foliation. L-S tectonites form via noncoaxial strain, such as plane strain, reflecting simultaneous flattening orthogonal to the shear zone and constriction, or extension parallel to the shear zone (Davis and Reynolds, 1996). The coexistence of steep and shallow plunging lineations cannot be explained by pure simple shear and have recently been described from transpressive shear zones resulting from combined simple shear and orthogonal shortening (Johnson and



Kattan, 2001). Oblique transpression produces a component of vertical movement of one block relative to the other block.



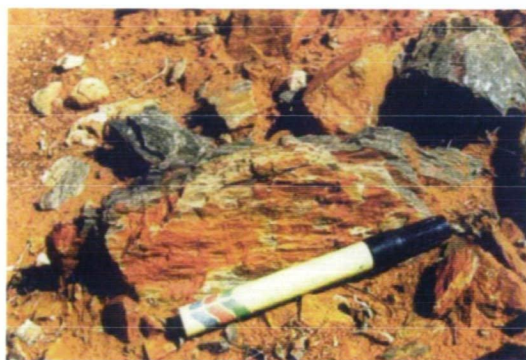
**Plate 51** Vertical face showing subvertical lineation in a rhyolite dyke from outcrop southwest of Childera (outcrop 8 on Figure 84) with ribbon quartz.



**Figure 88** Equal area stereonet of stretching lineations for rocks within the Yarlbirinda and Yerda Shear Zones.

The geology and geochemistry of granitoids in the CHILDARA region, western Gawler Craton, South Australia: implications for the Proterozoic tectonic history of the western Gawler Craton and the development of lode-style gold mineralisation at Tunkillia.





**Plate 52** Shallow plunging stretching lineations south of Yarlbrinda Hill (outcrop 12 on Figure 84).



**Plate 53** Shallow dipping stretching lineation within granites along vermin proof fence (outcrop 1 on Figure 84).



**Plate 54** Steeply plunging stretching lineation at Lakeside (outcrop 7 on Figure 84) (black line represents horizontal plane and pencil is parallel to the stretching lineation).

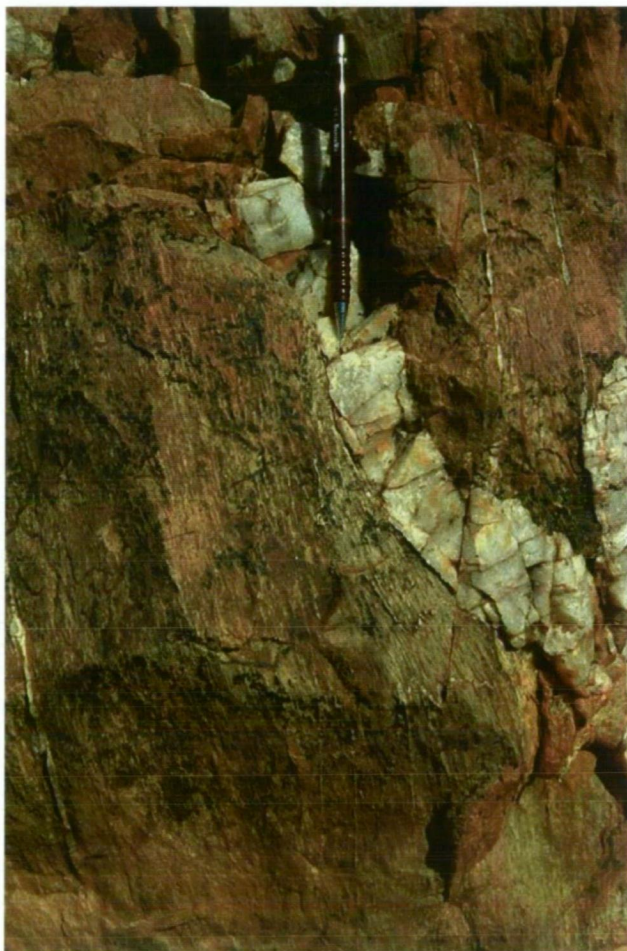
The existence of both shallow and steeply dipping stretching lineations with the opposite dip within the Yarlbrinda Shear Zone requires some explanation. The dominant stretching lineation within the Yarlbrinda Shear Zone is shallowly plunging to the north. Steeply dipping or dip-lineated mylonite at Lakeside is possibly derived from a precursor aplite dyke. A rhyolite dyke west of Childera Outstation shows evidence of both strike-slip and dip-slip deformation, with elongate quartz observed on both strike- and dip-surfaces (Plate 51). The dip-slip component of the deformation was late and relatively weak, and mostly observed within aplite and rhyolite dykes. A possible explanation for this is that the aplite and rhyolite dykes present a critical rheology contrast to the host granites and orthogneisses, hence they provided zones of weakness that localised the late dip-slip movement within the



Yarlbrinda Shear Zone. Tectonic interpretation of the significance of these observations will be discussed in the following section.

In thin section, deformation is mainly reflected by quartz grains which show plastic deformation forming ribbons within highly deformed rocks. Biotite is more stable and appears to wrap around quartz and feldspar aggregates. From these observation, the metamorphic grade is most likely greenschist facies ( $>400 - <600^{\circ}\text{C}$ : Winkler, 1974).

Abundant, black pseudotachylite is present at Yarlbrinda Hill (Plate 8). In thin section, the rock is massive to partly laminated, containing fragments and finer comminuted grains of quartz, K-feldspar, plagioclase and opaque oxide within in finer quartz-biotite-chlorite rich matrix. The pseudotachylite crosscuts the mylonitic foliation at Yarlbrinda Hill, which confirms that brittle deformation post-dates the ductile deformation within the Yarlbrinda Shear Zone. Hence, the initial deformation occurred at deep crustal levels which was followed by uplift and cataclasis.



**Plate 55** Folded, thin quartz vein (below main vein shown above). Fold axis rotates from horizontal to parallel to the stretching lineation.



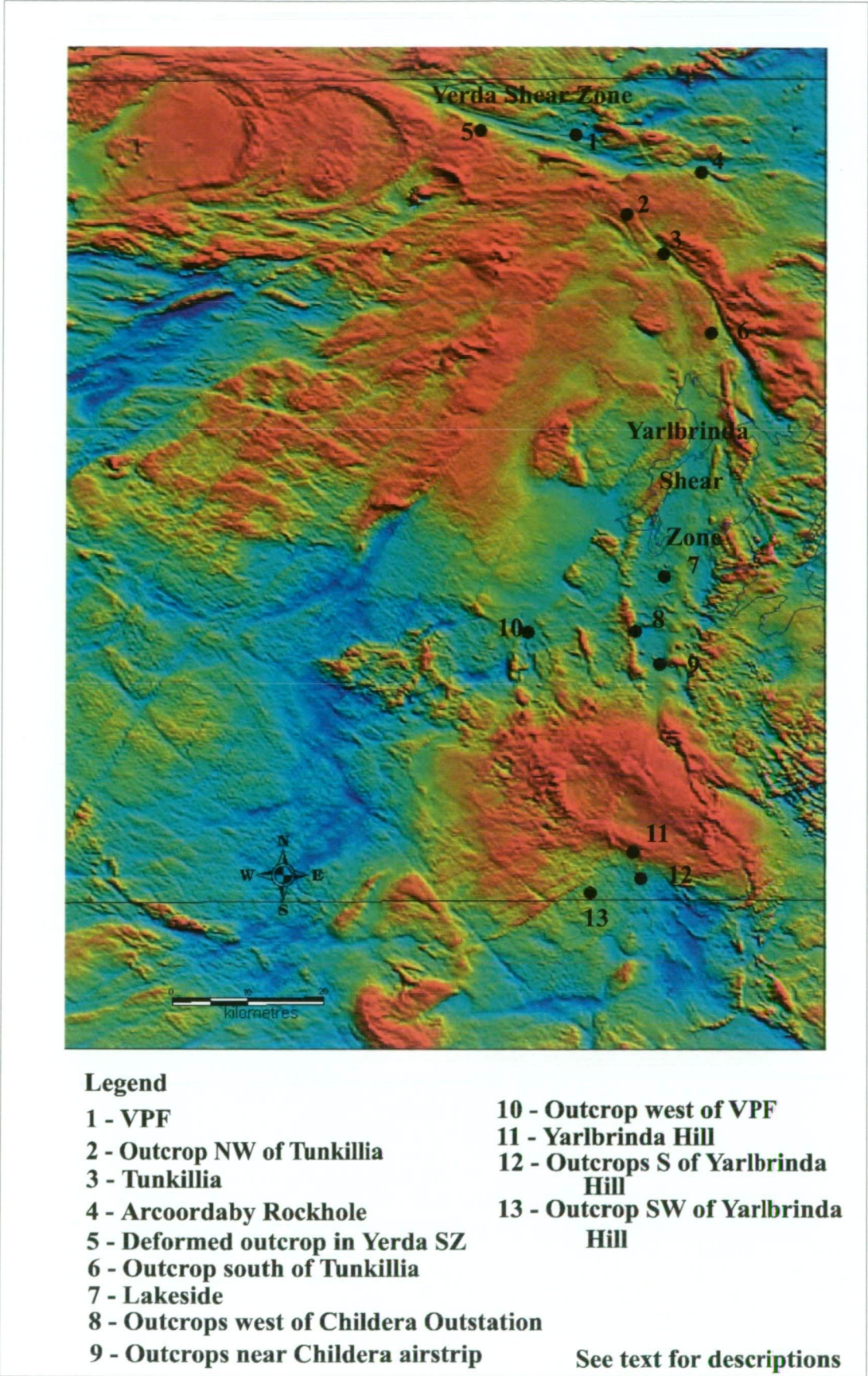


Figure 89 Location of outcrops within Yarlbrinda Shear Zone described in text over TMI image.

The geology and geochemistry of granitoids in the CHILDARA region, western Gawler Craton, South Australia: implications for the Proterozoic tectonic history of the western Gawler Craton and the development of lode-style gold mineralisation at Tunkillia.



In outcrop, rocks at Lakeside show evidence of two deformation events:

1. north-south shearing; and
2. crosscutting more brittle deformation trending  $060^\circ$ .

This implies a change in deformational environment from ductile to brittle regimes, and a major change in principal stress directions. Mylonite from west of VPF shows the main foliation is crenulated which also suggests a latter deformation not within the same stress orientation.

#### **4.6.2 Yerda Shear Zone**

The east-west trending Yerda Shear Zone separates the Nuyts and Wilgena Subdomains (Figure 3). An outcrop of foliated granodiorite located within the Yerda Shear Zone (outcrop 5 on Figure 89) has a U-Pb zircon age of  $1592 \pm 11$  Ma, which is interpreted to represent the crystallisation age. The foliation strikes northwest-southeast, and dips steeply to the west, with a shallowly plunging stretching lineation ( $20^\circ \rightarrow 296^\circ$ ). Rotated porphyroclasts indicate a sinistral sense of shear.

The discovery of deformed Hiltaba Suite granite within the Yerda Shear Zone and recent geochronology of fabric formation within the Fowler Subdomain, provides evidence that major crustal faults on the western Gawler Craton were active after the age of Hiltaba Suite emplacement. U-Pb isotope geochronology of metamorphic zircons in Nundroo DDH 3 on FOWLER indicates that mylonitic fabrics were still evolving within the Fowler Subdomain as late as  $1537 \pm 10$  Ma (Daly *et al.*, 1995; Fanning, 1997).

#### **4.6.3 Koonibba Fault Zone**

The Koonibba Fault is one of a series of northeast trending structures, which dissect the Gawler Craton. Outcrop within the Koonibba Fault Zone is rare, but stretching lineations where the fault zone is exposed at Point Bell, confirm the strike-slip nature of the Koonibba Fault Zone. Kinematic criteria in the form of fabric asymmetry and rotated porphyroclasts indicate localised sinistral movement, consistent with findings for other regional northeast trending faults (Rankin *et al.*, 1989; Teasdale, 1997). Porphyritic felsic mylonite within the Karari Fault Zone (drill hole Ooldea DDH3), show a sub-vertical foliation with steep down-dip stretching lineations (Teasdale, 1997). Teasdale (1997) reports that shear bands and asymmetric porphyroclasts indicate northwest-up with a component of sinistral strike-slip movement, which contradicts Rankin *et al.* (1989) who report an east up and sinistral strike-slip movement.

Structural interpretation of the aeromagnetic images indicates a significantly more complex picture than localised outcrop or drill hole data alone may suggest. Whilst the geophysical data show evidence for both dextral and sinistral strike-slip components along the major shears of the Fowler Suture zone (with the latter sense-of-shear dominating), outcrop scale observations are more consistent with dip-slip deformation. Stretching lineations in the Ifould Lake area generally pitch  $>60-70^\circ$  to the north, within subvertical foliation planes. The orientation and asymmetry of rare composite fabrics (S-C mylonites) are consistent with an east-block-up, dip-slip component of movement. These observations indicate that sinistral strike-slip

movement is locally only a minor component of the deformation, but the offset appears in plan view to be large.

#### **4.7 Relative chronology and timing of deformation within the Yarlbrinda Shear Zone**

The earliest fabric within the Yarlbrinda Shear Zone is the N-S to NNW-SSW  $S_0/S_1$  foliation (Figure 90) which was produced by N-S dextral strike-slip deformation with localised vertical shear. At the northern end of the shear zone, the foliation is rotated to the NNW due to dextral strike-slip movement on the Yerda Shear Zone to the north. The foliation is steeply dipping with dominantly sub-horizontal stretching lineations. The shear zone was affected by a later phase of dip-slip deformation, which produced steeply plunging stretching lineations. Poor exposure within the Yarlbrinda Shear Zone means there is no observable transition from shallowly, north plunging to steep south dipping stretching lineations. The stretching lineations switch from subhorizontal to subvertical along the Yarlbrinda Shear Zone indicates significant variation in finite strain consistent with an origin by oblique transpression. Drill holes located east of the “frogs eyes” plutons (CHL) show rapid change from vertical to horizontal foliation suggesting low angle thrusts. Unfortunately, the core is not oriented, hence no transport directions are deducible.

Petrology of quartz grains from granitoids at Lakeside show evidence of early phase of deformation, which was overprinted by the main deformation event producing the regional foliation. Hence, there may be an older deformation event, but it was within the same stress regime because the older deformation is not evident in mesoscopic outcrop observations.

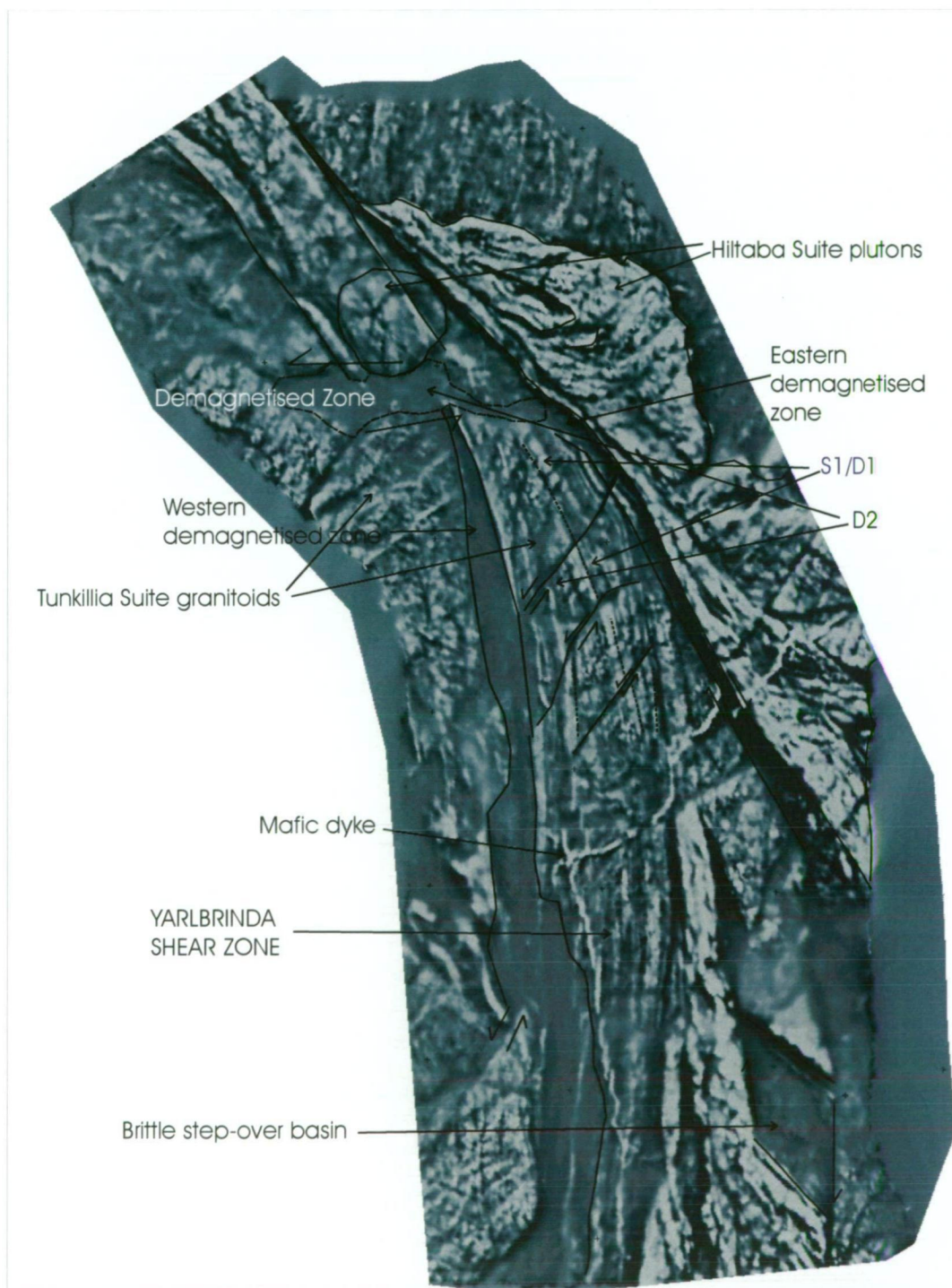
The  $S_1$  fabric is dissected by NE-SW trending, brittle structures ( $D_2$  on Figure 90). Fault offsets are apparent on aeromagnetic images and show a sinistral sense of movement. This indicates a change in the orientation of the major compressive stress from N-S to NNW-SSE. This event produced a prominent tear in the shear zone at the inflection point at the northern end, and appears to have been associated with a major zone of alteration (demagnetisation of magnetite to haematite). The tear in the shear zone may be related to thrusting of granite east of the Yarlbrinda Shear Zone (north over south) proposed by Martin (1996). This event also produced a major dilatational jog or pull apart basin (Figure 90) to the south of Tunkillia.

Mafic dykes intruded into the host sequence of granitoids show evidence for late reactivation of the shear zone within the original stress field, which suggests a reversal of the compressive stress back to N-S (Figure 90).

The relative timing of deformation is bracketed by the age of the host rocks at ~1680 Ma and intrusion of the Kondoolka Batholith at ~1580 Ma. Intrusion of the Kondoolka Batholith appears related to extensional movement on the shear zone providing space for granite emplacement. Granite within the Kondoolka Batholith is undeformed with the exception of minor brecciation/veining observed along the northern margin, and is most likely a stitching pluton. Syntectonic plutons of Hiltaba Suite were emplaced within the Yerda Shear Zone to the NW.

The geology and geochemistry of granitoids in the CHILDARA region, western Gawler Craton, South Australia: implications for the Proterozoic tectonic history of the western Gawler Craton and the development of lode-style gold mineralisation at Tunkillia.

Pontifex and Hand (1997) reports that the major mylonitic foliation at Tunkillia was reworked by a weak sericite-rich foliation due to deformation becoming increasingly partitioned. Major alteration and gold mineralisation within the Yarlbrinda Shear Zone appears to have occurred late within the deformation cycle. The switch from N-S to NNW-SSE directed compression and related extension at stepovers was relatively quick and occurred at ~1580 Ma (ie: intrusion of Kondoolka Batholith).



**Figure 90 Detailed TMI image of northern part of Yarlbrinda Shear Zone showing dominant fabrics and major features described within the text.**

The geology and geochemistry of granitoids in the CHILDARA region, western Gawler Craton, South Australia: implications for the Proterozoic tectonic history of the western Gawler Craton and the development of lode-style gold mineralisation at Tunkillia.



## Chapter 5 Tectonic Development of the CHILDARA region, Western Gawler Craton

### 5.1 Introduction

Granitoid rocks constitute the most voluminous rock type on the western Gawler Craton, hence, any model for the tectonic evolution of the western Gawler Craton, must encompass extensive episodes of predominantly silicic magmatism.

Palaeoproterozoic to Mesoproterozoic silicic magmatism on the western Gawler Craton, provides a record of crustal evolution spanning approximately 130 my (~1690-1560 Ma). During this time, magmatism was not continuous, but occurred in four distinct phases, which appear to represent different tectonic settings. The four phases of magmatism are:

1. 1690-1670 Ma Tunkillia Suite and equivalents, which represent a dominantly felsic suite with minor mafics;
2. 1630-1608 Ma St Peter Suite, a tonalitic to granitic suite, which tend to be sodic ( $\text{Na}_2\text{O} > \text{K}_2\text{O}$ ), with fractionated HREE, negligible Eu anomalies and high Sr contents, suggesting their generation from relatively mafic sources at depths sufficient to stabilise garnet;
3. 1595-1575 Ma Hiltaba Suite/Gawler Range Volcanics, which are potassic ( $\text{K}_2\text{O} > \text{Na}_2\text{O}$ ), and exhibit undifferentiated HREE patterns, negative Eu anomalies and low Sr contents, suggesting a shallower, more feldspathic source with abundant plagioclase; and
4. ~1560 Ma S-type Munjeela Granite.

Silicic magmatism within the CHILDARA region represents a major addition of crustal material within the Gawler Craton, during the four magmatic events outlined above. The Nuyts Subdomain was formerly interpreted to comprise predominantly Archaean basement with minor Palaeoproterozoic to Mesoproterozoic intrusives (Figure 85). Based on regional mapping, recent geochronology (this study and Teasdale, 1997) and Sm-Nd isotope analysis (Dove, 1997; Knight, 1997; Stewart and Foden, 2001), the Nuyts Subdomain does not contain any known Archaean rocks (Plan 2).

Previously, the St Peter Suite was considered a minor magmatic event within the Ceduna to Streaky Bay area. However, this study has shown the St Peter Suite magmatic event was a major crust-forming event within the Nuyts Subdomain. No known St Peter Suite magmatic rocks occur in other tectonic subdomains on the western Gawler Craton, hence it is unique to the Nuyts Subdomain.

#### 5.1.1 Problems with granite classification and discrimination diagrams

The geochemistry of granitoids has been widely used to determine tectonic settings for magmatic terranes and tectonic events. Various major and trace element discrimination diagrams have been used to distinguish tectonic settings, however many of these were produced for Phanerozoic plutonic rocks, from known tectonic settings. Hence, such diagrams must be used with caution when describing Archaean and Proterozoic rocks, due to possible differences in crustal composition with time. Pearce *et al.* (1984) report variations in geothermal gradients, mantle composition, degree of partial melting and contribution of crustal contamination between the Archaean and Phanerozoic. This is likely to have affected magma genesis, and resultant geochemical signatures.

Nonetheless, discrimination diagrams together with geochemical constraints and structural and barometric data provide the only available basis for speculation on the source regions and tectonic regimes of the western Gawler Craton plutonic rocks.

Pearce *et al.* (1984) defined a tectonic classification for granites based on trace elements, and grouped granites into ocean ridge, volcanic arc, within-plate and collisional types, using Rb, Y, Nb and Ta discrimination diagrams.

Rollinson (1993) outlines problems with using Rb in discrimination plots, as Rb is a very mobile element in hydrothermal fluids. Pearce *et al.* (1984) report that plagioclase accumulation may shift granites from the within-plate field on Nb-Y and Rb-(Yb + Nb) plots, and volcanic-arc and syn-collision granites can move to the within-plate or ocean granite field, by the accumulation of ferromagnesian and minor phases. Samples collected during regional mapping show little evidence of alteration, hence are considered reliable discriminators.

Wilson *et al.* (1985) report that the diagrams of Pearce *et al.* (1984) do not discriminate between the subalkaline to alkaline granites, formed on the continental side of Cordilleran belts and very different anorogenic granites formed during continental rifting.

Harris *et al.* (1986) reported that post-orogenic granites cannot be distinguished from volcanic arc and syn-collision granites using the Pearce *et al.* (1984) plots, and developed a Hf-Rb-Ta triangular plot to differentiate these granites (not used in this study due to lack of Hf data).

Pitcher (1982, 1987) defined five main tectonic environments;

1. Caledonian-type;
2. Hercynotype;
3. Andinotype;
4. Pacific-type; and
5. Nigeria-type.

The geological features of these are outlined in Figure 91. The Pitcher (1982, 1987) classification is used here because it defines the main tectonic environments for granite genesis and forms the basis for other classifications.

Batchelor and Bowden (1985) designed a set of discrimination diagrams to distinguish different granite types based on cationic/molecular values (R1-R2 multicationic scheme) previously defined by de la Roche *et al.* (1980). Batchelor and Bowden (1985) defined 6 groups (groups 1-5 relate to the tectonomagmatic divisions of Pitcher 1982):

1. Mantle plagiogranites – (oceanic island arc granites of Pitcher, 1982);
2. Destructive active plate margin (pre-plate collision – Andinotype of Pitcher, 1982);
3. Caledonian “permitted” plutons (post collision uplift);
4. Sub-alkaline plutons (late orogenic – Hercynotype of Pitcher, 1982);
5. Alkaline/peralkaline magmatism (post-orogenic – Nigeria type of Pitcher, 1982); and
6. Anatectic magmatism (syn-orogenic).

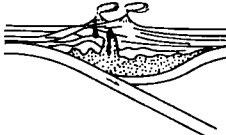
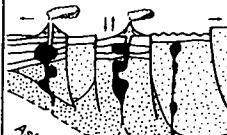

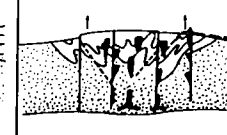
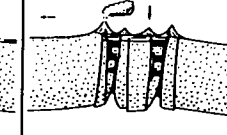
Batchelor and Bowden (1985) report that the R1-R2 discrimination diagram shows the progression of compositions through an orogenic cycle, starting at group 2 (pre-plate collision, subduction regime) to late orogenic plutons (group 4).

Maniar and Piccoli (1989) reported a tectonic discrimination of granites based on major element geochemistry, although again this is likely to be less useful where mass transfer due to alteration occurs. Maniar and Piccoli (1989) defined seven tectonic environments:

1. island arc granitoids (IAG) – formed by subduction of one oceanic plate beneath another oceanic plate (eg: PNG-Solomon Islands region);
2. continental arc granitoids (CAG) – formed on continents due to subduction of oceanic plate beneath continental plate (eg: Sierra Nevada and Idaho Batholiths, western USA);
3. continental collision granitoids (CCG) – intruded during continent-continent collision (eg: Himalayas);
4. post-orogenic granitoids (POG) – intruded during the last phase of an orogeny (eg: the younger granites of Egypt);
5. rift-related granitoids (RRG) – associated with rifting of the continental crust (eg: Oslo region of Norway);
6. continental epeirogenic uplift granitoids (CEUG) – associated with continental areas which have undergone epeirogenic crustal uplift (eg: younger granites of Nigeria); and
7. oceanic plagiogranites (OP) – minor group found in association with mafic rocks commonly at oceanic islands and mid-ocean ridges (eg: Canyon Mountain, Oregon).

The reader is referred to the various references cited above for further detail.

The various granite classification schemes outlined above have some limitations and must be used with caution, but remain the best tool for describing differences in granite geochemistry, and relating this difference to tectonic regimes.

OROGENIC				ANOROGENIC	
IOK	IMT	SS	St	IKK	IMA
W. Pacific -type  Oceanic Island Arc	Andinotype  Continental-lip arc, liminal basin	Hercynotype  Oblique continental collision		Caledonian-type  Post-closure uplift	Nigeria-type  Major rifting
					
Volcanic and volcanoclastic aprons Basalts Burial metamorphism  Gabbro, M-type granitoids in mature arcs Small zoned plutons	Sedimentation in fault margined turrows and marginal basins Andesites in great volume Burial metamorphism  I-type tonalite, granodiorite, with gabbro Disharmonious (Daly), linear, cauldron batholiths feeding volcanoes	Sedimentation in fore-thrust and pull-apart basins Rarely silicic lavas Regional, low-pressure metamorphism  Migmatites, reworked as S-type granites Harmonious (Suess) diapir batholiths in early phases		Erosion/flanking molasse basins Plateau-type basaltic volcanicity Strongly discordant aureoles  Biotite granite, appinitic diorite and gabbro Discordant plutons and distension diaps	Rift infills Alkali lavas, tuffs, as caldera infill  Biotite granite, alkali granite and syenite Resurgent subsidence cauldrons
Open folding	Spreading-Minimal shortening	Shortening and thickening		Tensional faulting, uplift	Rifting
Ocean-ocean subduction	Ocean-continental subduction	Continent-continent "subduction"		Rapid, post-closure uplift	Enclatonic or post-orogenic rifting
Short-lived  Partial melting of mantle-derived, metamorphosed underplate	Long-lived  Partial melting of mantle-derived underplate: crustal contribution within continental lip	Episodic recycling  Partial melting of recycled crustal material by metamorphic anatexis: reworking as batch-melts		Relatively short-lived  Partial melting of old, tonalitic lower crust plus mantle contribution	Relately short-lived  Partial melting of old mantle, or exhausted lower crust, under anhydrous but F,B-rich conditions
Hot, ?"dry," quartz-diorite magma	Hot, "dry" tonalitic magma rising high into the crust	Relatively warm, "wet," granitic mush freezing at depth, with autometamorphic recrystallization		Moderately hot and "dry," evolved, crystal-bearing magma rising to various levels	Relatively cool/alkal magma, rising to near surface with sub-solidus crystallization
Subduction energy - transfer of heat by basic magmas		Blanketing by tectonic thickening of radiogenic crust		Adiabatic decompression, heat transfer by basic magma	Decompression on release from deep crustal trap

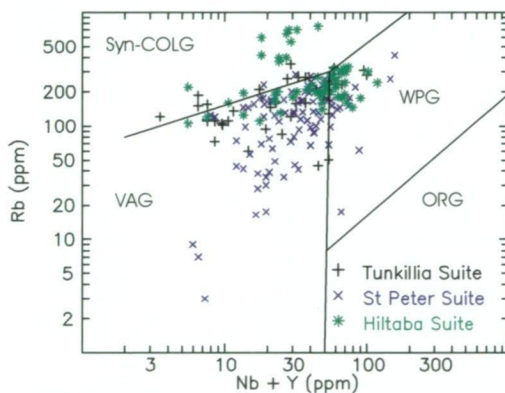
**Figure 91** Diagram showing different geological environments of Phanerozoic granitic rocks (from Pitcher, 1987).



## 5.2 Palaeoproterozoic to Mesoproterozoic magmatism on CHILDARA

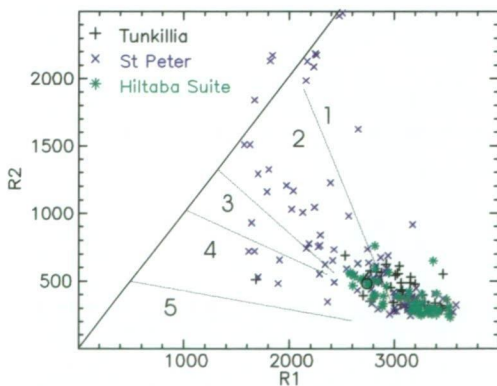
Four phases of Palaeoproterozoic to Mesoproterozoic magmatism spanning 130 My are present within the CHILDARA region and record major differences in geochemistry. This section will briefly summarise the geochemistry of the various magmatic events outlined in Chapter 3.

Samples from the Tunkillia Suite plot within the volcanic arc, syn-collision and within-plate granite fields on Rb v (Y + Nb) tectonic diagrams (Figure 92). In detail, Childera Airstrip samples plot predominantly in the volcanic arc field, whereas Lakeside samples, plot in the syn-collision and within-plate granite fields. VPF samples straddle the syn-collision and volcanic arc boundary (Figure 92). The St Peter Suite samples plot predominantly in the volcanic arc granite field on Pearce *et al.* (1984) tectonic discrimination diagram (Figure 92). Ultramafic/mafic rocks in the Kalanbi area are thought to be cumulates, from a fractionated tholeiitic magma, which is the cause of their high FeO contents, and the presence of hypersthene (Purvis, 1983). The inferred crystallisation sequence for these rocks is olivine-chromite, plagioclase, pyroxene, magnetite, sulphides and apatite (Purvis, 1983).



**Figure 92 Rb-(Y+Nb) tectonic discrimination plot for Tunkillia Suite, St Peter Suite and Hiltaba Suite granitoids (after Pearce *et al.*, 1984).**

(VAG - volcanic arc granite, syn-COLG - syn-collision granite, WPG - within-plate granite, ORG - ocean-ridge granite)



**Figure 93 Plot of R1-R2 multicationic points for Tunkillia Suite, St Peter Suite and Hiltaba Suite samples on CHILDARA.**

$$R1 = 4Si - 11(Na + K) - 2(Fe + Ti)$$

$$R2 = 6Ca + 2Mg + Al$$

Group 1 - Mantle fractionates (tholeiitic group)

Group 2 - Pre-plate collision (calc-alkaline and trondhjemitic)

Group 3 - Post collision uplift (high-potassic calc-alkaline)

Group 4 - Late-orogenic (sub-alkaline monzonitic)

Group 5 - Anorogenic (alkaline and peralkaline)

Group 6 - Syn-collision (anatectic 2-mica granites)

Groups based upon Pitcher (1979, 1982) and Harris *et al.*, (1982). Petrological equivalents (in brackets from Lameyre and Bowden, 1982).

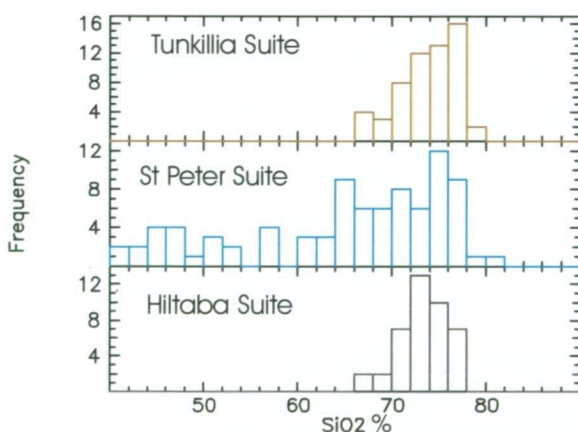
Samples of St Peter Suite plot within the pre-plate collision field on a R1-R2 diagram (Figure 93)(De la Roche, 1980). This progressive change in compositions from group 2 to 4 reflects a general increase in K and Na, and could be related to a common source (Batchelor and Bowden, 1980).

The Hiltaba Suite samples contain high SiO<sub>2</sub> contents, are potassic (K<sub>2</sub>O>Na<sub>2</sub>O) and plots on the boundary between the within-plate and volcanic arc fields (Figure 92). The S-type Munjeela Granite plots within the syn-collision field (not shown) on a Pearce *et al.* (1984) plot.

### 5.3 Petrogenesis of the St Peter Suite

The St Peter Suite was originally thought to represent a late- to syn-Kimban Orogeny intrusive (ie: member of the Lincoln Complex) based on deformational fabric. However, U-Pb dating by Flint *et al.* (1990) recorded a concordant crystallisation age of 1620±4 Ma, indicating that the St Peter Suite was not related to the Kimban Orogeny. Deformation of the St Peter Suite is related to the Kararan Orogeny (Daly *et al.*, 1998).

The St Peter Suite ranges in composition from gabbro through to granite, which is reflected in an SiO<sub>2</sub> histogram, with SiO<sub>2</sub> values being continuous other than minor gaps at 54-56 and 58-60 wt% (Figure 94) which may be due to lack of sampling.



**Figure 94 SiO<sub>2</sub> histogram for the St Peter Suite (Hiltaba and Tunkillia Suites shown for comparison).**

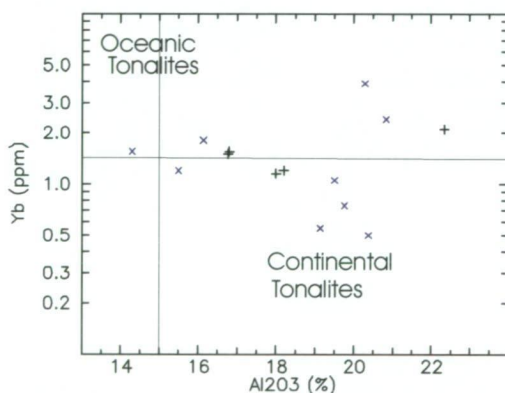
The major element chemistry of the St Peter Suite indicates calc-alkaline affinity and remain relatively enriched in CaO, MgO and FeO at high SiO<sub>2</sub> contents. This, and their wide composition range and unevolved trace element compositions, suggest them to have affinities to arc-type plutonic suites developed in convergent plate settings (ie: so-called VAG of Pearce *et al.*, 1984, or Cordilleran I-type granites, Pitcher, 1983). This is supported by tectonic discrimination diagrams using trace elements, and by other features such as late Ba depletion and Nb depletion, all of which are recognised as features of arc-type magmas. Knight (1997) reported a possible island arc setting for the St Peter Suite based on limited geochemistry, petrology and field relationships between units.



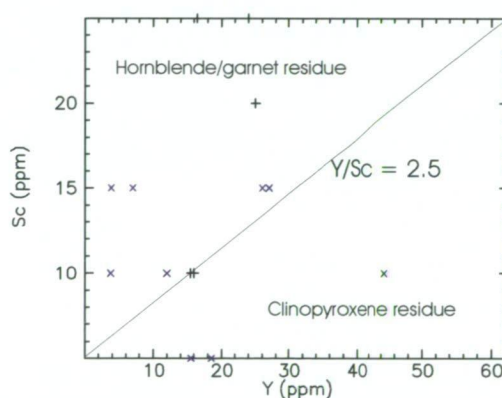
The St Peter Suite is characterised by a wide range of rock types including tonalite, granodiorite, monzogranite, quartz diorite, diorite, gabbro and anorthosite. Tonalites were intersected in drill holes in the Kalanbi area (Ferris, 2001), and crop out along the coast at Rocky Point, Cape Beaufort and Point James. Tonalitic rocks are common in the Archaean, and are generally considered to be formed by partial melting of young, hot and flat subducting oceanic slabs, with garnet and hornblende as residual phases (Martin, 1986; Defant and Drummond, 1990; McCulloch, 1993).

Barker (1979) and Arth (1976) divided Archaean tonalites into high Yb-low  $\text{Al}_2\text{O}_3$  (oceanic) and low Yb-high  $\text{Al}_2\text{O}_3$  (continental) varieties. Oceanic-type magmas are HREE-rich and Al-poor, compared to continental types. Yb enrichment reflects the release of HREE to melts by melting of garnet.

The St Peter Suite tonalites nearly all have high (>15 wt %)  $\text{Al}_2\text{O}_3$ , but most also have elevated Yb (Figure 95). Stone (1998) reports Y-Sc relations provide insight into possible residual minerals from partial melting or fractionation. The respective partition coefficient ( $K_d$ 's) for Y in hornblende, garnet and clinopyroxene are 3.2, 12.5 and 2.0 respectively, whereas, corresponding  $K_d$ 's for Sc are 2.7, 8.5 and 44 respectively (Stone, 1998). Melts with clinopyroxene residue should be enriched in Y and depleted in Sc relative to melts with hornblende and/or garnet residue (Stone, 1998). Y/Sc ratios of >2.5 – implies a clinopyroxene residue, samples <2.5 implies a hornblende or garnet residue. The St Peter Suite plots within both fields (Figure 96), suggesting possible input from both oceanic and continental magma types.



**Figure 95** Plot of  $\text{Al}_2\text{O}_3$  v Yb (after Arth, 1976) for tonalites of the St Peter Suite.



**Figure 96** Plot of Y v Sc for tonalites of the St Peter Suite.

Melting experiments show that the depth of melting influences tonalitic compositions. Basalts melted experimentally by Rapp *et al.* (1991) showed a residual assemblage of amphibole+plagioclase+pyroxene+Fe-Ti oxides at 8 kb, giving way to a garnet-dominant residue at 22 kb (Stone, 1998). The seemingly progressive change from garnet-bearing sources for the St Peter Suite to plagioclase dominant sources, would be consistent with a general trend of decreasing depth of magma generation with time in a subduction setting.

The St Peter Suite has trace element compositions consistent with magma generation at lower crust or upper mantle depths, where garnet is stable. The St Peter Suite is



geochemically similar to the Peninsular Range Batholith (Table 8)(Gromet and Silver, 1987) and Archaean tonalites (Taylor and McLennan, 1985).

**Table 8 Comparison of average values for St Peter Suite and Peninsular Ranges Batholith and Archaean TTG rocks.**

	St Peter Suite (1)	St Peter Suite (2)	Peninsular Ranges	Archaean TTG
SiO <sub>2</sub>	69.63	65.06	67.12	69.79
TiO <sub>2</sub>	0.37	0.47	0.63	0.34
Al <sub>2</sub> O <sub>3</sub>	15.49	17.04	15.98	15.56
Fe <sub>2</sub> O <sub>3</sub>	3.26	4.57	4.02	3.12
MnO	0.09	0.10	0.07	0.05
MgO	0.90	1.73	1.75	1.18
CaO	1.92	3.54	4.55	3.19
Na <sub>2</sub> O	3.89	3.43	4.15	4.88
K <sub>2</sub> O	3.74	3.18	2.13	1.76

**Notes:** St Peter Suite (1) = average of 49 samples having SiO<sub>2</sub> >53 wt %. St Peter Suite (2) average of 89 samples with full range of SiO<sub>2</sub> values from 40.8-80.85 wt%. Average of 297 analyses of granitic rocks from Peninsular Ranges Batholith having SiO<sub>2</sub> >53 wt % (Chappell & Stephens, 1988). Archaean TTG – average of 355 rocks (Martin, 1994).

The St Peter Suite appears to have been generated within a continental collision environment, producing dominantly calc-alkaline magmatic arc characteristics. The lack of associated voluminous andesitic volcanics, suggests a predominantly continental magmatic arc setting.

#### **5.4 Comparison of St Peter Suite with Australian Proterozoic granites and modern arc magmatism.**

Wyborn (1988) and Etheridge *et al.* (1987) report that Proterozoic crustal growth within Australia is the result of lower crustal underplating of mantle derived magma. The main line of evidence is the dominance of K-rich granite in the late Archaean and early Proterozoic, which are interpreted to be the result of a change of melting mafic sources within the Archaean to remelting Archaean crust in the Proterozoic. However, the previous sections have shown that the St Peter Suite does not fit this model and suggests a magmatic arc origin for the voluminous magma generated on the Western Gawler Craton.

Zhoa and McCulloch (1995) outline the two alternative models for production of continental crust during the Proterozoic:

1. a plate tectonic model which comprises mixing of a mantle-derived component with crustal rocks, either by lower crust assimilation or sediment subduction (eg., Patchett and Arndt, 1986; Bennett and DePaolo, 1987); and
2. mafic underplating and continental extension (eg., Etheridge *et al.*, 1987; Wyborn, 1988; Wyborn *et al.*, 1988, 1992).

Wyborn (2001) describes four main groups of I-type granites through geologic time:

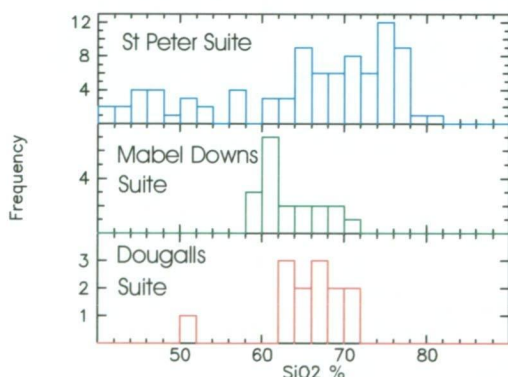
1. Archaean tonalites to granites;
2. Proterozoic granodiorites to granites;
3. early Palaeozoic granodiorites to granite; and
4. late Palaeozoic, Mesozoic and Cenozoic tonalites to granites.

The tonalitic rocks of the St Peter Suite do not fit any of these groups and are a unique magmatic event within the Gawler Craton.

Wyborn (2001) reports that I-type granites comprise >85% by area of all Proterozoic granites, with no major suites of I-(tonalitic) types. The St Peter Suite contradicts this: it is a suite of I-(tonalitic) type granites similar to other classic occurrences, such as the Peninsular Ranges Batholith (Martin, 1994; Silver and Chappell, 1998; Gromet and Silver, 1987).

Within Australia, the St Peter Suite is similar to the Sally Downs Association of Western Australia (Wyborn, 2001) and granites from the Arunta Block, central Australia (Zhao and McCulloch, 1995). The Mabel Downs Suite and Dougalls Suite (Sally Downs Association) show similar geochemistry to the St Peter Suite and plot within the VAG field on tectonic diagrams (not shown). Sheppard *et al.* (1995) report that the Bow River and Sally Downs batholiths are comparable in size to batholiths of the Cordillera and Andes, and that intrusives with high Na<sub>2</sub>O and Sr, and low K<sub>2</sub>O make up a large component of the Sally Downs batholith and Dougalls Suite.

Wyborn (2001) reports that mafic granites within these suites show strong evidence of restite, and they are characterised by little evidence of fractionation. Hence, they do not show the range of compositions generated within arc environments. Figure 97 shows the restricted range of the Mabel Downs and Dougalls Suites compared to the St Peter Suite.



**Figure 97** SiO<sub>2</sub> histogram for St Peter Suite, Mabel Downs Suite and Dougalls Suite showing restricted SiO<sub>2</sub> ranges for Mabel Downs and Dougalls suites. Data for Mabel Downs and Dougalls Suites from Sheppard *et al.*, (1997).

Zhao and McCulloch (1995) divided the Arunta granites into 3 groups:

1. Calcalkaline-trondjemitic Group (CAT);
2. Main Group;
3. High-heat-production group (HHP).

The CAT group occurs in the southern part of the Arunta Block is characterised by high Na<sub>2</sub>O, Na/K, Sr, K/Rb and Sr/Y and relatively low K<sub>2</sub>O, Rb, Rb/Sr, Th, U REE, Nb and Y (Zhao and McCulloch, 1995). These are characteristics of calcalkaline suites occurring in modern convergent plate margins. The HHP group crops out in the central part of the Arunta Block, is characterised by high K, Rb, Th, U, Rb/Sr and Rb/Zr and relatively low Sr, Ba, Na/K, K/Rb, Ba/Rb, MgO, Cr and Ni (Zhao and McCulloch, 1995). The Main Group are volumetrically the most significant granite



type in the Arunta Block, and are intermediate between the CAT and HHP groups (Zhao and McCulloch, 1995).

5.4.1 Comparative geochemistry

This section compares the geochemistry of the St Peter Suite with the Arunta Inlier granites of Zhao and Cooper (1992) and Zhao and McCulloch (1995), and modern arc granites from the pacific region (AGSO OZCHEM Database). On a major oxide triangular plot (Figure 98), the St Peter Suite plots predominantly within the trondhjemite, tonalite and granodiorite fields, the Arunta Inlier group plots within all fields. The modern island arc samples show a more restricted range and plot predominantly within the tonalite field (Figure 98), which most likely due to oceanic plate within the source region, whereas the St Peter Suite and Arunta Inlier granite are most likely continental magmatic arc rocks. On a SiO<sub>2</sub> histogram (Figure 99), all 3 groups show a relatively wide range of values with the modern island arc samples more mafic (mean 64 wt % SiO<sub>2</sub>). The mafic St Peter Suite samples were included to demonstrate the St Peter Suite shows the full range of SiO<sub>2</sub> values.

All 3 groups plot within the VAG field on Pearce *et al.* (1984) tectonic discrimination diagram (Figure 100) and are characterised by high Sr (Figure 101) and low Y (Figure 102) relative to highly fractionated HHP granites from the Arunta Inlier. Hence, all 3 groups are classified as Sr-undepleted and Y-depleted (Group 4 of Wyborn *et al.* 1992). On a chondrite normalised REE plot (Figure 103), the St Peter Suite and CAT group show similar trends with strongly fractionated REE patterns with HREE depletion, and no or negligible Eu anomaly, similar to Archaean TTG (Martin, 1986). In comparison, felsic suites on CHILDARA and the HHP (high heat producing) suite from the Arunta Inlier are slight to strongly enriched in REE and show large negative Eu anomalies (Figure 104).

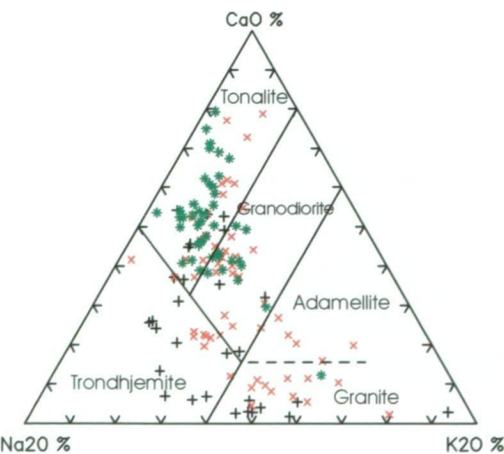
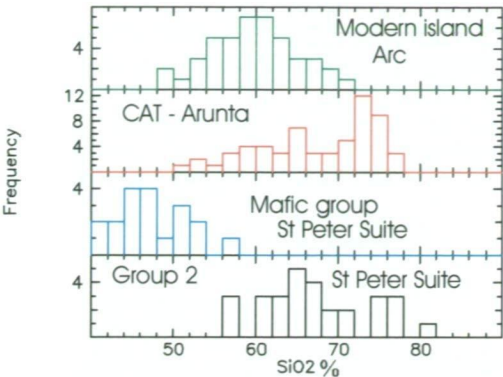


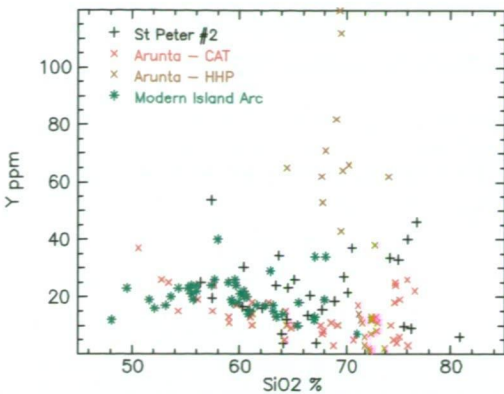
Figure 98 Major oxide classification diagram of Group 2 St Peter Suite, CAT Group Arunta Inlier and modern Island arc granites (group symbols same as Figure ). (fields from AJR White, Pers. comm., 1988).

- Legend
- + St Peter #2
  - x Arunta - CAT
  - \* Modern Island Arc

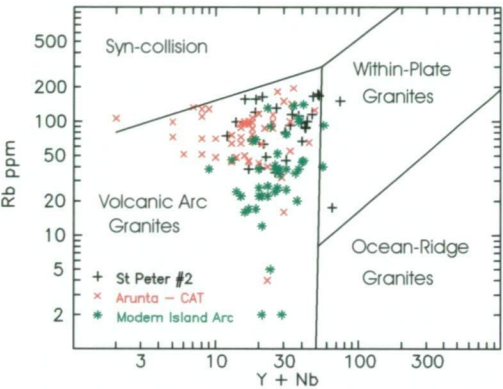




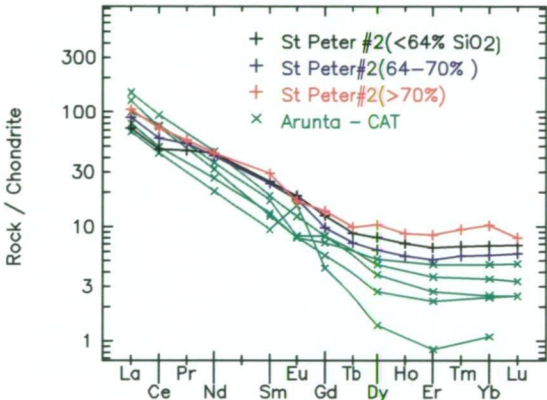
**Figure 99** SiO<sub>2</sub> histogram of St Peter Suite (Group 2 and mafic samples) and Arunta Inlier and modern island arc granites.



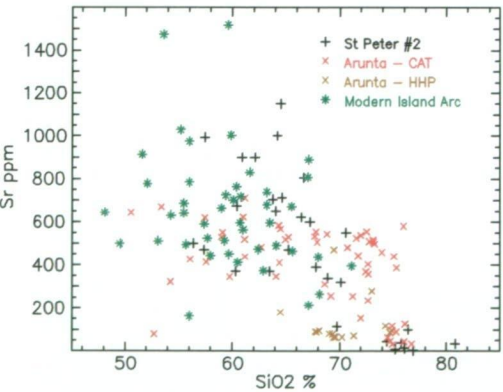
**Figure 102** Plot of SiO<sub>2</sub> v Y for Group 2 St Peter Suite, CAT Group from Arunta Inlier and modern island arc granites. Included is HHP granites from Arunta Inlier for comparison.



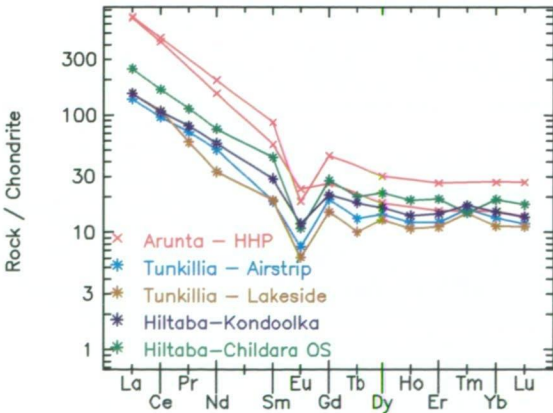
**Figure 100** Tectonic discrimination diagram of Pearce *et al.* (1984) for Group 2 St Peter Suite, CAT Group from Arunta Inlier and modern island arc granites.



**Figure 103** Chondrite normalised REE patterns for Average values of Group 2 St Peter Suite and CAT Group Arunta Inlier.



**Figure 101** Plot of SiO<sub>2</sub> v Sr for Group 2 St Peter Suite, CAT Group from Arunta Inlier and modern island arc granites. Included is HHP granites from Arunta Inlier for comparison.



**Figure 104** Chondrite normalised REE patterns for HHP Group Arunta Inlier and selected Tunkillia Suite and Hiltaba Suite groups from CHILDARA area.

## 5.5 Tectonic/Tectonothermal Evolution of the CHILDARA Area, Western Gawler Craton

The Nuyts Subdomain is dominated by granitoids ranging in age from ~1690 to ~1560 Ma. Aeromagnetic data shows large elliptical plutons, dissected by regional, low-grade shear zones, and intruded along major crustal shear zones. Hence, the Nuyts Subdomain is the product of voluminous intrusion of granitoids during periods of activation of these major framework faults.

The Nuyts Subdomain is bound to the north by the Wilgena Subdomain, and to the west by the Fowler Subdomain. The Gawler Range Volcanic province forms the northern section of the eastern boundary, and the Coultas Subdomain forms the southern section of the eastern boundary (see Figure 83).

The Wilgena Subdomain contains Archaean greenstones and Palaeoproterozoic to Mesoproterozoic intrusives, sediments and minor acid volcanics. The Yerda Shear Zone, which separates the subdomains, is a crustal-scale sinistral shear zone.

The Fowler Subdomain contains late Palaeoproterozoic mafic and intermediate intrusives, intruded into metasedimentary rocks, which subsequently underwent granulite facies metamorphism (Teasdale, 1997).

The Nuyts Subdomain is dominated by the addition of voluminous juvenile crust at 1630-1608 Ma, appears related to the continental collision within the Fowler Subdomain to the west. Geochemical evidence (Figure 95) suggests minor involvement of oceanic crust from the leading edge of the continent. The lack of major andesitic volcanics, which would be expected from the closing of an extensive oceanic crust, suggests that possibly only a small ocean or no ocean was developed, prior to amalgamation of the Nuyts, Wilgena and Fowler Subdomains. The St Peter Suite contains synchronous volcanics, the Nuyts Volcanics which only crop out within the Nuyts Archipelago. Only limited whole rock and trace element geochemistry exists and further geochemical analysis are required to determine their relationship to the St Peter Suite.

As demonstrated by various geochemical diagrams, the St Peter Suite corresponds closely to magmatic arc granitoids. While their chemical characteristics indicate their evolution at a collision margin, the analyses do not clearly discriminate between island arc, or Andean type arc settings. However, the St Peter Suite does contain a substantial volume of granodiorites and granites, which together with the lack of voluminous andesitic volcanics, suggests that continental crust was a significant part of the protolith.

### 5.5.1 *Sm-Nd isotope results for the St Peter Suite*

Sm-Nd and Sr-Rb isotopic analyses were undertaken by Knight (1997) and Dove (1997) to determine the crust-forming ages for the St Peter Suite. Knight (1997) reported initial  $\epsilon_{\text{Nd}}$ 's ranged from -0.25 to -0.65 at 1620 Ma, and calculated depleted mantle ages ranged from 2.03 to 2.16 Ga. Dove (1997) reported depleted mantle model ages ranged from 2.02 to 2.03 Ga. Limited U-Pb SHRIMP and Pb-Pb Kober analyses record a magmatic age between 1630-1608 Ma for the St Peter Suite, hence

the depleted model ages are ~400 My older. This suggests that accretion of new continental crust began at ~2 Ga, and the St Peter Suite is most likely related to subduction at >1630 Ma. This is similar to plutonism associated with magmatic arcs of the western margin of USA, which are predominantly crustally derived within areas underlain by older basement (Nelson and DePaolo, 1985). No inherited zircons were identified during SHRIMP dating.

Dove (1997) tested 2 possible units for crustal contamination. The Archaean Sleaford Complex was tested for Simple Mixing and Assimilation and Crystal Fractionation (ACF). Simple mixing between the depleted mantle and the Sleaford Complex did not support the isotope ratios for the St Peter Suite, and ACF was also not consistent with contamination by Sleaford Complex. Simple mixing between samples of Donnington Granitoid Suite (~1850 Ma) and the St Peter Suite did not explain the isotope ratios, but the mixing curve showed that the Donnington granitoid Suite may be a source of contamination of the depleted mantle to produce the St Peter Suite signature. However, it is observed that only a small proportion (~10%) of continental crust contamination was involved in this process, thus the St Peter Suite chemistry is derived mainly from a depleted mantle source.

### 5.5.2 Tectonic episode 1

At ~1710 Ma, the Fowler Subdomain was undergoing upper greenschist to amphibolite metamorphism, followed by intrusion of voluminous I-type granitoids at ~1690-1670 Ma (Teasdale, 1997).

The first major tectonic/tectonothermal event recorded within the Nuyts Subdomain was the intrusion of the Tunkillia Suite granites within the Yarlbirinda Shear Zone. U-Pb dating and Pb-Pb dating of a deformed granodiorite from the Yerda Shear Zone, shows inheritance at ~1670 Ma (this study and Stewart and Foden, 2001), suggesting 1690-1670 Ma magmatism was widespread within the northern part of the Nuyts Subdomain. Tunkillia Suite equivalents were intruded into the Coult (Little Pinbong), Christie (Lake Ifould, Lake Tallacootra, Wynbring Rocks and Barton South) and Fowler Subdomains (White Gin Rockhole).

Tunkillia Suite rocks at Lakeside within the Yarlbirinda Shear Zone, show evidence for two periods of deformation in thin section. Quartz crystals show low angle internal grain boundaries which may indicate pre-existing highly strained older grains. Hence, initial deformation may have been syn-tectonic which was overprinted by later deformation. The dominant foliation observed in these rocks is related to later movement within the Yarlbirinda Shear Zone (tectonic episode 3). Daly *et al.* (1998) report deformation within the Fowler Subdomain is related to continental collision between the proto-Yilgarn craton to the northwest. Hence fabrics formed within the Fowler Subdomain are referred to as the D<sub>1</sub> of the Kararan Orogeny. The lack of exposure within the area makes structural correlation difficult. Teasdale (1997) reports 3 major fabrics within the Nundroo Block of the Fowler Subdomain, an early tectonic foliation, which is overprinted by a steeply dipping stretching lineation. These fabrics are crosscut by narrow shear zones.



### 5.5.3 Tectonic episode 2

The second major tectonic/tectonothermal event within the Nuyts Subdomain is the voluminous intrusion of the St Peter Suite at 1630-1608 Ma. As previously outlined, major and trace element characteristics of the St Peter Suite are consistent with their formation in a continental arc setting.

The St Peter Suite ranges in deformation intensity from massive to mildly deformed with narrow mylonite zones. The dominant foliation trends roughly north-south, and is mostly vertical to steeply dipping. At Point Westall, the St Peter Suite forms a series of vertical dykes with the foliation aligned parallel to the dyke margins.

The St Peter Suite appears to have developed by a period of extension related to the initial continental collision to the west with a southward directed subduction of continental plate beneath the Nuyts Subdomain. This produced a breach in the crust and allowed the production of juvenile granites possibly within a back arc environment. This was short lived with a return to compressional event which resulted in a shift from initial calc-alkaline arc magmatism (ie: Group 2 of the St Peter Suite) to monzogranite to granodiorite (Groups 1,3,4,5 and 6 of the St Peter Suite).

### 5.5.4 Tectonic episode 3

The Hiltaba Suite/Gawler Range magmatic event (~1592-1575 Ma) represents the third major tectonic/tectonothermal event in the Nuyts Subdomain.

Associated with this magmatic event is major strike-slip movement within shear zones in the CHILDARA region. Contemporaneous, dextral strike-slip movement within the Yarlbirinda Shear Zone, producing a dominant north-south trending foliation ( $S_1$ ), and sinistral strike-slip movement within the Yerda Shear Zone resulted in the amalgamation of terranes. Stretching lineations switch from subhorizontal to subvertical within the Yarlbirinda Shear Zone, which may indicate deformation by oblique transpression. The change from subvertical to horizontal foliation observed within a drill hole east of the 'frogs eyes' plutons suggests a low angle thrust, which supports this concept.

The direction of major compressive stress was originally east-west, then reoriented to north-northwest/south-southeast on northern CHILDARA. During this event, the triple junction of the Yarlbirinda and Yerda Shear Zones with the Koonibba Fault Zone developed, and produced a rotation of the major strain axes from north-south to the northeast/southwest. During this event, several prominent Hiltaba Suite plutons were intruded into the Yerda Shear Zone/Oolabinna Shear Zone (eg: the 'frogs eyes'), possibly as a sheet within a zone of extension related to sinistral movement on the shear zones. U-Pb dating of magmatic zircons from a deformed granodiorite within the Yerda Shear Zone, recorded a crystallisation age of ~1592 Ma.

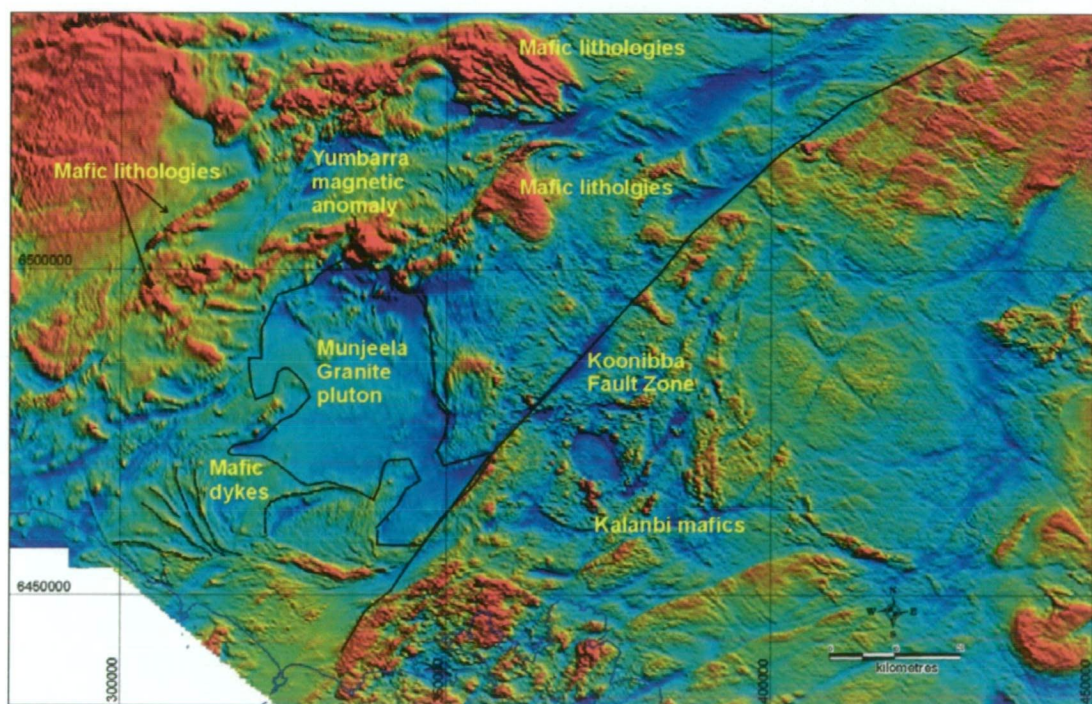
The Kondoolka Batholith appears to have exploited a northwest trending fracture. Granite within the Kondoolka Batholith is undeformed and is dated at  $1580 \pm 7$  Ma, suggesting the main phase of deformation had ceased. Outcrops of St Peter Suite located south of Yarlbirinda Hill, record the dominant north-south trending fabric (ie: they show no evidence of rotation due to intrusion of the Kondoolka Batholith).

In the northern part of the Yarlbirinda Shear Zone, the Yarlbirinda Shear Zone was pulled apart by combined movements on the Yarlbirinda and Yerda Shear Zones (Figure 90). The Yarlbirinda Shear Zone contains areas of significant alteration observed on the TMI image as demagnetised zones (Figure 89 and 90). Mineralisation at Tunkillia is located within the western demagnetised zone. These zones suggest fluid was focussed through the shear zone during this event.

The Hiltaba Suite/Gawler Range Volcanics magmatic event is the last major widespread plutonism within the western Gawler Craton (with the exception of local S-type Munjeela Granite and the Spilsby Suite). The Hiltaba Suite was interpreted to be an anorogenic suite produced within an intracratonic environment. However, based on this study and Daly *et al.* (1998), the Hiltaba Suite is an integral part of the deformation/tectonic history of the western Gawler Craton.

#### 5.5.5 Tectonic episode 4

The fourth major tectonic/tectonothermal event within the Nuyts Subdomain is the intrusion of the S-type Munjeela Granite at ~1560 Ma. Electron microprobe dating of monazite produced an interpreted crystallisation age of  $1562 \pm 15$  Ma (R.Berry, CODES, pers. comm., 2001). Granite at Munjeela Rockhole is undeformed, but equivalent granite at Point Bell, located within the Koonibba Fault Zone, shows evidence of sinistral strike-slip movement.



**Figure 105** TMI image showing main Munjeela Granite pluton west of the Koonibba Fault Zone. Diagram also shows location of mafic dykes and mafic lithologies and Yumbarra magnetic anomaly and Kalanbi mafic units.

The production of the Munjeela Granite is the last major magmatic event on the western Gawler Craton and is the only known S-type granite on the Gawler Craton. A period of extension, possibly during tectonic episode 3 resulted in basin formation.

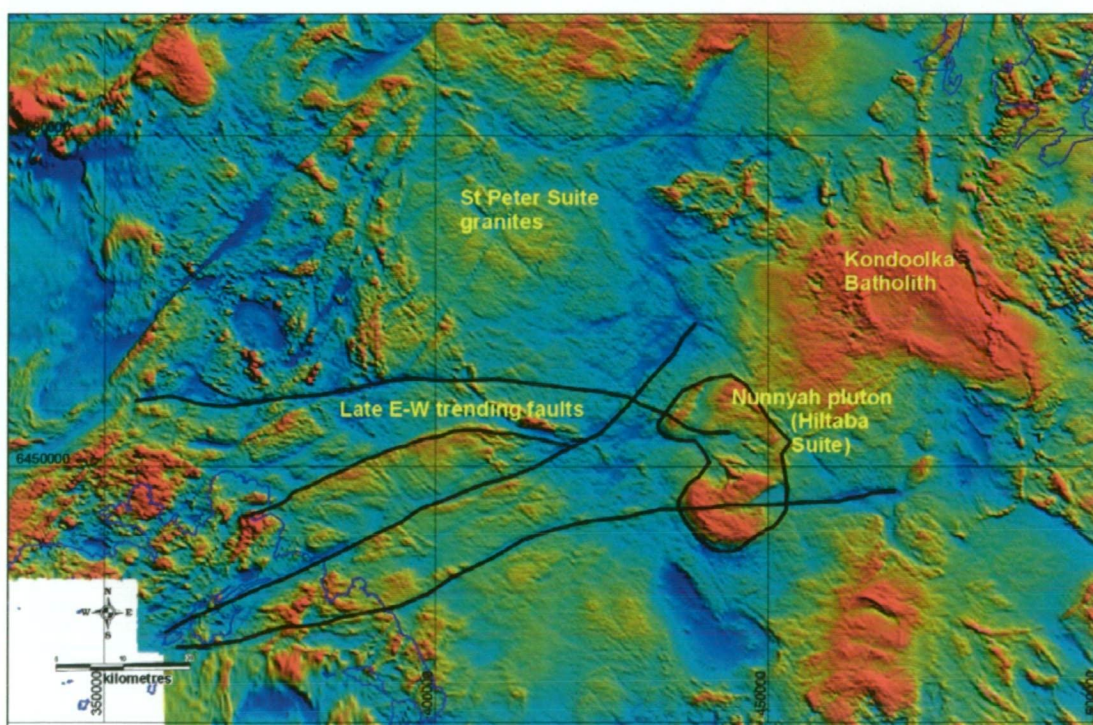
The geology and geochemistry of granitoids in the CHILDARA region, western Gawler Craton, South Australia: implications for the Proterozoic tectonic history of the western Gawler Craton and the development of lode-style gold mineralisation at Tunkillia.



The crust underwent thermal relaxation producing a suite of S-type granites. The most likely tectonic environment may be a small back arc basin with the subduction zone located to the east. The basin was subsequently closed during strike-slip motion on the Koonibba Fault Zone. The extension which produced the basin also produced mafic dykes to the west (Figure 105).

The Koonibba Fault Zone strikes northeast and is related to other major northeast trending shear zones on the western Gawler Craton. Mafic lithologies to the west and northwest of the Yumbarra magnetic anomaly show evidence of deformation related to movement on the Koonibba Fault Zone. The northeast striking sinistral deformation within the Yarlbirinda Shear Zone is most probably related to major shift in orientation of major stress observed across the western Gawler Craton.

The discovery of fabric forming events in Nundroo DDH2 within the Fowler Orogenic Belt (Daly and Fanning, 1993) to the west at ~1540 Ma, suggests that movement along the Koonibba Fault Zone occurred due to northwest compressive stress. Localised east-west trending shear zones on northern STREAKY BAY, are younger than intrusion of the Hiltaba Suite due to deformation of Hiltaba Suite plutons (Figure 106). They are most likely related to this tectonic event.



**Figure 106** TMI image showing mostly E-W trending late-stage faults. Faults cut Hiltaba Suite plutons, and hence are younger than ~1585 Ma.

Within the Fowler Subdomain, Teasdale (1997) also reports major compressional deformation between ~1560-1540 Ma, with granulite facies metamorphism in the Nundroo Block.

At Yarlbirinda Hill, the dominant N-S trending foliation is overprinted by pseudotachylite-generating brittle-ductile structures. At Lakeside, granites within the Yarlbirinda Shear Zone are truncated by a zone of intense shearing and associated



haematite and epidote alteration. The foliation strikes 060°. In summary, the northern part of the Yarlbirinda Shear Zone show abundant brittle, northeast trending structures, which clearly post date the main foliation forming event (Figure 90).

### **5.5.6 Tectonic episode 5**

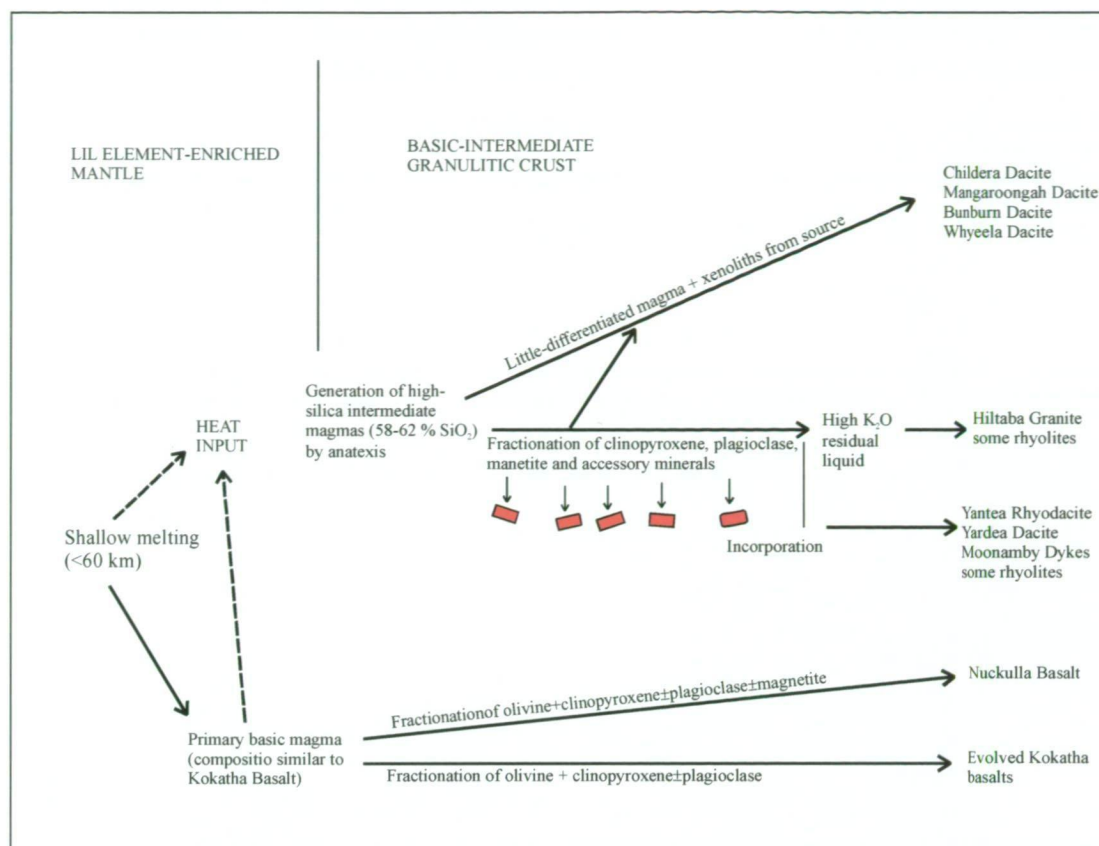
Teasdale reports minor felsic magmatism within the Fowler Subdomain at ~1490 Ma. Within the Yarlbirinda Shear Zone, K-Ar dating of late sericite alteration, gave an age of  $1516 \pm 16$  Ma, but this is due to fine grained and impure nature of the sample (Phillips, 1999).

Electron microprobe dating of monazite grains from the Munjeela Granite showed a small group of 3 analyses, which possibly show a resetting about 1200 Ma (R. Berry, CODES, pers. comm., 2001). This supports the 1100 Ma date reported by Teasdale from a aplite dyke at Lake Tallacootra. Ar-Ar dating of biotite grown in the fabric of major shear zones on the western Gawler Craton gave a range of ages between 1650 – 1450 Ma (G. Fraser, AGSO, pers. comm., 2001; C.M. Fanning, PRISE, pers. comm., 2001). No evidence for the 1100 Ma age was observed, hence these rocks have not been heated above 250° C, the closure temperature for biotite.

## **5.6 Implications for the development of the Hiltaba Suite/Gawler Range Volcanics**

The Gawler Range Volcanics represent a huge volume of Mesoproterozoic, dominantly felsic magma emplaced within the central Gawler Craton. The Gawler Range Volcanics is composed of two distinct units, the Upper and Lower, and the distribution of these units suggests initial volcanic activity occurred in several widely distributed centres including Kokatha and Lake Everard. Some units display linear outcrop pattern suggesting eruption from fissures. Aeromagnetic data shows the voluminous dacite units have prominent arcuate expression which suggest a more typical vent type eruption, but to date no vents have been located within the Gawler Range Volcanics.

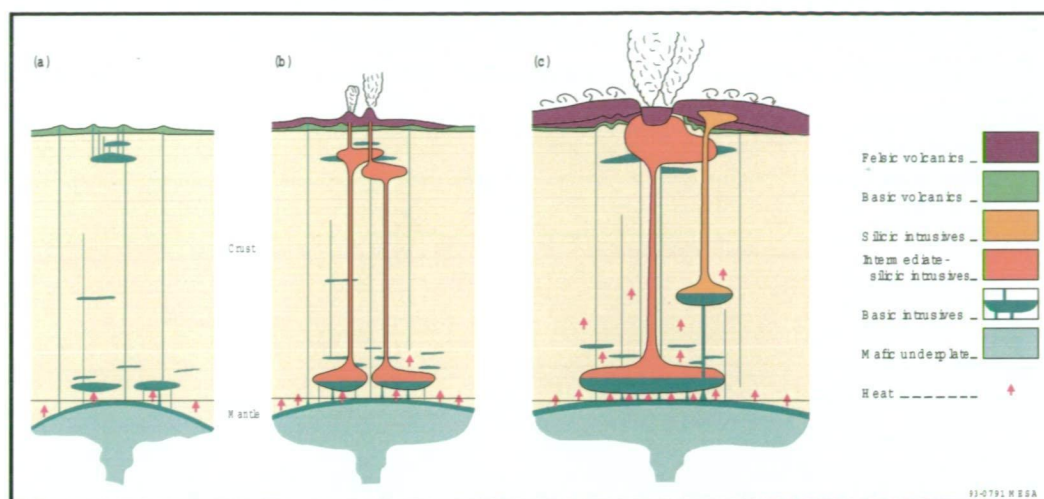
The source of the Gawler Range Volcanics remains enigmatic, with mantle underplating within an intracontinental setting the most widely accepted model (ie: Giles, 1980, 1988). Giles (1980) reported that units within the Glyde Hill Volcanic Complex showed evidence for two separate sources (Figure 107). Giles (1988) suggested that melting of the mantle produced magmas for both the mafic and felsic lithologies. The mafic units were erupted locally (eg: evolved Kokatha basalts, Nuckulla Basalt), and the felsic units were produced by increasing the thermal gradient of the continental crust to produce felsic magmas (Figure 107).



**Figure 107 Summary of postulated relationships between the various rock units in the Lake Everard area (from Giles, 1980).**

Stewart (1992) however, suggests that the Glyde Hill and other units of the developmental phase (Lower Gawler Range Volcanics) were derived from fractional crystallisation of a mantle derived magma, which digested Archaean to Palaeoproterozoic crustal rocks, within isolated magma chambers. The more extensive mature phase (Upper Gawler Range Volcanics) was possibly produced by the coalescence of these discrete chambers to form one large chamber (Stewart, 1992). This is supported by locally abundant basement xenoliths in the Nonning Rhyodacite (S Daly, PIRSA, pers. comm., 2001).

Huppert and Sparks (1988) modelled the process of mantle underplating of mafic magma producing high heat flow and melting (Figure 108). In the model, basic volcanics direct from the mantle (ie: evolved Kokatha basalts) are produced and felsic magmas are generally produced by partial melting of the lower crust. Increased underplating of the mafic magma to the crust generates greater volumes of silicic magma. The final stage is the eruption of large silicic ignimbrites (ie: Yardea Dacite) and high-level plutonism (ie: Hiltaba Suite).



**Figure 108** Diagrammatic scheme for generation of the Gawler Range Volcanics and Hiltaba Suite granitoids (Flint, 1993 after Huppert and Sparks, 1988).

Flint (1993) reports that the cause of extensive mafic underplating within an anorogenic tectonic setting remains unresolved. Using the model of Hoffman (1989), he suggested that a large mantle plume developed within the central Gawler Craton and acted as a thermal insulator which produced an increased heat regime, resulting in convective upwelling which lead to mafic underplating of the continent. If the Daly et al. (1998) continental collision model occurred, mantle heat loss would have been impaired by the very large continental mass formed by the East Antarctic Craton, the Gawler Craton and the proto-Yilgarn Craton.

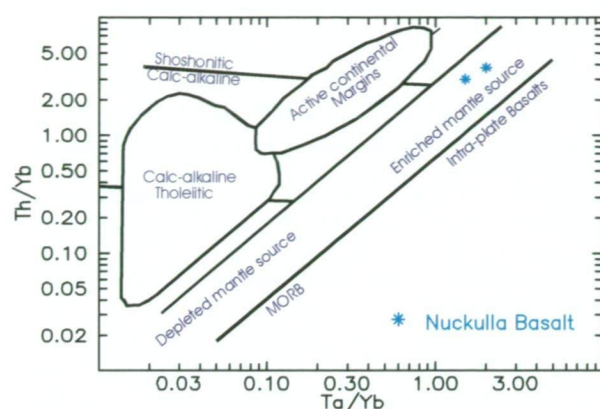
Within the tectonic framework outlined by this study, another model for the initial formation of the Hiltaba Suite is the underplating of the continental crust with a basaltic magma derived from the subducting slab, which produced the St Peter Suite magmatism. The introduction of a hot pulse of basaltic magma at the base of the crust with a mantle signature, would cause melting at higher crustal levels.  $\epsilon\text{Nd}$  values for Hiltaba Suite granites within the vicinity of known St Peter Suite magmatism record positive values including 0.11 (Nunyah Rockhole) and 1.19 (Wallala Rock) (Stewart and Foden, 2001), which suggest a depleted mantle source (Rollinson, 1993). Hiltaba Suite granites generally record negative  $\epsilon\text{Nd}$  values indicating a continental crustal source. Hiltaba Suite samples derived from Tunkillia Suite equivalent intrusives record  $\epsilon\text{Nd}$  values of -4 (eg: -4.50 at Arcoordaby Rockhole which records a zircon inheritance age of  $\sim 1670$  Ma; -4.39 from the 'frogs eyes' pluton on northern CHILDARA which records a zircon inheritance at  $\sim 1670$  Ma).

Zhao and McCulloch (1995) propose a multi-stage plate tectonic model for the formation of the Arunta granitoids, with an island arc/back arc developed at 1.9-1.7 Ga. This was followed by sedimentation and magmatism within this system and followed by closure of the back arc basins and development of Proterozoic crust (ie: production of CAT Group). The Main Group was produced by partial melting of arc-type underplates during collision of island arcs (Zhao and McCulloch, 1995). The HHP Group were produced by post-collision thermal relaxation and uplift which resulted in the water undersaturated remelting of the Main Group to produce the HHP Group. Zhao and McCulloch (1995) report that this process may have occurred



several times (eg: 1880-1850, 1780-1700 and 1650-1600 Ma), this last age overlaps the development of the St Peter Suite at 1630-1608 Ma.

The Nuckulla Basalt plots within the Enriched Mantle Source field (Figure 109) on a Th/Yb v Ta/Yb diagram of Pearce (1982), and not within the inter-plate field as would be expected for an intra-continental basalt.



**Figure 109** Nuckulla Basalt plotted on a discrimination diagram for the separation of subduction components from mantle components (after Pearce, 1983).

Within the Gawler Range Volcanics, basalts only occur within the Lower units in the Kokatha and Glyde Hill areas. This study has shown that the western Gawler Craton was tectonically active at ~1590 Ma and was undergoing terrane amalgamation by oblique compression along major shear zones. The geochemistry of the St Peter Suite indicates an calc-alkaline continental magmatic arc tectonic setting. The Glyde Hill and Kokatha areas are located on the western edge of the Gawler Range Volcanic province, hence may reflect a more direct heat source related to proximity to a magmatic arc. The Gawler Range Volcanics young to the east in the CHILDARA area, hence the heat source is most likely moving east and becoming more evolved.

More geochemical analysis of granites and mafic lithologies to the west of the Koonibba Fault Zone and within the southern Gawler Craton to determine the geochemistry and possible tectonic significance of these areas. West of the Koonibba Fault Zone, outcrop is sparse but recent drilling has provided samples suitable for geochemical interpretation.

Little is known about the southern margin of the Nuyts Subdomain and its relationships to the Coultas Subdomain and the type of tectonic processes which they formed. This study has focussed on the relationships between the Nuyts Subdomain and the subdomains to the west and north, but scant attention has been paid to the subdomains to the south and east. To fully test the model put forward by this study, this relationship needs to be studied.

### 5.6.1 Glyde Hill Volcanic Complex – Silicic Lava or Ignimbrite?

The extensive Gawler Range Volcanics, including the Glyde Hill Volcanic Complex have been interpreted as felsic ignimbrites (Giles, 1977, 1980, 1988; Blissett, 1979, 1986; Blissett *et al.*, 1993) based on the size of the volcanic province and the presence

of shards reported in several units. Table 9 outlines the physical features which characterise silicic ignimbrites and silicic lavas.

**Table 9 Physical features of silicic ignimbrites and lavas (from Henry and Wolff, 1992).**

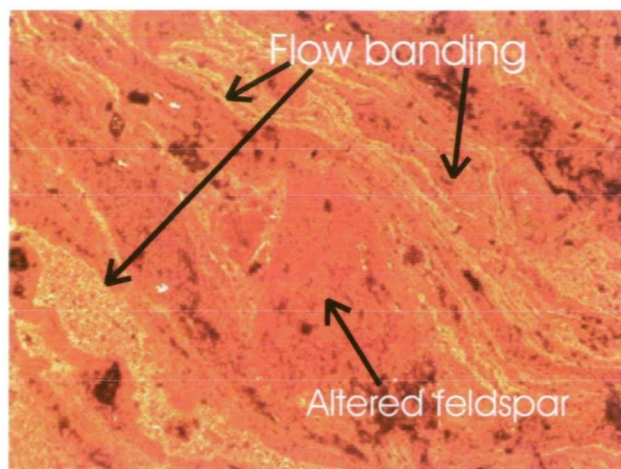
<u>Silicic Ignimbrite</u>	<u>Silicic Lava</u>
Extensive sheet like form	High aspect ratio
Low aspect ratio	
Fiamme	
Eutaxitic texture	
Abundant lithic fragments	Rare Lithic Fragments
Broken phenocrysts	Unbroken phenocrysts
Glass shards	
	Flow banding
Non welded to densely welded	Elongation of vesicles
Fumarolic pipes	Ramp structures

Bonnichsen and Kauffman (1987) distinguished rhyolite lava flows from pyroclastic flows in southwestern Idaho, using criteria outlined above, together with:

- the presence of blunt flow margins;
- abundant basal and marginal flow breccias;
- pervasive flow layering;
- laterally persistent zones of mismatched vertical shrinkage joints;
- complex contacts between basal vitrophyres;
- absence of lithic fragments;
- pumice fragments;
- bubble-wall shards;
- internal subhorizontal ash-emplacement layering; and
- sub-parallel flow marks.

These lavas had previously been interpreted as densely welded ash-flow sheets, which flowed like lava after emplacement (Ekren *et al.*, 1984).

Field mapping has shown that the Glyde Hill Volcanic Complex does contain a minor air-fall component, but is dominantly the result of extensive, most likely high-temperature lava flows with localised ignimbrites and epiclastic sedimentary units separating lava flows. The main outcropping units, the Childera Dacite, Mangaroongah Dacite and Yantea Rhyodacite show no evidence of an ignimbritic origin, all three units displaying similar features including rare lithic clasts, unbroken phenocrysts and some flow banding, more indicative of silicic lava. Plate 15 shows a hand specimen sample of Childera Dacite with flow banding and rare coarse lithic fragments. The sample has a pseudo-fiamme texture, but petrology showed diffuse flow banding with no fiamme present (Plate 56).



**Plate 56** Thin section view of flow banding within Childera Dacite wrapping around an altered feldspar phenocryst. The hand specimen (see Plate 16) has a pseudo-fiamme appearance, but the thin section shows diffuse flow banding with no fiamme present (field of view is 2.4 cm).

The basal margin of the Childera Dacite is covered by alluvium, but the Childera Dacite appears to maintain a relatively constant thickness with no apparent thinning towards the margin which is characteristic of ignimbrites. Between the Nuckulla Basalt and the overlying Yantea Rhyodacite is a thin layer of possible air-fall tuff, which may be a pre-eruptive pyroclastic air-fall deposit which characterises many silicic lavas (Henry *et al.*, 1990).

The main requirements for a silicic lava to form extensive flows are temperature and viscosity. Two-pyroxene geothermometry analysis of the Yardea Dacite indicated eruptive temperatures between 950-1000°C (Creaser, 1989; Creaser and White, 1991). Due to excessive high temperatures and low initial water content, Creaser (1989) and Creaser and White (1991) suggested that the Yardea Dacite formed via ash-flow tuffs which coalesced and flowed like lavas, with any pyroclastic features obliterated by compaction and devitrification. However, the high temperature and low volatile component indicate that the Yardea Dacite may be a silicic lava.

Table 10 outlines silicic volcanic units, which are controversial in origin, including the Gawler Range Volcanics, however there is sufficient evidence to support a silicic lava origin for the major dacite units of the Gawler Range Volcanics. The Glyde Hill Volcanic Complex does contain ignimbrites, the Wheepool and Arburee Rhyolites contain shards and hydrous minerals such as biotite, suggesting an ignimbritic origin.



**Table 10 Occurrence of extensive silicic volcanic rocks of controversial origin (from Henry and Wolff, 1992).**

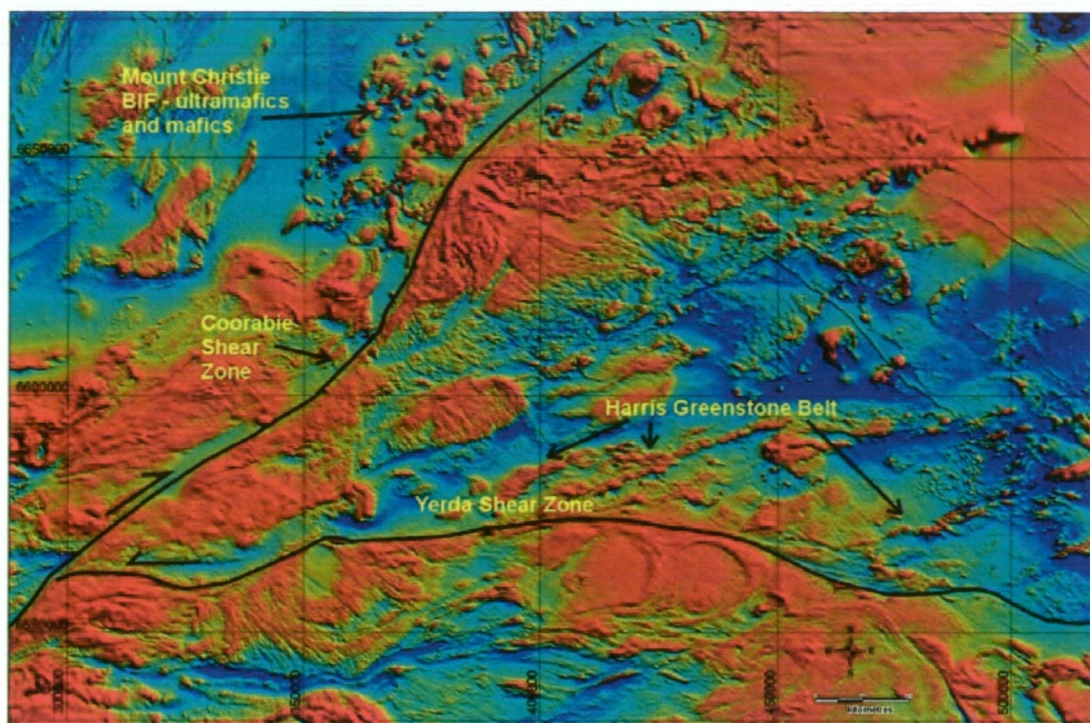
Volcanic province	Characteristics of silicic volcanic rocks			
	Basal breccia	Upper breccia	Distal thinning	Temp (° C)
Snake River, Idaho	Yes	Yes	No	850 – 1050
Yellowstone Park	Yes	Yes	No	>850
Trans-Peco Texas	Yes	Yes	No	>900
Keweenawan, Minnesota	Minor	Yes	No	>1000
Parana, Brazil	Minor	Yes	No	1000 - 1150
Etendeka, Namibia	Minor	Yes	No	1000 - 1100
Lebombo (Karoo) South Africa	Minor	Yes	No	900 - 1100
Rooiberg (Bushveld) South Africa	Minor	Yes	No	1100
Australia (Gawler Range Volcanics)	Yes	Yes	No	1100

## 5.7 CONCLUSIONS

The Palaeoproterozoic tectonic history of the western Gawler Craton appears to be related to a subduction event within a continental magmatic arc, which produced the calc-alkaline St Peter Suite. The Nuyts Subdomain represents a zone of extension and subsequent subduction to produce juvenile magma with geochemical characteristic similar to Archaean TTG's and Cordilleran magmatic arc rocks. This magmatic event was short lived and the Nuyts Subdomain was amalgamated with the Gawler Block during oblique transpression on the major shear zones of the western Gawler Craton. This also produced a major shift in magmatism from calc-alkaline magmatism of the St Peter Suite to fractionated, alkali-rich granites of the Hiltaba Suite. Within the western part of the area, the Hiltaba Suite records a depleted mantle signature with positive  $\epsilon_{\text{Nd}}$  values, which may reflect basaltic underplating of the crust due to subduction. To the east, the Hiltaba Suite generally records negative  $\epsilon_{\text{Nd}}$  values reflecting greater crustal contamination.

The location of a magmatic arc within the western Gawler Craton is unknown, more work is required to the west of the Koonibba Fault Zone, including geochemical sampling of Yumbarra and surrounding mafic lithologies, which may represent fragments of former oceanic crust. This project has not tried to reconstruct the former architecture of the western Gawler Craton, but one interesting possibility is the dismemberment of the Harris Greenstone Belt within the Wilgena Subdomain, initially by the Yerda Shear Zone and then the Coorabie Shear Zone to the north (Figure 110).

The Harris Greenstone belt comprises a sequence of ultramafics (komatiites), mafics (tholeiitic basalts) and metasediments including BIF. The Mount Christie area contains Archaean BIF and metasediments, calc-silicates, ultramafic (Blackfellow Hill Pyroxenite and Aristarchus Peridotite) and mafic lithologies (Figure 110). The tectonic scenario proposed which involves terrane separation and reformation by oblique transpression during the Mesoproterozoic would appear to validate this proposal, but more work is required, firstly to verify that the Harris Greenstone Belt is the same age as the sequence at Mount Christie.



**Figure 110** TMI image of part of the western Gawler Craton showing possible movement of the Harris Greenstone belt by Mesoproterozoic tectonics.

Syn-tectonic emplacement of a granodiorite within the Yerda Shear Zone recorded a crystallisation age  $\sim 1592$  Ma, hence the Yerda Shear Zone was active during the Mesoproterozoic. Dating of deformation/metamorphism at  $\sim 1540$  Ma within the Fowler Orogenic Zone (Daly *et al.*, 1998) indicates that the Coorabie Shear Zone was active at this time. Intrusion of the S-type Munjeela Granite at  $\sim 1560$  Ma was the last major magmatic event for the area. Plan 2 shows a solid geology interpretation of the CHILDARA map sheet.

## Chapter 6 Geology of Tunkillia Gold Prospect

### 6.1 Introduction

The Tunkillia prospect is located approximately 660 km northwest of Adelaide with access via sealed highway to Glendambo, then graded all weather road to Kingoonya, and to the prospect via station tracks (see Figure 2). Tunkillia is located within Exploration Licence 2028 originally granted to Helix Resources NL in November 1994. Acacia Resources Ltd entered into a 50:50 Joint Venture agreement with Helix Resources NL on 17 March 1998 with Acacia managing the project. In 1999, Acacia Resources Ltd was purchased by AngloGold Ltd and renamed AngloGold Australasia. Management of the Helix Resources NL and AngloGold Australia tenements in South Australia returned to Helix Resources NL during the year 2000.

Initial calcrete sampling in 1994 identified numerous anomalous zones of gold, which together define a large hydrothermal system associated with the Yarlbrinda Shear Zone. Figure 111 shows calcrete anomalism within the dextral strike-slip Yarlbrinda Shear Zone and major prospects within the main Tunkillia anomaly.

The aim of this chapter is to present new data obtained during this study, and incorporate it with published and confidential data, to determine the style and timing of mineralisation at Tunkillia. Data collected during this study include:

- Fluid inclusion microthermometry of vein quartz associated with mineralisation;
- Sulphur isotope determination of 21 samples of pyrite;
- Pb isotopic determination of 12 galena samples;
- K-Ar dating of sericite alteration; and
- U-Pb SHRIMP dating of host granite.

#### 6.1.1 Exploration History

Below is a brief description of exploration completed by 31 December 2000:

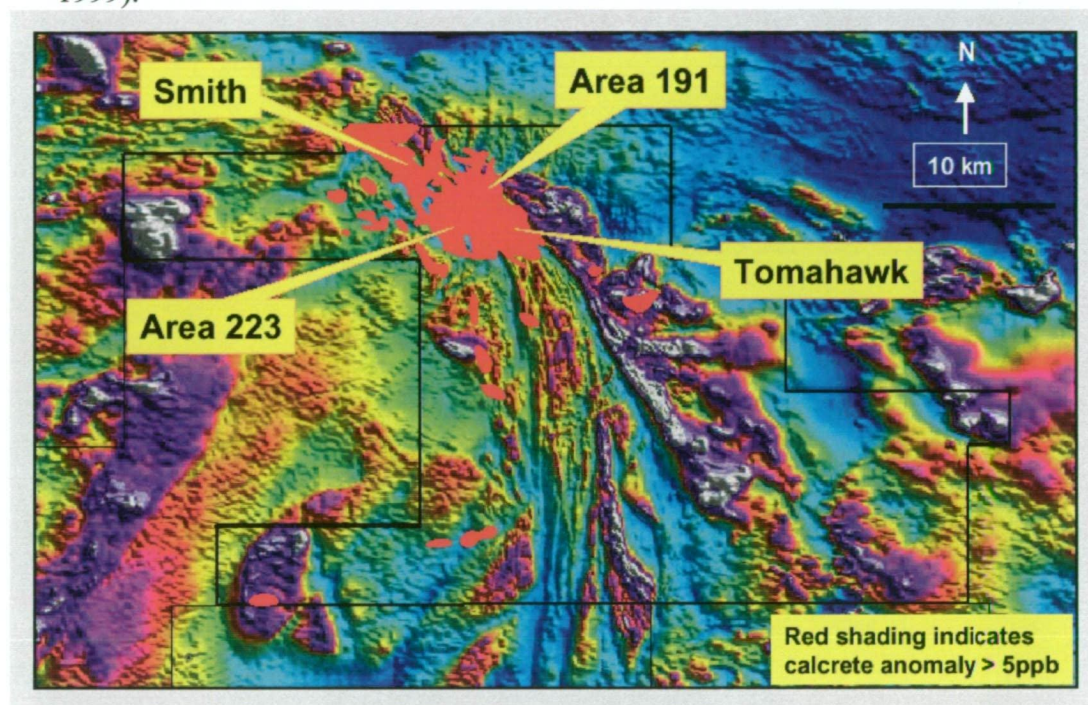
- A total of 1 945 calcrete samples were collected;
- Detailed analytical work was carried out to determining the location of gold and base metals within the carbonate profile to improve calcrete sampling technique;
- A 5 434 line kilometre of aeromagnetic and radiometric surveys were completed over the Yarlbrinda Shear Zone at 100m flight line spacing;
- A 4 880 line kilometre of aeromagnetic and radiometric surveys were completed over the Yarlbrinda Shear Zone at 25 m flight line spacing;
- 2 684 RAB holes were drilled totalling 153 161 m;
- 380 RC drill holes were drilled totalling 67 795m;
- 13 HQ and/or NQ diamond core holes or tails totalling 1 934.6 m were drilled at Area 223;
- 62.5 line kilometres of trial gravity survey on 5 lines were undertaken within the Tunkillia Prospect, and south over the Yarlbrinda Shear Zone;
- A detailed gravity survey over most of the Tunkillia Prospect;



- Detailed structural analysis of diamond drill core from Area 223 (Hill and Standish, 2000; various Helix Resources NL quarterly reports to the Australian Stock Exchange Ltd).

Gold is hosted in narrow steeply dipping quartz veins (lode gold-style) and is associated with sulphides, dominantly pyrite with minor galena, within an alteration zone comprising sericite and chlorite. Some of the best gold intersections from Area 223 include:

- LRC012: 36 m @ 3.68g/t Au (including 10 m @ 10.1g/t);
- LRC037: 13 m @ 5.47g/t Au (including 4 m @ 12.1g/t);
- LRC237: 19 m @ 5.1g/t Au (including 4 m @ 11.3g/t); and
- LRC033: 35 m @ 2.37g/t Au (including 3 m @ 15.2g/t) (Standish and Hill, 1999).



**Figure 111** Total magnetic intensity image showing location of calcrete anomalies at Tunkillia (Helix Resources NL website).

## 6.2 Rock Types

Regional mapping within the vicinity of Tunkillia and south near Childara Outstation has revealed a group of medium- to coarse-grained, partly-megacrystic, granite to granodiorite, which belong to the Tunkillia Suite. The Tunkillia Suite is a group of late Palaeoproterozoic (1690 - 1670 Ma) I-type intrusive rocks (see Chapter 2). Multigrain analyses of zircons from a sample of foliated drill core from hole LED 10 (155-157 m), gave an upper intercept age of  $1680 \pm 5$  Ma, which is interpreted as the crystallisation age. This is similar to the date obtained for a foliated rhyolite dyke intruded into granite southwest of Childara Outstation, which recorded a magmatic age of  $1679 \pm 12$  Ma (A.J. Parker, Geosurveys, pers. comm., 1997).

Petrological work by Pontifex and Hand (1997) described the host rock at Area 223 as medium-grained, with zones of megacrystic quartz monzonite to quartz poor



adamellite to granodiorite. There is no outcrop within the prospect area, but inspection of the drill core suggests that the rock types correlate with units L<sub>1</sub> and L<sub>2</sub> defined in chapter 2. Helix Resources NL defined six descriptive units to describe rocks intercepted within drill holes. Figure 112 shows a rock relationship diagram for a typical cross section for Area 223. A description of these units is presented below.

### 6.2.1 Tunkillia Augen Gneiss (TAG)

Tunkillia Augen Gneiss (TAG) is a medium-grained to megacrystic augen gneiss comprising coarse K-feldspar augen up to 8 x 15 mm, and finer-grained subhedral plagioclase grains which have been strongly deformed, producing protomylonitic to blastomylonitic gneiss (Plate 57). The rock is similar in appearance to rock from Yarlbirinda Hill, although the latter contains less plagioclase and have suffered predominantly brittle deformation. TAG most probably represents L<sub>1</sub> of the Tunkillia Suite.

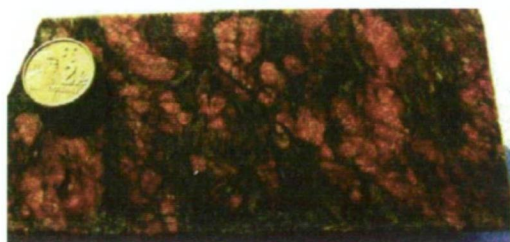


Plate 57 Drill core specimen of TAG.

K-feldspar grains are commonly contain numerous internal microfractures, which have been infilled with quartz and plagioclase. Plagioclase is more highly deformed and commonly shows sericitic alteration. Quartz is commonly strongly deformed and stretched into ribbon quartz, which defines the foliation. TAG shows a range of deformation features, from mylonitic foliation through to zones of intensely deformed dark chloritic phyllites. Sulphides are rare (<3%) and generally comprise pyrite only.

### 6.2.2 Fuzzy Granitoid (FUG)

This group describes a medium-grained, equigranular grey to pale green granodiorite to quartz monzonite which shows variable deformation from weakly foliated to protomylonitic fabric. FUG has a well defined granulo-granitoid crystalline texture comprising subhedral plagioclase grains (35-45%), K-feldspar (10-20%) and quartz which has been deformed and partly recrystallised, and minor primary biotite (Pontifex and Hand, 1997). Plagioclase is selectively sericitised and biotite is partly altered to chlorite and leucoxene.

### 6.2.3 Central Alteration Zone (CAZ)

The Central Alteration Zone (CAZ) defines a zone of intense sericite alteration and weak to moderate chlorite alteration (Plate 58). The original rock was a medium- to coarse-grained granite most probably correlated with L<sub>2</sub> of the Tunkillia Suite, but the original texture has been degraded by shearing and alteration. The rock is distinguished by pale green to dark green sericite and chlorite alteration.



**Plate 58** Drill core sample of CAZ showing intense sericite alteration.

CAZa (Central Alteration Zone - intensely altered) is a more altered member of CAZ and is associated with quartz±sulphide veins and gold mineralisation.

#### **6.2.4 Phyllite/ultra-mylonite shear (PUS)**

This TAG hosted unit is typically black to dark green and is strongly sheared producing a slaty cleavage. This unit may have formed due to compositional variations within TAG, or zones of higher strain within the shear zone. Pervasive chlorite and ilmenite alteration, and rare pyrite, are present.

#### **6.2.5 Mafic Dyke (MAD)**

Within the granitoid sequence outlined above, dark grey to green, fine- to medium-grained dolerite dyke were intruded (Plate 59). The dykes are variably foliated which suggests that they relate to the Tunkillia Suite (L<sub>4</sub>). This unit commonly shows brittle fracturing, calcite veining, haematite veinlets, rare sulphides, and does not generally contain anomalous gold.



**Plate 59** Drill core sample of mafic dyke (MAD) from Tunkillia prospect.

#### **6.2.6 Dacite/rhyolite Dyke (DAD)**

A dark red-brown dacite/rhyolite dyke comprising phenocrysts of quartz, K-feldspar and plagioclase within a massive microcrystalline matrix was intruded into the sequence, after the major regional deformation event (Plate 60). The dyke is undeformed and is possibly/probably related to the Gawler Range Volcanics, which places constraints on the timing of deformation. It shows brittle fracturing which has been infilled with late-stage chlorite (Pontifex and Hand, 1997). Some parts have been sericite altered which suggests that some alteration was post deformational and possibly related to waning stages of the Hiltaba Suite/Gawler Range Volcanic tectonothermal event.





Plate 60 Drill core sample of undeformed dacite dyke from Tunkillia prospect.

6.2.7 Other Minor Units

Minor units which occur within the Tunkillia prospect include (1) silicified fault breccia (SFB), which comprises milled country rock flooded by silica; and (2) a strongly haematite altered granite (GHA) which is commonly associated with SFB suggesting fluid movement along common fracture pathways (Standish *et al.*, 1997). South of Tunkillia near Boggy Crossing, within a possible compressional brittle flower structure, drill holes LEV 2355 and 2358 intersected metasediment. Petrological description reports a fine (muscovite-sericite) quartzite in LEV 2358 (Pontifex and Hand, 1997) which is similar to quartzite float located nearby. The quartzite has a protomylonitic fabric and rare laminae with titaniferous grains indicate a deformed metasediment. The stratigraphic position of this unit is unknown, but is thought to be pre-Hiltaba Suite and represent sedimentation within a compressional flower structure or step-over basin in the Yarlbirinda Shear Zone (Figure 90). This suggests a long-lived structural history for the Yarlbirinda Shear Zone.

6.2.8 Summary

The host rocks to the Tunkillia prospect are medium- to coarse-grained granitoids of the Tunkillia Suite ( $L_1$  and  $L_2$ ) which have been intensely sheared and brecciated within the Yarlbirinda Shear Zone. An idealised section through Tunkillia is presented in Figure 112.

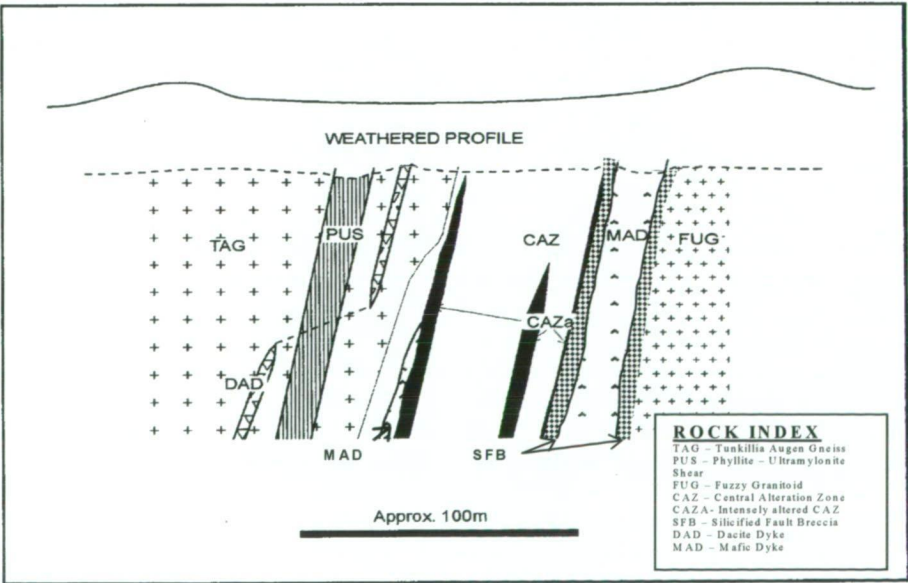


Figure 112 Generalised section of the Tunkillia prospect (Standish *et al.*, 1997).

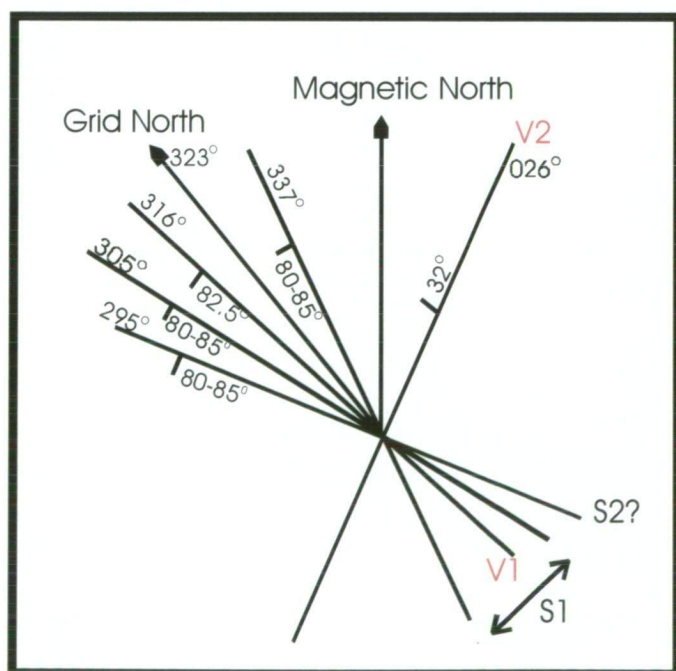
### 6.3 Structural Geology of the Tunkillia Area

Detailed structural interpretation of the Tunkillia Prospects has been undertaken by Rankin (1997a,b) and Laing (1998). Pontifex and Hand (1997) discussed the deformation history based on petrology of selected samples. This section will briefly summarise their findings and put them in a regional context discussed in chapter 4. The Tunkillia Prospect is located in the northern part of the Yarlbirinda Shear Zone, where it is reoriented to the NNW (See Figure 111). The rocks have undergone regional deformation within the shear zone, which has produced a range of fabrics, from a regional N-S, to NNW-SSE striking foliation with zones of intense deformation (mylonite zones).

Two generations of veins are observed within drill core:

1. V1 veins - quartz±sulphide (predominantly pyrite with minor galena and sphalerite) veins which host mineralisation. Laing (1998) divided the V1 veins into a “concordant to cleavage” set and a “discordant to cleavage” set;
2. V2 veins – barren calcite±quartz and chlorite veins that post-date regional shearing.

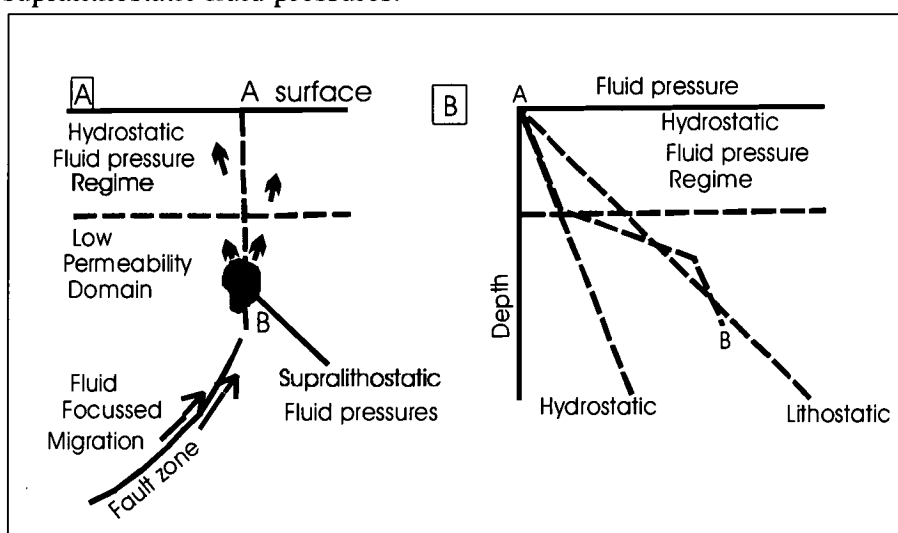
Drill holes were logged on-site by AngloGold geologists and structural data, including quartz ±sulphides and calcite±quartz veins (V1 and V2 respectively) and foliation ( $S_1$ ) measurements were made from oriented drill core. The main foliation strikes between  $285^\circ$  to  $340^\circ$  (magnetic north), dip steeply to the southwest (Figure 113). The V1 vein set is sub-parallel to  $S_1$  (Figure 113) which suggests they were formed during the main shearing event. The V2 vein set does not correlate well with the  $S_1$  and V1 structural orientation; the main cluster strikes  $026^\circ$  and dips  $32^\circ$  to the northeast (Standish, 1997). Relationships indicate that V2 veins formed after the main shearing event.



**Figure 113** Summary structural diagram of main structural orientations from diamond drill core from Area 223 (modified from Standish *et al.*, 1997).

Pontifex and Hand (1997) reported V1 veins, sometimes display a branching structure, suggestive of a stockwork structure. The early veins have been overprinted by the mylonitic deformation. This is a characteristic feature of these mesothermal lode deposits that show cyclic changes in fluid pressures from periods of lithostatic pressure to periods of sublithostatic to supralithostatic pressure (Cox *et al.*, 1991). The vein network at Tunkillia is narrow and does not penetrate the wallrocks for any great distance. Hence mineralised zones are likely to have been zones of high permeability and fluid flux at near lithostatic pressure during vein formation and mineralisation.

Lode gold mineralisation is commonly located not within the major shear zone, but within secondary splays off the main shear structure. Cox *et al.* (1991) report that major goldfields within the Ballarat-Bendigo area in Victoria are not located within first-order faults because major faults breach the base of the hydrostatic pressure regime, fluids quickly move through the system without major wallrock interaction and are focussed in the secondary structures (Figure 114). At Tunkillia, economic gold grades are localised at the intersection of the regional  $S_1$  foliation and steeply dipping stretching lineations, which leads to steeply dipping ore shoots. Ore shoots are related to a change in the plunge of the mineral/stretching lineation from shallow to steeply plunging. This produced localised dilatational zones, which are zones of supralithostatic fluid pressures.



**Figure 114 (A) schematic diagram showing how large-scale crustal fault architecture controls fluid migration pattern. First order localisation of near-lithostatic pressured regimes can be controlled by major fluid focussing faults terminating below low permeability crustal regimes. (B) Variation of fluid pressure within depth profile A-B in (A) (from Cox *et al.*, 1991).**

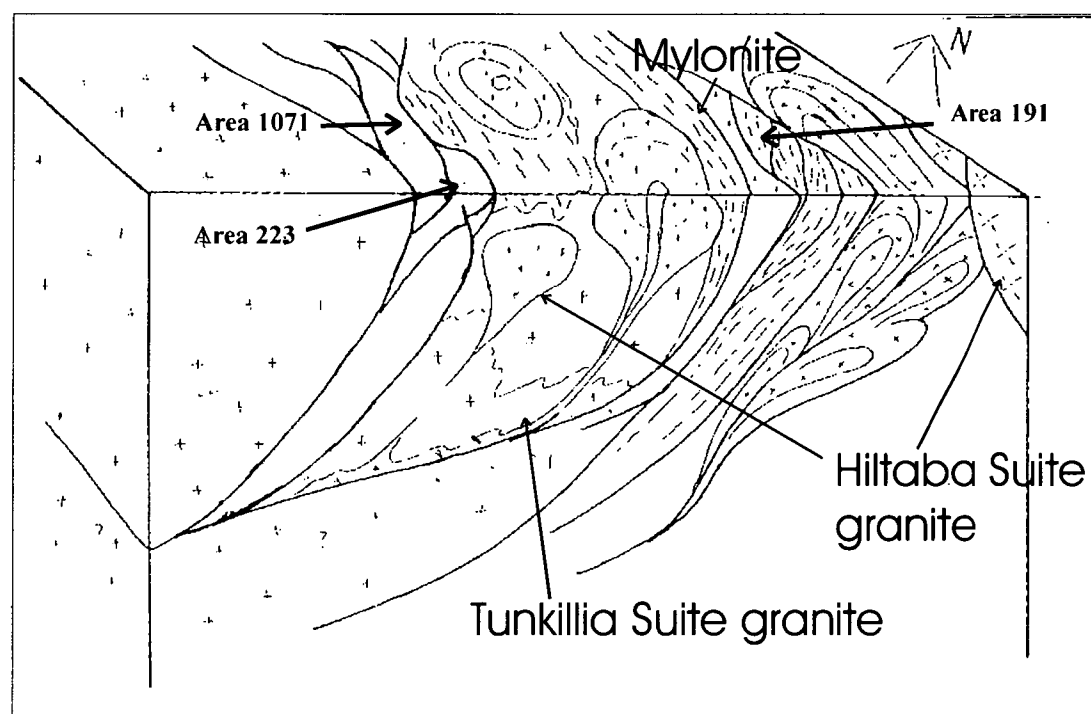
Within mesothermal lode deposits, deformation, fluid pressure fluctuations, fluid flow and hydrothermal alteration are intimately linked (Kerrick, 1986; Sibson *et al.*, 1988; Cox *et al.*, 1991). Hydrothermal alteration of the wallrocks produces new minerals which affect the permeability of these rocks. The production of sericite at Tunkillia would greatly enhance the porosity of the rocks and decrease the wallrock competency, hence focus deformation within these zones. This is referred to as 'strain softening' (McCuaig and Kerrich, 1994). The precipitation of anhydrous



minerals such as quartz and ankerite within the wallrocks increases the wallrock competency, and they become harder to deform, and restrict infiltration of hydrothermal fluids. This is termed 'strain hardening' (McCuaig and Kerrich, 1994).

Rankin (1997b) reported that mineralisation was related to complex structural control within the Tunkillia Prospect (Figure 115):

- At Area 223, a NW-SE trending shear zone with interpreted late-stage extensional reactivation is intersected by N-S transtensional faults extending from the western demagnetised zone;
- At Area 1071, complex interaction between strike-slip and high-angle reverse faults offsets the main western demagnetised zone. This offset may have accommodated the emplacement of a fluid-rich granite; and
- At Area 191, complex transpressive NW-SE to N-S "pop-up" structures near the margin of a granite in the eastern demagnetised zone appears related to major alteration.



**Figure 115** Schematic block diagram of structure within Tunkillia Region (Rankin, 1997b).

Rocks from Area 223 diamond drill core contain a strong, coarse grained foliation defined by ribbon quartz wrapped around coarse feldspar grains. Minor muscovite and ilmenite is present within the foliation. Unfortunately, there are no diagnostic minerals present which constrain the temperature and depth at which deformation and metamorphism occurred. Pontifex and Hand (1997) reports that quartz fabrics formed via subgrain rotation and recrystallisation, whereas K-feldspar underwent limited recrystallisation, and plagioclase grains showed limited evidence of ductile deformation, but did not recrystallise. They conclude that the temperature was between 400°-450° C during initial mylonitisation.

The main structure is a left stepping dextral wrench system in which the western side tries to over-ride the eastern side and in the process develops a range of ductile duplexes and brittle ‘pop up’ structures.

6.4 Alteration Assemblage

In a regional context, the Tunkillia area shows evidence of extensive alteration. Large zones of demagnetisation are observed in aeromagnetic images (see Figure 89 and 90). Helix Resources NL defined a western and eastern demagnetised zone (alteration of primary magnetite to ilmenite) within the northern Yarlbirinda Shear Zone; Area 223 is located within the western demagnetised zone. This indicates that large volumes of fluid were focussed within the shear zone, particularly along the margins.

At the prospect scale, gold mineralisation at Tunkillia is associated with zones of intense sericite alteration, and quartz and sulphide veining. Petrology shows that primary plagioclase grains have been extensively altered to sericite. In hand specimen, this has imparted a pale green-brown colour to the rock, that is in total contrast to zones of minor alteration (TAG). The sericite alteration provides evidence for strain softening having occurred at Tunkillia, with unaltered fragments of TAG found within zones of sericite alteration. Pontifex and Hand (1997) report that CAZ becomes more massive where vein quartz is abundant, which is further evidence of strain hardening. Two samples of sericite alteration were submitted for K-Ar dating to determine whether sericitic alteration is associated with intrusion of the Hiltaba Suite, or a younger deformation event.

6.4.1 K-Ar dating of sericite alteration

One sample of mildly sericite-altered rhyolite/rhyodacite dyke (R387439) and one sample of intensely sericite-altered granite (R387440) were forwarded to Precise Radiogenic Isotope Services (PRISE) for K-Ar dating. Sample R387440 comprises intensely foliated and altered granite, whereas sample R387439 is undeformed.

Mineral separates were analysed using the methods described in McDougall (1985). Results are presented in Table 11.

Table 11 Summary K-Ar data for Tunkillia samples.

Sample No.	K (wt %)	Radiogenic <sup>40</sup> Ar (10 <sup>-8</sup> mol/g)	% Radiogenic <sup>40</sup> Ar	Calculated age (±1 s.d.)
R387439	5.978	2.439	66.6	1510 ± 10 Ma
LRC 32D 376.2 m	5.924	2.453	66.8	1516 ± 16 Ma
R387440	6.456	2.907	90.6	1608 ± 13 Ma
LED01 108-109m	6.458	2.909	90.5	1609 ± 13 Ma

Sample R387439 yielded a mean K-Ar age of 1513 ±16 Ma and sample R387440 recorded a mean K-Ar age of 1609 ±12 Ma (Phillips, 1999). The difference in age may represent a geological/alteration feature or may be due to lower potassium concentration and possible <sup>40</sup>Ar loss from the separate due to its lower purity and

finer grain size (Phillips, 1999). Sample R387440 contained minor amounts of altered feldspar from the host and may have added an inherited component to the sericite age, making the age older than the Hiltaba Suite. Due to the fineness of the sericite, an accurate date is not possible with the two samples tested. The dates provide a minimum age for the alteration event at Tunkillia.

## 6.5 Fluid Inclusions

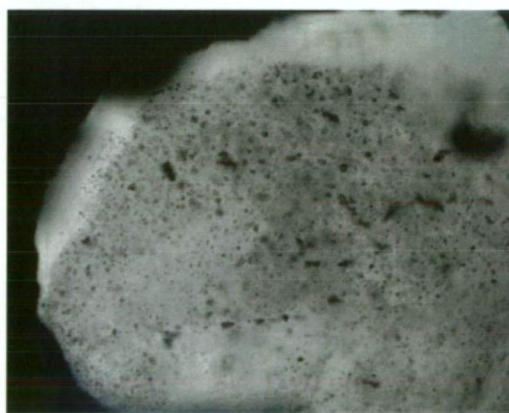
Mineralisation at Tunkillia is confined to quartz±sulphide veins, which are syn-deformational with respect to the main shearing and foliation forming event. The quartz veins appear intimately associated with sulphides, and therefore the fluid inclusion data is representative of the fluids responsible for gold deposition.

Milky white quartz is the main phase and comprises generally ≥90% of the veins, with sulphides (predominantly pyrite) comprising up to 10% of some veins. Four samples of quartz veins (V1) from Tunkillia were selected as suitable to obtain fluid-inclusion micro-thermometric data to establish temperature, composition and salinity of fluids related to sulphide precipitation.

Definitive petrographic evidence is difficult to find to link the fluid inclusion data to gold deposition. Gold was deposited as isolated blebs and in fractures in quartz and sulphides. Parker (1996) reports that petrology of sheared granite samples from Nuckulla Hill prospects suggest temperatures ranged from 350° to <100° C with different pH and XCO<sub>2</sub> levels.

### 6.5.1 Methods

Initial petrographic observations showed that numerous small (<3 µm) single phase fluid inclusions were present, largely with leakage characteristics, but rare zones of two phase primary fluid inclusions occur within enclosed pockets of sulphides which appear to have protected these sites from regional deformation (Plate 61).



**Plate 61** General view of quartz hosted fluid inclusions trapped within pyrite grain within quartz veins in hole LED 03. Width of view is 2.4 mm.

Three unmounted 150 µm thick sections were prepared at CODES. Microthermometric measurements were made using a Fluid Inc. modified USGS, gas-flow, freezing-heating stage (Sterner and Bodnar, 1984; Bodnar and Sterner, 1985). The slides were broken into smaller <1 cm diameter wafers to enable housing

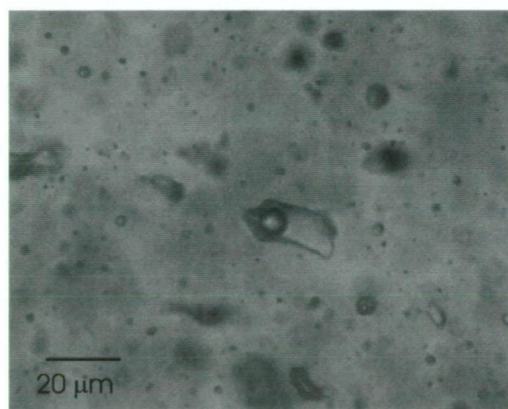


of samples within the sample chamber. Temperature data was recorded using a chromel-constant thermocouple that was placed directly on the fluid inclusion wafer in proximity to the fluid inclusion being analysed. Freezing and heating methods are outlined in Roedder (1984). Thermocouple measurements were calibrated against the triple point of CO<sub>2</sub> (-56.6° C), the freezing point of water (0.0° C) and the critical point of water (374.1° C) in synthetic fluid inclusions.

### 6.5.2 Fluid Inclusion Types

The majority of fluid inclusions observed from polished thin sections are small single phase (<5 µm); no microthermometric analyses were carried out on these inclusions. Within rare pockets of quartz enclosed within sulphides, fluid inclusions examined belonged to 3 groups (after Nash, 1976) based on phase relationships at room temperature.

- Type 1b - two-phase liquid rich (Plate 62) with a small vapour bubble represent a minor phase (≥5%);
- Less abundant Type 4 liquid-H<sub>2</sub>O and liquid CO<sub>2</sub> 3-phase inclusions found together with Type 1b; and
- Abundant Type 5 single phase liquid-filled aqueous inclusions which range in size from 1-15 µm. Many of these inclusions are thought to represent former 2- or 3-phase inclusions which decrepitated to produce single phase inclusions.



**Plate 62 Detailed view of type 1b fluid inclusion.**

No fluid inclusions containing daughter minerals were found in the samples examined. Types 1b and 4 occur in clusters randomly distributed through the quartz are considered primary and will be used for microthermometric analyses. Type 5 inclusions occur in planar groups and along healed fractures, and crosscut types 1b and 4, and are pseudosecondary to secondary. Freezing measurements were collected first to avoid decrepitation of inclusions.

Petrographic examination shows quartz veins from Tunkillia underwent substantial deformation which destroyed most fluid inclusions with only minor useable fluid inclusions found in protected areas. This is additional evidence that the inclusions used in this study relate to vein formation and sulphide growth, rather than to the subsequent history of deformation.

### 6.5.3 Microthermometric Results

Microthermometric cooling refers to the cooling of the fluid inclusions until solidification of the liquid phase occurs, then the sample is heated and phase changes observed. The temperature of first melting ( $T_m$ ) and the temperature of final melting ( $T_{fm}$ ) are used to determine the salinity of fluid inclusions. The majority of measurements come from one sample R387436 (LRC 32D 266.5-266.65 m). The other samples used are R387429 (LED 03 249.8-249.9 m) and R386308A (LED 01 127.7 m).

The small size of inclusions limited the number of reliable observations possible on freezing behaviour. Goldstein and Reynolds (1994) report that  $H_2O$ -NaCl liquid of low salinity (<5 wt. % NaCl) will contain minor hydrohalite, hence accurate determination of first melting is difficult to visually detect. Only 10 reliable temperatures were measured and they ranged from  $-38^\circ C$  to  $-30^\circ C$  with an average of  $-33.6^\circ C$  (Table 12). This value is below the  $H_2O$ -NaCl eutectic, which suggests the presence of salts other than NaCl.

Final melting temperatures ranged from  $-6.0^\circ C$  to  $6.8^\circ C$  with an average of  $-3.7^\circ C$  (Table 12). Some of these melting temperatures were made in the presence of clathrate and only provide maximum estimates of the salinity. Bodnar *et al.* (1985) have shown that it is very difficult to observe clathrate in inclusions containing less than 4 mole percent  $CO_2$ . Only one fluid inclusion recorded a positive value ( $6.8^\circ C$ ) which may represent a  $CaCl_2$  hydrate (mixing of aqueous and non aqueous phases).

Homogenisation temperatures ranged from  $165^\circ C$  to  $>350^\circ C$  with an average of  $247^\circ C$  (Table 12). Figure 116 shows that fluid inclusions formed over a wide range of temperatures which may be due to cooling of the hydrothermal system. The  $T_h$  temperatures need to be pressure corrected to temperatures of trapping. Pontifex and Hand (1997) estimated that mylonitisation at Tunkillia, occurred at temperatures between  $400$ - $450^\circ C$ . The depth of mylonitisation is estimated at approximately 8 km, and assuming a pressure gradient of 0.25 kbar/km, and a salinity of 5 wt% NaCl, using the pressure-temperature curves of Potter (1977), the veins require a temperature correction of  $165^\circ C$ , giving a trapping temperature range between  $330^\circ C$  to  $515^\circ C$ , with an average of  $412^\circ C$ .

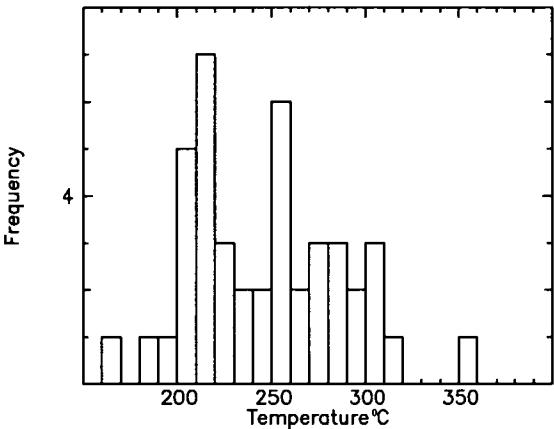
**Table 12 Fluid inclusion data for Tunkillia samples.**

Sample	Spot No.	Inclusion type	Size (µm)	Liquid: water	Temp. freezing (°C)	Tm – final melt (°C)	Te – 1 <sup>st</sup> melt (°C)	Homogen. temp. (°C)	Comments
R387436 Site 1	1	L-V (1b)	8-9	V=30%	-50	-4.9	-30.1	227	
	2	L-V (1b)	3	V= 40%		-4.3	-37	224	
	3	L-V (1b)	3	V = 20%	-78	-4.4		296	
	4	L-V (1b)	2	V = 20%		-3.7	-31.8	209	
	5	L-V (1b)	2	V = <10%		-4.2		221	
	6	L-V (1b)	10	V = 30%		-4.4	-30	286	
	7	L-V (1b)	5	V = 40%		-4.6	-38	268	
	8	L-V (1b)	2	V = 30%	-78	-4.6	-38	213	
	9	L-V (1b)	2	V = 20%		-3.2		253	
	10	L-V (1b)	5	V = 15%		-4.8		213	
	11	L-V (1b)	3	V = 40%		-4.8		254	
R387436 Site 2	1	L-V (1b)	5-10	V = 40%	-60	-3.3	-32	238	
	2	L-V (1b)	5-8	V = 30%		-3.4		214	
	3	L-V (1b)	10-15	V = 25%		-3.5		270	
	4	L-V (1b)							Inclusion went black
	5	L-V (1b)	8	V = 15%		-4.8		259	
	6	L-V (1b)	12-15	V = <10%		-4.3			Burnt
	7	L-V (1b)	8	V = 15%		-3.2			Burnt
	8	L-V (1b)	8	V = 10%		-2.7	-33		burnt
	9	L-V (1b)	4	V = 20%		-4.2		213	
	10	L-V (1b)	8	V = 30%		-3.8	-30.4	238	
	11	L-V (1b)	8	V = 30%		-3.8		277	
	12	L-V (1b)	6	V = 25%		-0.5		254	
	13	L-V (1b)	6	V = 15%	-53	-3.1		211	Clathrate present, disappeared after zero
	14	L-V (1b)	6	V = 20%	-44	-1.2		192	Bubble disappeared on freezing, kept moving above zero indicating clathrate production
	15	L-V (1b)	10	V = <10%				207	
R387436 Site 3	1	L-V (1b)	12	V = 60%	-55	-4.7		>305	Upon freezing edge went dark
	2	L-V (1b)	6	V = 25%		-4.4	-35.9	287	
	3	L-V (1b)	5	V = 20%		-3.0		186	
	4	L-V (1b)	5	V = 15%		-4.0		209	
	5	L-V (1b)	7	V = <10%		-3.6		244	Bubble continued activity below zero indicating possible clathrate formation
	6	L-V (1b)	5	V = 15%		-3.9		208	Bubble continued activity below zero indicating possible clathrate formation

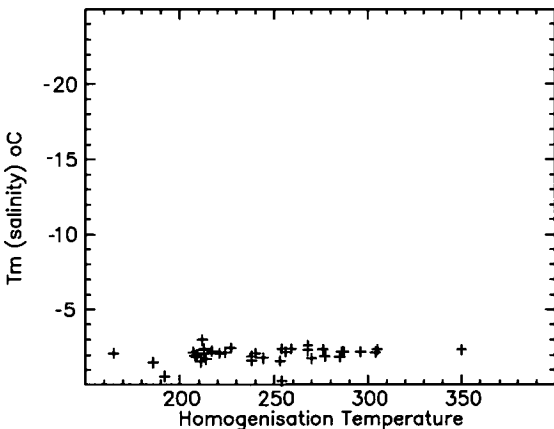


Sample	Spot No.	Inclusion type	Size (µm)	Liquid: water	Temp. freezing (°C)	Tm – final melt (°C)	Te – 1 <sup>st</sup> melt (°C)	Homogen. temp. (°C)	Comments
	7	L-V (1b)	9	V = 5%		-3.7		285	
	8	L-V (1b)	10	V = 35%		6.8		303	
	9	L-V (1b)	10	V = 25%		-4.7		276	
	10	L-V (1b)	5	V = 15%		-4.4		256	
R387429 Site 1	1	L-V (1b)	3			-4.2		165	
	2	L-V (1b)	3			-6.0		212	
	3	L-V (1b)	3			-4.3		304	
	4	L-V (1b)	3			-4.3		207	
	5	L-V (1b)	3			-4.5		217	
R387429 Site 2	1	L-V (1b)	4	V = 5%		-4.7		>350	decrepitated
	2	L-V (1b)	3	V = 10%		-3.7			
	3	L-V (1b)	5	V = 15%				301	
	4	L-V (1b)	5	V = 15%				293	
	5	L-V (1b)	5	V = 15%				253	
R386308A	1	L-V (1b)	4	V = 10%		-4.2		240	
	2	L-V (1b)	5	V = 5%		-5.2		268	
	3	L-V (1b)	5	V = 10%		-0.9			

Eutectic temperatures ranged between  $-37^{\circ}$  to  $-30^{\circ}$  C suggesting the presence of some  $\text{CaCl}_2$  with relatively high final melting temperatures, indicating a salinity  $\leq 6$  equivalent wt % NaCl. Figure 117 shows a plot of final melting temperature versus homogenisation temperature, which shows that the fluid is moderate temperature and low salinity. The ore fluids have uniform relatively low salinities and low  $\text{CO}_2$  contents.



**Figure 116 Histogram of homogenisation temperatures.**



**Figure 117 Tm (final melting temperature in °C) versus temperature of homogenisation for Tunkillia samples.**

**6.6 Sulphur Isotopes**

Sulphur isotope analysis was undertaken to place constraints on the source of sulphur within the Tunkillia ore system. Twenty two samples of pyrite were analysed using conventional and laser ablation methods.

Pyrite is the main sulphide at Tunkillia and is present as large euhedral grains within quartz veins (V1), as subhedral to anhedral grains within V1 veins, as fine-grained disseminated grains and as infillings of late-stage fractures. Pyrite grains with all three textures were selected for sulphur isotope analysis to assess the isotopic composition and source of sulphur in the Tunkillia prospect and to ascertain the

spatial variations in the physio-chemical conditions associated with sulphide deposition.

Sulphur may be derived;

1. directly from magmatic fluids;
2. metamorphic fluids;
3. from leaching or desulphidation of primary or secondary minerals in igneous rocks; and
4. from leaching or desulphidation of sulphide minerals from sediments or older hydrothermal alteration;

or by some combination of these three sources.

Sulphur isotope geothermometry is not reported due to difficulties in establishing isotopic equilibrium between mineral pairs.

Results from this study will be compared to limited sulphur isotope data available for Mesoproterozoic deposits at Moonta (Cu-Au), Tarcoola (Au) and Menninnee Dam (Pb-Zn).

### 6.6.1 Analytical Techniques

Coarse-grained pyrites screened to be inclusion free were drilled out by hand using a dentist drill, and these samples were analysed by conventional analytical techniques (Robinson and Kusakabe, 1975). 16 samples were combusted to develop O<sub>2</sub> and then SO<sub>2</sub> was then separated to determine the <sup>34</sup>S/<sup>32</sup>S ratios. The results were expressed in standard per mil (‰) notation relative to the Canyon Diablo Troilite (CDT), and calculated as:

$$^{34}\text{S}_{\text{sample}} = \frac{(^{34}\text{S}/^{32}\text{S})_{\text{sample}} - (^{34}\text{S}/^{32}\text{S})_{\text{standard}}}{(^{34}\text{S}/^{32}\text{S})_{\text{standard}}} * 1000 \text{ ‰}$$

Measurements were performed using a Finnigan Isogass 2000 mass spectrometer and results are presented in Table 13. The precision of conventional analyses is  $\pm 0.3 \text{ ‰}$ .

Six fine-grained pyrite samples too fine for conventional analysis were analysed by laser ablation in accordance with the procedure of Huston *et al.* (1993), using a Nd:YAG laser. Unmounted polished thin sections were prepared and broken into 10 mm x 10 mm wafers. Pyrite grains analysed had to be  $>70 \text{ }\mu\text{m}$  because ablation pits ranged in size from 100  $\mu\text{m}$  to 250  $\mu\text{m}$ . SO<sub>2</sub> gas was collected and passed into an automatic clean-up line on a VG Sira 10 mass spectrometer. The precision of the laser ablation technique was established by Huston *et al.* (1993) as  $\pm 0.3 - 0.5\text{‰}$ . Pyrite analysis by laser are corrected for laser effects according to calibrations in Huston *et al.* (1993). Results are presented in Table 12. Both techniques were carried out in the Central Science Laboratory, University of Tasmania, under the supervision of Keith Harris and Christine Cook.

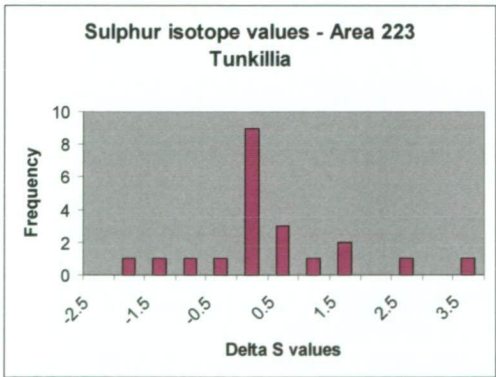


6.6.2 Results

Results are presented in Table 13 and shown in Figure 118.  $\delta^{34}\text{S}$  values range from – 2.23 to 3.19 ‰, with a mean of 0.09 ‰, and fall within the range of sulphides in mantle-derived melts and intracontinental granitic rocks (Nielsen, 1979; Hoefs, 1987).

**Table 13 Sulphur isotope analyses of pyrite from Tunkillia (values in per mil relative to Canon Diablo Troilite). (\* laser samples).**

D/Hole	Interval (m)	Description	Weight (mg)	Yield mm Hg	$\delta^{34}\text{S}$ ‰
LED 03	289	coarse aggregate	7.5	13.3	-0.48
LED 08	106.3	scattered ragged pyrite	4.2	5.7	-0.23
LED 08	119.3	coarse aggregate	2.4	2.8	-1.21
LED 08	129.9	massive pyrite	5.3	7	-0.63
LED 03	186.1	Massive pyrite	7.6	11.2	-0.39
LED 03	289.6	Massive pyrite	1.7	2	-0.31
LED 03	375.9	Vein	1.3	2.2	-0.20
LED 01	107.2	massive pyrite	0.9	1.9	-0.15
LED 02	143.05	scattered ragged pyrite	1.2	1.9	-1.54
LED 09	145.9	Coarse euhedral crystal	5.8	4.8	2.13
LED 10	145.15	vein	0.9	1.2	-2.23
LED 10	258	massive	4.8	5.8	1.22
LED 10	317.8-317.85	vein	6	7	0.29
LED 10*	318.75-318.8	Coarse euhedral crystal	2.9	4.8	-0.04
LED 10*	345.2	folded pyrite vein	0.3	0.8	1.31
LED 03*	249.8-249.9	scattered ragged pyrite	2.3	3.8	3.19
LED 08*	140.8-140.9	coarse pyrite	3.4	5.4	-0.05
LED 04*	187.25-187.3	scattered pyrite	2	2.1	-0.13
LRC 32D*	266.5-266.65	scattered pyrite	2	5.7	0.65
LRC 32D	290-290.15	scattered pyrite	0.4	1.5	0.36
LED 10	274.1	Massive pyrite	9.3	12.2	0.33



**Figure 118 Graph showing sulphur isotope values from Tunkillia.**

In summary, sulphur isotope results from pyrite within the Tunkillia ore system are similar but form a narrower range, than isotopic values of some other similar-aged hydrothermal systems on the Gawler Craton influenced by Hiltaba Suite granitoids. The  $\text{H}_2\text{S}$  values inferred are consistent with a magmatic origin for sulphur. This fits

The geology and geochemistry of granitoids in the CHILDARA region, western Gawler Craton, South Australia: implications for the Proterozoic tectonic history of the western Gawler Craton and the development of lode-style gold mineralisation at Tunkillia.

with the geological environment since the Tunkillia prospect is hosted by granite, with no sediments observed in the immediate area. However, the data do not preclude an origin from a metamorphic source dominated by magmatic rocks. Other deposits on the Gawler Craton show mixing of a variety of sources but all with a possible link to magmatic sources, though more rigorous analysis is required to more fully constrain this interpretation.

## 6.7 Lead Isotopes

Lead isotope analysis was carried out on galena samples from V1 veins from Tunkillia to determine the source of lead and the relative timing of mineralisation compared to other Pb-bearing mineralisation in the district.

### 6.7.1 Analytical Methods

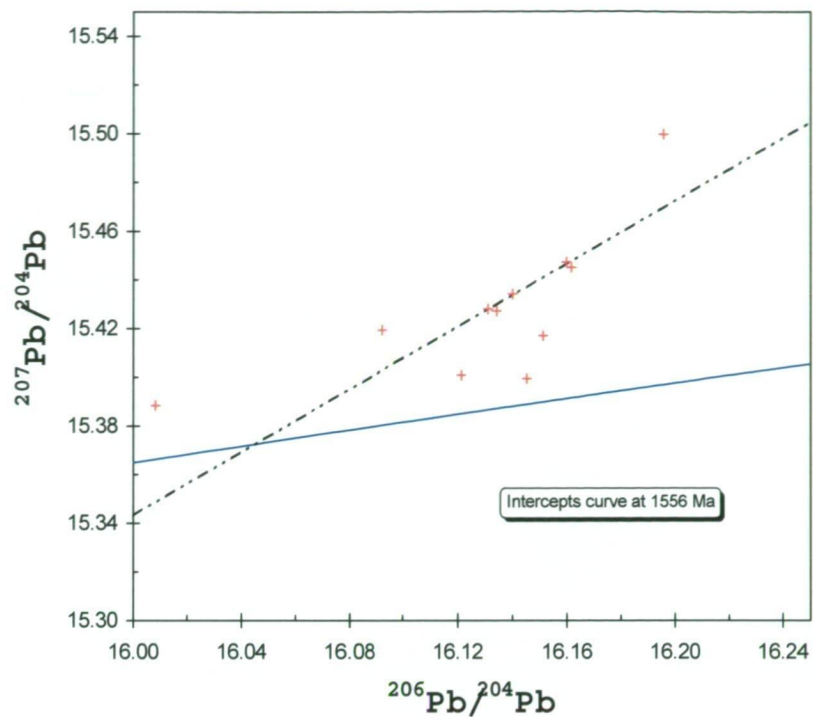
Twelve galena samples from diamond drill core of the Area 223 prospect at Tunkillia were submitted for Pb lead isotope analysis at CODES. Samples were collected from quartz veins with galena associated with pyrite, and rarely with minor sphalerite. Fine-grained galena grains were drilled by hand using a dentist drill at University of Adelaide and forwarded to CODES for Pb analysis. All analyses were obtained using High Resolution inductively coupled plasma mass spectrometry (HR-ICP-MS). The method is outlined in Townsend *et al.* (1998).

### 6.7.2 Results

Results are presented in Table 14 and Pb isotope ratio plots are presented in the standard format of  $^{207}\text{Pb}/^{204}\text{Pb}$  versus  $^{206}\text{Pb}/^{204}\text{Pb}$  and are compared with the Stacey and Kramers (1975) average crustal growth curve (Figure 119). Gulson (1986) reported that the Stacey and Kramers (1975) average crustal growth curve was more applicable for Proterozoic rocks than other growth curves including, that of Cumming and Richards (1975).

**Table 14 Results for lead isotope determinations of galena samples from V1-generation veins from Area 223, Tunkillia.**

D/Hole	Interval (m)	Pb206/Pb204	Pb207/Pb204	Pb208/Pb204	Pb208/Pb206	Pb207/Pb206
LED 03	289	16.1213	15.4009	35.8259	2.2223	0.9553
LED 08	98.7	16.1452	15.3994	35.9513	2.2268	0.9538
LED 08	119.3	16.1513	15.4171	35.8934	2.2223	0.9545
LED 08	129.9	16.1342	15.4272	35.9095	2.2257	0.9561
LED 03	289.6	16.1311	15.4280	35.9174	2.2266	0.9564
LED 01	109.6	16.1617	15.4450	35.9536	2.2246	0.9556
LED 02	143.05	16.0081	15.3884	35.8305	2.2383	0.9613
LED 03	249.8-249.9	16.0921	15.4194	35.9513	2.2341	0.9582
LED 08	116.1-116.25	16.1956	15.4997	36.1627	2.2329	0.9570
LRC 32D	266.5-266.65	16.1401	15.4342	35.9085	2.2248	0.9562
LRC 32D	288.7-288.8	16.1598	15.4473	35.9926	2.2273	0.9559



**Figure 119** Plot of  $^{207}\text{Pb}/^{206}\text{Pb}$  vs  $^{206}\text{Pb}/^{204}\text{Pb}$  showing Tunkillia data and Stacey and Kramers (1975) growth curve (blue line). The data intersects the curve at 1556 Ma.

**6.8 DISCUSSION**

Tunkillia gold prospect is located within the N-S to NW-SW trending Yarlbirinda Shear Zone and is hosted within 1690-1670 Ma Tunkillia Suite granitoids (units L<sub>1</sub> and L<sub>2</sub>). However, cross-cutting unaltered Gawler Range Volcanic dykes, the Pb model age, and less reliable K-Ar dating of sericite suggest that mineralisation occurred between 1600 Ma and 1580 Ma. Mineralisation is hosted within quartz and sulphide veins which strike ~325° and dip steeply to the west. Ore zones are located at the intersection of mineralised structures, which results in steeply plunging lodes. The mineralised zones are characterised by erratic gold grades with sub-economic grade occurring adjacent to high-grade zones.

**6.8.1 Comparisons to Moonta-Wallaroo (Au-Cu) Tarcoola (Au), Menninnee Dam (Pb-Zn) and Olympic Dam Cu-U-Au-Ag deposits**

The Moonta-Wallaroo (see Figure 2) region on the eastern Gawler Craton contains the Wheal Hughes and Poona copper mines, which were discovered in 1985/86 and mined until 1994, with 355, 000 tonnes of copper and 2 tonnes of gold extracted (Conor, 1995). Mineralisation is hosted in the Palaeoproterozoic Moonta Porphyry at Moonta and the Doora Schist at Wheal Hughes. Mineralisation and regional alteration are linked to the Mesoproterozoic Hiltaba Suite (Conor, 1995).

The geology and geochemistry of granitoids in the CHILARA region, western Gawler Craton, South Australia: implications for the Proterozoic tectonic history of the western Gawler Craton and the development of lode-style gold mineralisation at Tunkillia.



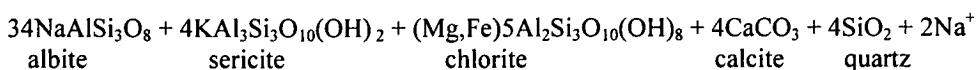
The Menninnee Dam Pb-Zn-Ag prospect is located north of the township of Kimba on central Eyre Peninsula. Discovered 1981, the prospect is hosted by Palaeoproterozoic Hutchinson Group metasediments, with an inferred resource of 1.7 Mt containing 5% lead, 8% zinc and 100g/t silver (Higgins *et al.*, 1990). Hydrothermal alteration and mineralisation are related to the Hiltaba Suite/Gawler Range Volcanics magmatic event (Roache, 1994).

The Olympic Dam copper-uranium-gold-silver deposit is located approximately 520 km north-northwest of Adelaide (see Figure 2), and contains reserves of > 600 Mt averaging 1.8% Cu, 0.5 kg/t U<sub>3</sub>O<sub>8</sub>, 0.5 g/t Au and 3.6 g/t Ag (Reynolds, 2001). Olympic Dam is hosted by the Olympic dam Breccia Complex, which occur within the Roxby Downs Granite, a member of the Hiltaba Suite.

At Tunkillia, sericite is the dominant alteration mineral. This constrains conditions for pH, with a pH of 3.5-5 is inferred (Figures 120-122). Mikucki and Groves (1990) report that sericite ( $\pm$ albite and K-feldspar) alteration at Golden Mile system indicates a restricted range of pH values between 5.2 to 6.2, for a system with fluid conditions of 300° – 400° C at 2 kbar and salinities of 1-3 wt % NaCl equivalent. However, feldspar is not stable in the Tunkillia system.

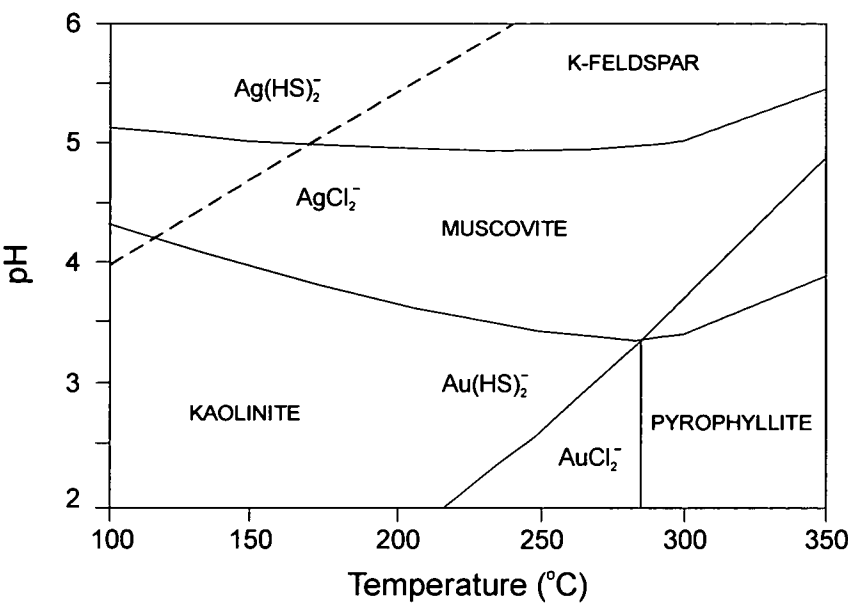
1. Chlorite-ilmenite± sericite; and
2. Chlorite-sericite-leucoxene, generally with pyrite.

Albite is present within the system, and a possible alteration reaction may comprise (Colvine *et al.*, 1988);



**The geology and geochemistry of granitoids in the CHILDARA region, western Gawler Craton, South Australia: implications for the Proterozoic tectonic history of the western Gawler Craton and the development of lode-style gold mineralisation at Tunkillia.**

plagioclase grains. Undeformed rhyolite/rhyodacite dykes, that obviously post-date regional deformation, are selectively sericite altered. Hence, the introduction of the fluids appears to have been a long-lived or repeated process.

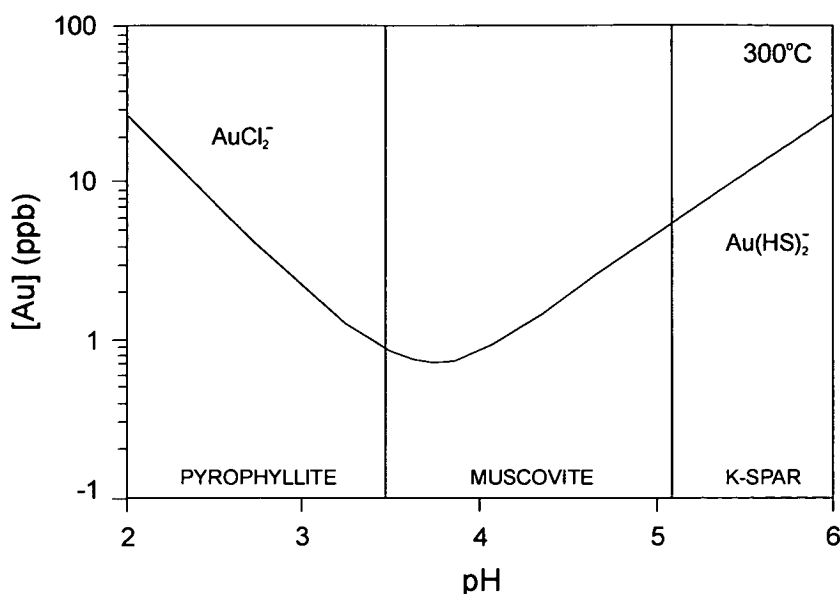


**Figure 120** Stability fields of silver and gold thio and chloro complexes and K-Al-silicates with temperature and pH (from Cooke and Large, 1995).

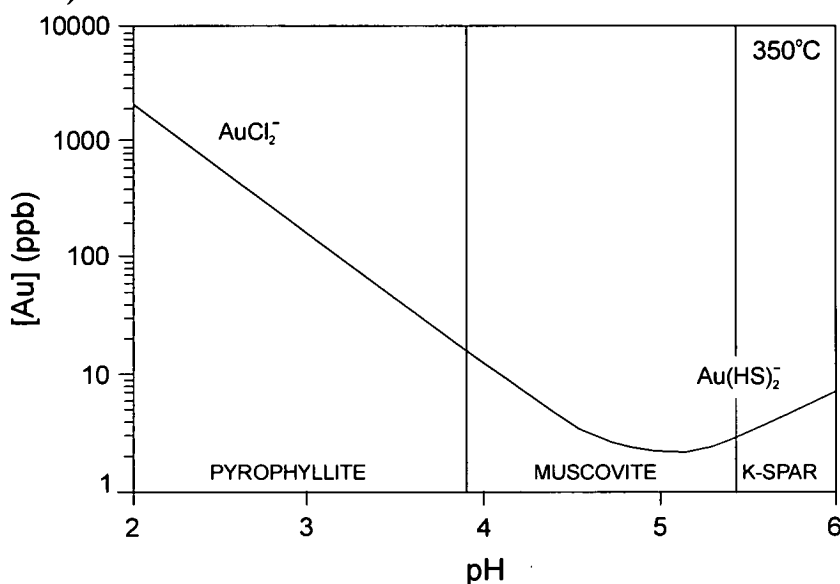
The mineralising fluid at Tunkillia was a moderate to high temperature (average trapping temperature of 412° C), relatively low salinity (<3.5 wt% NaCl) with minor CO<sub>2</sub>. On a temperature versus salinity diagram, Tunkillia plots just above the field of Archaean lode deposits (Figure 123). Under these conditions gold deposition largely occurs from a bisulphide complexes ( $\text{Au(HS)}_2^-$ ). Benning and Seward (1996) reported that gold is transported principally as AuHS rather than  $\text{Au(HS)}_2^-$  or  $\text{AuCl}_2^-$  in reduced, weakly acidic (muscovite stable), dilute, 250° – 350° C H<sub>2</sub>S rich fluids. Table 15 summarises temperature-salinity conditions for some classes of hydrothermal ore deposits. Tunkillia falls within the mesothermal deposit type. Figures 121 and 122 show the gold solubility with pH at 300° C, and 350° C respectively.

**Table 15** Temperature-salinity conditions for selected hydrothermal ore deposit types (from Cooke and Large, 1995).

Temperature	Salinity	Ore Type
High (>300° C)	High (>10wt. % NaCl)	Porphyry Cu-Au-Mo
Low (<200° C)	High (>10wt. % NaCl)	MVT; shale hosted Pb-Zn-Ag
Moderate (200-300° C)	Moderate (5-10wt. % NaCl)	VHMS Cu-Pb-Zn-Ag-Au
High (>300° C)	Low (0-5wt. % NaCl)	Mesothermal Au
Moderate (200-300° C)	Low (0-5wt. % NaCl)	Epithermal Au-Ag

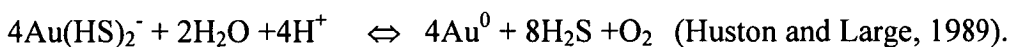


**Figure 121** Variations in gold solubility with pH at 300° C (from Cooke and Large, 1995).



**Figure 122** Variations in gold solubility with pH at 350° C (from Cooke and Large, 1995).

Gold deposition from a bisulphide complex occurs due to the following reaction:

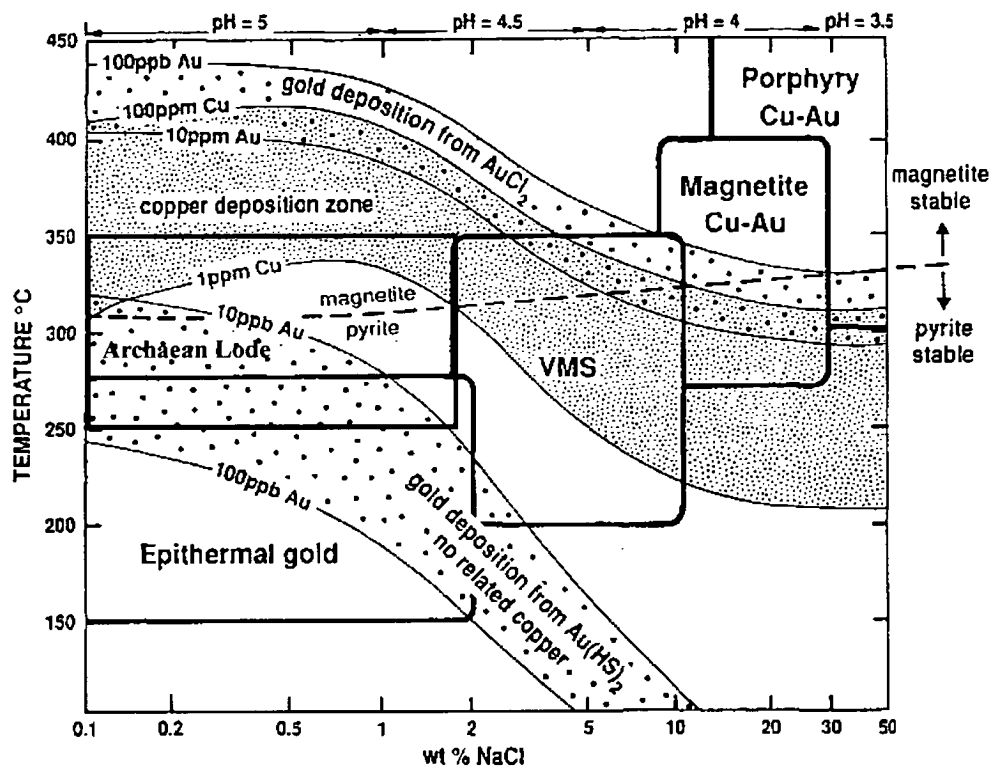


Gold transport as the  $\text{Au}(\text{HS})_2^-$  complex is favoured by:

- low to moderate temperatures (150° - 300° C);
- neutral to alkaline pH (>4.5);
- low salinity (less than seawater); and
- moderate  $f\text{O}_2$ .

These conditions are characteristic of the mineralising system at Tunkillia.





**Figure 123** A temperature-salinity diagram, which models the relationships between fluid chemistry for various ore deposit types based on fluid inclusion data (the boxes) with zones of gold and copper deposition based on chloride complex and thio complex solubility data (from Cooke and Large, 1995).

**Table 16** Relationships between temperature and redox conditions for selected hydrothermal ore types (from Cooke and Large, 1995).

Redox conditions	Gangue	Temperature	Ore Type
Highly oxidised (SO <sub>4</sub> <sup>-</sup> rich fluids)	Haematite	Moderate (200-300° C)	Cu-U-haematite
Oxidised (SO <sub>4</sub> <sup>-</sup> rich fluids)	Magnetite/haematite	Moderate (200-300° C)	Cu-Au-Fe oxide
Oxidised (SO <sub>4</sub> <sup>-</sup> rich fluids)	Haematite/pyrite	Low (<200° C)	Sediment hosted Cu
Reduced (H <sub>2</sub> S-rich fluids)	Pyrite	Moderate (200-300° C)	Au + pyrite; no Cu
Highly reduced (H <sub>2</sub> S-rich fluids)	pyrrhotite	High (>300° C)	Au-Cu-pyrrhotite

At Tarcoola, the interpreted T-fO<sub>2</sub>-pH conditions during sulphide deposition indicate a reduced fluid with H<sub>2</sub>S as the dominant sulphur species, with fluid inclusion data showing homogenisation temperatures between 202° to 358° C (Hein *et al.*, 1994). They report that gold was possibly transported as AuCl<sub>2</sub><sup>-</sup> at high temperatures, but as the temperature and fO<sub>2</sub> decreased gold was transported as Au(HS)<sub>2</sub><sup>-</sup>. Hein *et al.* (1994) report that the decrease in fO<sub>2</sub> was a major cause of gold precipitation at around 260° – 250° C.

Hein *et al.* (1994) suggest the contact between the Tarcoola Formation and the granite at Tarcoola is an unconformity, with no evidence for an intrusive contact. Daly *et al.* (1990) report the contact is intrusive. Hein *et al.* (1994) report localised intermediate intrusives, which intrude the Tarcoola Formation in the area, and represent a possible source of fluids.

Roache (1994) reports that intrusion of the Menninnie Dam granite (Hiltaba Suite), was a major factor in the formation of the Menninnie Dam deposit. The Menninnie Dam deposit has a magmatic isotopic signature, which may have been produced via:

- an acidic Na-Ca-K-Cl-rich metal brine which was exsolved from the granite; or
- heated, circulating meteoric waters leached metals and chlorine from the granite (Roache, 1994).

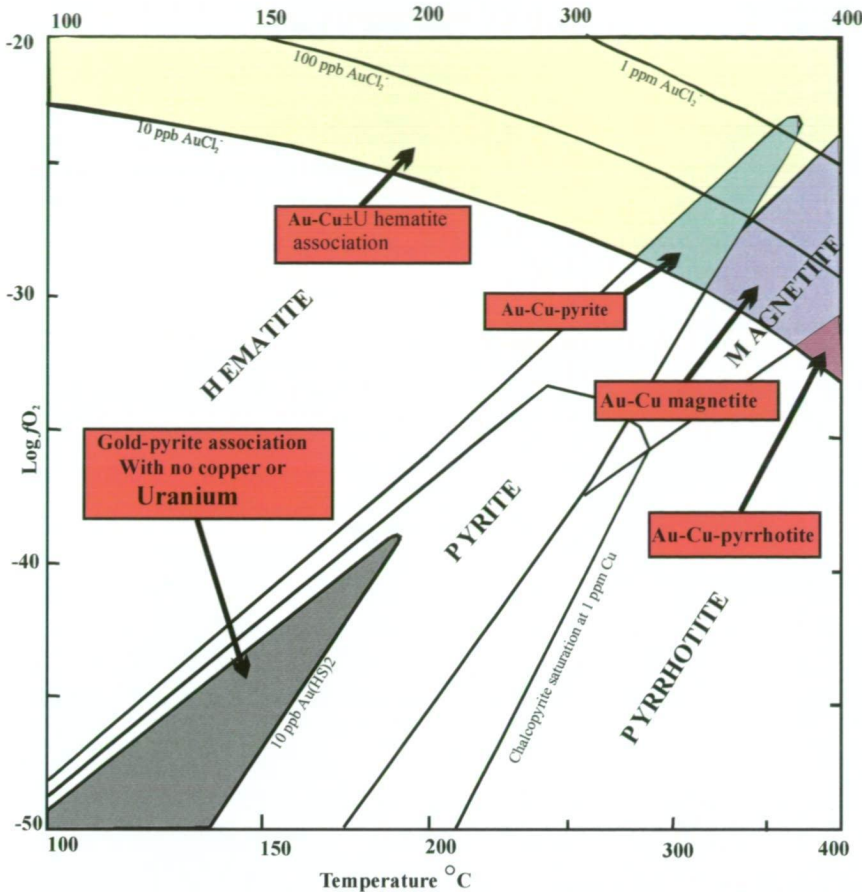
These fluids deposited metals within the Katunga Dolomite (Hutchinson Group) via replacement of the marble and calc-silicate lithologies (Roache, 1994).

At Menninnie Dam, three populations of fluid inclusions were observed, with two related to mineralisation (Roache, 1994). The trapping temperatures and salinities for each fluid are: (1) 180° C and 0-3 wt% NaCl equivalent, and (2) 140° C and  $\geq 27$  wt% NaCl equivalent.

At Moonta and Wheal Hughes copper mines, fluid inclusion studies showed the presence of co-existing vapour-rich and liquid-rich inclusions indicative of boiling of hydrothermal fluids, with salinities between 0-27 wt% NaCl equivalent (Hough, 1990; Hafer, 1991). Sulphur isotopes are within the range of magmatic values, which suggests that these deposits are related to intrusion of the Hiltaba Suite at ~1585 Ma.

At Olympic Dam, Haynes *et al.* (1995) propose that ore deposition resulted from mixing a high temperature ( $>250^{\circ}$  C) saline magmatic (?) fluid with a lower temperature ( $150^{\circ}$  –  $200^{\circ}$  C) less saline fluid. Three mineral assemblages are recognised:

- Association 1 – magnetite±haematite, chlorite, sericite, siderite, pyrite, chalcopryrite and pitchblende;
- Association 2 – haematite, sericite, chalcocite, bornite, pitchblende, barite, fluorite and chlorite; and
- Association 3 – massive haematite±quartz, vein barite and silicification (Haynes *et al.*, 1995).



**Figure 124** Fields of gold transport and deposition in  $fO_2$  – temperature space. The gold association is controlled by the stability of  $AuCl_2^-$  complexes (high temperature and  $fO_2$ ). The gold-pyrite-copper association is absent where gold transport is dominated by  $Au(HS)_2^-$ , at lower temperatures and only in the pyrite field (calculated from data provided in Huston and Large, 1989:  $a(\Sigma_s) = 10^{-3}$ ,  $a(Cl) = 10^{0.5}$ ,  $pH = 4$ ).

Tunkillia is a gold-only prospect, with pyrite the dominant gangue mineral. Figure 124 and Table 16 show that gold as  $Au(HS)_2^-$  is most stable in the pyrite field and would suggest that the lower temperature fluids at Tunkillia are responsible for gold deposition within the Tunkillia system. Figure 124 and Table 16 indicate that gold as  $Au(HS)_2^-$  is relatively insoluble within the pyrrhotite field, hence gold will not be transported as  $Au(HS)_2^-$  within very reduced or very oxidised fluids within hydrothermal ore systems.

6.8.1.2 Sulphur isotopes

At Tarcoola gold deposit,  $\delta^{34}S$  values ranged from 3.4 to 13.6‰, with an average of 7.3‰ (Hein, 1989). Hein (1989) suggested the source of sulphur for the Tarcoola deposit was seawater sulphate. Daly (PIRSA, pers. comm., 2001) reports  $\delta^{34}S$  values between 17.6-37.8‰ for pyrite samples from Wilgena 1 drill hole, located approximately 15 km east of Tarcoola. These imply a reduction of sulfate by biogenic processes with limited sulphate replenishment. The  $\delta^{34}S$  values reported by



Hein (1989) for Tarcoola suggests possible mixing between the biogenically reduced values from Wilgena 1 and magmatic sulphur.

Sulphur isotope analysis from Wheal Hughes and Poona copper deposits, showed  $\delta^{34}\text{S}$  values from  $-1.3$  to  $6.4\text{‰}$ , which is within the range for magmatic sulphur from intracontinental melts (Hough, 1990; Hafer, 1991).

At Menninnie Dam Pb-Zn deposit,  $\delta^{34}\text{S}$  values ranged from  $-3.04$  to  $7.38\text{‰}$  (Roche, 1994). Roche (1994) concluded that the source of the sulphur is not readily discernible, with possible sources including:

- saline groundwaters circulating at ore-time;
- magmatic sulphur from Menninnie Dam granite (Hiltaba Suite); and
- a combination of magmatic sulphur and country rock sources.

Roache (1994) reported that the sulphur and metals were introduced; hydrogen and oxygen isotope analysis of the mineralising fluid supported a magmatic/meteoric fluid origin.

Sulphur isotope values of Olympic Dam range from  $-10.8$  to  $-4.6\text{‰}$  (Roberts and Godden, unpublished report) which overlaps magmatic and sedimentary sulphides.

Archaean lode gold deposits of WA have  $\delta^{34}\text{S}$  values cluster around  $0\text{‰}$  (Lambert *et al.*, 1984), which may also indicate a relationship to granite magmatism. Colvine *et al.* (1988) report  $\delta^{34}\text{S}$  values for Archaean gold deposits in Canada show two broad groups; (1)  $0$  to  $10\text{‰}$  and, (2)  $<0\text{‰}$ . Many of the deposits show evidence for either mixing of more than one sulphur source or major isotopic fractionation (Colvine *et al.*, 1988).

#### 6.8.1.3 Lead isotopes

Doe and Zartman (1979) produced a 'Plumbotectonics' model to explain the relationship between small changes in the Pb-isotopic ratios of ore bodies and their tectonic settings. The model contains four growth curves, with three curves representing the three different lead reservoirs (eg: upper crust, mantle and lower crust) and the fourth curve, the orogene, representing mixing between the three lead reservoirs. All Tunkillia and Tarcoola samples and the majority of Menninnie Dam samples plot between the upper crust and the orogene curves (Figure 125). This suggests that they contain a component of lead from the orogene, mantle or lower crust reservoirs.

No Pb isotope analysis of Hiltaba Suite and Tunkillia Suite granites was undertaken to investigate the source of the lead and/or mineralisation. However, at Menninnie Dam, Roache (1994) reported that Hiltaba Suite granite Pb isotope results plot close to the orogene curve of Doe and Zartman (1979). Roache (1994) interpreted the data as a mixing array between a Hiltaba Suite component and upper crustal rocks, possibly the Hutchinson Group metasediments that surround the deposit. At Tarcoola, Pb isotope data for pyrite, galena and gold samples are similar to feldspar Pb data from the adjacent Hiltaba Suite granite, which suggests that the Hiltaba Suite is the source of the metals (Flintoft and Horn, 1989).

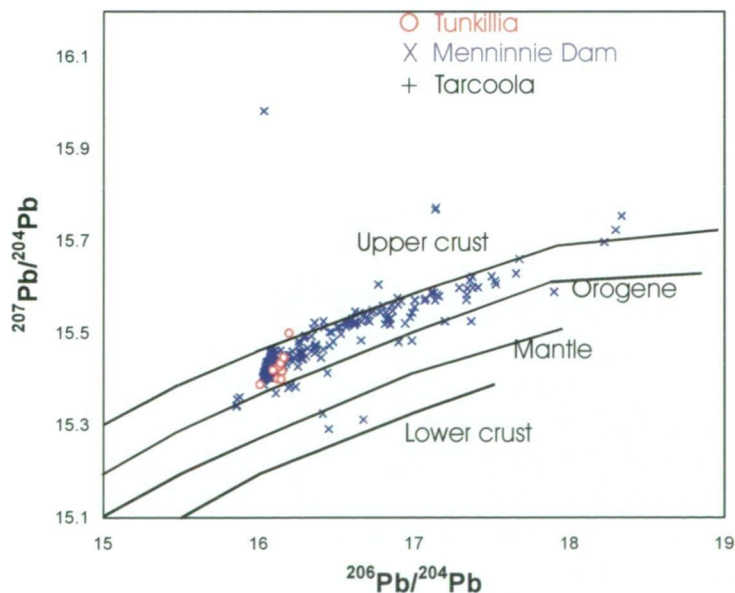
At Tunkillia, Pb isotope results lie close to the magmatic end of the mixing line at Menninnie Dam. This suggests the fluids are dominantly magmatic in origin.

Figure 126 shows lead isotope data from Tunkillia and Menninnie Dam (Roache, 1994) and Tarcoola (Fanning, 1988). All of the Tunkillia samples lie above the Stacey and Kramer (1975) growth curve, as do the majority of Menninnie Dam and Tarcoola samples (Figure 126).

Mineralisation at Tunkillia is interpreted to have related to the waning stages of major deformation within the Yarlbrinda Shear Zone and intrusion of the Hiltaba Suite (~1590 – 1575 Ma), supported by the application of a single stage lead model age approach. Gulson (1986) summarised the criteria for the appropriateness of a single stage lead model age determination:

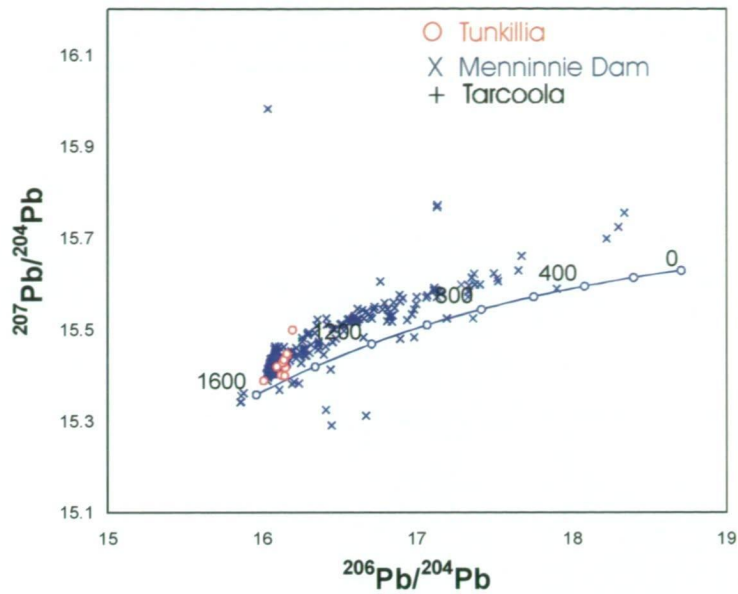
- Homogeneous isotopic composition for deposit and within a metallogenic province;
- The data should plot on or close to an accepted growth curve; and
- The model age should correlate with the geologic age (within 150 My).

Tunkillia Pb data does plot close to and intersects the Stacey-Kramers (1975) model age curve at ~1556 Ma, which is within error of the Hiltaba Suite (Figure 119). Another method of determining the model lead age is to use a terrain specific growth curve, but due to lack of data for Proterozoic rocks within South Australia, this is not a viable option. A close similarity between the least radiogenic data from Menninnie Dam, and Tunkillia, is consistent with both deposits sharing a component of Pb derived from Hiltaba Suite plutons, which are inferred to have influenced ore deposition at both sites.



**Figure 125** Plumbotectonics of Doe and Zartman (1979) with four growth curves that result from the evolution of three lead reservoirs: mantle, lower crustal and upper crustal and a fourth growth curve, the orogene curve, that results from mixing of the three curves.

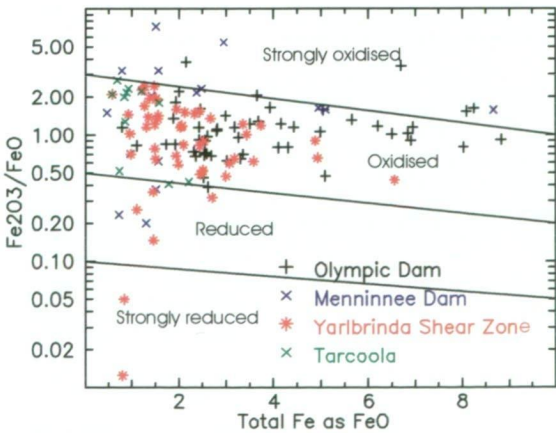
The geology and geochemistry of granitoids in the CHILDARA region, western Gawler Craton, South Australia: implications for the Proterozoic tectonic history of the western Gawler Craton and the development of lode-style gold mineralisation at Tunkillia.



**Figure 126** Lead isotope determinations fro Tunkillia, Menninnie Dam and Tarcoola samples. Most samples plot above the Stacey and Kramer (1975) average crustal growth curve shown in blue with figures in millions of years.

6.6.1.4 Fluid chemistry

The Hiltaba Suite is largely oxidised with a small number of samples plotting in the reduced field (Figure 127). The original host rock at Tunkillia (Tunkillia Suite) is not characteristically red in colour like the Hiltaba Suite, hence is more reduced than the Hiltaba Suite. No FeO determinations were carried out for the host Tunkillia Suite granitoids.



**Figure 127** Redox plot of Champion and Heinemann (1994) showing Hiltaba Suite granites located near Olympic Dam, Menninnie Dam, the Yarlbirinda Shear Zone and Tarcoola areas.

The geology and geochemistry of granitoids in the CHILDARA region, western Gawler Craton, South Australia: implications for the Proterozoic tectonic history of the western Gawler Craton and the development of lode-style gold mineralisation at Tunkillia.



The inferred trapping temperature for fluids related to gold precipitation at Tunkillia is between 330°-515° C with an average of 412° C. This is slightly lower than magmatic fluids related to porphyry Cu deposits (400° to 700° C), and is lower than the granite solidus under conditions of excess H<sub>2</sub>O (eg: Wyllie, 1977). McDonald (1983) report the lower temperature may be a result of irreversible, adiabatic expansion of the fluid, which can produce a temperature decrease of up to 300° C. Heat loss to the environment during transport away from the source granite will also reduce fluid temperature. Within lode gold deposits of the Superior Province, Canada, fluid inclusion data suggests the fluid responsible for gold precipitation was of low salinity (< 6 wt % NaCl equivalent), aqueous, but CO<sub>2</sub>-bearing, with a moderate to high CO<sub>2</sub> density (0.7- >1.0 g/cm<sup>3</sup>), and homogenisation temperatures ranged between 200° to 400° C, and cluster around 350° C (Colvine *et al.*, 1988).

Cassidy and Bennett (1993) summarise physiochemical processes in which hydrothermal fluids precipitate gold within hydrothermal systems:

- decrease in temperature;
- extensive mixing of fluids with contrasting compositions;
- fluid:wallrock interactions; and
- phase separation into immiscible fluids.

The moderate temperature range from 325° – 375° C would not result in major gold precipitation, and the lack of fluid inclusion data which suggesting the presence of two distinct fluid populations discounts the first two processes outlined above. The host rocks appear to have extensively altered, and they are possibly more reduced than the Hiltaba Suite granite. The fluid inclusion data suggests that metamorphic fluid is a possibility because of the low salinity observed at Tunkillia, however the data does not preclude a mixing of magmatic and/or metamorphic fluids.

### **6.8.2 Tunkillia: Magmatic versus Metamorphic Fluid Source**

At Tunkillia and the other deposits discussed above all are associated with Hiltaba Suite granites, hence, the question about how much influence did the Hiltaba Suite have on these deposits. Cameron and Hattori (1987) report that oxidised, CO<sub>2</sub> rich felsic magmas are the most likely source of Au-bearing oxidised fluids, within several Archaean deposits, including Matachewan, Hemlo and McIntyre-Hollinger deposits in Ontario, Canada and Kalgoorlie in Western Australia. The two main models for ore fluids for mesothermal gold deposits are magmatic and metamorphic fluid models (Hodgson, 1993).

The source of hydrothermal fluids at Tunkillia, possibly represent a mixture of low salinity metamorphic fluids and oxidised magmatic fluids from the Hiltaba Suite. Tunkillia is hosted by 1690-1670 Ma granitoids within the Yarlbirinda Shear Zone. Hiltaba Suite plutons do intrude the shear zone and were a possible source of fluids. However, fluid inclusion data indicates that mineralisation was associated with a low salinity fluid (<3 wt% NaCl equivalent), which suggests involvement of metamorphic fluids.

Sulphur and lead isotopes show a relationship to Hiltaba Suite granites.  $\delta^{34}\text{S}$  values between  $-2.23$  to  $3.19\%$  indicate a possible magmatic origin, however, mixing of magmatic and metamorphic fluids cannot be ruled out.

All of the deposits discussed above have a spatial relationship to Hiltaba Suite plutons and it is apparent that the Hiltaba Suite magmatic event was a major thermal event on the Gawler Craton, which provided fluids and/or metals to the deposits discussed above. Table 17 outlines the geologic characteristics of the deposits discussed above which contain gold (ie: not Menninnie Dam). So why do we see different types of deposits from gold-only at Tunkillia to Cu-Au at Wallaroo to Cu-U-Au-Ag at Olympic Dam, when they all appear to be related to Hiltaba Suite granites.

Budd *et al.* (2001) divided the Hiltaba Association into two groups:

1. Roxby Downs type – oxidised, haematite to magnetite stable granites related to Cu-Au deposits; and
2. Kokatha type – reduced, magnetite to ilmenite stable granites related to Au only deposits.

Limited FeO determinations show the majority of the Hiltaba Suite is oxidised (see Figure 127). Five samples of Hiltaba Granite from near the Yarlbirinda Shear Zone plot within the strongly reduced to reduced fields on Figure 127, these include Arcoordaby Rockhole, located to the northeast of Tunkillia, and Cooritta Hill located near Kokatha. Hence, the reduced nature of these granites, may be a major factor in location of gold mineralisation within regional shear zones.

Tunkillia is a lode-style, gold only deposit, which was most probably produced from the syn-tectonic emplacement of Hiltaba Suite granite within the Yarlbirinda Shear Zone. Fluids derived from the granite mixed with oxidised metamorphic fluids (from  $\sim 8$  km depth), and were localised by changes in lithostatic pressure producing steeply dipping vein sets. Hodgson (1993) outlines a possible mechanism for modifying external derived fluid within a shear zone by alternating periods of chemical pumping processes within a supra-lithostatic environment, and fault valve behaviour within a sub-lithostatic environment (Figure 128).

Fluids associated with deposits discussed above including Tarcoola and Olympic Dam were radically different that at Tunkillia; they were formed at lower temperatures, lower pressures and salinities were much higher. The current data for Tunkillia favours either a tapping of deep seated metamorphic reservoirs, perhaps driven by Hiltaba Suite magmatism, or separation of low salinity vapours from magmatic fluids.

Granites generally have very low gold contents (generally below detection - 1 ppb), even where they closely associated with gold mineralisation. Bettenay (1988) in a study of the relationships between gold mineralisation and granitoids in the Eastern Goldfields Province of the Yilgarn Craton, Western Australia, found no spatial or genetic relationship existed. The data obtained by this study does not answer the question as to the source of fluids, but further granite geochemistry within the Tunkillia prospect, and within the Yarlbirinda and Yerda Shear Zones to locate reduced granites is warranted.

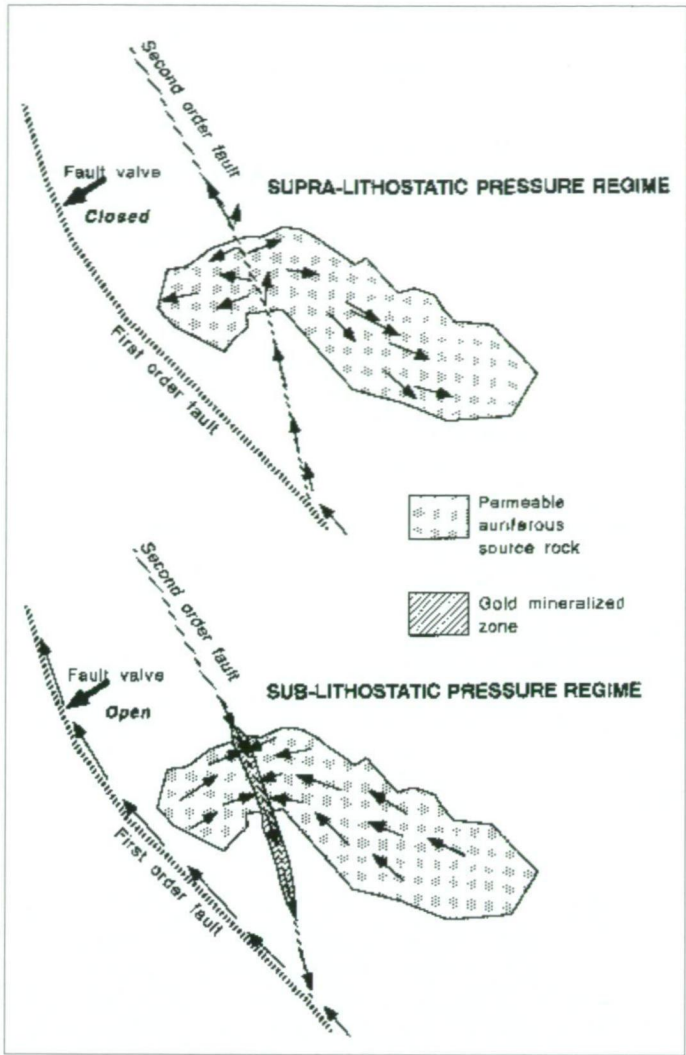


Figure 128 Diagrammatic representation of chemical pumping process possibly accompanying fault-valve behaviour on major fault zones associated with mesothermal gold deposits (Hodgson, 1993).



## 6.9 CONCLUSIONS

1. Tunkillia gold prospects are hosted within Tunkillia Suite intrusives (1690-1670 Ma) which range in composition from adamellite to granodiorite with minor mafic and rhyolite dykes;
2. Gold is hosted within quartz±sulphide veins striking 325° and dipping steeply to the west. Ore shoots plunge steeply to the north;
3. Sericite is the main alteration mineral, which constrains pH to 3.5-5. The fluid inclusion data which shows the mineralising fluid to be moderate temperature (about 375° C), low salinity (up to 6 equivalent wt % NaCl, average <3.5 wt%), with minor CO<sub>2</sub> content;
4. Gold is associated with sulphides, dominantly pyrite. This association and the fluid type indicate that gold was transported as a Au(HS)<sub>2</sub><sup>-</sup> complex within the pyrite stability field;
5. Sulphur isotope data suggests a magmatic source for sulphur;
6. Pb isotope data suggests a link to the Hiltaba Suite with some contamination from the host granitoids;
7. The prospects are related to fluid influx from syn-tectonic Hiltaba Suite granites emplaced within the active Yarlbrinda Shear Zone, which may have mixed with low salinity metamorphic fluids produced at depth. Structure appears to be the dominant control on mineralisation with the shear zone focussing the fluids and fault intersections acting as trap sites.

**Table 17 Geologic features of mineral deposits discussed in text.**

Geologic features	Tunkillia (Au only)	Tarcoola (Au only)	Olympic Dam (Cu-U-Au)	Walleroo and Moonta (Cu-Au)
Age	Mesoproterozoic ~1590-1580 Ma	Mesoproterozoic	Mesoproterozoic	Mesoproterozoic
Deposit-type	Shear zone lode-gold	?lode-gold (quartz vein)	Replacement deposit	
Fe-S-O Host	S-poor granite	S-rich pyritic shales and dolomites	Sulfate rich	S – rich pyritic sediments of Doora Schist, Moonta Porphyry less S-rich
Alteration minerals	<b>Dominantly sericite, chlorite</b>	Sericite, chlorite	Sericite,	Chlorite, sericite, tourmaline
Sulphur isotopes	$\delta^{34}\text{S}$ -2.23 –3.19‰	$\delta^{34}\text{S}$ 3.4 – 13.6‰	$\delta^{34}\text{S}$ -10 to –4.6‰	$\delta^{34}\text{S}$ -1.3 to 6.4‰
Dominant Sulphur species	pyrite	Pyrite and galena	pyrite	Chalcopyrite and pyrite
Fluid chemistry	Low salinity High temperature (av. 412° C)	Two fluids 1. Low salinity, low temp. 180° C 2. Low to high salinity, low temp. 140° C	Two fluids 1. High salinity, high temperature 2. Low salinity, lower temp.	Co-existing vapour-rich and liquid-rich, low to high salinity inclusions (
Depth of formation	Deep 8km	Relatively shallow	shallow	shallow
Granites	Hiltaba Suite intruded into Yarlbrinda Shear Zone, source of fluids. Dominantly oxidised, but some reduced granites (see Figure 127).	Mesoproterozoic intermediate intrusives intruded into Tarcoola Formation. Oxidised.	Olympic Dam Breccia Complex hosted in Hiltaba Suite Roxby Downs granite. Oxidised.	Associated with Mesoproterozoic Hiltaba Suite granite. Oxidised.

## Chapter 7 Summary

This chapter summarises the contributions made by this study to the understanding of the geological and tectonic history of the western Gawler Craton. Prior to geochronology reported in Teasdale (1997), the Palaeoproterozoic geological history of the western Gawler Craton was poorly constrained, with much of the structural and tectonic history of the region assigned to the Kimban Orogeny defined from the southern Gawler Craton. Teasdale (1997) defined a new suite of granitoids emplaced between 1690-1670 Ma, which he termed the Ifould Complex. Daly *et al.* (1998) defined the Kararan Orogeny to explain the deformation and magmatic events between 1650-1540 Ma, and referred to all granitoids within this time range as the Ifould Complex. This includes the St Peter Suite, Hiltaba Suite and Munjeela Granite.

Host rocks for the Tunkillia gold prospect are a comagmatic suite of granitoids, mafic and felsic dykes which were intruded at ~1680 Ma. These rocks are referred to as the Tunkillia Suite, but are time equivalents of the more spatially more restricted Ifould Complex described Teasdale (1997), but are not included within the definition reported in Daly *et al.* (1998). The use of the term Ifould Complex is misleading and the granites need to be renamed to avoid confusion. The 'suite' terminology of this thesis is advanced as an alternative nomenclature.

Five main periods of magmatism have been described for the study area:

1. Archaean to early Palaeoproterozoic Glenloth Granite (~2440 Ma metamorphic age);
2. Tunkillia Suite and equivalents (1690-1670 Ma);
3. St Peter Suite (1630-1608 Ma);
4. Gawler Range Volcanics (1592 Ma)/Hiltaba Suite granite (1595-1575 Ma); and
5. S-type, two mica  $\pm$  garnet Munjeela Granite (~1560 Ma).

Prior to this study, the Nuyts tectonic subdomain was interpreted to represent Archaean basement with minor Palaeoproterozoic to Mesoproterozoic intrusives. This study has shown the Nuyts Subdomain contains a significant proportion of juvenile crust, with no known Archaean crust. The St Peter Suite magmatic event represents a major addition to the crust of rocks with a distinct magmatic arc-type geochemistry, during a subduction event that began at least 2.1 Ga, based on Nd-model ages of the granitoids across the area.

This study defined the Munjeela Granite, a two mica  $\pm$  garnet S-type granite which has a monazite crystallisation age of  $1562 \pm 15$  Ma, and is the only known S-type granite on the Gawler Craton. The Munjeela Granite is interpreted to have formed during a period of extension, which produced localised fault-bound basins. This basin related to the Munjeela Granite was subsequently buried, possibly during reactivation of the Koonibba Fault Zone.

The western Gawler Craton records a multi-stage Proterozoic tectonic history, beginning with continental collision between the Fowler Orogenic Zone and the proto-Yilgarn Craton between 1750-1700 Ma (Daly *et al.*, 1998). This was probably



the initiation of the Kararan Orogeny, although major deformation within the Kalinjala Mylonite Zone (Kimban Orogeny) on the eastern margin of the Gawler Craton was occurring at this time.

Continental collision within the Fowler Orogenic Zone produced major crustal thickening which resulted in the formation of a crustal suite of granites between 1690-1670 Ma (Ifould Complex of Teasdale, 1997). Within the Yarlbirinda Shear Zone, these granites are termed the Tunkillia Suite. The Tunkillia Suite and equivalents are predominantly felsic with minor mafic dykes, but the full extent of this magmatic event is still unknown. The intracratonic rift signature of these granites is most consistent with a back-arc environment, given the overall compressive character of the region (e.g. Zhao and McCulloch, 1995).

At approximately 1630 Ma, the St Peter Suite was intruded into the Nuyts Subdomain, within a continental magmatic arc setting, producing a suite of tonalitic to granodioritic rocks, similar in chemistry to Archaean tonalite-trondhjemite-granodiorites. The Nuyts Subdomain was amalgamated within the proto-Gawler Block during the Palaeoproterozoic and subsequently cratonised during the Mesoproterozoic. The Mesoproterozoic Hiltaba Suite granite ranges from syn-tectonic to post-tectonic, with Hiltaba Suite granites located close to St Peter Suite rocks recording positive  $\epsilon\text{Nd}$  values. This indicates a juvenile source, possibly related to basaltic underplating of the subducting slab at the base of the crust in an overall return to back-arc extensional conditions.

The discovery of gold within the Yarlbirinda Shear Zone has major implications for mineral exploration on the western Gawler Craton, particularly in areas where multiphase plutons were intruded adjacent to major shear zones. Gold mineralisation is intimately related to intrusion of felsic, oxidised Hiltaba Suite granite within or adjacent to the shear zone, which produced major, regional scale alteration zones.

The significance of shear zones in the localisation of lode-gold deposits in general is well documented, with mineralisation concentrated in secondary splays off the main structures or at sites of crosscutting faults. Mineralisation may be present in such structures as intersection of faults with favourable rock types, mutual fault intersections and fault jogs. Many mineralised shear zones also show a spatial and genetic link with metamorphism, which suggests that both are related to the same regional tectonic processes. Some mineralisation within shear zones is developed on the margins of anorogenic granites with no obvious relation to the deformation zone.

Within the Yarlbirinda Shear Zone, strain associated with deformation appears to have been variable, with brittle-ductile deformation seen at Yarlbirinda Hill and mylonites intersected at Tunkillia and Nuckulla Hill prospects, this implies different crustal levels or strain rates. Within shear zones, areas of ductile deformation are characterised by high fluid flow due to fluid infiltration at deep crustal levels, whereas within the brittle to brittle—ductile zone, deformation is more episodic and the result of fluid pumping into fractures and dilatational zones. The transition from brittle to ductile deformation is dependent upon the geometry and mode of faulting, crustal composition and temperature.

---

At Tunkillia, gold mineralisation is hosted within quartz+sulphide veins, which are located within steeply plunging zones, at the intersection of the regional foliation and steeply plunging stretching lineations. Mineralisation is heterogeneous with narrow zones of high-grade mineralisation located within zones of barren granite. To date no economic deposit has been delineated. South of Tunkillia is a major step-over basin produced by dextral shearing occurs within the Yarlbirinda Shear Zone, and represent a potential gold target. Drilling by Helix Resources NL in the area failed to intersect significant a significant Au anomaly, but the drilling was probably not deep enough to fully test the feature.

**REFERENCES**

- Arth, J.G., 1976. Behaviour of trace elements during magmatic processes – A summary of theoretical models and their applications. *Journal of Research, U.S. Geological Survey*, 4:41-47.
- Arth, J., Barker, F., Peterman, Z.E. and Friedman, I., 1978. Geochemistry of the gabbro-diorite-tonalite-trondhjemite suite of southwest Finland and its implications for the origin of tonalitic and trondhjemitic magmas. *Journal of Petrology*, 19:289-316.
- Barbarin, B., 1990. Granitoids: main petrogenetic classifications in relation to origin and tectonic setting. *Geological Journal*, 25:227-238.
- Barker, F., 1979. Trondhjemite: definition, environment and hypotheses of origin. In Barker, F. (Ed.) *Trondhjemites, Dacites and Related Rocks*. Elsevier, New York, p1-12.
- Barker, F. and Arth, J. G., 1976. Generation of trondhjemitic-tonalitic liquids and Archaean bimodal trondhjemitic-basalt suites. *Geology*, v4, p596-600.
- Batchelor, R.A. and Bowden, P., 1985. Petrogenetic interpretation of granitoid rock series using multicationic parameters. *Chemical Geology*, 48, 43-55.
- Bennett, C. J., 1968. Preliminary report on 1:250 000 scale maps of KINGOONYA, GAIRDNER, YARDEA and CHILDARA sheet areas. *South Australia. Department of Mines and Energy. Report Book 67/98*.
- Bennett, V.C. and DePaolo, D.J., 1987. Proterozoic crustal history of the western United States as determined by neodymium isotopic mapping. *Geological Society of America. Bulletin*, 99:674-685.
- Benning, L.G. and Seward, T.M., 1996. Hydrosulphide complexing of Au(I) in hydrothermal solutions from 150-400 C and 500-1500 bar. *Geochimica et Cosmochimica Acta*, 60:1849-1871.
- Bettenay, L.F., 1988. Granitoid batholiths of the Eastern Goldfields Province, Yilgarn Block: characteristics and significance to gold mineralization. In Ho, S.E. and Groves, D.I. *Advances in Understanding Precambrian Gold Deposits, Volume II*. Geology Department and University Extension, The University of Western Australia, Publication 12, p227-237.
- Berry, R.F. and Flint, R.B., 1988. Magmatic banding within Proterozoic granodiorite dykes near Streaky Bay, South Australia. *Royal Society of South Australia. Transactions*, 112:66-73.
- Blissett, A.H., 1975. Rock units in the Gawler Range Volcanics, South Australia. *South Australia. Geological Survey. Quarterly Geological Notes*, 55:2-14.



- Blissett, A.H., 1977. CHILDARA map sheet. South Australia. *Geological Survey. Geological Atlas 1:250 000 Series*, sheet SH/53-14.
- Blissett, A.H., 1980. CHILDARA, South Australia, Sheet SH/53-14. *South Australia. Geological Survey. 1:250 000 Series - Explanatory Notes*.
- Blissett, A.H., 1985. GAIRDNER, South Australia, Sheet SH/53-15. *South Australia. Geological Survey. 1:250 000 Series - Explanatory Notes*.
- Blissett, A.H., 1986. Subdivision of the Gawler Range Volcanics in the Gawler Ranges. *South Australia. Geological Survey. Quarterly Geological Notes*, 97:2-11.
- Blissett, A.H., Creaser, R.A., Daly, S.J., Flint, R.B. and Parker, A.J., 1993. Gawler Range Volcanics. In Drexel, J.F., Preiss, W.V. and Parker, A.J. (eds.), *The geology of South Australia. Vol. 1, The Precambrian. Geological Survey of South Australia, Bulletin 54*.
- Blissett, A.H. and Vitols, V. 1974. Helicopter Geological Survey of the Gawler Block, 1973. *South Australia. Department of Mines and Energy. Report Book 74/144*.
- Bodnar, R.J., Reynolds, T.J. and Kuehn, C.A., 1985. Fluid-inclusion systematics in epithermal systems. In Berger, B.R. and Bethke, P.M. (Eds.) *Geology and Geochemistry of Epithermal Systems. Society of Economic Geologists, Reviews in Economic Geology*, 2:73-97.
- Bodnar, R.J. and Sterner, S.M., 1985. Synthetic fluid inclusions in natural quartz. II. Application to PVT studies. *Geochimica et Cosmochimica Acta*, 49:1855-1859.
- Bonnichsen, B. and Kauffman, D.F., 1987. Physical features of rhyolite lava flows in the Snake River Plain volcanic province, southwestern Idaho. *Geological Society of America. Special Paper 212*, p119-145.
- Boynton, W.V., 1984. Geochemistry of the rare earth elements: meteorite studies. In Henderson, P. (Ed.), *Rare earth element geochemistry*. Elsevier, pp63-114.
- Branch, C.D., 1978. Evolution of the Middle Proterozoic Chandabooka caldera, Gawler Range acid volcano-plutonic province, South Australia. *Geological Society of Australia. Journal*, 25:199-218.
- Brown, H.Y.L., 1885. Report on geological character of country passed over from Port Augusta to Eucla. *Parliamentary paper, South Australia*, 45:7p.
- Budd, A.R., Wyborn, L.A.I. and Bastrakova, I.V., 2001. The metallogenic potential of Australian Proterozoic granites: summary volume. *AGSO Record 2001/12*.
- Busby-Spera, C.J. and White, J.D.L., 1987. Variation in peperite textures associated with differing host-sediment properties. *Bulletin of Volcanology*, v49, p765-775.

- Cameron, E.M. and Hattori, K., 1987. Archaean gold mineralization and oxidised hydrothermal fluids. *Economic Geology*, 87, 1177-1191.
- Cassidy, K.F. and Bennett, J.M., 1993. Gold mineralisation at the Lady Bountiful Mine, Western Australia: an example of a granitoid-hosted Archaean lode gold deposit. *Mineralium Deposita*, 28(6): 388-408.
- Champion, D.C., and Heinemann, M.A., 1994. Igneous rocks of North Queensland: 1:50 000 map and explanatory notes. *Australian Geological Survey Organisation, Record*, 1994/11, 82pp.
- Chappell, B.W. and Stephens, W.E., 1988. Origin of infracrustal (I-type) granite magmas. *Transactions of the Royal Society of Edinburgh, Earth Sciences*, 79, 71-86.
- Chappell, B.W. and White, A.J.R., 1974. Two contrasting granite types. *Pacific Geology*, 8, p173-174.
- Chappell, B.W., and White, A.J.R., 1992. I- and S-type granites in the Lachlan Fold Belt. *Transactions of the Royal Society of Edinburgh, Earth Sciences*, v83, p1-26.
- Chappell, B.W., White, A.J.R. and Wyborn, D. 1987. The importance of residual source material (restite) in granite petrogenesis. *Journal of Petrology*, v28, p1111-1138.
- Collins, W.J., Beams, S.D., White, A.J.R., and Chappell, B.W., 1982. Nature and origin of A-type granites with particular reference to southeastern Australia. *Contributions to Mineralogy and Petrology*, 80, 189-200.
- Colvine, A.C, Fyon, J.A., Heather, K.B., Marmont, S., Smith, P.M. and Troop, D.G., 1988. Archaean Lode gold deposits in Ontario, Canada. *Ontario Geological Survey, Miscellaneous Paper* 139, 210p.
- Conor, C.H.H., 1995. Moonta-Wallaroo region: an interpretation of the geology of the Maitland and Wallaroo 1:100 000 sheet areas. *Mines and Energy, South Australia. Open file Envelope* 8886.
- Cooke, D.R. and Large, R.R., 1995. Hydrothermal Geochemistry. In Exploration Geochemistry and Hydrothermal Geochemistry, Part 2. *Masters of Economic Geology Course Manual 12*, Centre for Ore Deposit and Exploration Studies, Tasmania.
- Cooper, J.A., Mortimer, G.E., Rosier, C.M. and Upphill, R.K., 1985., Gawler Range magmatism – further isotopic age data. *Australian Journal of Earth Science*, 32:115-123.
- Cox, S.F., Wall, V.J., Etheridge, M.A. and Potter, T.F., 1991. Deformational and metamorphic processes in the formation of mesothermal gold deposits – examples from the Lachlan Fold Belt in central Victoria, Australia. *Ore Geology Reviews*, 6:391-423.

Creaser, R.A., 1989. The geology and petrology of Middle Proterozoic felsic magmatism of the Stuart Shelf, South Australia. *Latrobe University. Ph.D. thesis* (unpublished).

Creaser, R.A. and White, A.J.R., 1991. Yardea Dacite — Large-volume, high-temperature felsic magmatism from the Middle Proterozoic of South Australia. *Geology*, 19:48-51.

Cumming, G.L. and Richards, J.R., 1975. Ore lead isotope ratios in a continuously changing earth. *Earth and Planetary Science Letters*, 28:155-171.

Daly, S.J., 1985. TARCOOLA map sheet. *South Australia. Geological Survey. Geological Atlas 1:250 000 Series*, sheet SH/53-10.

Daly, S.J., 1986. The Mulgathing Complex. *South Australia. Department of Mines and Energy. Report Book*, 86/41.

Daly, S.J., 1993. Mineralisation associated with the Gawler Range Volcanics and Hiltaba Suite granitoids: Earea Dam Goldfield Glenloth Goldfield and Tarcoola Goldfield. In: Drexel, J.E, Preiss, WY & Parker, A.J. (editors), The geology of South Australia. Vol. 1, The Precambrian. *Geological Survey of South Australia, Bulletin* 54.

Daly, S.J., 1996. Gawler Craton. In Newton, A.W. (compiler), Mineral Exploration and Development in South Australia. *Department of Mines and Energy. Report Book* 96/1 (unpublished).

Daly, S.J., Benbow, M.C. and Blissett, A.H., 1979. Archaean to Early Proterozoic geology of the northwestern Gawler Craton. In: Parker, A.J. (Compiler). *Symposium on the Gawler Craton, Adelaide, 1979. Extended abstracts*. Geological Society of Australia (SA Division), pp.16-19.

Daly, S.J. and Fanning, C.M. 1990. Archaean geology of the Gawler Craton, South Australia. In: Glover, J.E. and Ho, S.E. (Compilers), *3<sup>rd</sup> International Archaean Symposium, Perth, 1990. Extended abstracts*. Geoconferences (WA) Inc., Perth, pp91-92.

Daly, S.J. and Fanning, C.M. 1993. Archaean. In Drexel (Eds). The geology of South Australia Volume 1. The Precambrian. *Geological Survey of South Australia. Bulletin* 54.

Daly, S.J., Fanning, C.M. and Fairclough, M.C. (1998). Tectonic evolution and implications for exploration potential of the western Gawler Craton. *AGSO Journal of Australian Geology and Geophysics*, 17:145-168.

Daly, S.J., Fairclough, M.C., Fanning, C.M. and Rankin, L.R., 1995. Tectonic evolution of the western Gawler Craton: A Palaeoproterozoic collision zone and likely plate margin. *Geological Society of Australia, Abstracts*. 40.



- Daly, S.J., Horn, C.M. & Fradd, W.P., 1990. Tarcoola Goldfield. In: Hughes, F.E., (editor), *Geology of the mineral deposits of Australia and Papua New Guinea. Australasian Institute of Mining and Metallurgy, Monograph 14*, 1049-1053.
- Davis, G.H. and Reynolds, S.J., 1996. *Structural Geology of Rocks and Regions*, 2<sup>nd</sup> edition. Wiley, New York, 776p.
- De la Roche, H., Leterrier, J., Grande, C.P. and Marchal, M., 1980. A classification of volcanic and plutonic rocks using R1-R2 diagrams and major element analyses – its relationships and current nomenclature. *Chemical Geology*, 29:183-210.
- Doe, B.R. , and Zartmen, R.E., 1979. Plumbotectonics: The Phanerozoic. In H.L. Barnes (ed.), *Geochemistry of Hydrothermal Ore Deposits. Wiley Interscience*, New York:22-70.
- Dove, M.B., 1997. The geology, petrology, geochemistry and isotope geology of the eastern St Peter Suite, western Gawler Craton, South Australia. *BSc Hons University of Adelaide* (unpublished).
- Drexel, J.F., Preiss, W.V. & Parker, A.J. (Eds.), 1993, The geology of South Australia. Vol. 1, The Precambrian. *Geological Survey of South Australia, Bulletin 54*.
- Drummond, M.S. and Defant, M.J., 1990. A model for trondhjemite-tonalite-dacite genesis and crustal growth via slab melting. *Journal of Geophysical Research*, 95:21,503-21,521.
- Drummond, M.S., Neilson, M.J., Allison, D.T. and Tull, J.F., 1997. Igneous petrogenesis and tectonic setting of granitic rocks from the eastern Blue Ridge and Inner Piedmont, Alabama Appalachians, in Sinha, A.K., Whalen, J.B., and Hogan, J.P., eds., *The Nature of Magmatism in the Appalachian Orogen*: Boulder, Colorado, Geological Society of America Memoir 191.
- Eby, G.N., 1990. The A-type granitoids: a review of their occurrence and chemical characteristics and speculation on their petrogenesis. *Lithos*, 26, 115-134.
- Ekren, E.B., McIntyre, D.H. and Bennett, E.H., 1984. High-temperature, large-volume, lavalike ash-flow tuffs without calderas in southwestern Idaho. *United States Geological Survey Professional Paper 1272*.
- El Bouseily, A.M., and El Sokkary, A.A., 1975. The relationship between Rb, Ba and Sr in granitic rocks. *Chemical Geology*, 16, 207-219.
- Etheridge, M.A., Rutland, R.W.R., and Wyborn, L.A.I., 1987. Orogenesis and tectonic processes in the Early to Middle Proterozoic of northern Australia. *American Geophysical Union Geodynamic Series*, 17, 131-147.
- Evensen, N.M, Hamilton, P.J. and O’Nions, R.K., 1978. Rare earth abundances in chondritic meteorites. *Geochimica et Cosmochimica Acta*, 42, 1199-1212.

- Fairclough, M.C. and Daly, S.J., 1994. Western Gawler Craton. Interpreted Precambrian geology. *South Australia. Department of Mines and Energy. Digital dataset.*
- Fanning, C.M., 1988. Tarcoola gold mine: U-Pb and Pb isotope study. Amdel Report G7519/88 (unpublished).
- Fanning, C.M., 1997. Geochronological Synthesis of South Australia. Part II: The Gawler Craton. *Unpublished PRISE report.* Research School of Earth Sciences, Australian National University.
- Fanning, C. M., Flint, R.B., Parker, A.J., Ludwig, K.R. and Blissett, A.H., 1988. Refined Proterozoic evolution of the Gawler Craton, South Australia, through U-Pb zircon geochronology. *Precambrian Research*, 40/41:363-386.
- Ferris, G.M., 2001., Childara bedrock drilling program. *Primary Industries and Resources, South Australia. Report Book*, 2001/04.
- Flint, R.B., 1993. Chapter 5: Mesoproterozoic. In Drexel, J.F., Preiss, W.V. and Parker, A.J., 1993. The geology of South Australia. Vol 1. The Precambrian. *South Australian Geological Survey Bulletin*, 54.
- Flint, R.B., Rankin, L.R. and Fanning, C.M., 1990. Definition – The Palaeoproterozoic St Peter Suite of the western Gawler Craton. *South Australia. Geological Survey. Quarterly Geological Notes*, 114, p2.
- Flintoft, M.W. and Horn, C.M., 1988. Compilation of Exploration data available on the Tarcoola Blocks goldmine, Tarcoola, South Australia. *South Australia. Geological Survey. Report Book* 89/88 (unpublished).
- Giles, C.W., 1977. Rock units in the Gawler Range Volcanics, Lake Everard area, South Australia. *South Australia. Geological Survey. Quarterly Geological Notes*, 61:7-16.
- Giles, C.W., 1980. A comparative study of Archaean and Proterozoic felsic volcanic associations in southern Australia. *University of Adelaide. Ph.D. thesis* (unpublished).
- Giles, C.W., 1988. Petrogenesis of the Proterozoic Gawler Range Volcanics, South Australia. *Precambrian Research*, 40/41:407-427.
- Goldstein, R.H. and Reynolds, T.J., 1994. *Systematics of fluid inclusions in diagenetic minerals. SEPM Short Course* 31. Society of Sedimentary Geology. Oklahoma, USA.
- Gromet, L.P and Silver, L.T., 1987. REE variations across the Peninsular Ranges Batholith: implications for batholithic petrogenesis and crustal growth in magmatic arcs. *Journal of Petrology*, 28:75-125.
- Gulson, B.L., 1986. *Lead Isotopes in Mineral Exploration*, Elsevier, Amsterdam, p.245.

- Hafer, M.R., 1991. Origin and controls of deposition of the Wheal Hughes and Poona copper deposits, Moonta, South Australia. *B.Sc (Hons) Thesis, University of Adelaide* (unpublished).
- Hanmer, S. and Passchier, C., 1991. Shear-sense indicators: a review. *Geological Survey of Canada, Paper* 90-17.
- Hanson, G.N., 1978. The application of trace elements to the petrogenesis of igneous rocks of granitic composition. *Earth and Planetary Science Letters*, v38, p26-43.
- Hanson, R.E. and Schweickert, R.A., 1982. Chilling and brecciation of a Devonian rhyolite sill intruded into wet sediments, northern Sierra Nevada, California. *Journal of Geology*, v90, p717-724.
- Harris, N.B.W., Pearce, J.A. and Tindle, A.G., 1986. Geochemical characteristics of collision-zone magmatism. In Coward, M.P and Ries, A.C. (Eds) *Collision Tectonics. Geological Society of London, Special Publication* 19, p67-81.
- Haynes, D.W., Cross, K.C., Bills, R.T. and Reed, M.H., 1995. Olympic Dam ore genesis: a fluid-mixing model. *Economic Geology*, 90:281-307.
- Hein, K.A.A., 1989. The geology and mineralization at the Tarcoola goldfield, South Australia. *B.Sc (Hons) Thesis, University of Adelaide* (unpublished).
- Hein, K.A.A., Both, R.A. and Bone, Y., 1994. The geology and genesis of the Tarcoola gold deposits, South Australia. *Mineralium Deposita*, 29:224-236.
- Henry, C.D., Price, J.G., Rubin, J.N. and Laubach, S.E., 1990. Case study of an extensive silicic lava: the Bracks Rhyolite. Trans-Pecos Texas. *Journal of Volcanology and Geothermal Research*, v43, p113-132.
- Henry, C.D., Price, J.G., Rubin, J.N., Parker, D.F., Wolff, J.A., Self, S., Franklin, R. and Barker, D.S. 1988. Widespread, lavalike silicic volcanic rocks of Trans-Peco Texas. *Geology*, v16, p509-512.
- Henry, C.D. and Wolff, J.A., 1992. Distinguishing strongly rheomorphic tuffs from extensive silicic lavas. *Bulletin of Volcanology*, 54(3):171-186.
- Higgins, M.L., Berg, R.C. and Hellesten, K.J., 1990. Menninnie Dam lead-zinc-silver prospect, Eyre Peninsula. In Hughes, F.E. (Ed.), *Geology of the Mineral Deposits of Australia and Papua New Guinea*. Australasian Institute of Mining and Metallurgy, p1055-1058.
- Hill, R.I., Chappell, B.W. and Campbell, I.H., 1992. Late Archaean granites of the southeastern Yilgarn Block, Western Australia: age, geochemistry, and origin. *Transactions of the Royal Society of Edinburgh. Earth Sciences*, 83:211-226.



- Hodgson, C.J., 1993. Mesothermal lode-gold deposits. In Kirkham, R.V., Sinclair, W.D., Thorpe, R.I. and Duke, J.M., (Eds.) *Mineral Deposit Modelling*. Geological Association of Canada, Special Paper 40, p635-678.
- Hoefs, J., (1973). *Stable Isotope Geochemistry*, New York. Springer-Verlag.
- Hoffman, P.F., 1989. Speculations on Laurentia's first gigayear (2.0-1.0 Ga). *Geology*, 17:135-138.
- Huppert, H.E. and Sparks, R.S.J., 1988. The generation of granitic magmas by intrusion of basalt into continental crust. *Journal of Petrology*, 29:599-624.
- Huston, D.L., Bolger, C. and Cozens, G., 1993. A comparison of mineral deposits at Gecko and White Devil deposits: implications for ore genesis in the Tenant Creek district, Northern Territory, Australia. *Economic Geology*, 88:1198-1225.
- Huston, D.L. and Large, R.R., 1989. A chemical model for the concentration of gold in volcanogenic massive sulfide deposits. *Ore Geology Reviews*, 4(3):171-200.
- Huston, D.L., Sie, S., Cooke, D.R., Both, R.A. and Suter, G.F., 1995. Trace elements in sulfide minerals from eastern Australian volcanic-hosted massive sulfide deposits: Part II, selenium levels in pyrite: comparison with  $\delta^{34}\text{S}$  values and implications for the source of sulphur in volcanogenic hydrothermal sources. *Economic Geology*, 90:1167-1196.
- Irvine, T.N. and Baragar, W.R.A., 1971. A guide to the chemical classification of the common volcanic rocks. *Canadian Journal of Earth Sciences*, 8:523-548.
- Janz, J., 1990. The mineralogy and paragenesis of the Poona Mine copper deposit. *B.Sc (Hons) Flinders University* (unpublished).
- Johnson, P.R. and Kattan, F., 2001., Oblique sinistral transpression in the Arabian shield: the timing and kinematics of a Neoproterozoic suture zone. *Precambrian Research*, 107:117-138.
- Kerrick, R., 1986. Archaean lode gold deposits of Canada: Part II, characteristics of the hydrothermal systems, and models of origin. *Information Circular 183*. *Economic Geology Research Unit, University of Witwatersand, Johannesburg*, 34p.
- Knight, J., 1997. Geochemistry and geochronology of the St Peter Suite west of Ceduna. *University of Adelaide. Honours Thesis* (unpublished).
- Laing, W.P., 1998. The Tunkillia ore system: preliminary assessment. Confidential report to Acacia Resources Ltd (unpublished).
- Lambert, I.B., Phillips, G.N. and Groves, D.I., 1984. Sulphur isotope compositions and genesis of Archaean gold mineralization, Australia and Zimbabwe. In Foster, R.P. (Ed.), The geology, geochemistry and genesis of gold deposits. *Proceedings, Symposium Gold '82. Geological Society of Zimbabwe, Special Publication 1*, Rotterdam, the Netherlands.

- Le Bas, M.J., Le Maite, R.W., Streckeisen, A. and Zanettin, B., 1986. A chemical classification of volcanic rocks based on the total alkali – silica diagram. *Journal of Petrology*, 27:745-750.
- Lister, G.S. and Snoke, A.W., 1984. S-C mylonites. *Journal of Structural Geology*, 6:617-638.
- MacDonald, A.J., 1983. The iron formation-gold association: evidence from the Geraldton area. *Ontario Geological Survey, Miscellaneous Paper* 110, 75-83.
- Maniar, P.D. and Piccoli, P.M., 1989. Tectonic discrimination of granitoids. *Geological Society of America, Bulletin*, 101:635-643.
- Martin, A.R., 1996. Gold mineralisation at the Tunkillia prospect (Yarlbrinda Shear Zone), Lake Everard. In Preiss, W.V. (ed.) Resources '96. Convention Abstracts. South Australia Department of Mines and Energy.
- Martin, A.R., Rankin, L.R., Benbow, M.C. and Daly, S.J., 1989. Helicopter survey of the geology of the BARTON and TARCOOLA 1:250 000 map sheets. *South Australia. Department of Mines and Energy. Report Book* 89/58.
- Martin, H., 1986. Effect of steeper Archaean geothermal gradient on geochemistry of subduction-zone magmas. *Geology*, 14:753-756.
- Martin, H., 1994. The Archaean grey gneisses and the genesis of continental crust. In Condie, K.C. (Ed). *Archaean Crustal Evolution*, Elsevier, Amsterdam, Holland.
- Mason, D.R., 1998. Petrographic descriptions for twenty one thin sections of rock samples from the Gawler Craton, South Australia. Mason Geoscience Pty Ltd Report 2432 (unpublished).
- McCuaig, T.C. and Kerrich, R., 1994. P-T-t-deformation-fluid characteristics of lode gold deposits: evidence from alteration systematics. In Lentz, D.R. (Ed.), Alteration and Alteration Processes Associated with Ore-forming Systems. *Geological Association of Canada, Short Course Notes* 11: 339-379.
- McDougall, I., 1985. K-Ar and  $^{40}\text{Ar}/^{39}\text{Ar}$  dating of hominid-bearing Pliocene-Pleistocene sequences at Koobi For a, Lake Turkana, northern Kenya. *Geological Society of America. Bulletin* 96:159-175.
- Mikucki, E.J. and Groves, D.I., 1990. Mineralogical constraints. In , Ho, S.E., Groves, D.I. and Bennett, J.M. (Eds.) Gold deposits of the Archaean Yilgarn Block, Western Australia. *Geology Department (Key Centre) and University Extension, The University of Western Australia, Publication No.* 20.
- Montel, J.M., Foret, S., Veschambre, M., Nicollet, C. and Provost, A., 1996. Electron microprobe dating of monazite. *Chemical Geology*, 131:37-53.

- Nakamura, N., 1974. Determinations of REE, Ba, Fe, Mg, Na and K in carbonaceous and ordinary chondrites. *Geochimica et Cosmochimica Acta*, 38, 757-775.
- Nash, J.T., 1976. Fluid-inclusion petrology-data from porphyry copper deposits and applications to exploration. *United States Geological Survey Professional Paper* 907-D, 16p.
- Nielsen, H., 1979. *Sulphur Isotopes*. In *Lectures in Isotope Geology*. Ed. E. Jaeger and J.C. Hunziker. Springer-Verlag publishers, p283-313.
- O'Connor, J.T., 1965., A classification for quartz-rich igneous rock based on feldspar ratios. *United States Geological Survey Professional Paper*, 525-B: 79-84.
- Parker, A.J., 1980. The Kalinjala Mylonite Zone, eastern Eyre Peninsula. *South Australia. Geological Survey. Quarterly Geological Notes*, 75:6-11.
- Parker, A.J., 1987. Structural, stratigraphic and metamorphic geology of Lower Proterozoic rocks in the Cowell/Cleve district, eastern Eyre Peninsula. *Ph.D thesis, University of Adelaide*.
- Parker, A.J., (1990). Gawler Craton and Stuart Shelf – regional geology and mineralisation. In: Hughes, F.E. (Ed.). *Geology of the mineral deposits of Australia and Papua New Guinea. Australasian Institute of Mining and Metallurgy. Monograph Series*, 14:999-1008.
- Parker, A.J., 1993. Geological Framework. In Drexel, J.F., Preiss, W.V. and Parker, A.J. (Eds). *The geology of South Australia. Vol. 1, The Precambrian. South Australia. Geological Survey, Bulletin*, 54:9-31.
- Parker, A.J., 1996. Shear hosted Proterozoic gold, Nuckulla Hill. In Preiss, W.V. (Ed.) *Resources '96. Convention Abstracts. South Australia Department of Mines and Energy*.
- Parker, A.J., Fanning, C.M. and Flint, R.B., 1981. Archaean to Middle Proterozoic geology of the southern Gawler Craton, South Australia. Excursion guide. *South Australia. Department of Mines and Energy. Report Book*, 81/91.
- Parker, A.J. and Lemon, N.M., 1982. Reconstruction of the Palaeoproterozoic stratigraphy of the Gawler Craton, South Australia. *Geological Society of Australia, Journal*, 29,221-238.
- Parker, A.J., Rickwood, P.C., Baillie, P.W., McClenaghan, M.P., Boyde, D.M., Freeman, M.J., Pietsch, B.A., Murray, C.G. and Myers, J.S., 1987. Mafic Dyke Swarms of Australia. In: Halls, A.C. and Fahrig, W.F. (Eds), *Mafic dyke swarms. Geological Association of Canada Special Paper*, 34:401-417.
- Passchier, C.W. and Simpson, C., 1986. Porphyroclast systems as kinematic indicators. *Journal of Structural Geology*, 8, 831-844.
- Patchett, J. and Arndt, N.T., 1986. Nd isotopes and tectonics of 1.9-1.7 Ga crustal genesis. *Earth and Science Planetary Letters*, 78:329-338.



Pearce, J.A., 1982. Trace element characteristics of lavas from destructive plate boundaries. In Thorpe, R.S. (Ed.) *Andesites*. Wiley, Chichester, pp525-548.

Pearce, J.A. and Cann, J.R., 1973. Tectonic setting of basic volcanic rocks determined using trace element analysis. *Earth and Planetary Science Letters*, v19, p290-300.

Pearce, J.A., Harris, N.B.H. and Tindle, A.G., 1984. Trace element discrimination diagrams for the tectonic interpretation of granitic rocks. *Journal of Petrology*, v25, p956-983.

Pettifer, G.R. and Fraser, A.R., 1974. Reconnaissance helicopter gravity survey, South Australia, 1970. *Record of the Bureau of Mineral Resources, Geology and Geophysics, Australia*, 1974/88.

Phillips, D., 1999. K-Ar dating of sericite samples R387439 and R387440. PRISE Report AR98-550. For *Primary Industries and Resources, South Australia* (unpublished).

Pitcher, W.S., 1979., Comments on the geological environments of granites. In Atherton, M.P. and Tarney, J. (Eds). *Origin of Granite Batholiths: geochemical evidence*. Shiva Publishing Ltd, Kent, UK.

Pitcher, W.S., 1982. Granite type and tectonic environment. In: *Mountain Building Processes*. K.J. Hsu (editor). Academic Press, London, 19-40.

Pitcher, W.S., 1987. Granites and yet more granites forty years on. *Geologische Rundschau*, v76 (1), 51-79.

Pitcher, W.S., 1993. *The Nature and Origin of Granite*. Chapman and Hall, London, 387p.

Pontifex, I.R. and Hand, M., 1997. Mineralogical Report No. 7367. Pontifex & Associates Pty Ltd. Unpublished report fro Helix Resources NL.

Potter, R.W., 1977. Pressure correction for fluid-inclusion homogenization temperatures based on the volumetric properties of the system NaCl-H<sub>2</sub>O. *United States Geological Survey, Journal of Research*, 5:603-607.

Purvis, A.C., 1983. Pontifex and Associates Pty Ltd mineralogical report for CRA Exploration Pty Ltd. *Primary Industries. Open file Envelope* 5048.

Purvis, A.C., 1997. Pontifex and Associates Pty Ltd mineralogical report 7938 for Primary Industries and Resources.

Purvis, A.C., 1998a. Pontifex and Associates Pty Ltd mineralogical report 7580 for Primary Industries and Resources.

- Purvis, A.C., 1998b. Pontifex and Associates Pty Ltd mineralogical report 7723 for Primary Industries and Resources.
- Purvis, A.C., 2000. Pontifex and Associates Pty Ltd mineralogical report 7938 for Primary Industries and Resources.
- Quilty, J.H., 1962. CHILDARA/GAIRDNER, airborne magnetic and radiometric survey, South Australia, 1961. *Record Bureau of Mineral Resources. Geology and Geophysics, Australia, 1962/192* (unpublished).
- Rankin, L.R., 1986. Petrography of mylonitic lithologies from the Karari Fault Zone in SADME Ooldea 3 DDH. *South Australia. Department of Mines and Energy. Report Book, 86/84*.
- Rankin, L.R., 1997a. Geological Interpretation. Lake Everard Survey. For Helix Resources NL (unpublished).
- Rankin, L.R., 1997b. Lake Everard EL 2028 Ultra-detailed magnetic survey. Geological Interpretation. For Helix Resources NL (unpublished).
- Rankin, L.R. and Flint, R.B., 1991. 1:250 000 Geological Series -Explanatory Notes, STREAKY BAY, South Australia. *South Australia. Department of Mines and Energy*.
- Rankin, L.R., Flint, R.B. and Fanning, C.M., 1990. Palaeoproterozoic Nuyts Volcanics of the western Gawler Craton. *South Australia. Department of Mines and Energy. Report Book, 90/60*.
- Rankin, L.R., Martin, A.R. and Parker, A.J. 1989. Early Proterozoic history of the Karari Fault Zone, northwest Gawler Craton, South Australia. *Australian Journal of Earth Sciences*, 36:123-134.
- Rapp, R.P., Watson, E.B. and Miller, C.F., 1991. Partial melting of amphibolite/eclogite and the origin of Archaean trondhjemites and tonalites. *Precambrian Research*, 51:1-25.
- Roache, M.W., 1994. The geology, timing of mineralisation, and genesis of the Menninnie Dam Zn-Pb-Ag deposit, Eyre Peninsula, South Australia. *Ph.D. Thesis, University of Tasmania* (unpublished).
- Robinson, B.W. and Kusakabe, M., 1975. Quantitative preparation of SO<sub>2</sub> for <sup>34</sup>S/<sup>32</sup>S analyses, from sulphides by combustion with cuprous oxide. *Analytical Chemistry*, 47:1179-1181.
- Roedder, E., 1984. *Fluid Inclusions*. Mineralogical Society of America, Reviews in Mineralogy, 12, 654p.
- Rollinson, H., 1993. *Using geochemical data: evaluation, presentation, interpretation*. Longman, Singapore, 352p.

- Sheperd, T.J., Rankin, A.H. and Alderton, D.H.M., 1985. A Practical Guide to Fluid Inclusion Studies. Blackie.
- Sheppard, S., Griffin, T.J. and Tyler, I.M., 1995. Geochemistry of felsic igneous rocks from the southern Halls Creek Orogen. . *Geological Survey of Western Australia, Record* 1995/4.
- Sheppard, S., Griffin, T.J. and Tyler, I.M., 1997. Compilation of whole-rock geochemical data for the King Leopold and Halls Creek Orogens. *Geological Survey of Western Australia, Record* 1997/4.
- Sibson, R.H., 1986. Brecciation processes in fault zones: inferences from earthquake rupturing. *Pure and Applied Geophysics*, 124:159-175.
- Sibson, R.H., Robert, F. and Poulsen, K.H., 1988. High-angle reverse faults, fluid-pressure cycling, and mesothermal gold deposits. *Geology*, 16:551-555.
- Silver, L.T. and Chappell, B.W., 1988. The Peninsular Ranges batholith: an insight into the evolution of the Cordilleran batholiths of southeastern North America. *Transactions of the Royal Society of Edinburgh, Earth Sciences*, 79:105-121.
- Simpson, C. and Schmid, S.M., 1983. An evaluation of criteria to deduce the sense of movement in sheared rocks. *Geological Survey of America, Bulletin* 94, 1281-1288.
- Stacey, J.S. and Kramers, J.D., 1975. Approximation of terrestrial lead isotope evolution by a two-stage model. *Earth and Planetary Science Letters*, 26:207-221.
- Standish, T.R. and Hill, R.J., 1999. Technical report No. 08.9849. Lake Everard – South Australia, EL 2028. Fourth Annual Report for the period ending 7 November 1998. Acacia Resources Limited Gawler Craton Joint Venture. Unpublished report.
- Standish, T.R., Treloar, K. and Hill, R.J., 1997. Technical report No. 2213 Lake Everard – South Australia, EL 2028. Third Annual Report for the period ending 7 November, 1997. Helix Resources NL. Unpublished report.
- Sterner, S.M. and Bodnar, R.J., 1984. Synthetic fluid inclusions in natural quartz. I. Compositional types synthesized and applications to experimental geochemistry. *Geochimica et Cosmochimica Acta*, 48:2659-2668.
- Stewart, K.P., 1992. High temperature felsic volcanism and the role of mantle magmas in Proterozoic crustal growth: The Gawler Range Volcanic Province. *University of Adelaide, Ph.D thesis* (unpublished).
- Stewart, K.P. and Foden, J. 1998. Mesoproterozoic granitoids of South Australia: progress report. *Department of Geology and Geophysics, University of Adelaide* (unpublished).



- Stewart, K.P. and Foden, J. 2001. Mesoproterozoic granitoids of South Australia: Part 1 – the Gawler Craton. *Department of Geology and Geophysics, University of Adelaide* (unpublished).
- Stone, D., 1998., Precambrian geology of the Berens River area, northwest Ontario. *Ontario Geological Survey. Open file Report 5963*.
- Streckeisen, A., 1976. To each plutonic rock its proper name. *Earth Science Reviews*, 12:1-33.
- Sun, S.S. and McDonough, W.F., 1989. Chemical and isotopic systematics of oceanic basalts: implications for mantle composition and processes. In: Saunders, A.D. and Norry, M.J. (eds), *Magmatism in Ocean Basins. Geological Society of London, Special Publication 42*, 313-345.
- Taylor, S.R. and McLennan, S.M., 1985. *The continental crust: its composition and evolution*. Oxford, England, Blackwell Scientific, 312p.
- Teasdale, J., 1997. The interpretive geology and tectonothermal evolution of the western Gawler Craton. *Ph.D thesis, University of Adelaide*.
- Thomson, B.P., 1966. The lower boundary of the Adelaide System and older basement relationships in South Australia. *Geological Society of Australia. Journal*, 13:203-228.
- Thomson, B.P., 1969. Precambrian crystalline basement. In Parkin, L.W. (Ed.), *Handbook of South Australian Geology*. Geological Survey of South Australia, pp21-48.
- Thomson, B.P., 1970. A review of the Precambrian and Lower Palaeozoic tectonics of South Australia. Royal Society of South Australia. *Transactions*, 94:193-221.
- Thomson, B.P., 1975. Gawler Craton, S.A. In Knight, C.L. (Ed.) *Economic Geology of Australia and Papua New Guinea*, 1, Metals. *Australasian Institute of Mining and Metallurgy. Monograph Series*, 5:461-466.
- Thomson, B.P., 1980., (Compiler), Geological map of South Australia. *South Australia. Geological Survey. Maps of South Australia Series*, 1:1 000 000.
- Townsend, A.T., Zongshou, Y, McGoldrick, P. and Hutton, J.A., 1998. Precise lead isotope ratios in Australian galena samples by high resolution inductively coupled plasma mass spectrometry. *Journal of Analytical Atomic Spectrometry*, 13:809-813.
- Webb, A.W., 1976. Geochronology of the younger granites of the Gawler Craton and its northwest margin. Amdel report for project 1/1/122, progress report 24. *South Australia. Department of Mines and Energy. Open file Envelope*, 1582 (unpublished).
- Webb, A.W., 1978. Geochronology of the younger granites of the Gawler Craton and its northwest margin. Amdel report 1215. *South Australia. Department of Mines and Energy. Open file Envelope*, 1582 (unpublished).

- Webb, A.W., Thomson, B.P., Blissett, A.H., Daly, S.J., Flint, R.B. and Parker, A.J., 1986. Geochronology of the Gawler Craton, South Australia. *Australian Journal of Earth Sciences*, 33:119-143.
- Whalen, J.B., Currie, K.L. and Chappell, B.W., 1987. A-type granites: geochemical characteristics, discrimination and petrogenesis. *Contributions to Mineralogy and Petrology*, v95, p407-419.
- White, A.J.R., 1979. Sources of granite magmas. Abstracts with programs. *Geological Society of America. Annual General Meeting*, p539.
- White, A.J.R. and Chappell, B.W., 1983. Granitoid types and their distribution in the Lachlan Fold Belt, southeastern Australia. *Geological Society of America, Memoirs*, 159:21-34.
- Whitten, G.F., 1963. Drilling of the Warramboo aeromagnetic anomalies, central Eyre Peninsula. *Mining Review, Adelaide*, 115:70-79.
- Wilson, M.R., Hamilton, P.J., Fallick, A.E., Aftalion, M. and Michard, A. 1985. Sm-Nd, U-Pb and O systematics of granites and Proterozoic crustal evolution in Sweden. *Earth and Science Planetary Letters*, 72:376-388.
- Winkler, H.G.F., 1976. *Petrogenesis of metamorphic rocks*. Springer Verlag, New York, 4<sup>th</sup> edition.
- Wyborn, L.A.I., 1988. Petrology, geochemistry and origin of a major Australian 1880-1840 Ma felsic volcano-plutonic suite: a model for intracontinental felsic magma generation. *Precambrian Research*, 40/41:37-60.
- Wyborn, L.A.I., 1993. Constraints on interpretations of lower crustal structure, tectonic setting and metallogeny of the Eastern Goldfields and Southern Cross Provinces provided by granite geochemistry. *Ore Geology Reviews*, 8:125-140.
- Wyborn, L.A.I., 2001. Granites and copper gold metallogenesis in the Australian Proterozoic. In Budd, A., Wyborn, L and Bastrakova, I. *The Metallogenesis Potential of Australian Proterozoic Granites*. AGSO Record 2001/12.
- Wyborn, L.A.I., Page, R.W. and Parker, A.J., 1987. Geochemical and geochronological signatures in Australian Proterozoic igneous rocks. In: Pharaoh, T.C., Beckinsale, R.D. and Richard, D. (Eds), *Geochemistry and mineralisation of Proterozoic volcanic suites*. *Geological Society Special Publication*, 33:377-394.
- Wyborn, L.A.I., Page, R.W., and McCulloch, M.T., 1988. Petrology, geochronology, and isotope geochemistry of the post-1820 Ma granites of the Mount Isa Inlier: mechanisms for the generation of Proterozoic anorogenic granites. In Wyborn, L.A.I. and Etheridge, M.A., (Editors), *The early to middle Proterozoic of Australia*. *Precambrian Research*, 40/41: 509-541.

Wyborn, L.A.I., Wyborn, D., Warren, R.G. and Drummond, B.J., 1992. Proterozoic granite types in Australia: implications for lower crust composition, structure and evolution. *Transactions of the Royal Society of Edinburgh, Earth Sciences*, 83,201-209.

Wyllie, P.J., 1977. Effects of H<sub>2</sub>O and CO<sub>2</sub> on magma generation in the crust and mantle. *Geological Society of London*, 134:215-234.

Yamagishi, H. and Goto, Y., 1992. Cooling joints of subaqueous rhyolite lava flows at Kuriowa, Yakumo, Southern Hokkaido, Japan. *Bulletin of Volcanological Society of Japan*, 4:205-207.

Zen, E.A., 1986. Aluminium enrichment in silicate melts by fractional crystallisation: some mineralogic and petrographic constraints. *Journal of Petrology*, v27, p1095-1117.

Zhao, J. and Cooper, J.A., 1992. The Atnarpa Igneous Complex, S.E. Arunta Inlier, central Australia: implications for subduction at an early-mid Proterozoic continental margin. *Precambrian Research*, 56:227-253.

Zhao, J. and McCulloch, M.T., 1995. Geochemical and Nd isotope systematics of granites from the Arunta Inlier, central Australia: implications for Proterozoic crustal evolution. *Precambrian Research*, 71:265-299.



## **APPENDIX A**

# **GEOCHEMICAL SAMPLE LOCATIONS AND FULL GEOCHEMICAL ANALYSIS**

# Archaeon

SAMPNO R378930 R378931

GROUP Archaeon Archaeon

Easting 485624 497589

Northing 6569151 6569356

## Major elements (wt%)

SiO <sub>2</sub>	71.4	74.9
Al <sub>2</sub> O <sub>3</sub>	14.9	13.5
CaO	2.4	0.82
Fe <sub>2</sub> O <sub>3</sub>	2.91	1.78
K <sub>2</sub> O	2.35	4.37
MgO	0.83	0.31
MnO	0.05	0.02
Na <sub>2</sub> O	4.69	3.8
P <sub>2</sub> O <sub>5</sub>	0.2	0.14
TiO <sub>2</sub>	0.38	0.22
LOI	0.31	0.73

## Trace elements (ppm)

Be	1	1
Sc	5	2.5
V	40	10
Cr	30	20
As	0.5	1
Ba	650	1200
Bi	1.5	1.5
Cd	1.5	1.5
Co	4	1
Cs	1.5	1.5
Ga	28	18
Hf	4	5
In	0.25	0.25
Mo	4	4
Nb	0.5	0.5
Rb	130	105
Sb	1	84
Sn	0.5	0.5
Sr	440	195
Ta	4	3
Te	2.5	2.5
Tl	1.5	1.5
Th	32	32
U	3.5	4.5
W	1.5	1.5
Y	12	8
Zr	180	170

### Archaean

SAMPNO R378930 R378931

GROUP Archaean Archaean

Easting 485624 497589

Northing 6569151 6569356

#### Rare earth elements (ppm)

Ce	66	71
Dy	1.5	1.5
Er	0.5	0.5
Eu	1	1
Gd	2	2
Ho	0.25	0.25
La	44	46
Lu	0.25	0.25
Nd	25	27.5
Pr	7	8
Sm	2.5	2
Tb	0.25	0.25
Tm	0.5	0.5
Yb	0.5	0.5

#### Economic elements (ppm)

Cu	6	2
Pb	8	18
Zn	61	24
Ni	5	9



# Tunkillia Suite

SAMPNO	R350424	R350426	R350427	R350428	R350429	R350431	R350433	R350434	R350435	R363434	R363435	R363436	R363437	444825	R370938	R378933	R444828	R444829	R444830	R444831
GROUP	airstrip	airstrip	airstrip	airstrip	airstrip	airstrip	airstrip	airstrip	airstrip	airstrip	airstrip	airstrip	airstrip	Barton	Childara	Childara	Lake Ifould	Lake Ifould	Lake Ifould	Lake Ifould
Easting	466840	475717	475730	477797	477663	478064	481010	480106	480718	481130	480020	480361	480406	283614	474771	477000	225023	225631	224536	221438
Northing	6500257	6494570	6494556	6490815	6490718	6490150	6491265	6491383	6491498	6490622	6490385	6471129	6491366	7E+06	6494106	6491863	6585730	6583112	6581750	6577403
Major elements (wt%)																				
SiO <sub>2</sub>	72.0	62.9	71.8	76.4	76.8	76.3	73.7	74.4	71	70.5	67.7	71.6	72.5	72.028	72.9	75.6	76.068	70.645	70.041	70.208
Al <sub>2</sub> O <sub>3</sub>	14.9	19.3	13.5	11.5	12	12.3	13.2	12.9	14.5	14.7	15.6	13.7	12.5	15.308	13.1	12.2	13.467	14.63	15.047	17.171
CaO	1.64	1.1	1.01	0.45	0.55	0.64	0.55	0.79	0.72	2.32	1.95	1.74	0.17	2.017	0.57	0.68	2.425	1.545	2.207	2.998
Fe <sub>2</sub> O <sub>3</sub>	1.73	2.43	2.72	1.47	1.36	1.31	0.9	1.06	2.42	2.67	2.84	2.92	2.53	1.944	3.32	1.36	1.74	3.255	2.62	1.798
K <sub>2</sub> O	4.15	8.24	5.84	5.41	4.42	4.5	6.69	5.87	4.77	3.7	6.05	5.16	6.01	4.064	5.93	5.3	2.262	4.573	5.538	1.226
MgO	0.36	0.3	0.34	0.13	0.14	0.15	0.13	0.13	0.62	0.5	0.71	0.57	0.72	0.778	0.45	0.15	0.546	0.859	0.673	0.621
MnO	0.05	0.06	0.06	0.03	0.07	0.06	0.03	0.05	0.08	0.11	0.09	0.08	0.05	0.021	0.05	0.04	0.038	0.03	0.03	0.023
Na <sub>2</sub> O	4.22	4.16	2.64	2.72	3.85	3.87	2.93	2.66	3.94	3.7	3.21	2.63	2.5	3.476	3.03	2.96	3.622	3.447	3.148	5.495
P <sub>2</sub> O <sub>5</sub>	0.13	0.09	0.11	0.04	0.03	0.03	0.04	0.02	0.1	0.11	0.13	0.08	0.05	0.029	0.07	0.18	0.077	0.046	0.095	0.017
TiO <sub>2</sub>	0.21	0.22	0.31	0.14	0.11	0.11	0.14	0.08	0.23	0.22	0.49	0.3	0.24	0.202	0.43	0.1	0.226	0.546	0.316	0.199
LOI	1.11	1.33	1.31	0.73	0.56	0.92	1.11	1.08	1.55	1.33	1.43	1.44	1.65	0.14	0.32	0.64	0.671	0.134	0.159	0.019
Trace elements (ppm)																				
Be	2	3	1	3	4	4	1	1	1	1	1	1	1	1.8	1	2	2	1.9	1.3	2.2
Sc	2.5	2.5	2.5	2.5	2.5	2.5	2.5	2.5	2.5	2.5	2.5	5	2.5	4	2.5	2.5	4	5	2	4
V	10	10	10	10	10	10	10	10	10	10	20	20	10	31	10	10	16	43	18	30
Cr	10	10	10	10	10	10	10	10	10	10	10	30	20	17	20	20	9	23	3	18
As	0.5	3	2	2	0.5	2	1	0.5	1	2	2	1	3	0.8	2	0.5	0.9	1.1	1.1	0.7
Ba	1100	600	490	260	180	200	1450	500	2750	2350	2750	1300	750	1422	1150	400	880	1194	2779	587
Bi	1.5	1.5	1.5	1.5	1.5	1.5	1.5	1.5	1.5	1.5	1.5	1.5	1.5	0	1.5	1.5	0	0	0	0
Cd	1.5	1.5	1.5	1.5	1.5	1.5	1.5	1.5	1.5	1.5	1.5	1.5	1.5	0.26	1.5	1.5	0.14	0.05	0.05	0.06
Co	2	3	3	1	0.5	1	2	0.5	2	2	3	4	2		7	0.5				
Cs	4	10	6	4	4	1.5	1.5	1.5	4	1.5	1.5	1.5	1.5	1.2	1.5	4	0.77	0.76	0.95	4
Ga	20	31	25	23	21	23	18	18	22	25	25	26	21	15.2	24	18	14.1	19.6	13.7	19
Hf	2	3	2	3	3	3	3	2	2	3	6	3	4	3.4	9	5	3.3	6.5	5.3	1.9
In	0.25	0.25	0.25	0.25	0.25	0.25	0.25	0.25	0.25	0.25	0.25	0.25	0.25		0.25	0.25				
Mo	2	1	2	1	1	1	1	1	1	2	1	3	3	2.9	2	3	5	4.6	2.8	3.4
Nb	10	15	15	10	20	20	0.5	0.5	15	0.5	0.5	15	15	5.2	25	0.5	5.3	18.6	3.2	4.5
Rb	130	350	250	200	190	200	150	115	120	73	110	160	210	93.9	280	260	60.4	126.8	101.5	48.9
Sb	3	3	3	4	3	3	3	3	3	3	3	5	3	0	3	2	0	0	0.1	0
Sn	0.5	0.5	0.5	0.5	0.5	0.5	0.5	0.5	0.5	0.5	0.5	0.5	0.5	1.6	0.5	0.5	1.2	1.6	1.8	0.8
Sr	350	55	60	35	40	40	140	125	340	470	410	290	75	385.9	85	65	341	250.3	503.9	914.9
Ta	4	4	4	4	4	4	3	3	3	3	3	3	3	0.5	7	4	0.6	0.5	0.3	0.6
Te	2.5	2.5	2.5	2.5	2.5	2.5	2.5	2.5	2.5	2.5	2.5	2.5	2.5		2.5	2.5				
Tl	1.5	1.5	1.5	1.5	1.5	1.5	1.5	1.5	1.5	1.5	1.5	1.5	1.5		1.5	1.5				
Th	9	17.5	21	21	32	20.5	7.5	3.5	4.5	2	9.5	12.5	20.5	11.7	25	21	4.9	66.6	11.6	3.9
U	3	3.5	5.5	5.5	6.5	5	0.5	1	1.5	0.25	1.5	2	3	1.51	3.5	6	0.71	2.58	0.46	0.87
W	500	160	350	410	650	500	500	320	350	300	200	210	240		1.5	1.5				
Y	14	15	41	35	33	38	6	7	14	8	10	22	39	14.2	75	27	9.3	35.1	6.4	5.1
Zr	140	160	120	140	120	130	170	90	180	180	380	180	220	122	500	140	128	258	249	76

# Tunkillia Suite

SAMPNO	R350424	R350426	R350427	R350428	R350429	R350431	R350433	R350434	R350435	R363434	R363435	R363436	R363437	444825	R370938	R378933	R444828	R444829	R444830	R444831
GROUP	airstrip	airstrip	airstrip	airstrip	airstrip	airstrip	airstrip	airstrip	airstrip	airstrip	airstrip	airstrip	airstrip	Barton	Childara	Childara	Lake Ifould	Lake Ifould	Lake Ifould	Lake Ifould
Easting	466840	475717	475730	477797	477663	478064	481010	480106	480718	481130	480020	480361	480406	283614	474771	477000	225023	225631	224536	221438
Northing	6500257	6494570	6494556	6490815	6490718	6490150	6491265	6491383	6491498	6490622	6490385	6471129	6491366	7E+06	6494106	6491863	6585730	6583112	6581750	6577403
Rare earth elements (ppm)																				
Ce	43	26	87	140	50	60	49	19	60	58	89	97	115	66.71	180	47	32.2	300.3	165.3	14.94
Dy	2.5	3	7	7	6.5	7	1.5	1.5	3	2	2.5	4	8	2.76	12	4	1.56	8.87	1.09	0.89
Er	2	2	5	4	4	4	0.5	1	2	0.5	1	2	4	1.15	7	2	0.82	1.99	0.57	0.58
Eu	0.5	0.5	0.5	0.5	0.25	0.25	0.25	0.5	0.25	0.5	1	1	1	1.024	1	0.25	0.883	1.391	1.192	0.622
Gd	3	3	7	9	6	7	2	2	3	2	3	5	9	4.05	11	4	2.21	19.18	2.72	0.88
Ho	0.5	0.5	1.5	1	1.5	1.5	0.25	0.25	0.5	0.25	0.25	0.5	1.5	0.46	2.5	1	0.31	1.2	0.22	0.19
La	25	15	50	80	24	29	29	10	32	34	45	47	70	34.35	93	26	18.52	122.2	94.27	7.75
Lu	0.25	0.25	0.5	0.5	0.5	0.5	0.25	0.25	0.25	0.25	0.25	0.25	0.5	0.12	1	0.25	0.13	0.13	0.12	0.1
Nd	16	11.5	34	57	25	29	19.5	8.5	23.5	21	30	30.5	51	25.62	60	22	12.49	108.5	47.38	4.57
Pr	5	3	11	15	8	8	6	2	7	6	9	9	16	7.1	16	5	3.51	30.58	15.48	1.39
Sm	0.25	2	6.5	9	6.5	7	0.25	0.25	0.25	0.25	0.25	0.25	10	4.44	8	3	2.35	22.6	5.33	0.88
Tb	0.25	0.25	1	1	1	1	0.25	0.25	0.25	0.25	0.25	0.5	1	0.63	1.5	0.5	0.3	2.49	0.27	0.16
Tm	0.5	0.5	0.5	0.5	0.5	0.5	0.5	0.5	0.5	0.5	0.5	0.5	0.5	0.5	1	0.5				
Yb	2	2	5	4	5	4	0.5	1	2	0.5	1	2	4	0.77	7	3	0.88	0.82	0.64	0.74
Economic elements (ppm)																				
Cu	4	8	2	3	3	2	2	0.5	3	27	36	39	47	13	11	3	8	14	9	6
Pb	14	10	10	16	20	20	8	14	6	8	14	6	4	40.9	18	12	19.2	41.8	24.4	14.4
Zn	34	39	51	46	47	40	12	14	48	55	52	34	59	29.2	74	30	25.8	60.6	29.4	33.4
Ni	2	4	2	1	0.5	2	2	3	1	1	2	3	4	10.1	4	2	3.5	7.2	0.15	4.6

# Tunkillia Suite

SAMPNO	R370928	R370929	R370930	R370931	R370932	R370933	R370934	R370935	R370936	R444835	R444824	R444832	R444833	R444834	R387449	R337010	R337011	R337017	R368571	R368573
GROUP	Lakeside	Lakeside	Lakeside	Lakeside	Lakeside	Lakeside	Lakeside	Lakeside	Lakeside	Mulgathing	Pinbong	Tallacootra	Tallacootra	Tallacootra	Tunkillia	VPF	VPF	VPF	VPF	VPF
Easting	477656	478426	478416	478402	478400	477187	477039	489996	489674	399000	544166	232344	232451	231647		484124	472307	469620	484124	472307
Northing	6503959	6503346	6503114	6503092	6503092	6504581	6506538	6511884	6512791	6653600	6367104	6567634	6567700	6564845		6535828	6553627	6554690	6535828	6553627
Major elements (wt%)																				
SiO <sub>2</sub>	72.9	75.6	75.8	72.4	68.9	76.9	75.3	76	77.1	75.9	76.459	72.826	71.391	75.711	69.784	74.3	72	73.8	66.7	72.7
Al <sub>2</sub> O <sub>3</sub>	11.9	12.8	13.1	13.8	14	12.4	12.9	13.1	12	13.1	12.104	12.862	14.28	13.01	14.411	14.1	14.4	13.6	14.6	14.3
CaO	0.26	0.36	0.41	1.29	2.63	0.31	0.18	0.31	0.64	0.78	0.785	1.053	0.559	1.05	2.319	1.73	1.49	1.44	2.58	1.78
Fe <sub>2</sub> O <sub>3</sub>	5.14	1.99	1.89	2.68	5.11	0.76	2.11	0.85	1.62	0.87	1.589	2.755	2.321	1.278	4.129	1.51	1.27	1.69	4.14	1.3
K <sub>2</sub> O	5.23	6.58	4.76	6.1	3.7	6.51	6.36	6	4.73	5.57	5.38	6.521	6.534	4.4	3.992	4.31	5.06	3.97	4.98	4.43
MgO	0.09	0.17	0.07	0.41	1.34	0.05	0.14	0.12	0.21	0.03	0.306	0.59	0.22	0.278	0.911	0.3	0.22	0.3	0.95	0.3
MnO	0.005	0.04	0.03	0.06	0.16	0.005	0.01	0.02	0.08	0.005	0.036	0.059	0.041	0.021	0.072	0.05	0.02	0.04	0.14	0.05
Na <sub>2</sub> O	2.13	2.13	3.78	2.7	3.07	2.62	2.86	2.95	2.91	3.13	2.883	2.072	3.255	3.802	3.628	3.39	3.39	3.77	1.96	3.44
P <sub>2</sub> O <sub>5</sub>	0.02	0.03	0.005	0.06	0.12	0.01	0.03	0.08	0.03	0.08	0.026	0.049	0.109	0.033	0.157	0.04	0.04	0.04	0.14	0.04
TiO <sub>2</sub>	0.17	0.2	0.09	0.3	0.64	0.11	0.2	0.11	0.14	0.05	0.269	0.403	0.208	0.222	0.607	0.13	0.12	0.17	0.51	0.13
LOI	1.65	0.85	0.57	0.83	1.05	0.66	0.54	0.68	0.77	0.3	0.001	0.582	0.945	0.023	0.327	0.54	0.72	0.52	3.31	0.68
Trace elements (ppm)																				
Be	1	1	4	1	3	1	1	3	3	1	4.1	2.3	0.9	1.6	2.3	1	2	4	1	1
Sc	2.5	2.5	2.5	2.5	15	2.5	2.5	2.5	2.5	2.5	5	6	2	1	6	2.5	2.5	2.5	10	2.5
V	140	10	10	10	50	10	10	10	10	10	14	16	8	9	31	10	10	10	40	10
Cr	50	90	300	100	30	50	140	10	110	20	9	8	5	6	11	10	20	20	40	10
As	11	0.5	3	2	2	0.5	0.5	0.5	1	0.5	1.3	0.7	1.1	0.8	1	0.5	0.5	1	4	1
Ba	850	360	55	1050	600	150	700	320	270	1100	289	766	313	1135	1179	1100	4900	900	1250	950
Bi	1.5	1.5	1.5	1.5	1.5	1.5	1.5	1.5	1.5	1.5	0.1	0	0	0	0	1.5	1.5	1.5	1.5	1.5
Cd	1.5	1.5	1.5	1.5	1.5	1.5	1.5	1.5	1.5	1.5	0.025	0.24	0.22	0.06	0.1	1.5	1.5	1.5	1.5	1.5
Co	0.5	4	2	6	17	2	3	2	2	0.5					3	2	3	6	2	
Cs	4	4	4	4	8	1.5	6	6	6	1.5	3.38	3.14	1.09	0.13	0.4	1.5	1.5	1.5	6	1.5
Ga	22	18	23	21	24	17	21	19	20	18	14.9	15	16	15.4	19.4	16	20	19	22	22
Hf	4	3	4	6	5	3	4	3	3	2	6.3	8.6	5.5	4.7	10.1	2	2	3	3	1
In	0.25	0.25	0.25	0.25	0.25	0.25	0.25	0.25	0.25	0.25						0.25	0.25	0.25	0.25	0.25
Mo	3	3	4	3	3	2	3	2	2	1	5.8	4.3	3.4	3.7	3.3	4	1	4	4	1
Nb	30	20	40	25	25	15	20	20	25	0.5	21.7	16.4	8.5	11.1	15	0.5	0.5	15	0.5	0.5
Rb	210	270	310	220	230	270	270	350	320	120	289.1	327.2	84.9	44.4	50.5	135	110	145	210	110
Sb	4	3	3	3	3	3	3	4	3	0.5	0	0	0	0	0	2	3	2	0.5	4
Sn	0.5	0.5	0.5	0.5	0.5	0.5	0.5	0.5	0.5	0.5	3.3	7	1.2	1.5	1.1	0.5	0.5	0.5	0.5	0.5
Sr	85	50	25	110	150	35	130	75	145	220	58.2	79.6	80.8	206.8	308.9	400	370	300	250	380
Ta	11	8	9	8	8	6	7	7	7	3	1.9	1.5	0.6	1.1	0.5	4	1	4	1	1
Te	2.5	2.5	2.5	2.5	2.5	2.5	2.5	2.5	2.5	2.5						2.5	2.5	2.5	2.5	2.5
Tl	1.5	1.5	1.5	1.5	1.5	1.5	1.5	1.5	1.5	1.5						1.5	1.5	1.5	1.5	1.5
Th	16.5	26	26	27.5	23.5	29	24	19.5	24	12	35.9	41.3	3	3.8	10.1	11	6	30	25.5	6.5
U	2	4	7	5	6.5	3.5	4	5.5	6.5	1	6.56	4.64	1.22	0.46	0.82	2.5	1	4.5	2	1.5
W	4	1.5	1.5	1.5	4	1.5	1.5	1.5	1.5	1.5						4	300	4	6	360
Y	14	19	55	25	42	18	17	9	12	3	42	41.9	16.7	34	38.6	11	8	6	17	7
Zr	170	100	150	280	220	110	190	80	90	80	203	306	252	176	402	80	120	130	250	70



# Tunkillia Suite

SAMPNO	R370928	R370929	R370930	R370931	R370932	R370933	R370934	R370935	R370936	R444835	R444824	R444832	R444833	R444834	R387449	R337010	R337011	R337017	R368571	R368573
GROUP	Lakeside	Lakeside	Lakeside	Lakeside	Lakeside	Lakeside	Lakeside	Lakeside	Lakeside	Mulgathing	Pinbong	Tallacootra	Tallacootra	Tallacootra	Tunkillia	VPF	VPF	VPF	VPF	VPF
Easting	477656	478426	478416	478402	478400	477187	477039	489996	489674	399000	544166	232344	232451	231647		484124	472307	469620	484124	472307
Northing	6503959	6503346	6503114	6503092	6503092	6504581	6506538	6511884	6512791	6653600	6367104	6567634	6567700	6564845		6535828	6553627	6554690	6535828	6553627
Rare earth elements (ppm)																				
Ce	18	160	100	155	110	80	86	44	64	12	137.8	144.8	70.58	87.53	268	52	37	88	115	34
Dy	2	3.5	8.5	5	8	3.5	3	1.5	1.5	0.25	5.96	6.69	2.59	5.23	7.31	2	2	1.5	4	2
Er	1	2	5	3	4	2	2	1	1	0.5	4.04	3.93	1.48	3.24	3.58	0.5	0.5	0.5	2	0.5
Eu	0.25	0.5	0.25	1	1	0.25	0.25	0.25	0.25	0.25	0.71	0.811	0.768	1.227	2.044	0.25	0.25	1	1.5	0.25
Gd	1	4	8	5	7	4	3	1	1	0.5	6.37	7.59	3.01	6.39	11.06	3	2	3	6	2
Ho	0.25	0.5	2	1	1.5	0.5	0.5	0.25	0.25	0.25	1.29	1.39	0.57	1.1	1.39	0.25	0.25	0.25	0.5	0.25
La	11	77	44	89	55	38	61	30	41	9	65.77	69.74	37.44	39.07	141.1	34	23	53	63	22
Lu	0.25	0.25	1	0.25	0.5	0.25	0.25	0.25	0.25	0.25	0.6	0.5	0.15	0.44	0.37	0.25	0.25	0.25	0.25	0.25
Nd	5	21	27.5	34.5	31.5	23.5	15.5	6.5	7	5	48.71	50.88	25.53	41.9	95.53	19	14.5	28.5	44.5	14.5
Pr	1	12	9	12	10	7	6	3	4	1	14.45	15	7.08	10.72	27.78	5	4	9	13	5
Sm	0.25	6.5	9	6.5	7.5	5	0.25	0.25	0.5	0.25	8.16	8.87	3.67	7.49	14.94	0.25	0.25	2.5	7.5	0.25
Tb	0.25	0.5	1	0.5	1	0.25	0.25	0.25	0.25	0.25	1.11	1.26	0.45	0.99	1.63	0.25	0.25	0.25	0.5	0.25
Tm	0.5	0.5	0.5	0.5	0.5	0.5	0.5	0.5	0.5	0.5						0.5	0.5	0.5	0.5	0.5
Yb	2	2	5	3	3	2	2	1	1	0.5	4.12	3.46	1.02	3.27	2.57	0.5	0.5	0.5	2	0.5
Economic elements (ppm)																				
Cu	8	51	10	13	29	10	39	7	18	2	6	7	8	6	11	5	51	4	15	76
Pb	14	22	91	14	6	10	12	12	14	4	32.6	32	18	16.7	19	6	8	12	4	10
Zn	9	32	25	41	74	9	12	8	17	6	23.2	29.2	33.8	24.7	78.8	25	22	23	42	30
Ni	0.5	4	0.5	3	7	2	9	3	1	1	3.5	3.7	2	3.4	4.7	1	2	3	5	2

# Tunkillia Suite

SAMPNO	R378920	R378921	R378922	R378923	R378924	R444826
GROUP	VPF	VPF	VPF	VPF	VPF	Wynbring
Easting	466420	466740	468036	467050	484352	360107
Northing	6561795	6561175	6561342	6563550	6536030	6619258

## Major elements (wt%)

SiO <sub>2</sub>	72.2	74.6	75.3	77.3	73	73.16
Al <sub>2</sub> O <sub>3</sub>	15	13.5	12.9	12.6	14.2	13.407
CaO	2.14	1.15	1.09	0.66	2.15	1.307
Fe <sub>2</sub> O <sub>3</sub>	1.74	1.29	0.9	0.62	1.72	1.886
K <sub>2</sub> O	4.21	5.26	4.67	5.41	3.95	5.529
MgO	0.37	0.16	0.09	0.05	0.39	0.411
MnO	0.05	0.02	0.01	0.005	0.05	0.034
Na <sub>2</sub> O	3.54	3.37	3.52	2.98	3.36	3.095
P <sub>2</sub> O <sub>5</sub>	0.07	0.17	0.12	0.11	0.13	0.049
TiO <sub>2</sub>	0.16	0.14	0.07	0.05	0.17	0.286
LOI	0.5	0.46	0.42	0.55	0.56	0.603

## Trace elements (ppm)

Be	1	2	1	3	1	2.4
Sc	2.5	2.5	2.5	2.5	2.5	4
V	10	10	10	10	30	17
Cr	20	40	40	30	30	6
As	0.5	1	0.5	0.5	0.5	1.5
Ba	1600	900	220	210	1400	986
Bi	1.5	1.5	1.5	1.5	1.5	0
Cd	1.5	1.5	1.5	1.5	1.5	0.05
Co	4	0.5	0.5	0.5	1	
Cs	1.5	1.5	1.5	1.5	1.5	1.24
Ga	15	22	19	19	17	16.1
Hf	2	4	2	3	3	5.3
In	0.25	0.25	0.25	0.25	0.25	
Mo	3	2	2	3	1	5.8
Nb	0.5	0.5	0.5	15	0.5	12.1
Rb	105	185	155	160	110	156.9
Sb	3	1	1	1	0.5	0.1
Sn	0.5	0.5	0.5	0.5	0.5	1.8
Sr	650	420	165	145	440	157
Ta	3	7	7	6	4	0.9
Te	2.5	2.5	2.5	2.5	2.5	
Tl	1.5	1.5	1.5	1.5	1.5	
Th	4.5	17	23	23.5	13	18
U	1.5	2.5	2	0.25	1	2.45
W	30	1.5	1.5	1.5	1.5	
Y	9	6	7	8	8	19.6
Zr	70	120	80	70	110	197

# **Tunkillia Suite**

<b>SAMPNO</b>	R378920	R378921	R378922	R378923	R378924	R444826
<b>GROUP</b>	VPF	VPF	VPF	VPF	VPF	Wynbring
<b>Easting</b>	466420	466740	468036	467050	484352	360107
<b>Northing</b>	6561795	6561175	6561342	6563550	6536030	6619258
<b>Rare earth elements (ppm)</b>						
<b>Ce</b>	29	43	32	6	42	125.4
<b>Dy</b>	2	1	1	1	1.5	2.97
<b>Er</b>	1	0.5	0.5	0.5	0.5	1.78
<b>Eu</b>	0.25	0.25	0.25	0.25	0.25	1.025
<b>Gd</b>	2	1	1	0.5	2	4.3
<b>Ho</b>	0.25	0.25	0.25	0.25	0.25	0.63
<b>La</b>	18	31	20	4	27	629.5
<b>Lu</b>	0.25	0.25	0.25	0.25	0.25	0.28
<b>Nd</b>	14	16.5	12.5	2.5	18.5	42.1
<b>Pr</b>	4	5	3	0.5	5	12.73
<b>Sm</b>	0.25	0.25	1	0.25	0.25	6.09
<b>Tb</b>	0.25	0.25	0.25	0.25	0.25	0.64
<b>Tm</b>	0.5	0.5	0.5	0.5	0.5	
<b>Yb</b>	0.5	0.5	0.5	1	0.5	1.64
<b>Economic elements (ppm)</b>						
<b>Cu</b>	4	3	3	25	2	8
<b>Pb</b>	4	10	10	14	6	25.8
<b>Zn</b>	24	14	9	4	30	29.8
<b>Ni</b>	3	2	1	1	1	10.9



# St Peter Suite

SAMPNO	PGPJ2	HCBI	CGCBI	R432570	R432580	R432586	R432589	R432591	R434791	R434792	R434793	R432595	R432602	R434794	R434795	R432671	R432673	R432715	R432728	R432734	R389875	1077-136
GROUP	1	1	1	2	2	2	2	2	2	2	2	2	2	2	2	2	2	2	2	2	2	2
Easting	349677	363566	363566	359500	362500	363702	368415	370856	376313	376313	376313	376313	382983	382983	382983	382372	382382	379119	377266	368538	387290	388368
Northing	6E+06	6E+06	6E+06	6472935	6477136	6473003	6475810	6E+06	6477039	6477039	6477039	6E+06	6477039	6477039	6477039	6471500	6470300	6467446	6466145	6469390	6473464	6470039
Major elements (wt%)																						
SiO <sub>2</sub>	76.74	76.63	77.75	67.22	64.19	64.04	65.25	69.75	68.9	56.4	67.8	70.12	64.5	60.9	62.1	76.4	80.85	70.57	63.47	60.33	75.2	75.74
Al <sub>2</sub> O <sub>3</sub>	12.92	12.44	11.94	19.13	20.37	19.76	20.83	16.13	14.3	16.8	15.5	17.32	19.5	18	18.2	14.01	12.61	17.54	22.34	16.77	13.1	12.97
CaO	0.47	0.03	0.03	1.62	0.53	2.81	0.46	0.19	3.2	6.4	3.44	0.54	3.69	5.37	5.17	0.4	0.13	1.51	1.12	4.36	0.29	0.36
Fe <sub>2</sub> O <sub>3</sub>	0.67	1.14	0.87	4.95	5.07	5.47	6.75	1.46	4.49	8.9	4.56	4.28	4.41	5.41	4.38	0.97	0.78	2.77	6.51	9.86	0.88	1.01
K <sub>2</sub> O	4.38	4.64	4.49	1.84	3	1.67	1.8	6.1	3.68	2.14	2.47	2.87	1.42	1.61	1.58	4.24	4.13	3.02	2.34	1.73	4.43	4.54
MgO	0.13	0.13	0.09	0.76	0.49	1.51	0.62	0.15	1.26	3.88	1.26	0.68	1.25	2.08	1.89	0.06	0.06	0.5	1.05	3.71	0.04	0.13
MnO	0.14	0.05	0.01	0.04	0.02	0.06	0.06	0.01	0.09	0.12	0.09	0.03	0.05	0.1	0.09	0.01	0.01	0.05	0.06	0.65	0.1	0.06
Na <sub>2</sub> O	4.2	4.43	4.15	4.45	5.3	4.58	4.3	4.3	3.09	3.63	3.84	4.41	4.83	4.78	4.8	2.74	0.22	3.96	2.67	2.8	4.57	4.18
P <sub>2</sub> O <sub>5</sub>	0.01	0.02	0.01	0.17	0.31	0.08	0.14	0.03	0.1	0.2	0.14	0.09	0.09	0.22	0.2	0.01	0.01	0.15	0.26	0.16	0.03	0.08
TiO <sub>2</sub>	0.05	0.17	0.12	0.54	0.78	0.61	0.54	0.36	0.315	0.775	0.35	0.47	0.43	0.485	0.465	0.19	0.17	0.65	0.75	0.53	0.06	0.1
LOI	0.34	0.22	0.15																			
Trace elements (ppm)																						
Be				1.5	3	1.5	2	1	1.5	2.5	2	1.5	1	1	1.5	1.5	0.5	2	1.5	1	3	
Sc	5.3	4.2	2.1	15	10	15	15	15	5	20	5	15	10	10	10	2.5	2.5	15	25	25	2.5	2.9
V	5	13	5	70	60	80	100	10	50	160	40	50	60	60	60	10	10	50	60	100	10	8
Cr	1	2	2	80	90	120	120	160	30	60	30	60	80	20	10	110	70	70	40	440	10	312
As				0.5	0.25	1	19.5	2.5	2.5	1	0.25	0.25	0.5	0.5	0.5	0.25	0.25	1	0.25	0.25	0.5	1.18
Ba	70	69	58	460	1600	700	400	3600	750	750	600	1100	1300	950	1000	950	650	1300	1450	900	60	437
Bi				0.2	3.1	0.1	0.2	0.05	0.4	0.1	0.05	0.2	0.05	0.05	0.05	0.05	0.1	0.1	0.1	0.05	1.5	
Cd				0.05	0.05	0.1	0.2	0.1	0.05	0.05	0.05	0.05	0.1	0.05	0.05	0.05	0.05	0.05	0.05	0.3	1.5	
Co				6.5	8.5	12.5	64	3750	9.5	33.5	10	8.5	18.5	13	12	16	85	15.5	27	63	0.5	2
Cs				1.7	5.5	2.7	2.2	0.3	3.1	2.7	2.1	2.4	2	1	0.9	1.5	1.2	2	6.5	2.8	1.5	1.52
Ga	22.7	18.3	18.8	20	21.5	21.5	17.5	16	21.5	23	23	16.5	22	26	25.5	14.5	13	21	26.5	19	18	15.5
Hf				3	6	12	5	7	6	5	4	4	3	4	4	3	3	4	4	2	4	3.04
In				0.025	0.025	0.025	0.05	0.025	0.025	0.05	0.025	0.025	0.025	0.025	0.025	0.025	0.025	0.1	0.1	0.05	0.25	
Mo				1.6	2.2	3.2	3.9	32.5	0.5	0.3	0.3	2.1	0.9	0.4	0.4	1.4	1.5	2.2	2.3	0.5	4	7.7
Nb	37.9	14.3	6.3	10	15	5	5	20	25	15	15	5	5	5	10	10	10	5	10	5	15	11.5
Rb	416.7	166.8	127.8	98	120	74	45.5	115	100	67	80	130	38	39	35.5	155	155	88	115	63	165	163.6
Sb				0.25	1	0.25	0.25	0.25	1	0.5	0.25	0.25	0.25	0.25	0.25	0.25	0.25	0.25	0.25	0.25	0.5	0.2
Sn				5	5	5	5	5	5	5	5	5	5	5	5	5	5	5	5	5	5	
Sr	11.2	3.8	3.2	600	1000	650	470	115	340	500	390	320	1150	900	900	100	35	550	370	370	10	38.7
Ta				1	1	1	1	44	3	3	2	1	1	2	1	4	3	1	1	1	1	1.47
Te				0.1	1.7	0.1	0.1	0.1	0.1	0.1	0.1	0.1	0.1	0.1	0.1	0.1	0.1	0.1	0.1	0.1	2.5	5
Tl				0.4	0.5	0.3	1.2	0.5	1.4	0.5	0.4	0.5	0.2	0.1	0.05	0.6	0.7	0.5	0.5	0.3	1.5	
Th	29.5	13.1	9.2	8.5	6	5	5.5	6	18	10.5	12	4.5	2.6	3.4	2.6	17.5	11.5	5.5	7	3.5	22.5	10.3
U	4.3	1.7	0.5	2.1	3.7	1.05	4.1	0.95	3.3	2.6	4.1	4.2	2.3	1.35	0.58	1.1	0.78	3.1	3.7	0.97	2	0.9
W				12	115	24	74	10700	1.5	1.5	18	260	165	1.5	1.5	500	460	52	91	16	1.5	2.53
Y	119	41.3	24.3	3.9	3.8	7	26	27	18.5	25	15.5	21.5	12	15.5	16	9	6	37	24	16.5	33	9.7
Zr	105.3	235	161	100	240	550	200	330	150	100	110	180	140	140	150	110	110	160	170	100	80	96.7

# St Peter Suite

SAMPNO	PGPJ2	HCB1	CGCB1	R432570	R432580	R432586	R432589	R432591	R434791	R434792	R434793	R432595	R432602	R434794	R434795	R432671	R432673	R432715	R432728	R432734	R389875	1077-136
GROUP	1	1	1	2	2	2	2	2	2	2	2	2	2	2	2	2	2	2	2	2	2	2
Easting	349677	363566	363566	359500	362500	363702	368415	370856	376313	376313	376313	376313	382983	382983	382983	382372	382382	379119	377266	368538	387290	388368
Northing	6E+06	6E+06	6E+06	6472935	6477136	6473003	6475810	6E+06	6477039	6477039	6477039	6E+06	6477039	6477039	6477039	6471500	6470300	6467446	6466145	6469390	6473464	6470039
Rare earth elements (ppm)																						
Ce	30	88	27	40.5	72	30	54	100	37.5	39.5	37.5	135	33.5	30.5	29	56	30.5	49	64	42.5	42	38.2
Dy				0.67	1.3	1.45	4.3	3.4	2.2	2.8	1.9	4.9	1.95	2.1	2.2	1.55	0.92	4.9	4.5	2.2	5.5	
Er				0.4	0.5	0.7	2.2	1.95	1.4	1.65	1.15	2.1	1	1.15	1.2	0.75	0.55	3.1	2.1	1.3	3	
Eu				0.45	1.25	1.15	1.7	3.1	0.88	1.45	0.82	2.7	1.3	1.05	1.2	0.94	0.51	2	2.1	1.35	0.25	0.5
Gd				0.8	2.1	1.75	4.8	4.5	2.7	3.8	2.6	7.5	2.4	2.7	2.9	1.7	1	4.7	5.5	2.4	4	
Ho				0.12	0.19	0.25	0.83	0.67	0.48	0.59	0.4	0.81	0.37	0.42	0.45	0.27	0.19	0.98	0.8	0.44	1	
La	11	37	13	23.5	37	14	28.5	66	24.5	26	25.5	74	18	18.5	17	40	19	25	35.5	22.5	14	11
Lu				0.09	0.08	0.12	0.37	0.32	0.23	0.24	0.19	0.3	0.17	0.16	0.18	0.15	0.12	0.53	0.33	0.25	0.25	
Nd	19	38	12	12	29	16.5	34.5	47	25.5	32	26.5	67	18.5	25.5	25.5	18	9	30	34	20.5	14.5	10
Pr				4.3	9	4.2	8	13	5.5	6	5.5	17.5	4.5	4.6	4.5	6	3	7	9	5.5	3	
Sm				1.9	4.9	3.9	7	9.5	3.7	4.6	3.5	12.5	4.1	3.8	4.1	3.5	2.1	7.5	8	4.3	4	2.35
Tb				0.12	0.26	0.24	0.7	0.57	0.35	0.46	0.32	0.92	0.32	0.34	0.37	0.24	0.13	0.69	0.67	0.35	0.5	0.5
Tm				0.1	0.05	0.1	0.4	0.3	0.2	0.25	0.2	0.35	0.15	0.15	0.2	0.15	0.1	0.5	0.35	0.2	0.5	
Yb				0.55	0.5	0.75	2.4	1.8	1.55	1.55	1.2	2	1.05	1.15	1.2	1	0.85	3.4	2.1	1.5	4	1.49
Economic elements (ppm)																						
Cu	7	4	3	6.5	26	36	53	14.5	13.5	77	33	20.5	55	61	45.5	4.5	5.5	35	14.5	36.5	2	11
Pb	51.1	18.4	10.8	13	8	15.5	12.5	16.5	22	14.5	19	11.5	12	12	12.5	25	14	17.5	14.5	12	10	21.9
Zn	37	34	13	42	37.5	72	42.5	53	85	115	79	77	84	105	100	13.5	16	100	130	140	29	23
Ni	-2		-2	11	9	28	46	12	8	40	7	12	31	13	11	15	10	18	8	98	0.5	10

# St Peter Suite

SAMPNO	1077-137	1077-138	1077-139	GPJ1	MZPJ1	CMPJ7	GGPJ10	GDCB7	GDRP8	MDPJ8	1096-4	1096-9	1096-14	1096-15	1096-17	R432607	R432617	R432620	R389873	R389874	1077-140	1077-141
GROUP	2	2	2	2	2	2	2	2	2	2	3	3	3	3	3	4	4	4	4	4	4	4
Easting	388133	387347	387347	651690	651690	351499	351366	361695	336691	351325	413703	413670	412848	412848	392329	389796	399776	403416	393477	393933	393450	393920
Northing	6471076	6473355	6473355	6E+06	6E+06	6E+06	6E+06	6E+06	6E+06	6E+06	6E+06	6E+06	6E+06	6E+06	6E+06	6475500	6469137	6466965	6474827	6474626	6474858	6474625
Major elements (wt%)																						
SiO <sub>2</sub>	74.43	76.04	76.86	63.76	66.65	64.63	66.4	60.41	57.4	57.49	70.15	69.71	68.36	64.79	65.31	74.93	69.59	78.79	72.9	73.7	72.68	74.93
Al <sub>2</sub> O <sub>3</sub>	13.29	12.47	12.65	18.23	17.23	17.88	16.93	18.23	15.77	17.77	14.34	14.78	16.75	16.14	17.32	15.56	18.01	14.18	12	13.4	12.45	13.57
CaO	0.56	0.27	0.23	2.84	1.41	2.92	2.56	4.4	6.46	6.28	2.35	2.62	2.43	3.57	3.2	0.87	0.44	0.09	0.75	0.99	0.63	0.95
Fe <sub>2</sub> O <sub>3</sub>	1.25	0.74	0.79	3.6	2.7	3.39	3.03	5.27	9.8	7.43	2.94	3.31	2.03	4.15	3.39	1.02	4.63	0.82	3.95	1.63	4.12	1.22
K <sub>2</sub> O	4.46	4.37	3.94	1.6	2.43	1.69	1.78	2.01	0.77	1.61	4.82	2.86	3.65	3.38	2.92	4.38	3.9	5.09	5.69	4.57	6.48	4.42
MgO	0.26	0.09	0.09	1.18	0.82	1.14	1.02	2.04	3.19	2.95	1.19	1.27	0.64	1.52	1.17	0.11	0.9	0.02	0.1	0.16	0.25	0.3
MnO	0.11	0.04	0.06	0.14	0.11	0.17	0.12	0.16	0.23	0.15	0.08	0.1	0.07	0.13	0.11	0.01	0.28	0.01	0.11	0.08	0.12	0.08
Na <sub>2</sub> O	4.55	4.33	4.55	6.6	6.69	6.59	6.25	5.62	4.71	3.92	3.1	4.11	4.87	4.55	4.93	2.98	2.37	0.86	2.78	3.72	2.39	3.83
P <sub>2</sub> O <sub>5</sub>	0.03	0.02	0.02	0.19	0.13	0.19	0.17	0.34	0.46	0.44	0.11	0.12	0.08	0.22	0.17	0.03	0.03	0.02	0.08	0.06	0.13	0.04
TiO <sub>2</sub>	0.14	0.05	0.07	0.46	0.35	0.42	0.38	0.65	0.99	0.84	0.37	0.4	0.25	0.56	0.41	0.38	0.46	0.09	0.4	0.16	0.42	0.12
LOI				0.78	0.86	0.43	0.38	0.46	0.46	0.92	0.37	0.39	0.47	0.32	0.45				1	1		
Trace elements (ppm)																						
Be																1.5	3	0.5	1	3		
Sc	3.9	2.1	3.2	5.9	3.9	9.1	5.6	12.1	31.9	17.5	8.1	9.6	10.4	10.7	9.5	10	10	2.5	2.5	2.5	5.7	4
V	9	6	6	29	17	26	23	71	132	166	60	58	23	70	68	20	50	10	10	10	10	13
Cr	274	234	268	0.5	0.5			11	0.5	0.5	9	13	4	1	2	110	80	130	10	10	204	272
As	1	1	1													0.5	0.25	2	3	0.5	1	1.12
Ba	618	100	100	1348	2001	1606	2124	1600	315	1159	837	674	2456	1233	1700	2100	1050	360	270	500	347	674
Bi																0.1	0.1	0.3	1.5	1.5		
Cd																0.05	0.1	0.05	1.5	1.5		
Co	2	2	3													7.5	47.5	2.5	1	1	4	4
Cs	2.62	3.18	1.79													0.9	6	2.7	1.5	1.5	1	2.75
Ga	16.2	16.1	19.8	22	21.8	21.8	20.6	21.6	22	22	15.8	17.6	16.9	19	19.5	17	22	17	19	15	20.5	16.7
Hf	4.2	3.8	4.79													5	4	3	17	0.5	14.5	2.92
In																0.025	0.025	0.025	0.5	0.25		
Mo	5	5	5													4.3	2.8	6.5	4	4	5	5
Nb	19.2	11.7	27.9	8	17.5	10	4.5	9.3	11.6	3	14.3	11.7	8.1	12.1	12.4	5	15	5	10	5	21	11.6
Rb	168.2	172.9	149.9	86.5	111.5	92.3	69	96.6	17.5	48.7	210.3	132.8	124	162.9	130.3	110	260	195	145	170	176.5	200.4
Sb	0.2	0.2	0.2													0.25	0.25	0.25	1	0.5	0.2	0.4
Sn																5	5	5	15	5		
Sr	45.2	14.2	2.6	704	805.7	713.3	621.8	672.7	468.9	994.1	301.6	403.7	639.8	430.8	627.8	230	110	80	40	135	35.5	154.2
Ta	2.95	1	3.88													1	2	1	1	1	2.32	1.95
Te	5	5	5													0.1	0.1	0.1	2.5	2.5	5	5
Tl																0.6	1.2	0.9	1.5	1.5		
Th	14.6	17.6	33.5	16.2	40.4	17.6	15.1	5.4	2	3.9	33.5	32.4	6.8	14.7	14	7	21	22.5	15	8	14.6	8.65
U	3.4	4.4	4	2.7	3.6	2.1	1.3	0.3	-0.3	0.3	2.1	1.2	1.6	2.8	4.9	1.75	7.5	2.8	3.5	4	0.9	4.2
W	2	2	2													105	92	53	4	1.5	2	2
Y	33.6	40.1	46.1	34.4	20.5	23.1	13.5	30.4	53.7	19.5	27.3	18.9	14.2	29.4	32.8	19	130	34	54	21	54.7	25
Zr	136.3	82.6	95.3	391.9	321.3	329.7	303.4	268.7	175.1	121.2	175.3	161	128.9	217.6	191.6	210	160	110	650	170	564.4	89.4



**St Peter Suite**

SAMPNO	1077-137	1077-138	1077-139	GPJ1	MZPJ1	CMPJ7	GGPJ10	GDCB7	GDRP8	MDPJ8	1096-4	1096-9	1096-14	1096-15	1096-17	R432607	R432617	R432620	R389873	R389874	1077-140	1077-141
GROUP	2	2	2	2	2	2	2	2	2	2	3	3	3	3	3	4	4	4	4	4	4	4
Easting	388133	387347	387347	651690	651690	351499	351366	361695	336691	351325	413703	413670	412848	412848	392329	389796	399776	403416	393477	393933	393450	393920
Northing	6471076	6473355	6473355	6E+06	6E+06	6E+06	6E+06	6E+06	6E+06	6E+06	6E+06	6E+06	6E+06	6E+06	6E+06	6475500	6469137	6466965	6474827	6474626	6474858	6474625
Rare earth elements (ppm)																						
Ce	61.1	36.1	56.2	163	149	150	137	71	75	53	155	125	62	84	115	64	57	51	170	37	216	25
Dy																3.5	14.5	5	10.5	3		
Er																1.65	9.5	2.9	5	2		
Eu	0.5	0.5	0.5													1.85	3.1	1.3	1	0.25	1.24	0.5
Gd																4	12.5	5	13	3		
Ho																0.62	3.2	1	2.5	0.5		
La	24	14	5	92	74	86	72	31	22	23	82	66	32	47	61	37.5	69	41.5	95	21	91	9
Lu																0.26	1.9	0.56	0.5	0.25		
Nd	19	17	9	54	38	45	44	26	42	25	52	39	15	28	42	30	64	37	72	16	67	9
Pr																8	17	10	19	4		
Sm	4.9	4.67	3.69													7	14.5	7.5	12.5	1.5	12.3	2.46
Tb	0.9	1.04	0.74													0.58	2	0.72	1.5	0.25	1.63	0.53
Tm																0.25	1.75	0.5	0.5	0.5		
Yb	3.73	3.61	5.37													1.7	11.5	3.5	5	2	5.87	2.92
Economic elements (ppm)																						
Cu	5	5	10	10	11	9	14	19	18	12	17	15	8	14	26	6.5	14	8	5	4	16	20
Pb	24.9	23.4	25.5	18.3	33.8	17.3	16.5	15.2	13.7	5.7	32	22.2	25.9	22.8	22.2	21	32.5	53	12	20	29	35.8
Zn	41	20	32	122	109	113	86	101	130	107	42	61	49	64	60	29.5	105	20	67	33	112	30
Ni	8	8	9	2	3	3	4	9	4	5	7	10	4	3	1	14	9	28	1	2	8	9

# St Peter Suite

SAMPNO	1077-142A	1077-142B	1096-23	1096-2	1096-22	1096-7	1096-11	1096-13	1096-1	1096-10	1096-8	1096-16	1096-18	1096-19	R432624	R434797	R434798	R434799	R432666	R434800	R434657	R434658
GROUP	4	4	4	4	4	4	4	4	4	4	4	4	4	4	5	5	5	5	mafic	mafic	mafic	mafic
Easting	393920	393920	422035	413703	394676	374500	412169	380817	374500	392232	393501	413994	380703	412848	409959	416831	416831	416831	386657	386657	386657	386657
Northing	6474625	6474625	6E+06	6E+06	6E+06	6E+06	6E+06	6E+06	6E+06	6E+06	6E+06	6E+06	6E+06	6E+06	6463072	6455696	6455696	6455696	6E+06	6475133	6475133	6475133
Major elements (wt%)																						
SiO <sub>2</sub>	74.61	67.36	69.39	70.06	70.82	74.35	75.28	75.65	76.02	77.47	75.18	75.75	76.17	75.7	73.21	65.7	66.2	64.8	46.7	42.8	41.4	40.8
Al <sub>2</sub> O <sub>3</sub>	13.64	16.14	14.76	15.53	14.09	13.54	12.93	12.66	12.93	11.77	13.62	13.68	13.11	13	16.7	15.2	15.8	16.1	21.31	19.5	19.9	19.9
CaO	1	1.84	2.62	2	1.24	0.99	0.2	0.83	0.98	0.27	0.42	0.98	0.72	0.66	0.21	2.72	3.38	3.5	9.34	11.2	14	14.4
Fe <sub>2</sub> O <sub>3</sub>	1.1	2.81	3.27	2.25	2.67	1.29	1.28	1.11	1.23	1.33	0.47	0.68	0.62	0.56	2.58	5.39	4.62	4.85	14.96	14.2	13.7	15.5
K <sub>2</sub> O	4.73	4.24	3.99	4.43	6.06	5.06	6.23	4.69	4.63	6.29	4.56	4.55	4.79	5.94	4.86	4.27	4.08	4.29	0.98	1.27	0.87	0.62
MgO	0.23	0.74	1.16	0.54	0.6	0.4	0.2	0.31	0.35	0.21	0.11	0.17	0.18	0.15	0.3	1.26	1.21	1.29	1.85	5.16	4.87	4.83
MnO	0.05	0.09	0.1	0.05	0.07	0.06	0.03	0.07	0.06	0.02	0.16	0.02	0.05	0.02	0.02	0.13	0.1	0.1	0.1	0.17	0.17	0.15
Na <sub>2</sub> O	3.51	4.57	3.97	4.12	3.24	3.72	3.16	3.62	3.62	2.32	4.44	3.74	3.77	2.99	2.17	3.7	3.88	3.95	2.73	1.81	1.3	1.08
P <sub>2</sub> O <sub>5</sub>	0.36	0.47	0.11	0.08	0.1	0.04	0.02	0.03	0.04	0.02	0.01	0.01	0.02	0.01	0.02	0.21	0.2	0.2	0.12	0.04	0.03	0.03
TiO <sub>2</sub>	0.1	0.43	0.41	0.27	0.42	0.2	0.17	0.16	0.18	0.19	0.03	0.09	0.07	0.07	0.25	0.66	0.615	0.675	1.06	1.32	1.28	1.28
LOI			0.27	0.29	0.38	0.29	0.3	0.27	0.41	0.39	0.42	0.27	0.32	0.23								
Trace elements (ppm)																						
Be															1.5	2	2	2	8.5	2	1.5	1.5
Sc	2.6	4.4	10	3.5	7.7	2.7	4.7	2.9	2.3	1.3	4.6	1.5	3.7	2	2.5	10	10	10	35	40	40	40
V	11	32	63	23	25	12	4	9	12	15	6	8	5	6	10	50	40	60	250	380	380	380
Cr	263	208	8	9	1	1	0.5			1	2			9	110	10	30	30	40	20	10	10
As	1	1													2	0.25	2.5	1	1.5	1	1	2
Ba	558	1390	908	1995	748	458	325	266	425	718	58	1258	485	403	1750	1200	1150	1300	310	430	300	220
Bi															1.5	0.05	0.2	0.1	0.4	0.4	0.1	0.3
Cd															0.05	0.1	0.05	0.05	0.2	0.05	0.4	0.3
Co	3	6													16.5	8	7.5	8.5	67	46.5	30	43
Cs	3.68	3.58													4.7	2.6	2.9	3.2	11.5	4.6	2.5	3.1
Ga	14.4	18	16.4	16.1	17.5	15.5	16.1	16.1	13.2	14.4	19.9	13	15.2	14.8	20	24.5	24	24.5	21	24.5	19	27
Hf	2.06	7.84													3	5	4	5	1	3	2	2
In															0.025	0.05	0.05	0.05	0.05	0.05	0.025	0.05
Mo	5	9.9													3.1	1.2	1	0.9	12	83	9	3.7
Nb	7.3	15.7	13.2	8.5	13.8	14.1	10.8	16.4	13.9	10	15.2	3.7	13.1	7	10	20	20	25	5	5	5	5
Rb	169.9	134.5	169	132.7	182.1	246.4	220	275.1	225.5	175.4	254.4	124.4	283.7	230.7	200	150	125	140	160	77	56	35.5
Sb	0.2	0.2													0.25	0.25	0.25	0.25	0.25	0.25	0.5	0.25
Sn															5	5	5	5	5	5	5	5
Sr	178.2	222.9	306.4	532	107	103.7	59.7	74.8	99.9	149.3	23.8	317.6	77.5	140.6	290	230	250	260	550	360	490	500
Ta	1	2.09													1	2	2	1	1	1	1	1
Te	5	5													0.1	0.1	0.1	0.1	0.1	0.1	0.1	0.1
Tl															1	0.7	0.8	0.7	0.4	0.5	0.2	0.2
Th	6.57	6.87	22.7	12.1	22.6	28.8	24.2	34.1	31	25.5	10.7	7.3	17.3	15.4	20.5	12.5	14.5	12.5	4.2	2.1	1.15	1.4
U	2.3	2.5	2.8	0.3	3.3	3.1	2.2	5.4	4.7	1.7	3.5	0.9	9.1	1.7	4.9	2.6	3.5	3.2	3.9	0.39	0.25	0.35
W	2.21	2													83	4	16	1.5	38	48	14	12
Y	13.8	26	21.9	26.6	51.6	26.5	72.1	23.6	24.2	7.6	35.1	4.2	18.4	11.7	19.5	36.5	37	36.5	27.5	15.5	10	14.5
Zr	85.8	285.8	175.4	174.8	280.6	113.1	239.2	105.1	104.3	209.7	65.7	103.8	67.8	57.7	130	270	290	370	60	100	60	60

# St Peter Suite

SAMPNO	1077-142A	1077-142B	1096-23	1096-2	1096-22	1096-7	1096-11	1096-13	1096-1	1096-10	1096-8	1096-16	1096-18	1096-19	R432624	R434797	R434798	R434799	R432666	R434800	R434657	R434658
GROUP	4	4	4	4	4	4	4	4	4	4	4	4	4	4	5	5	5	5	mafic	mafic	mafic	mafic
Easting	393920	393920	422035	413703	394676	374500	412169	380817	374500	392232	393501	413994	380703	412848	409959	416831	416831	416831	386657	386657	386657	386657
Northing	6474625	6474625	6E+06	6E+06	6E+06	6E+06	6E+06	6E+06	6E+06	6E+06	6E+06	6E+06	6E+06	6E+06	6463072	6455696	6455696	6455696	6E+06	6475133	6475133	6475133
Rare earth elements (ppm)																						
Ce	16.1	67.2	110	106	183	88	199	70	76	12	6	18	27	24	95	57	59	55	20.5	13.5	8.5	12
Dy															3	5	5	5.5	3.4	1.9	1.2	1.8
Er															1.65	3.1	3	3.2	2	1.1	0.7	1
Eu	0.51	0.55													1.8	1.6	1.6	1.65	1.05	0.8	0.5	0.73
Gd															3.7	6	6	6	3	2.1	1.35	1.95
Ho															0.55	1.1	1.1	1.15	0.69	0.42	0.26	0.38
La	3	14	52	54	91	49	105	39	40	5		7	14	12	44.5	37.5	38.5	36	13	7	4	6
Lu															0.35	0.49	0.5	0.51	0.32	0.16	0.1	0.15
Nd	4	17	41	36	65	24	72	18	23	1	0.5	5	9	11	39.5	47.5	48.5	47	13	11.5	7	10.5
Pr															11	9	9.5	9	3.2	1.9	1.15	1.7
Sm	1.53	4.96													7.5	7	7	7.5	3.3	2.2	1.35	2
Tb	0.5	0.76													0.52	0.79	0.78	0.83	0.46	0.28	0.19	0.27
Tm															0.3	0.5	0.45	0.5	0.35	0.15	0.1	0.15
Yb	1.58	3.36													2.1	3.2	3.2	3.3	2.1	1.1	0.65	1
Economic elements (ppm)																						
Cu	13	14	14	10	13	4	10	9	4	19	7	14	10	10	46	61	26	24.5	125	87	48.5	66
Pb	35.4	21.5	31.7	26	29.6	38	34.3	27.2	27.2	26.5	28.6	25.1	37.3	28.7	26.5	19.5	19.5	20.5	12.5	8	13.5	8
Zn	25	60	78	40	55	34	38	22	21	13	3	11	21	8	64	88	83	80	200	93	75	100
Ni	9	9	5	2	1		1	-2	0.5	-2	0.5	0.5		0.5	9	4	3	4	44	11	6	9



# St Peter Suite

SAMPNO	R434659	R432678	R434661	R434662	R432683	R434663	R432688	R432693	R434666	R434667	R434668	R432698	R434669	R432710	R432721	R368554	R378937	R378938	R378939	R378934
GROUP	mafic	mafic	mafic	mafic	mafic	mafic	mafic	mafic	mafic	mafic	mafic	mafic	mafic	mafic	mafic	Pureba	Pureba	Pureba	Pureba	Pureba
Easting	386657	381410	381410	381410	311810	311810	372450	37300	37300	37300	37300	372530	372530	374613	379097	476797	476800	475120	475120	460088
Northing	6475133	6E+06	6462822	6462822	6462404	6462404	6464140	6466700	6466700	6466700	6466700	6465948	6465948	6465368	6467900	6461087	6461044	6462710	6462710	6462929
Major elements (wt%)																				
SiO <sub>2</sub>	44.4	56.25	51	47.6	45.26	42.9	51.72	52.53	46.7	46.2	45.8	53.17	45.9	50.39	48.52	70.4	70.8	71.5	72.1	72.1
Al <sub>2</sub> O <sub>3</sub>	18.4	18.43	16.6	16.6	18.21	16.7	33.97	42.65	31.7	31	24.7	22.32	24.8	19.38	20.89	14.9	15	14.4	13	14.4
CaO	14.1	4.81	7.18	8.62	8.41	9.15	0.02	0.61	16.9	16.9	13.3	4.99	13.7	7.87	6.32	1.95	1.89	2.45	1.37	1.79
Fe <sub>2</sub> O <sub>3</sub>	13.9	10.33	11.3	12	10.19	10.2	8.84	1.77	1.51	1.99	6.04	9.8	5.72	12.7	13.82	1.91	1.87	1.93	2.66	1.65
K <sub>2</sub> O	0.56	1.91	2.19	2.14	0.78	0.5	0.91	0.25	0.34	0.21	1.1	1.27	1.09	0.33	1.37	4.04	4.04	4.32	5.52	4.39
MgO	4.36	3.38	4.64	5.28	14.63	16.5	0.09	0.23	0.69	1.44	5.28	5.13	4.62	8.04	4.15	0.53	0.5	0.31	0.3	0.4
MnO	0.16	0.12	0.17	0.16	0.18	0.14	0.01	0.01	0.02	0.03	0.09	0.22	0.09	0.13	0.37	0.07	0.08	0.05	0.05	0.05
Na <sub>2</sub> O	0.79	2.79	2.85	2.83	1.42	1.04	0.55	0.7	1.57	1.4	1.43	2.1	1.5	0.92	2.8	3.96	3.92	3.6	3.06	3.9
P <sub>2</sub> O <sub>5</sub>	0.04	0.94	1.23	1.37	0.05	0.08	0.12	0.01	0.01	0.005	0.04	0.04	0.03	0.03	0.17	0.08	0.16	0.12	0.16	0.17
TiO <sub>2</sub>	1.27	1.36	1.59	1.77	0.29	0.2	2.03	0.08	0.075	0.095	0.255	0.51	0.255	0.66	1.2	0.21	0.2	0.17	0.37	0.21
LOI																1.11	0.99	0.59	0.89	1
Trace elements (ppm)																				
Be	1.5	1.5	1.5	1.5	2	0.25	1	0.25	0.25	0.25	0.5	2	0.25	0.25	5	2	1	1	3	6
Sc	35	65	40	40	15	10	30	40	2.5	10	15	30	15	75	40	2.5	2.5	2.5	5	2.5
V	400	170	220	260	70	50	310	10	30	40	90	130	120	260	300	20	10	10	10	10
Cr	10	60	10	10	600	600	90	50	50	90	70	150	90	90	30	20	30	20	20	30
As	2.5	0.25	0.5	0.5	1	2.5	0.25	0.25	0.25	0.25	0.25	0.25	5	1	0.25	0.5	0.5	0.5	1	0.5
Ba	175	700	800	750	250	190	260	90	105	175	350	330	350	110	440	800	900	1350	850	1050
Bi	0.4	0.05	0.05	0.05	0.3	0.1	0.2	0.2	0.05	0.05	0.05	0.3	0.2	0.1	0.05	1.5	1.5	1.5	1.5	1.5
Cd	0.2	0.1	0.05	0.05	0.1	0.05	0.05	0.05	0.05	0.05	0.05	0.1	0.05	0.1	0.3	1.5	1.5	1.5	1.5	1.5
Co	36	24	26.5	25.5	98	70	42.5	12.5	4.2	6.5	30.5	200	30	52	95	3	2	0.5	1	1
Cs	2.8	3.6	3.4	2.8	2	2	0.5	1.9	0.3	0.8	10.5	6.5	9.5	4.5	7	6	1.5	1.5	4	4
Ga	29	20.5	26.5	26.5	12.5	15	35	19	22.5	21.5	21	17.5	21.5	18	27	20	17	17	18	19
Hf	2	3	2	2	1	1	4	1	0.5	0.5	0.5	1	0.5	1	3	2	3	3	8	4
In	0.1	0.05	0.1	0.1	0.025	0.025	0.05	0.025	0.025	0.025	0.025	0.025	0.025	0.05	0.1	0.25	0.25	0.25	0.25	0.25
Mo	5.5	1.4	0.7	0.5	0.7	0.3	3.2	1.7	0.5	0.5	0.1	0.8	0.5	1.5	0.9	2	2	2	2	3
Nb	5	5	10	10	5	5	5	5	5	5	5	5	5	5	5	0.5	0.5	0.5	10	0.5
Rb	30	165	98	68	41.5	16.5	17.5	9	7	3	44	61	42	28	73	145	145	120	230	175
Sb	1	0.25	0.25	0.25	0.25	0.25	0.25	1	1.5	1	1	0.25	1	0.25	0.25	3	2	2	2	2
Sn	5	5	5	5	5	5	5	5	5	5	5	5	5	5	5	10	0.5	0.5	0.5	0.5
Sr	450	600	480	500	450	480	105	50	800	800	600	300	600	185	750	410	450	550	125	390
Ta	1	1	1	1	1	1	1	1	1	1	1	1	1	1	1	1	4	3	4	4
Te	0.1	0.1	0.1	0.1	0.1	0.1	0.1	0.1	0.1	0.1	0.1	0.1	0.1	0.1	0.1	2.5	2.5	2.5	2.5	2.5
Tl	0.1	0.7	0.6	0.4	0.2	0.1	0.1	0.05	0.05	0.05	0.2	0.3	0.1	0.05	0.4	1.5	1.5	1.5	1.5	1.5
Th	1.4	10.5	12.5	6.5	2.4	1.65	10	0.76	1.25	0.49	0.6	1.75	2.1	2.8	1.65	7.5	13.5	3	29	18
U	0.58	3.8	2.6	1.65	0.68	0.29	3.1	1.8	0.14	0.07	0.14	1.7	0.21	0.82	0.27	2	2	1	5	3
W	18	65	1.5	1.5	24	1.5	32	40	1.5	4	1.5	28	1.5	40	48	350	1.5	1.5	1.5	1.5
Y	14.5	29.5	45	43.5	28	11.5	14.5	0.95	1.5	2.2	7	83	8.5	12	24	13	14	8	38	18
Zr	50	90	100	100	50	50	230	60	20	20	20	50	20	60	120	100	120	130	300	130

# St Peter Suite

SAMPNO	R434659	R432678	R434661	R434662	R432683	R434663	R432688	R432693	R434666	R434667	R434668	R432698	R434669	R432710	R432721	R368554	R378937	R378938	R378939	R378934
GROUP	mafic	mafic	mafic	mafic	mafic	mafic	mafic	mafic	mafic	mafic	mafic	mafic	mafic	mafic	mafic	Pureba	Pureba	Pureba	Pureba	Pureba
Easting	386657	381410	381410	381410	311810	311810	372450	37300	37300	37300	37300	372530	372530	374613	379097	476797	476800	475120	475120	460088
Northing	6475133	6E+06	6462822	6462822	6462404	6462404	6464140	6466700	6466700	6466700	6466700	6465948	6465948	6465368	6467900	6461087	6461044	6462710	6462710	6462929
Rare earth elements (ppm)																				
Ce	11.5	81	61	54	12.5	12.5	125	3	2.5	2.5	6.5	40	6.5	64	34	39	36	46	135	57
Dy	1.75	5.5	6.5	6.5	3.2	1.1	2.1	0.16	0.19	0.26	0.8	9	0.88	3.5	3.8	3	2	1.5	7	2.5
Er	1	2.7	3.6	3.4	1.95	0.7	1.1	0.05	0.1	0.15	0.45	6	0.5	1.3	2	2	1	0.5	4	1
Eu	0.67	2.5	2.7	2.7	0.91	0.49	0.91	0.11	0.22	0.27	0.57	2.7	0.61	2.2	1.8	0.5	0.25	0.25	1.5	0.25
Gd	1.9	6	8.5	9	2.6	1.25	2.2	0.15	0.25	0.35	1.05	7.5	1.2	5	4.4	3	2	2	8	3
Ho	0.37	0.97	1.35	1.3	0.71	0.25	0.41	0.01	0.04	0.05	0.17	1.95	0.19	0.55	0.74	0.25	0.25	0.25	1.5	0.5
La	5.5	44	37.5	32	11	7	43.5	1.8	1.5	1.5	5.5	25	6.5	23.5	16	22	22	28	83	36
Lu	0.15	0.44	0.48	0.44	0.32	0.1	0.17	0.01	<0.02	<0.02	0.07	1	0.08	0.16	0.35	0.25	0.25	0.25	0.5	0.25
Nd	10.5	43.5	60	58	11	9	17	1.3	1.75	2.1	7.5	29	8	36.5	25.5	16.5	16	17.5	62	24.5
Pr	1.65	11	10	9.5	2.5	1.6	5.5	0.35	0.3	0.35	1.3	6.5	1.4	9	5.5	5	4	5	15	6
Sm	1.95	10	10	10	2.7	1.35	3.2	0.33	0.29	0.39	1.2	7.5	1.35	8.5	6	0.25	0.25	0.25	9	0.25
Tb	0.26	0.84	1.05	1.05	0.41	0.16	0.31	0.01	0.03	0.05	0.13	1.2	0.14	0.65	0.6	0.25	0.25	0.25	1.5	0.5
Tm	0.15	0.45	0.5	0.5	0.35	0.1	0.15	0.025	0.025	0.025	0.05	1	0.1	0.2	0.35	0.5	0.5	0.5	0.5	0.5
Yb	1	2.9	3.3	3	2	0.7	1.1	0.1	0.1	0.15	0.4	6	0.5	1.15	2.2	2	1	0.5	4	2
Economic elements (ppm)																				
Cu	67	24	35	32	10.5	32	41	78	23	12	68	240	66	140	145	190	2	2	4	6
Pb	10	8.5	7.5	5.5	1	3	21.5	4.5	3.5	2	2.5	5.5	3.5	5	5	20	10	8	22	10
Zn	88	99	80	88	71	86	99	10.5	12	17.5	63	160	62	90	220	35	23	30	43	36
Ni	11	20	4	2	340	290	18	52	8	17	48	115	52	49	27	3	5	2	0.5	3

# Hiltaba Suite

SAMPNO	R215524	R215522	R215525	R350422	R215521	R350423	RS203991	RS203990	R363439	RS203985	RS203981	R368559	RS203986	R363440	RS203975	R378936	RS203974	RS215369
GROUP	Childara	Childara	Childara	Childara	Childara	Childara	Kondoolka	Kondoolka	Kondoolka	Kondoolka	Kondoolka	Kondoolka	Kondoolka	Kondoolka	Kondoolka	Kondoolka	Kondoolka	Kondoolka
Easting	459168	458600	464686	467660	456961	467857	488333	487480	463680	490340	484565	488313	493520	463993	463700	470812	464720	469620
Northing	6498257	6503308	6504370	6500578	6502562	6500121	6457250	6458840	6474457	6463460	6466590	6463354	6466630	6474445	6474333	6470853	6478715	6554690
Major elements (wt%)																		
SiO <sub>2</sub>	72.7	74.2	76	76	76.2	77.9	67.6	67.8	67.8	68.1	70.2	70.6	70.7	70.7	70.8	71.3	72.1	72.1
Al <sub>2</sub> O <sub>3</sub>	12.9	12.6	11.9	12	11.4	11.8	13.7	13.7	14.8	13.7	14.8	13.3	13.3	12.3	13	14.3	13.9	15.4
CaO	1.13	1	0.31	0.52	0.62	0.34	2.36	2.3	1.27	1.62	1.68	1.72	1.08	3.44	1.2	1.84	0.5	2.23
Fe <sub>2</sub> O <sub>3</sub>	2	2.24	1.33	1.26	1.61	1.11	5.59	5.58	3.98	3.96	2.38	4.13	2.97	4.26	4.05	1.81	2.5	1.62
K <sub>2</sub> O	5.29	5.18	5.71	5.77	5.07	5.31	4.96	4.95	5.38	4.95	4.05	5.19	5.23	4.82	5.8	4.24	6.44	4.36
MgO	0.23	0.27	0.1	0.09	0.12	0.09	0.8	0.7	0.78	0.65	0.81	0.49	0.33	0.74	0.31	0.46	0.11	0.38
MnO	0.04	0.05	0.01	0.04	0.04	0.03	0.13	0.13	0.08	0.1	0.08	0.09	0.09	0.11	0.08	0.06	0.07	0.06
Na <sub>2</sub> O	3.22	3.23	2.81	2.86	2.98	3.14	3.34	3.38	3.29	3.11	4.11	3.42	3.38	1.85	3.13	3.99	3.07	3.67
P <sub>2</sub> O <sub>5</sub>	0.07	0.07	0.02	0.02	0.04	0.01	0.24	0.23	0.05	0.16	0.11	0.12	0.11	0.07	0.09	0.15	0.04	0.06
TiO <sub>2</sub>	0.27	0.295	0.165	0.165	0.165	0.105	0.76	0.73	0.6	0.55	0.24	0.55	0.35	0.385	0.47	0.195	0.26	0.16
LOI	1.02	1.08	0.89	1.03	1.1	0.9	0.78	0.78	1.06	0.99	1.04	0.77	0.79	1.2	0.45	0.8	0.66	0.57
Trace elements (ppm)																		
Be	3	4	4	3	4	3	1	1	2	1	1	4	1	3	1	2	1	1
Sc	2.5	2.5	2.5	2.5	2.5	2.5	15	10	5	10	2.5	10	5	2.5	2.5	2.5	2.5	2.5
V	10	10	10	10	10	10	30	30	50	30	30	10	10	10	10	10	10	10
Cr	10	10	10	10	10	10	10	10	40	30	30	10	10	10	10	30	100	10
As	3	2	4	1	3	2	4	5	2	0.5	0.5	2	0.5	2	0.5	0.5	1	2
Ba	850	700	470	550	160	190	1100	1100	850	850	900	1150	700	900	850	1100	430	1500
Bi	1.5	1.5	1.5	1.5	1.5	1.5	1.5	1.5	1.5	1.5	1.5	1.5	1.5	1.5	1.5	1.5	1.5	1.5
Cd	1.5	1.5	1.5	1.5	1.5	1.5	1.5	1.5	1.5	1.5	1.5	1.5	1.5	1.5	1.5	1.5	1.5	1.5
Co	2	2	0.5	0.5	0.5	0.5	6	6	9	6	5	2	4	3	6	2	2	4
Cs	6	6	10	8	10	6	4	4	8	6	6	4	6	4	4	4	14	1.5
Ga	23	23	20	22	21	19	18	18	22	14	16	24	15	30	17	19	20	15
Hf	4	5	3	4	4	3	9	9	5	6	3	5	6	8	12	5	11	2
In	0.25	0.25	0.25	0.25	0.25	0.25	0.25	0.25	0.25	0.25	0.25	0.25	0.25	0.25	0.25	0.25	0.25	0.25
Mo	1	2	3	1	3	1	3	3	2	2	2	5	3	1	2	3	3	2
Nb	15	20	15	20	20	15	20	20	10	15	0.5	20	15	15	20	0.5	25	0.5
Rb	210	220	280	270	290	270	175	190	200	185	160	180	200	160	175	185	300	105
Sb	4	4	4	4	4	3	7	2	3	1	1	3	1	4	2	2	2	3
Sn	0.5	0.5	0.5	0.5	0.5	0.5	0.5	0.5	15	0.5	0.5	0.5	0.5	0.5	0.5	0.5	0.5	0.5
Sr	105	90	40	55	30	30	160	165	145	140	600	135	120	165	75	440	30	750
Ta	6	7	5	5	7	5	1	1	2	1	1	2	1	3	1	4	1	1
Te	2.5	2.5	2.5	2.5	2.5	2.5	2.5	2.5	2.5	2.5	2.5	2.5	2.5	2.5	2.5	2.5	2.5	2.5
Tl	1.5	1.5	1.5	1.5	1.5	1.5	1.5	1.5	1.5	1.5	1.5	1.5	1.5	1.5	1.5	1.5	1.5	1.5
Th	27	29	25.5	28	47	27.5	21	21.5	19.5	19	8.5	25.5	19.5	11	13.5	19	23.5	3
U	5	6.5	3.5	4.5	14.5	4.5	4.5	5	3	4	2	4.5	3	3	3	3	6	0.5
W	600	550	480	850	450	460	1.5	1.5	210	1.5	1.5	280	4	210	1.5	1.5	6	1.5
Y	36	40	41	38	46	30	47	49	22	31	10	42	40	57	70	22	77	5
Zr	220	250	190	170	170	150	390	360	310	240	110	400	240	550	490	150	420	90



# Hiltaba Suite

SAMPNO	R215524	R215522	R215525	R350422	R215521	R350423	RS203991	RS203990	R363439	RS203985	RS203981	R368559	RS203986	R363440	RS203975	R378936	RS203974	RS215369
GROUP	Childara	Childara	Childara	Childara	Childara	Childara	Kondoolka	Kondoolka	Kondoolka	Kondoolka	Kondoolka	Kondoolka	Kondoolka	Kondoolka	Kondoolka	Kondoolka	Kondoolka	Kondoolka
Easting	459168	458600	464686	467660	456961	467857	488333	487480	463680	490340	484565	488313	493520	463993	463700	470812	464720	469620
Northing	6498257	6503308	6504370	6500578	6502562	6500121	6457250	6458840	6474457	6463460	6466590	6463354	6466630	6474445	6474333	6470853	6478715	6554690
Rare earth elements (ppm)																		
Ce	155	140	185	120	170	85	140	145	99	105	47	130	115	72	135	56	160	25
Dy	7.5	7.5	7.5	7	8	7	9.5	10	5	6	2	8	8	11	13.5	3	14	1
Er	4	4	4	5	5	4	5	5	3	3	1	4	4	6	8	2	9	0.5
Eu	1.5	1.5	1	0.5	0.25	0.25	2.5	2.5	1.5	1.5	0.25	1.5	1.5	2.5	2	0.25	1.5	0.25
Gd	8	8	8	8	8	6	10	11	6	7	2	8	9	10	14	4	14	1
Ho	1.5	1.5	1	1.5	1.5	1.5	1.5	2	1	1	0.25	1.5	1.5	2	2.5	0.5	3	0.25
La	83	85	115	71	97	39	63	70	50	45	22	77	56	44	57	32	66	12
Lu	0.5	0.5	0.5	0.5	1	0.5	0.5	0.5	0.25	0.25	0.25	0.5	0.5	1	1	0.25	1	0.25
Nd	48.5	54	58	45.5	51	30.5	63	70	41	44.5	20	51	56	42.5	70	25	73	11
Pr	16	15	17	14	16	9	17	18	12	11	5	15	14	12	18	6	18	3
Sm	9.5	9.5	10	8	9.5	6.5	11.5	12	7.5	7.5	0.25	6	10	7.5	13.5	0.25	14.5	0.25
Tb	1	1	1	1	1	1	1.5	1.5	1	1	0.25	1.5	1	1.5	2	0.5	2	0.25
Tm	0.5	0.5	0.5	0.5	0.5	0.5	0.5	0.5	0.5	0.5	0.5	0.5	0.5	0.5	1	0.5	1	0.5
Yb	4	4	4	4	5	4	5	5	3	3	1	5	4	6	8	2	8	0.5
Economic elements (ppm)																		
Cu	4	5	3	2	3	4	6	7	125	10	4	30	5	19	3	5	6	2
Pb	16	28	6	18	100	18	14	22	14	20	12	22	16	6	6	12	18	1.5
Zn	40	47	18	33	26	28	68	68	78	47	41	31	35	75	80	33	92	26
Ni	1	1	0.5	0.5	0.5	2	5	3	13	5	9	2	2	2	4	4	2	5

# Hiltaba Suite

SAMPNO	R368574	RS203976	R368563	R368557	R368565	R363441	R363442	R368562	RS215375	R368575	R368560	R363443	R368561	R368555	RS203988	R368550	RS203977
GROUP	Kondoolka	Kondoolka	Kondoolka	Kondoolka	Kondoolka	Kondoolka	Kondoolka	Kondoolka	Kondoolka	Kondoolka	Kondoolka	Kondoolka	Kondoolka	Kondoolka	Kondoolka	Kondoolka	Kondoolka
Easting	497272	464350	484140	484767	486900	463778	469704	487375	478600	497453	490143	479068	491563	476110	477625	476049	465285
Northing	6468650	6474035	6463385	6469767	6465166	6474410	6472948	6473950	6461000	6465290	6472569	6468305	6472007	6474522	6470975	6466450	6472495
Major elements (wt%)																	
SiO <sub>2</sub>	72.3	72.4	72.4	72.7	73	73.2	74.2	74.7	75	75.2	75.3	75.4	75.4	75.6	76.2	76.3	76.7
Al <sub>2</sub> O <sub>3</sub>	13	13.3	14.5	12.9	13.9	13.6	12.3	12.3	13.4	11.5	11.9	12.4	12	12	11.6	11.6	11.9
CaO	0.38	0.96	1.76	1.01	0.78	0.74	1.27	0.18	0.7	0.51	0.41	0.58	0.17	0.5	0.45	0.14	0.3
Fe <sub>2</sub> O <sub>3</sub>	2.23	3.47	1.78	2.48	1.84	2.25	1.46	2.33	1.27	1.62	1.72	0.93	1.9	0.98	1.01	1.26	2.08
K <sub>2</sub> O	5.79	5.93	4.25	5.52	4.65	4.6	4.04	5.52	6.29	6.15	5.53	5.24	5.92	5.19	4.83	4.79	5.68
MgO	0.34	0.09	0.53	0.28	0.63	0.33	0.48	0.21	0.3	0.2	0.29	0.16	0.14	0.14	0.09	0.08	0.06
MnO	0.05	0.1	0.05	0.06	0.07	0.06	0.07	0.04	0.02	0.07	0.03	0.05	0.02	0.05	0.04	0.03	0.06
Na <sub>2</sub> O	3.36	3.5	4.04	2.98	3.87	2.18	3.28	3.13	2.88	2.43	3.04	3.41	2.69	3.29	3.11	3.46	3.01
P <sub>2</sub> O <sub>5</sub>	0.19	0.05	0.07	0.07	0.06	0.05	0.12	0.09	0.08	0.02	0.02	0.04	0.03	0.04	0.03	0.02	0.03
TiO <sub>2</sub>	0.235	0.35	0.21	0.345	0.185	0.345	0.17	0.16	0.11	0.315	0.175	0.18	0.17	0.165	0.13	0.125	0.2
LOI	0.97	0.48	1.1	1.01	1.28	1.1	1.17	1.1	0.48	0.76	1.14	0.49	1.08	0.54	0.6	0.69	0.54
Trace elements (ppm)																	
Be	3	1	3	3	4	4	4	4	1	1	4	8	2	7	4	6	1
Sc	2.5	2.5	2.5	2.5	2.5	2.5	2.5	2.5	2.5	5	2.5	2.5	2.5	2.5	5	2.5	2.5
V	10	10	10	10	20	10	10	10	10	10	10	10	10	10	10	10	10
Cr	10	10	20	10	10	30	30	10	20	10	20	10	10	10	10	20	10
As	3	0.5	0.5	2	1	3	2	2	4	5	2	2	2	2	0.5	1	1
Ba	550	750	850	800	650	650	900	240	460	400	460	240	300	300	115	310	210
Bi	1.5	1.5	1.5	1.5	1.5	1.5	10	1.5	1.5	1.5	1.5	1.5	1.5	1.5	1.5	1.5	1.5
Cd	1.5	1.5	1.5	1.5	1.5	1.5	1.5	1.5	1.5	1.5	1.5	1.5	1.5	1.5	1.5	1.5	1.5
Co	0.5	2	2	2	5	3	3	0.5	2	1	0.5	1	2	0.5	0.5	0.5	4
Cs	4	4	6	4	6	8	12	4	6	4	4	10	6	10	8	8	4
Ga	22	21	20	21	21	24	19	22	11	17	22	22	19	21	13	23	19
Hf	5	13	2	5	3	5	2	5	2	2	4	2	5	3	3	4	10
In	0.25	0.25	0.25	0.25	0.25	0.25	0.25	0.25	0.25	0.25	0.25	0.25	0.25	0.25	0.25	0.25	0.25
Mo	1	3	3	1	1	4	2	1	2	2	3	2	1	1	3	3	3
Nb	15	15	0.5	15	15	15	0.5	20	0.5	10	20	15	15	15	15	15	25
Rb	230	145	160	200	180	160	195	240	165	210	250	400	240	370	400	420	240
Sb	3	1	2	2	6	3	3	4	1	3	3	3	2	3	2	3	2
Sn	0.5	0.5	0.5	0.5	0.5	0.5	0.5	0.5	0.5	0.5	0.5	0.5	0.5	0.5	0.5	0.5	0.5
Sr	50	35	400	100	220	90	290	40	115	95	40	60	25	60	30	20	15
Ta	1	1	1	2	2	3	1	3	1	1	1	2	2	1	1	2	1
Te	2.5	2.5	2.5	2.5	2.5	2.5	2.5	2.5	2.5	2.5	2.5	2.5	2.5	2.5	2.5	2.5	2.5
Tl	1.5	1.5	1.5	1.5	1.5	1.5	1.5	1.5	1.5	1.5	1.5	1.5	1.5	1.5	1.5	1.5	1.5
Th	23.5	13.5	11	25.5	11	20.5	10	28	9	34	20	42.5	26	43.5	37	52	24.5
U	3.5	3	2	5	5	3	2.5	3	5.5	2.5	2.5	7	2	6	9.5	5.5	5.5
W	280	1.5	350	480	270	155	430	280	1.5	410	240	440	290	450	4	700	1.5
Y	45	64	10	28	15	33	13	50	22	28	41	12	35	9	9	3	93
Zr	310	600	120	270	120	280	120	220	60	90	210	120	220	140	100	150	330

# Hiltaba Suite

SAMPNO	R368574	RS203976	R368563	R368557	R368565	R363441	R363442	R368562	RS215375	R368575	R368560	R363443	R368561	R368555	RS203988	R368550	RS203977
GROUP	Kondoolka	Kondoolka	Kondoolka	Kondoolka	Kondoolka	Kondoolka	Kondoolka	Kondoolka	Kondoolka	Kondoolka	Kondoolka	Kondoolka	Kondoolka	Kondoolka	Kondoolka	Kondoolka	Kondoolka
Easting	497272	464350	484140	484767	486900	463778	469704	487375	478600	497453	490143	479068	491563	476110	477625	476049	465285
Northing	6468650	6474035	6463385	6469767	6465166	6474410	6472948	6473950	6461000	6465290	6472569	6468305	6472007	6474522	6470975	6466450	6472495
Rare earth elements (ppm)																	
Ce	145	130	40	105	40	115	46	140	30	410	105	78	100	64	52	43	170
Dy	8	13	2	6	3	7	3	11.5	4	9	7	2	9	1.5	1.5	0.5	17.5
Er	5	7	0.5	4	2	4	2	7	3	3	5	1	6	1	0.5	0.5	11
Eu	1	3	0.5	1.5	0.25	1	0.25	1	0.25	1	1	0.25	0.5	0.25	0.25	0.25	1
Gd	9	14	2	7	3	8	3	9	3	12	9	2	8	1	1	0.5	16
Ho	1.5	2.5	0.25	1	0.5	1	0.25	2.5	1	1	1.5	0.25	1.5	0.25	0.25	0.25	3.5
La	76	54	28	50	21	67	25	58	12	210	70	52	51	51	40	46	72
Lu	0.5	1	0.25	0.5	0.25	0.5	0.25	1	0.25	0.5	0.5	0.25	0.5	0.25	0.25	0.25	1.5
Nd	53	70	15.5	43	16	51	18	56	13.5	130	51	16.5	45.5	13	11	6.5	83
Pr	13	16	6	12	5	14	6	19	4	46	13	6	12	5	4	3	21
Sm	9.5	13.5	0.25	8	0.5	7	0.5	11.5	1	20	8	2.5	8.5	1.5	1.5	1	17
Tb	1.5	2	0.25	1	0.25	1	0.25	1.5	0.5	1.5	1.5	0.25	1.5	0.25	0.25	0.25	2.5
Tm	0.5	0.5	0.5	0.5	0.5	0.5	0.5	1	0.5	0.5	0.5	0.5	0.5	0.5	0.5	0.5	2
Yb	5	7	1	4	2	4	2	7	2	3	4	2	5	1	2	0.5	11
Economic elements (ppm)																	
Cu	40	5	12	66	40	37	340	16	6	55	11	5	34	19	2	12	4
Pb	6	12	10	34	14	10	14	4	1.5	18	6	18	6	28	22	10	16
Zn	64	66	26	60	33	41	41	56	8	36	43	17	21	39	15	9	88
Ni	2	2	3	2	7	4	5	0.5	3	0.5	1	0.5	2	0.5	0.5	0.5	2



# Hiltaba Suite

SAMPNO	R368556	RS215376	R368564	RS203982	RS203979	RS203984	RS203989	R368567	R378917	R378926	R378925	R378935	R378916	R378915	R378940	R 387447	R378929	R378927	R378928
GROUP	Kondoolka	Kondoolka	Kondoolka	Kondoolka	Kondoolka	Kondoolka	Kondoolka	Meelera	Meelera	Meelera	Meelera	Pureba	Tolmer	Tolmer	Tunkillia	Tunkillia	Tunkillia	Tunkillia	Tunkillia
Easting	476322	466400	487457	482495	474400	488445	478010	463680	454274	468907	457065	451973	434840	424592	483588	482452	483662	491236	498406
Northing	6475000	6561700	6466222	6466060	6467130	6465465	6473200	6518422	6561869	6536895	6524010	6469194	6557500	6566327	6547050	6547726	6557828	6548902	6547216
Major elements (wt%)																			
SiO <sub>2</sub>	76.8	76.9	77.2	77.6	77.9	78.4	79.8	70.2	70.3	76.8	77.2	69.6	68.6	75.7	66.7	72.6	74.2	75.5	77.3
Al <sub>2</sub> O <sub>3</sub>	12.3	13	12.5	12.2	12.2	12.2	11.6	15.2	13.2	11.9	11.3	13.5	14.1	12.3	14.6	14.1	12.9	12.2	11.7
CaO	0.13	0.56	0.09	0.13	0.47	0.08	0.03	2.05	1.6	0.55	0.76	2.06	2.6	1.4	3.72	0.71	1.41	0.9	0.5
Fe <sub>2</sub> O <sub>3</sub>	0.54	0.83	0.62	0.87	0.77	0.72	0.63	1.87	3.42	1.67	1.48	3.9	3.95	1.66	4.12	1.78	2.66	1.89	1.53
K <sub>2</sub> O	4.81	5	4.76	5.24	5.08	4.79	4.66	3.39	5.3	5.43	5.48	5.01	4.93	4.46	3.7	5.19	5.3	5.54	5.3
MgO	0.09	0.02	0.03	0.07	0.05	0.03	0.03	0.39	0.59	0.13	0.11	0.67	0.74	0.25	1.47	0.72	0.31	0.16	0.08
MnO	0.04	0.02	0.06	0.07	0.04	0.04	0.04	0.08	0.06	0.03	0.03	0.08	0.09	0.07	0.1	0.05	0.05	0.03	0.03
Na <sub>2</sub> O	3.59	3.68	3.74	3.3	3.58	3.49	3.43	4.53	2.94	2.95	2.63	3.47	2.99	3.01	3.05	3.85	3.11	2.98	2.96
P <sub>2</sub> O <sub>5</sub>	0.02	0.02	0.02	0.02	0.02	0.12	0.02	0.07	0.23	0.09	0.1	0.22	0.3	0.18	0.25	0.08	0.12	0.1	0.07
TiO <sub>2</sub>	0.11	0.06	0.07	0.11	0.1	0.1	0.09	0.215	0.49	0.18	0.17	0.565	0.6	0.23	0.43	0.255	0.335	0.215	0.15
LOI	0.86	0.39	0.6	0.75	0.56	0.7	0.49	0.82	0.55	0.45	0.52	0.97	0.4	0.57	0.62	0.94	0.15	0.52	0.53
Trace elements (ppm)																			
Be	5	1	10	1	5	3	1	3	1	3	4	2	1	3	1	1	1	4	4
Sc	5	2.5	5	5	2.5	5	5	2.5	2.5	2.5	2.5	10	10	2.5	10	2.5	2.5	2.5	2.5
V	10	10	10	10	10	10	10	10	10	10	10	20	20	10	40	10	10	10	10
Cr	10	10	10	10	20	20	10	10	40	20	30	30	40	30	40	40	10	30	30
As	0.5	3	0.5	0.5	0.5	0.5	0.5	0.5	2	1	2	0.5	0.5	1	1	2	0.5	2	0.5
Ba	145	130	15	110	50	45	25	950	1200	270	360	950	850	240	800	850	750	390	115
Bi	1.5	1.5	1.5	1.5	1.5	1.5	1.5	1.5	1.5	1.5	1.5	1.5	1.5	1.5	1.5	1.5	1.5	1.5	1.5
Cd	1.5	4	1.5	1.5	1.5	1.5	1.5	1.5	1.5	1.5	1.5	1.5	1.5	1.5	1.5	1.5	1.5	1.5	1.5
Co	1	2	0.5	3	2	1	0.5	2	3	0.5	0.5	3	4	0.5	6	3	0.5	0.5	0.5
Cs	6	1.5	12	10	10	10	10	4	4	4	4	1.5	4	10	6	4	1.5	4	4
Ga	21	17	27	17	18	20	19	24	22	21	18	21	22	18	18	17	20	21	20
Hf	3	3	3	3	4	5	4	2	9	5	6	9	7	5	4	1	7	7	7
In	0.25	1	0.25	0.25	0.25	0.25	0.25	0.25	0.25	0.25	0.25	0.25	0.25	0.25	0.25	0.25	0.25	0.25	0.25
Mo	1	2	3	2	3	5	3	1	4	3	3	3	3	3	2	23	4	3	5
Nb	25	0.5	30	15	20	40	25	0.5	15	15	10	10	15	15	0.5	0.5	10	15	20
Rb	550	220	700	600	650	750	700	110	230	310	270	190	140	230	130	200	200	320	330
Sb	3	20	4	3	1	10	1	4	2	1	1	2	2	1	3	0.5	1	0.5	0.5
Sn	0.5	0.5	0.5	0.5	0.5	0.5	0.5	0.5	0.5	0.5	0.5	0.5	0.5	0.5	0.5	0.5	0.5	0.5	0.5
Sr	25	120	10	30	15	30	10	390	190	55	75	165	185	80	380	185	115	65	30
Ta	3	1	2	1	1	1	1	1	7	5	5	4	7	8	4	1	4	5	5
Te	2.5	2.5	2.5	2.5	2.5	2.5	2.5	2.5	2.5	2.5	2.5	2.5	2.5	2.5	2.5	2.5	2.5	2.5	2.5
Tl	1.5	1.5	1.5	1.5	1.5	1.5	1.5	1.5	1.5	1.5	1.5	1.5	1.5	1.5	1.5	1.5	1.5	1.5	1.5
Th	32.5	23	36	33.5	47.5	53	39.5	7	36	38.5	42.5	24	19.5	27	24	17	41.5	54	53
U	5.5	5	11	3.5	11.5	11.5	8.5	2.5	6	5.5	9.5	4.5	2.5	8	3	2	7.5	10	12
W	310	1.5	390	6	4	6	4	230	44	1.5	1.5	1.5	1.5	1.5	1.5	1.5	1.5	1.5	4
Y	4	5	2	3	7	5	3	17	37	54	45	39	33	26	24	23	37	44	54
Zr	110	70	100	90	110	120	100	130	380	150	180	380	280	160	180	110	230	220	180

# Hiltaba Suite

SAMPNO	R368556	RS215376	R368564	RS203982	RS203979	RS203984	RS203989	R368567	R378917	R378926	R378925	R378935	R378916	R378915	R378940	R 387447	R378929	R378927	R378928
GROUP	Kondoolka	Kondoolka	Kondoolka	Kondoolka	Kondoolka	Kondoolka	Kondoolka	Meelera	Meelera	Meelera	Meelera	Pureba	Tolmer	Tolmer	Tunkillia	Tunkillia	Tunkillia	Tunkillia	Tunkillia
Easting	476322	466400	487457	482495	474400	488445	478010	463680	454274	468907	457065	451973	434840	424592	483588	482452	483662	491236	498406
Northing	6475000	6561700	6466222	6466060	6467130	6465465	6473200	6518422	6561869	6536895	6524010	6469194	6557500	6566327	6547050	6547726	6557828	6548902	6547216
Rare earth elements (ppm)																			
Ce	44	16	38	37	71	66	18	39	230	105	175	105	145	95	97	85	125	140	105
Dy	1	1	0.5	0.5	1	0.5	0.25	3	6	8.5	6.5	6.5	5.5	4.5	3.5	5.5	7	6.5	8
Er	0.5	0.5	0.5	0.5	0.5	0.5	0.5	2	3	4	3	3	3	2	2	2	3	4	5
Eu	0.25	0.25	0.25	0.25	0.25	0.25	0.25	0.5	1.5	0.5	1	1.5	1	0.5	1	1	1.5	1	0.25
Gd	0.5	1	0.5	0.5	0.5	0.5	0.5	3	7	7	7	7	7	5	5	6	7	7	7
Ho	0.25	0.25	0.25	0.25	0.25	0.25	0.25	0.5	1	2	1.5	1.5	1	1	1	1	1.5	1.5	2
La	33	9	36	29	59	56	14	23	135	60	110	63	91	55	57	43	76	91	64
Lu	0.25	0.25	0.25	0.25	0.25	0.25	0.25	0.25	0.25	0.25	0.5	0.5	0.25	0.25	0.25	0.25	0.5	0.5	1
Nd	6	6.5	4	7	9.5	6.5	2.5	15	70	48	66	49	61	44.5	42	36	57	60	46.5
Pr	3	2	2	3	4	3	0.5	6	20	12	19	12	15	11	11	10	15	16	13
Sm	1	1	0.5	1	1	1	0.25	0.25	8	9	9.5	5.5	5.5	7	2.5	7	8.5	8.5	8
Tb	0.25	0.25	0.25	0.25	0.25	0.25	0.25	0.25	1	1.5	1	1	1	1	1	0.5	1	1	1
Tm	0.5	0.5	0.5	0.5	0.5	0.5	0.5	0.5	0.5	0.5	0.5	0.5	0.5	0.5	0.5	0.5	0.5	0.5	0.5
Yb	1	0.5	0.5	0.5	2	1	0.5	2	3	6	5	4	2	3	2	3	4	5	6
Economic elements (ppm)																			
Cu	12	2	6	3	1	4	2	13	9	2	2	5	13	6	19	18	2	2	1
Pb	10	8	4	20	12	4	4	8	10	22	24	32	4	12	6	4	14	16	16
Zn	5	5	11	5	12	9	9	42	54	25	19	55	49	29	45	37	38	23	19
Ni	1	2	0.5	1	1	2	1	1	4	0.5	0.5	3	3	2	12	4	0.5	0.5	0.5

# Hiltaba Suite

SAMPNO R370937 R370939  
 GROUP Yathong Yathong  
 Easting 472870 473012  
 Northing 6510632 6510256

## Major elements (wt%)

SiO <sub>2</sub>	75.1	77.8
Al <sub>2</sub> O <sub>3</sub>	12.6	11.3
CaO	0.22	0.27
Fe <sub>2</sub> O <sub>3</sub>	1.31	1.22
K <sub>2</sub> O	6.15	5.57
MgO	0.18	0.09
MnO	0.03	0.02
Na <sub>2</sub> O	2.97	2.76
P <sub>2</sub> O <sub>5</sub>	0.03	0.04
TiO <sub>2</sub>	0.17	0.175
LOI	0.49	0.63

## Trace elements (ppm)

Be	1	2
Sc	2.5	2.5
V	10	10
Cr	10	170
As	1	2
Ba	800	750
Bi	1.5	24
Cd	1.5	1.5
Co	3	0.5
Cs	4	4
Ga	19	18
Hf	5	5
In	0.25	0.25
Mo	2	4
Nb	25	25
Rb	320	300
Sb	3	3
Sn	0.5	25
Sr	55	50
Ta	7	6
Te	2.5	2.5
Tl	1.5	1.5
Th	31	30.5
U	8	5
W	1.5	4
Y	43	46
Zr	190	230

### Hiltaba Suite

<b>SAMPNO</b>	R370937	R370939
<b>GROUP</b>	Yathong	Yathong
<b>Easting</b>	472870	473012
<b>Northing</b>	6510632	6510256
<b>Rare earth elements (ppm)</b>		
<b>Ce</b>	155	155
<b>Dy</b>	7.5	7.5
<b>Er</b>	4	4
<b>Eu</b>	1	1
<b>Gd</b>	7	7
<b>Ho</b>	1.5	1.5
<b>La</b>	77	67
<b>Lu</b>	0.5	1
<b>Nd</b>	40	30.5
<b>Pr</b>	13	10
<b>Sm</b>	8.5	7.5
<b>Tb</b>	1	1
<b>Tm</b>	0.5	0.5
<b>Yb</b>	4	4
<b>Economic elements (ppm)</b>		
<b>Cu</b>	13	43
<b>Pb</b>	10	12
<b>Zn</b>	39	31
<b>Ni</b>	1	1



# Gawler Range Volcanics

SAMPNO	R370943	R370976	R370978	R370980	R370981	R370982	R370940	R370941	R370944	R370946	R370956	R370957	R370960	R370965	R370964	R370966	R370968	R370983	R370985	R370951	R370952	R370972
GROUP	Myb	Myc	Myc	Myc	Myc	Myc	Myl	Myl	Myl	Myl	Myl	Myl	Myl	Myl	Mym	Mym	Mym	Mym	Mym	Myn	Myn	Myn
Easting	498926	482588	483304	483451	484878	486638	495452	495452	498860	497893	486978	487341	491475	487538	487190	487250	486400	486674	484878	493210	492364	486173
Northing	6492875	6489046	6490152	6487192	6486839	6486401	6494638	6494638	6494053	6497131	6493147	6494999	6498195	6495982	6496610	6495995	6496597	6489802	6490780	6489744	6489744	6500310
Major elements (wt%)																						
SiO <sub>2</sub>	70.00	63.20	63.40	61.40	69.50	63.80	80.90	78.50	76.00	75.70	71.30	72.50	73.40	77.00	65.40	61.00	64.30	65.10	63.70	50.80	51.00	53.90
Al <sub>2</sub> O <sub>3</sub>	13.90	14.30	13.70	13.40	13.00	14.40	9.77	11.50	13.00	11.80	15.60	13.40	14.50	12.00	13.40	16.10	14.80	14.20	14.30	17.00	17.10	14.60
CaO	0.34	2.59	2.58	2.37	0.30	1.10	0.51	0.51	0.48	0.25	0.42	0.55	0.28	0.37	1.06	0.80	1.39	0.57	2.04	6.10	6.80	1.77
Fe <sub>2</sub> O <sub>3</sub>	3.81	5.97	6.03	6.24	2.42	4.60	0.94	1.15	1.14	1.74	1.86	2.55	1.64	0.85	6.01	7.01	4.99	4.67	4.89	10.40	10.20	10.90
K <sub>2</sub> O	6.47	5.12	4.45	4.90	9.14	5.24	5.05	5.07	6.21	9.29	3.27	6.11	4.89	6.78	5.94	4.20	5.33	5.48	5.48	1.99	1.62	3.89
MgO	0.64	2.05	1.65	2.11	1.00	1.84	0.16	0.20	0.18	0.44	0.17	0.42	0.34	0.13	1.85	2.66	1.69	1.50	1.55	5.27	5.67	5.00
MnO	0.10	0.14	0.17	0.18	0.06	0.11	0.07	0.04	0.07	0.09	0.03	0.06	0.03	0.03	0.09	0.11	0.10	0.08	0.13	0.17	0.17	0.17
Na <sub>2</sub> O	2.97	2.65	3.36	2.99	0.79	3.71	2.07	3.03	2.57	0.14	6.41	3.02	4.41	2.16	2.75	4.46	3.64	3.60	3.20	3.61	3.03	2.72
P <sub>2</sub> O <sub>5</sub>	0.07	0.41	0.53	0.54	0.11	0.29	0.02	0.02	0.03	0.02	0.04	0.06	0.04	0.05	0.35	0.37	0.26	0.25	0.30	0.23	0.24	1.14
TiO <sub>2</sub>	0.42	0.91	0.99	1.00	0.49	0.85	0.10	0.13	0.16	0.15	0.15	0.35	0.17	0.14	0.89	1.11	0.88	0.81	0.87	1.19	1.16	1.89
LOI	1.3	2.7	1.9	2.2	3.4	1.8	0.5	0.6	0.8	1.0	0.2	1.0	0.9	0.2	2.0	2.2	1.4	1.8	1.4	2.6	2.6	4.4
Trace elements (ppm)																						
Be	2.0	1.0	1.0	1.0	1.0	1.0	2.0	1.0	3.0	1.0	1.0	3.0	1.0	1.0	1.0	1.0	1.0	1.0	1.0	1.0	1.0	1.0
Sc	10.0	15.0	15.0	15.0	5.0	10.0	2.5	2.5	2.5	2.5	2.5	2.5	2.5	2.5	15.0	15.0	15.0	10.0	15.0	25.0	25.0	25.0
V	10	100	90	90	40	70	10	10	10	10	10	20	30	10	90	90	70	60	70	200	200	170
Cr	10	20	20	30	10	10	20	10	10	10	10	10	10	10	10	10	10	10	10	60	80	10
As	2.0	0.5	0.5	0.5	1.0	1.0	2.0	2.0	1.0	2.0	4.0	1.0	0.5	2.0	0.5	0.5	1.0	0.5	1.0	2.0	2.0	0.5
Ba	1450	1500	1350	1800	1950	3600	250	310	70	1400	1700	1100	1950	2150	4400	3500	3250	3600	3150	700	700	1750
Bi	1.5	1.5	1.5	1.5	1.5	1.5	1.5	1.5	1.5	1.5	1.5	1.5	1.5	1.5	1.5	1.5	1.5	1.5	34.0	1.5	1.5	1.5
Cd	1.5	1.5	1.5	1.5	1.5	1.5	1.5	1.5	1.5	1.5	1.5	1.5	1.5	1.5	1.5	1.5	1.5	1.5	1.5	1.5	1.5	1.5
Co	2.0	19.0	18.0	21.0	3.0	11.0	0.5	0.5	1.0	0.5	0.5	4.0	2.0	0.5	8.0	14.0	11.0	7.0	15.0	39.0	38.0	22.0
Cs	4.0	4.0	1.5	4.0	1.5	1.5	4.0	1.5	4.0	4.0	1.5	1.5	1.5	4.0	1.5	1.5	1.5	1.5	1.5	4.0	1.5	1.5
Ga	27.0	22.0	23.0	28.0	19.0	25.0	11.0	15.0	20.0	17.0	13.0	21.0	13.0	10.0	14.0	21.0	22.0	23.0	23.0	25.0	26.0	27.0
Hf	15.0	7.0	7.0	7.0	9.0	12.0	9.0	5.0	6.0	6.0	4.0	8.0	4.0	4.0	11.0	11.0	12.0	12.0	12.0	5.0	5.0	9.0
In	0.3	0.3	0.3	0.3	0.3	0.3	0.3	0.3	0.3	0.3	0.3	0.3	0.3	0.3	0.3	0.3	0.3	0.3	0.3	0.3	0.3	0.3
Mo	4.0	4.0	4.0	4.0	3.0	5.0	4.0	5.0	4.0	6.0	5.0	4.0	4.0	4.0	4.0	3.0	3.0	3.0	3.0	4.0	4.0	4.0
Nb	35.0	20.0	25.0	25.0	25.0	25.0	25.0	25.0	35.0	35.0	20.0	30.0	20.0	15.0	20.0	25.0	20.0	25.0	25.0	15.0	15.0	20.0
Rb	210.0	135.0	165.0	180.0	190.0	150.0	210.0	185.0	270.0	240.0	78.0	220.0	125.0	155.0	135.0	100.0	150.0	155.0	150.0	70.0	45.5	93.0
Sb	10.0	4.0	6.0	6.0	9.0	5.0	15.0	6.0	6.0	5.0	5.0	3.0	4.0	4.0	4.0	5.0	5.0	5.0	6.0	7.0	4.0	5.0
Sn	10.0	0.5	0.5	0.5	0.5	0.5	15.0	10.0	0.5	30.0	0.5	0.5	0.5	0.5	0.5	0.5	0.5	0.5	0.5	0.5	10.0	0.5
Sr	95.0	290.0	300.0	400.0	50.0	190.0	30.0	30.0	25.0	45.0	370.0	110.0	150.0	200.0	165.0	320.0	185.0	145.0	330.0	550.0	550.0	135.0
Ta	6.0	1.0	6.0	5.0	4.0	4.0	6.0	6.0	6.0	4.0	3.0	4.0	3.0	2.0	3.0	3.0	3.0	4.0	4.0	4.0	3.0	3.0
Te	2.5	2.5	2.5	2.5	2.5	2.5	2.5	2.5	2.5	2.5	2.5	2.5	2.5	2.5	2.5	2.5	2.5	2.5	2.5	2.5	2.5	2.5
Tl	1.5	1.5	1.5	1.5	1.5	1.5	1.5	1.5	1.5	1.5	1.5	1.5	1.5	1.5	1.5	1.5	1.5	1.5	1.5	1.5	1.5	1.5
Th	22.5	17.0	20.0	19.5	18.5	17.0	17.5	16.5	20.0	20.0	15.0	27.0	15.5	13.0	16.0	16.5	17.5	15.0	15.5	7.5	6.0	16.5
U	3.0	2.0	3.0	3.0	2.5	2.5	2.0	1.5	3.0	1.5	2.5	5.5	1.0	1.5	2.5	2.5	2.5	2.0	2.5	1.0	1.0	2.5
W	1.5	1.5	1.5	1.5	1.5	1.5	4.0	1.5	1.5	1.5	1.5	1.5	1.5	1.5	1.5	1.5	1.5	1.5	1.5	1.5	1.5	1.5
Y	51.0	37.0	39.0	44.0	40.0	44.0	26.0	23.0	34.0	42.0	18.0	40.0	18.0	15.0	33.0	46.0	38.0	41.0	41.0	25.0	25.0	57.0
Zr	800.0	300.0	290.0	280.0	420.0	650.0	320.0	170.0	220.0	220.0	210.0	310.0	190.0	160.0	490.0	550.0	650.0	650.0	550.0	230.0	210.0	450.0

### Gawler Range Volcanics

SAMPNO	R370943	R370976	R370978	R370980	R370981	R370982	R370940	R370941	R370944	R370946	R370956	R370957	R370960	R370965	R370964	R370966	R370968	R370983	R370985	R370951	R370952	R370972
GROUP	Myb	Myc	Myc	Myc	Myc	Myc	Myl	Myl	Myl	Myl	Myl	Myl	Myl	Myl	Mym	Mym	Mym	Mym	Mym	Myn	Myn	Myn
Easting	498926	482588	483304	483451	484878	486638	495452	495452	498860	497893	486978	487341	491475	487538	487190	487250	486400	486674	484878	493210	492364	486173
Northing	6492875	6489046	6490152	6487192	6486839	6486401	6494638	6494638	6494053	6497131	6493147	6494999	6498195	6495982	6496610	6495995	6496597	6489802	6490780	6489744	6489744	6500310
Rare earth elements (ppm)																						
Ce	160.0	130.0	105.0	110.0	210.0	180.0	80.0	66.0	87.0	84.0	105.0	160.0	105.0	98.0	125.0	165.0	155.0	165.0	165.0	62.0	67.0	155.0
Dy	8.5	7.0	7.0	8.5	8.0	8.0	5.5	4.5	6.5	7.0	3.5	8.0	3.5	3.0	7.5	9.0	8.0	8.0	7.5	5.0	5.0	10.5
Er	4.0	3.0	4.0	4.0	4.0	4.0	2.0	2.0	4.0	3.0	2.0	4.0	2.0	1.0	4.0	4.0	4.0	4.0	4.0	3.0	3.0	5.0
Eu	2.0	1.5	2.0	2.5	1.5	2.0	0.5	0.3	0.5	0.3	0.3	1.5	0.3	0.3	1.5	2.0	2.5	1.5	2.0	1.5	1.5	3.5
Gd	8.0	7.0	8.0	8.0	9.0	9.0	5.0	4.0	6.0	5.0	3.0	8.0	4.0	4.0	8.0	10.0	9.0	10.0	9.0	5.0	5.0	12.0
Ho	1.5	1.5	1.5	1.5	1.5	1.5	1.0	1.0	1.5	1.5	0.5	1.5	0.5	0.5	1.5	1.5	1.5	1.5	1.5	1.0	1.0	2.0
La	86.0	61.0	53.0	51.0	105.0	89.0	36.0	40.0	44.0	45.0	55.0	89.0	49.0	54.0	62.0	85.0	77.0	86.0	81.0	31.0	32.0	73.0
Lu	1.0	0.3	0.5	0.5	0.5	0.5	0.3	0.3	0.5	0.3	0.3	0.5	0.3	0.3	0.5	0.5	0.5	0.5	0.5	0.3	0.3	0.5
Nd	55.0	48.0	43.0	43.5	63.0	60.0	25.5	23.0	29.5	27.5	29.5	51.0	26.5	31.0	49.5	60.0	61.0	56.0	57.0	27.0	26.0	63.0
Pr	15.0	11.0	10.0	11.0	17.0	14.0	7.0	6.0	9.0	8.0	9.0	14.0	7.0	8.0	12.0	15.0	15.0	14.0	15.0	6.0	6.0	14.0
Sm	8.0	2.5	6.5	6.0	3.0	0.3	4.0	2.5	6.0	0.3	0.3	7.0	0.3	0.3	0.3	0.3	0.3	0.3	0.3	2.0	2.0	5.0
Tb	1.5	1.0	1.5	1.0	1.5	1.5	0.5	0.5	1.0	1.0	0.5	1.0	0.5	0.5	1.0	1.5	1.5	1.5	1.5	1.0	1.0	2.0
Tm	0.5	0.5	0.5	0.5	0.5	0.5	0.5	0.5	0.5	0.5	0.5	0.5	0.5	0.5	0.5	0.5	0.5	0.5	0.5	0.5	0.5	0.5
Yb	5.0	3.0	4.0	4.0	4.0	4.0	3.0	2.0	4.0	3.0	1.0	4.0	2.0	1.0	3.0	4.0	4.0	4.0	3.0	2.0	2.0	5.0
Economic elements (ppm)																						
Cu	6.0	12.0	10.0	10.0	2.0	25.0	7.0	5.0	2.0	2.0	4.0	4.0	1.0	2.0	3.0	9.0	9.0	2.0	10.0	30.0	54.0	5.0
Pb	6.0	8.0	22.0	24.0	8.0	10.0	1.5	1.5	8.0	4.0	1.5	8.0	1.5	1.5	4.0	6.0	8.0	6.0	8.0	4.0	4.0	14.0
Zn	76.0	74.0	84.0	100.0	37.0	87.0	11.0	35.0	34.0	13.0	5.0	48.0	11.0	18.0	52.0	98.0	88.0	88.0	80.0	84.0	67.0	155.0
Ni	4.0	13.0	9.0	10.0	3.0	9.0	2.0	3.0	3.0	5.0	2.0	2.0	2.0	2.0	10.0	12.0	10.0	9.0	10.0	77.0	80.0	12.0

# Gawler Range Volcanics

SAMPNO	R370973	R370970	R370947	R370975	R370942	R370945	R370948	R370950	R370953	R370954	R370958	R370959	R370962	R370949	R370955	R370961	R370963	R370967	R370969	R370971	R370974	R370977
GROUP	Myn	Myp	Myw	Myw	Myy	Myy	Myy	Myy	Myy	Myy	Myy	Myy	Myy	Myz	Myz	Myz	Myz	Myz	Myz	Myz	Myz	Myz
Easting	485883	486568	498432	492406	496144	499292	494046	494480	492334	489064	491469	491225	492047	492734	488999	491773	492212	486976	486370	487475	491059	482868
Northing	6495892	6496205	6487590	6488685	6493450	6497290	6494722	6491300	6499695	6493386	6500169	6498825	6497974	6494585	6493370	6497969	6497149	6496149	6496157	6498555	6489929	6489648
Major elements (wt%)																						
SiO <sub>2</sub>	56.10	76.20	75.00	76.00	69.40	70.90	70.50	70.20	73.70	72.10	69.80	70.90	73.40	76.00	71.00	73.20	71.20	75.50	69.70	69.30	76.00	71.30
Al <sub>2</sub> O <sub>3</sub>	14.40	12.40	12.50	12.70	14.30	13.90	14.00	13.80	13.20	13.50	13.40	13.90	12.50	10.60	14.50	13.20	13.80	12.60	14.00	13.70	12.10	13.70
CaO	4.46	0.35	0.25	0.34	0.35	0.82	0.29	0.25	0.64	0.24	0.84	0.38	0.35	0.17	0.29	0.21	0.88	0.41	1.16	1.60	0.25	0.93
Fe <sub>2</sub> O <sub>3</sub>	9.95	0.99	2.15	1.51	3.84	3.53	3.75	3.70	2.64	3.26	3.46	3.79	3.06	2.74	2.66	2.76	2.98	1.92	3.93	3.78	2.20	3.14
K <sub>2</sub> O	3.04	6.05	5.91	2.59	5.46	5.85	6.36	6.28	6.10	6.21	9.32	6.41	6.24	6.01	3.54	6.25	6.42	6.02	5.42	5.23	5.61	5.72
MgO	2.77	0.19	0.45	0.57	0.63	0.37	0.52	1.17	0.54	0.31	0.56	0.34	0.70	0.49	1.05	0.61	0.43	0.29	0.61	0.68	0.17	0.58
MnO	0.22	0.04	0.03	0.04	0.08	0.08	0.07	0.08	0.04	0.07	0.10	0.05	0.16	0.08	0.09	0.04	0.08	0.03	0.08	0.08	0.02	0.06
Na <sub>2</sub> O	3.47	2.95	2.37	4.75	3.61	3.49	3.19	2.78	1.30	3.07	0.89	2.77	2.35	1.54	4.81	2.07	2.96	2.64	3.01	3.25	2.71	3.33
P <sub>2</sub> O <sub>5</sub>	1.00	0.01	0.08	0.06	0.08	0.07	0.07	0.07	0.06	0.07	0.07	0.08	0.06	0.06	0.07	0.06	0.08	0.03	0.12	0.12	0.03	0.10
TiO <sub>2</sub>	1.72	0.10	0.30	0.33	0.42	0.42	0.43	0.42	0.40	0.42	0.43	0.42	0.33	0.36	0.40	0.39	0.40	0.23	0.57	0.52	0.19	0.44
LOI	2.6	1.4	1.4	1.7	1.6	1.1	1.4	1.6	1.8	1.2	1.5	1.4	0.9	1.3	1.8	1.6	1.2	1.0	1.0	1.7	1.3	1.2
Trace elements (ppm)																						
Be	1.0	3.0	2.0	2.0	2.0	2.0	3.0	3.0	4.0	1.0	1.0	1.0	2.0	1.0	4.0	2.0	3.0	3.0	2.0	3.0	3.0	3.0
Sc	25.0	2.5	2.5	2.5	10.0	10.0	10.0	10.0	2.5	10.0	10.0	10.0	2.5	5.0	10.0	5.0	5.0	2.5	5.0	5.0	2.5	5.0
V	150	10	10	30	10	10	10	10	20	10	30	30	10	10	10	30	20	20	40	40	20	30
Cr	10	10	10	10	10	10	10	10	10	10.00	10	10	110	10	10	10	10	10	20	30	10	10
As	0.5	2.0	2.0	2.0	2.0	1.0	2.0	0.5	2.0	0.5	1.0	1.0	3.0	2.0	2.0	0.5	0.5	0.5	2.0	2.0	2.0	0.5
Ba	2450	600	650	460	1300	1300	1400	1400	2150	1100	2200	1500	1350	1400	1600	2000	1500	1100	1600	1250	440	1400
Bi	1.5	1.5	1.5	1.5	1.5	1.5	1.5	1.5	1.5	30.0	1.5	1.5	1.5	1.5	1.5	1.5	1.5	1.5	1.5	1.5	1.5	1.5
Cd	1.5	1.5	1.5	1.5	1.5	1.5	1.5	1.5	1.5	1.5	1.5	1.5	1.5	1.5	1.5	1.5	1.5	1.5	1.5	1.5	1.5	1.5
Co	23.0	2.0	0.5	1.0	3.0	3.0	2.0	0.5	0.5	2.0	0.5	2.0	1.0	2.0	3.0	3.0	6.0	2.0	6.0	9.0	3.0	3.0
Cs	1.5	1.5	4.0	4.0	1.5	1.5	1.5	1.5	4.0	1.5	4.0	1.5	4.0	4.0	1.5	4.0	1.5	1.5	1.5	1.5	1.5	4.0
Ga	25.0	20.0	17.0	13.0	26.0	28.0	25.0	25.0	20.0	18.0	17.0	22.0	17.0	18.0	22.0	23.0	21.0	22.0	21.0	22.0	20.0	23.0
Hf	9.0	5.0	9.0	8.0	14.0	14.0	14.0	16.0	9.0	13.0	15.0	13.0	7.0	12.0	12.0	9.0	8.0	7.0	9.0	9.0	6.0	9.0
In	0.3	0.3	0.3	0.3	0.3	0.3	0.3	0.3	0.3	0.3	0.3	0.3	0.3	0.3	0.3	0.3	0.3	0.3	0.3	0.3	0.3	0.3
Mo	3.0	3.0	3.0	2.0	5.0	4.0	5.0	3.0	3.0	3.0	3.0	3.0	14.0	3.0	4.0	4.0	4.0	4.0	4.0	5.0	3.0	3.0
Nb	20.0	30.0	30.0	30.0	30.0	35.0	30.0	30.0	35.0	25.0	30.0	25.0	25.0	25.0	30.0	30.0	25.0	30.0	25.0	25.0	30.0	25.0
Rb	79.0	230.0	210.0	63.0	170.0	185.0	210.0	180.0	240.0	180.0	230.0	200.0	210.0	190.0	92.0	230.0	270.0	270.0	190.0	190.0	340.0	240.0
Sb	4.0	8.0	5.0	4.0	6.0	6.0	6.0	4.0	5.0	4.0	4.0	7.0	7.0	4.0	4.0	4.0	5.0	5.0	4.0	4.0	4.0	5.0
Sn	0.5	0.5	0.5	0.5	10.0	0.5	10.0	10.0	15.0	0.5	0.5	0.5	0.5	0.5	0.5	10.0	0.5	0.5	0.5	0.5	10.0	0.5
Sr	550.0	105.0	60.0	85.0	85.0	80.0	60.0	55.0	145.0	80.0	70.0	85.0	130.0	55.0	130.0	125.0	175.0	120.0	200.0	150.0	55.0	135.0
Ta	1.0	3.0	4.0	3.0	6.0	6.0	5.0	6.0	5.0	4.0	4.0	4.0	3.0	5.0	4.0	3.0	4.0	4.0	2.0	4.0	5.0	3.0
Te	2.5	2.5	2.5	2.5	2.5	2.5	2.5	2.5	2.5	2.5	2.5	2.5	2.5	2.5	2.5	2.5	2.5	2.5	2.5	2.5	2.5	2.5
Tl	1.5	1.5	1.5	1.5	1.5	1.5	1.5	1.5	1.5	1.5	1.5	1.5	1.5	1.5	1.5	1.5	1.5	1.5	1.5	1.5	1.5	1.5
Th	11.5	33.0	20.0	23.0	23.0	24.0	22.5	23.5	31.0	21.0	25.0	21.5	29.5	18.5	20.0	30.0	27.5	27.5	22.0	30.5	46.0	27.5
U	2.0	4.5	2.5	3.0	3.5	5.0	4.5	5.5	5.0	4.0	3.5	4.0	3.0	4.0	4.0	4.0	5.5	3.0	5.0	5.0	4.0	7.0
W	1.5	1.5	1.5	1.5	4.0	1.5	1.5	1.5	1.5	1.5	1.5	1.5	1.5	1.5	1.5	1.5	1.5	1.5	1.5	1.5	1.5	1.5
Y	47.0	19.0	36.0	41.0	47.0	49.0	50.0	46.0	51.0	37.0	45.0	44.0	39.0	44.0	37.0	49.0	42.0	37.0	29.0	36.0	38.0	43.0
Zr	400.0	140.0	380.0	330.0	750.0	800.0	800.0	800.0	410.0	650.0	800.0	700.0	330.0	600.0	750.0	410.0	450.0	320.0	410.0	370.0	200.0	370.0

# Gawler Range Volcanics

SAMPNO	R370973	R370970	R370947	R370975	R370942	R370945	R370948	R370950	R370953	R370954	R370958	R370959	R370962	R370949	R370955	R370961	R370963	R370967	R370969	R370971	R370974	R370977
GROUP	Myn	Myp	Myw	Myw	Myy	Myy	Myy	Myy	Myy	Myy	Myy	Myy	Myz	Myz	Myz	Myz	Myz	Myz	Myz	Myz	Myz	Myz
Easting	485883	486568	498432	492406	496144	499292	494046	494480	492334	489064	491469	491225	492047	492734	488999	491773	492212	486976	486370	487475	491059	482868
Northing	6495892	6496205	6487590	6488685	6493450	6497290	6494722	6491300	6499695	6493386	6500169	6498825	6497974	6494585	6493370	6497969	6497149	6496149	6496157	6498555	6489929	6489648
Rare earth elements (ppm)																						
Ce	140.0	95.0	290.0	165.0	150.0	175.0	170.0	195.0	220.0	160.0	220.0	170.0	135.0	185.0	175.0	175.0	165.0	74.0	120.0	150.0	165.0	175.0
Dy	10.0	2.5	7.5	8.0	8.0	9.0	9.0	10.0	9.0	7.5	8.5	8.5	7.5	8.0	7.0	8.5	7.5	5.5	6.5	7.5	7.0	7.5
Er	5.0	2.0	4.0	4.0	4.0	4.0	5.0	4.0	5.0	4.0	4.0	4.0	4.0	4.0	4.0	4.0	4.0	4.0	3.0	4.0	4.0	4.0
Eu	3.0	0.3	1.5	1.5	2.0	2.0	1.5	2.0	1.5	2.0	2.0	1.5	1.0	1.0	1.5	1.5	1.5	0.5	1.5	2.0	0.5	1.5
Gd	11.0	3.0	10.0	8.0	9.0	9.0	10.0	10.0	10.0	9.0	9.0	8.0	7.0	8.0	8.0	8.0	7.0	3.0	6.0	8.0	6.0	8.0
Ho	1.5	0.5	1.5	1.5	1.5	1.5	1.5	1.5	2.0	1.5	1.5	1.5	1.5	1.5	1.5	1.5	1.5	1.5	1.0	1.5	1.5	1.5
La	67.0	49.0	150.0	68.0	76.0	91.0	87.0	99.0	110.0	80.0	105.0	66.0	69.0	91.0	100.0	98.0	92.0	23.0	54.0	77.0	71.0	96.0
Lu	0.5	0.3	0.5	0.5	0.5	0.5	1.0	0.5	1.0	0.5	0.5	0.5	0.5	0.5	0.5	0.5	0.5	0.5	0.5	0.5	1.0	0.5
Nd	60.0	18.0	94.0	51.0	49.0	58.0	53.0	69.0	64.0	58.0	61.0	49.0	42.0	54.0	59.0	51.0	51.0	12.5	33.5	49.5	40.0	56.0
Pr	15.0	6.0	25.0	13.0	13.0	15.0	14.0	18.0	17.0	15.0	16.0	12.0	12.0	15.0	15.0	15.0	12.0	3.0	9.0	13.0	12.0	14.0
Sm	1.5	2.0	11.5	8.0	8.0	9.0	8.0	10.0	7.0	8.0	9.0	7.0	5.0	3.5	2.5	7.0	6.0	1.5	4.0	6.5	6.0	7.5
Tb	1.5	0.3	1.5	1.0	1.5	1.5	1.5	1.5	1.5	1.5	1.5	1.5	1.0	1.5	1.0	1.5	1.0	1.0	1.0	1.5	1.0	1.0
Tm	0.5	0.5	0.5	0.5	0.5	0.5	0.5	0.5	0.5	0.5	0.5	0.5	0.5	0.5	0.5	0.5	0.5	0.5	0.5	0.5	0.5	0.5
Yb	4.0	2.0	4.0	4.0	4.0	4.0	4.0	4.0	5.0	4.0	4.0	5.0	4.0	4.0	4.0	4.0	4.0	4.0	3.0	4.0	5.0	4.0
Economic elements (ppm)																						
Cu	13.0	7.0	2.0	2.0	4.0	4.0	14.0	3.0	1.0	17.0	2.0	3.0	4.0	4.0	3.0	4.0	13.0	2.0	9.0	26.0	2.0	6.0
Pb	22.0	4.0	4.0	1.5	6.0	24.0	4.0	6.0	1.5	8.0	1.5	4.0	4.0	6.0	4.0	4.0	42.0	6.0	12.0	30.0	6.0	12.0
Zn	125.0	4.0	9.0	43.0	69.0	78.0	77.0	74.0	39.0	69.0	99.0	64.0	46.0	52.0	89.0	67.0	71.0	27.0	46.0	62.0	20.0	60.0
Ni	9.0	3.0	2.0	2.0	3.0	3.0	2.0	2.0	5.0	3.0	3.0	2.0	3.0	4.0	5.0	3.0	3.0	2.0	6.0	3.0	2.0	3.0



# Gawler Range Volcanics

SAMPNO R370979 R370984 R370986 R370987

GROUP Myz Myz Myz Myz

Easting 483175 485542 486457 484413

Northing 6490294 6490059 6491760 6493523

## Major elements (wt%)

SiO <sub>2</sub>	73.90	66.40	67.30	72.90
Al <sub>2</sub> O <sub>3</sub>	12.10	13.60	13.70	12.10
CaO	0.35	1.40	0.74	0.24
Fe <sub>2</sub> O <sub>3</sub>	2.39	4.47	4.23	2.03
K <sub>2</sub> O	6.20	5.15	5.51	6.18
MgO	0.20	1.19	1.25	0.29
MnO	0.04	0.08	0.07	0.03
Na <sub>2</sub> O	2.68	3.31	3.02	2.65
P <sub>2</sub> O <sub>5</sub>	0.05	0.18	0.17	0.03
TiO <sub>2</sub>	0.20	0.62	0.61	0.21
LOI	0.8	1.6	1.7	1.1

## Trace elements (ppm)

Be	3.0	2.0	2.0	3.0
Sc	2.5	10.0	10.0	2.5
V	20	50	40	10
Cr	30	10	10	10
As	1.0	2.0	2.0	1.0
Ba	950	1450	1550	2750
Bi	1.5	1.5	1.5	1.5
Cd	1.5	1.5	1.5	1.5
Co	0.5	8.0	5.0	0.5
Cs	4.0	1.5	4.0	1.5
Ga	18.0	25.0	24.0	21.0
Hf	8.0	10.0	10.0	7.0
In	0.3	0.3	0.3	0.3
Mo	4.0	4.0	2.0	4.0
Nb	25.0	25.0	25.0	25.0
Rb	280.0	195.0	200.0	260.0
Sb	6.0	5.0	5.0	5.0
Sn	0.5	0.5	0.5	0.5
Sr	65.0	150.0	140.0	75.0
Ta	6.0	5.0	5.0	4.0
Te	2.5	2.5	2.5	2.5
Tl	1.5	1.5	1.5	1.5
Th	34.5	24.5	25.5	32.0
U	2.5	4.5	3.0	2.0
W	1.5	1.5	1.5	1.5
Y	47.0	39.0	41.0	45.0
Zr	280.0	440.0	430.0	260.0

# **Gawler Range Volcanics**

**SAMPNO** R370979 R370984 R370986 R370987

**GROUP** Myz Myz Myz Myz

**Easting** 483175 485542 486457 484413

**Northing** 6490294 6490059 6491760 6493523

## **Rare earth elements (ppm)**

<b>Ce</b>	200.0	155.0	155.0	195.0
<b>Dy</b>	9.0	7.5	7.0	7.5
<b>Er</b>	5.0	4.0	4.0	4.0
<b>Eu</b>	1.0	2.0	2.0	1.0
<b>Gd</b>	9.0	8.0	8.0	9.0
<b>Ho</b>	2.0	1.5	1.5	1.5
<b>La</b>	98.0	86.0	89.0	105.0
<b>Lu</b>	1.0	0.5	0.5	0.5
<b>Nd</b>	57.0	51.0	49.5	55.0
<b>Pr</b>	16.0	13.0	13.0	14.0
<b>Sm</b>	8.5	6.5	6.5	6.5
<b>Tb</b>	1.5	1.5	1.0	1.5
<b>Tm</b>	0.5	0.5	0.5	0.5
<b>Yb</b>	5.0	4.0	4.0	4.0

## **Economic elements (ppm)**

<b>Cu</b>	3.0	7.0	3.0	3.0
<b>Pb</b>	6.0	12.0	6.0	1.5
<b>Zn</b>	8.0	65.0	68.0	31.0
<b>Ni</b>	2.0	4.0	6.0	6.0

### Munjeela Granite

SAMPNO	R368576	R389867	R389869	1077-118	1077-120	1077-122	1077-123	1077-143	1077-144	1077-129	1077-121
GROUP	Munjeela	Munjeela	Munjeela	Munjeela	Munjeela	Munjeela	Munjeela	Munjeela	Munjeela	Munjeela	Munjeela
Easting	309100	309545	323390	309240	323390	246806	246806	336838	336838	350273	263343
Northing	6446100	6446716	6434860	6445790	6434860	6463710	6463710	6479630	6479630	6471116	6469912
Major elements (wt%)											
SiO <sub>2</sub>	71.90	72.40	73.40	72.42	74.53	73.29	67.53	72.45	70.44	74.44	72.90
Al <sub>2</sub> O <sub>3</sub>	14.70	14.50	13.10	14.80	14.09	13.68	13.94	14.12	15.49	14.42	13.35
CaO	0.82	0.85	0.87	0.93	0.54	0.89	2.77	0.60	0.76	0.33	1.51
Fe <sub>2</sub> O <sub>3</sub>	0.87	1.44	2.15	1.16	0.78	1.90	5.63	1.08	1.72	0.93	2.33
K <sub>2</sub> O	5.57	5.28	5.23	5.60	4.92	5.34	4.23	5.59	5.26	3.64	5.07
MgO	0.25	0.35	0.44	0.35	0.19	0.53	1.22	0.28	0.55	0.15	0.61
MnO	0.10	0.14	0.12	0.10	0.06	0.12	0.18	0.14	0.12	0.62	0.10
Na <sub>2</sub> O	3.38	3.15	2.64	3.46	3.50	2.91	2.82	2.94	3.80	4.56	2.86
P <sub>2</sub> O <sub>5</sub>	0.12	0.14	0.16	0.15	0.08	0.15	0.23	0.20	0.16	0.14	0.11
TiO <sub>2</sub>	0.10	0.14	0.29	0.12	0.09	0.29	0.91	0.12	0.19	0.02	0.38
LOI	0.8	0.9	0.7	0.5	0.5	0.7	0.6	0.7	0.8	0.5	0.5
Trace elements (ppm)											
Be	13.0	10.0	3.0								
Sc	2.5	5.0	10.0	4.1	6.7	7.7	16.6	3.6	6.2	1.9	7.6
V	10	10	10	12	11	18	67	11	17	5	26
Cr	20	10	10	237	256	1	6	240	213	233	2.00
As	0.5	1.0	1.0	1.0	1.1	1.0	1.0	1.0	1.3	1.0	1.0
Ba	280	310	380	265	214	390	656	280	408	100	605
Bi	1.5	1.5	1.5								
Cd	1.5	1.5	1.5								
Co	1.0	2.0	3.0	3.0	3.0	107.0	45.0	4.0	6.0	1.0	80.0
Cs	36.0	51.0	34.0	38.8	24.3	31.8	11.0	37.9	34.5	36.2	28.8
Ga	18.0	15.0	15.0	14.9	16.4	16.5	20.4	18.6	18.1	19.9	16.3
Hf	1.0	3.0	3.0	1.9	1.2	5.8	7.6	1.3	3.4	1.0	5.6
In	0.3	1.0	0.5								
Mo	1.0	3.0	3.0	5.0	5.7	20.0	5.0	10.0	10.0	10.0	8.5
Nb	10.0	25.0	25.0	18.8	19.2	28.9	18.9	35.6	32.3	42.1	22.2
Rb	290.0	330.0	400.0	338.1	337.7	422.6	211.5	519.3	498.6	483.0	352.8
Sb	3.0	1.0	0.5	0.2	0.2	0.2	0.2	0.2	0.2	0.2	0.2
Sn	0.5	5.0	5.0								
Sr	55.0	55.0	55.0	62.5	182.1	56.3	136.7	41.4	70.7	8.1	83.8
Ta	1.0	3.0	3.0	3.7	1.7	5.2	4.0	5.6	3.9	4.5	4.4
Te	2.5	2.5	2.5	5.0	5.0	5.0	5.0	5.0	5.0	5.0	5.0
Tl	1.5	1.5	1.5								
Th	9.5	10.5	21.5	13.9	10.4	31.4	27.6	13.9	42.6	1.2	33.6
U	3.0	4.0	11.0	3.4	5.0	12.8	4.7	8.8	9.2	6.0	7.2
W	320.0	4.0	6.0	4.1	3.4	709.0	231.0	4.1	3.0	5.5	533.0
Y	25.0	34.0	52.0	43.8	25.3	58.8	69.4	21.6	46.9	7.5	81.1
Zr	60.0	80.0	120.0	83.2	56.3	157.2	272.2	56.6	131.2	38.4	170.9

### Munjeela Granite

SAMPNO	R368576	R389867	R389869	1077-118	1077-120	1077-122	1077-123	1077-143	1077-144	1077-129	1077-121
GROUP	Munjeela	Munjeela	Munjeela	Munjeela	Munjeela	Munjeela	Munjeela	Munjeela	Munjeela	Munjeela	Munjeela
Easting	309100	309545	323390	309240	323390	246806	246806	336838	336838	350273	263343
Northing	6446100	6446716	6434860	6445790	6434860	6463710	6463710	6479630	6479630	6471116	6469912
Rare earth elements (ppm)											
Ce	35.0	46.0	80.0	49.3	36.7	97.8	125.0	42.6	118.0	6.3	119.0
Dy	4.0	6.0	7.0								
Er	3.0	2.0	4.0								
Eu	0.3	0.3	0.5	0.6	0.5	0.7	2.2	0.5	0.5	0.5	0.9
Gd	4.0	4.0	8.0								
Ho	1.0	1.0	2.0								
La	19.0	25.0	42.0	20.0	14.0	36.0	60.0	16.0	42.0	3.0	45.0
Lu	0.3	0.3	0.5								
Nd	16.0	19.5	38.5	16.0	10.0	38.0	55.0	14.0	42.0	1.0	40.0
Pr	4.0	5.0	9.0								
Sm	2.0	4.0	7.0	5.1	2.8	9.4	11.6	4.1	11.0	0.9	9.7
Tb	0.5	1.0	1.5	0.9	0.6	1.8	2.1	0.7	1.9	0.5	2.3
Tm	0.5	0.5	0.5								
Yb	3.0	3.0	5.0	3.5	2.2	5.3	6.2	1.8	3.6	0.9	8.4
Economic elements (ppm)											
Cu	32.0	20.0	17.0	15.0	15.0	20.0	25.0	14.0	37.0	15.0	20.0
Pb	8.0	8.0	10.0	36.1	37.2	30.4	30.8	28.2	32.3	8.4	33.6
Zn	24.0	35.0	40.0	27.0	11.0	40.0	81.0	41.0	53.0	17.0	40.0
Ni	1.0	2.0	4.0	11.0	8.0	7.0	4.0	10.0	11.0	8.0	4.0



## **APPENDIX B**

### **GEOCHRONOLOGY DATA TABLES**

## Sample R469813

Spot	% $^{206}\text{Pb}_c$	ppm U	ppm Th	$^{232}\text{Th}$ / $^{238}\text{U}$	ppm $^{206}\text{Pb}^*$	(1) $^{207}\text{Pb}^*$ / $^{206}\text{Pb}^*$	(1) $^{207}\text{Pb}^*$ / $^{235}\text{U}$	(1) $^{206}\text{Pb}^*$ / $^{238}\text{U}$	err corr	(1) $^{206}\text{Pb}$ / $^{238}\text{U}$ Age	(1) $^{207}\text{Pb}$ / $^{206}\text{Pb}$ Age	% Dis- cor- dant
1.1	0.03	514	347	0.70	123	0.09918 ± 0.00035	3.808 ± 0.045	0.2785 ± 0.0032	.953	1,584 ± 16	1,608.7 ± 6.7	2
2.1	0.74	487	419	0.89	109	0.09591 ± 0.00066	3.425 ± 0.045	0.2590 ± 0.0029	.854	1,485 ± 15	1,546 ± 13	4
3.1	0.04	403	206	0.53	97.6	0.09878 ± 0.00041	3.836 ± 0.047	0.2817 ± 0.0032	.941	1,600 ± 16	1,601.3 ± 7.7	0
4.1	--	443	258	0.60	110	0.09962 ± 0.00035	3.954 ± 0.047	0.2879 ± 0.0033	.955	1,631 ± 16	1,617.0 ± 6.6	-1
5.1	0.06	537	137	0.26	129	0.09915 ± 0.00037	3.813 ± 0.045	0.2789 ± 0.0032	.949	1,586 ± 16	1,608.1 ± 7.0	1
6.1	0.03	596	370	0.64	144	0.09938 ± 0.00032	3.856 ± 0.045	0.2814 ± 0.0032	.961	1,599 ± 16	1,612.5 ± 6.0	1
7.1	0.22	300	168	0.58	73.8	0.10014 ± 0.00056	3.952 ± 0.051	0.2862 ± 0.0033	.901	1,623 ± 17	1,627 ± 10	0
8.1	0.28	466	439	0.97	101	0.09953 ± 0.00053	3.447 ± 0.043	0.2512 ± 0.0028	.905	1,445 ± 15	1,615.3 ± 9.9	11
8.2	0.49	425	311	0.75	105	0.0999 ± 0.0010	3.944 ± 0.061	0.2863 ± 0.0033	.738	1,623 ± 16	1,622 ± 19	0
9.1	0.08	399	12	0.03	96.9	0.09941 ± 0.00042	3.873 ± 0.047	0.2826 ± 0.0032	.938	1,604 ± 16	1,613.0 ± 7.8	1
10.1	0.05	470	373	0.82	116	0.09914 ± 0.00035	3.917 ± 0.047	0.2865 ± 0.0032	.954	1,624 ± 16	1,608.0 ± 6.7	-1
11.1	0.06	318	211	0.69	76.1	0.09965 ± 0.00042	3.825 ± 0.047	0.2784 ± 0.0032	.939	1,583 ± 16	1,617.5 ± 7.9	2
12.1	0.12	359	198	0.57	85.9	0.09881 ± 0.00047	3.788 ± 0.047	0.2780 ± 0.0032	.924	1,581 ± 16	1,601.7 ± 8.9	1
13.1	0.03	612	567	0.96	148	0.09925 ± 0.00030	3.851 ± 0.045	0.2814 ± 0.0032	.965	1,599 ± 16	1,610.1 ± 5.7	1
14.1	0.03	508	561	1.14	123	0.09997 ± 0.00032	3.867 ± 0.045	0.2805 ± 0.0032	.963	1,594 ± 16	1,623.4 ± 5.9	2
15.1	0.54	364	306	0.87	87.3	0.09872 ± 0.00064	3.783 ± 0.050	0.2779 ± 0.0032	.871	1,581 ± 16	1,600 ± 12	1
16.1	0.03	402	253	0.65	97.9	0.10055 ± 0.00040	3.930 ± 0.048	0.2834 ± 0.0032	.944	1,609 ± 16	1,634.3 ± 7.4	2
17.1	0.32	464	312	0.70	114	0.09875 ± 0.00056	3.877 ± 0.049	0.2847 ± 0.0032	.895	1,615 ± 16	1,601 ± 11	-1
18.1	0.02	914	229	0.26	222	0.09927 ± 0.00026	3.862 ± 0.044	0.2821 ± 0.0032	.973	1,602 ± 16	1,610.5 ± 4.9	1
19.1	0.07	580	409	0.73	141	0.09939 ± 0.00040	3.864 ± 0.046	0.2820 ± 0.0032	.942	1,601 ± 16	1,612.6 ± 7.5	1

Errors are 1-sigma;  $\text{Pb}_c$  and  $\text{Pb}^*$  indicate the common and radiogenic portions, respectively.

Error in Standard calibration was 0.20% (not included in above errors).

(1) Common Pb corrected using measured  $^{204}\text{Pb}$ .

## Sample R469740

Spot	% % $^{206}\text{Pb}_c$	ppm U	ppm Th	$^{232}\text{Th}$ / $^{238}\text{U}$	ppm $^{206}\text{Pb}^*$	(1) $^{207}\text{Pb}^*$ / $^{206}\text{Pb}^*$	(1) $^{207}\text{Pb}^*$ / $^{235}\text{U}$	(1) $^{206}\text{Pb}^*$ / $^{238}\text{U}$	err corr	(1) $^{206}\text{Pb}$ / $^{238}\text{U}$ Age	(1) $^{207}\text{Pb}$ / $^{206}\text{Pb}$ Age	% Dis- cor- dant
1.1	0.18	54	83	1.59	13.0	0.0988 ±0.0011	3.829 ±0.069	0.2812 ±0.0040	.786	1,597 ±20	1,601 ± 21	0
1.2	0.32	69	122	1.81	17.6	0.0971 ±0.0011	3.936 ±0.092	0.2939 ±0.0059	.866	1,661 ±30	1,569 ± 22	-6
2.1	0.23	114	103	0.94	27.5	0.09594 ±0.00086	3.713 ±0.058	0.2807 ±0.0036	.816	1,595 ±18	1,547 ± 17	-3
2.2	0.65	81	82	1.05	18.8	0.0968 ±0.0014	3.605 ±0.071	0.2700 ±0.0036	.672	1,541 ±18	1,564 ± 27	2
3.1	0.42	74	79	1.10	17.6	0.0989 ±0.0012	3.785 ±0.069	0.2776 ±0.0037	.739	1,579 ±19	1,603 ± 23	1
4.1	0.16	152	215	1.47	35.4	0.09790 ±0.00067	3.667 ±0.057	0.2717 ±0.0038	.896	1,549 ±19	1,584 ± 13	2
4.2	0.15	152	223	1.51	34.2	0.09847 ±0.00066	3.54 ±0.12	0.2610 ±0.0086	.980	1,495 ±44	1,595 ± 13	6
5.1	0.60	47	105	2.29	11.6	0.0966 ±0.0018	3.785 ±0.090	0.2841 ±0.0043	.641	1,612 ±22	1,560 ± 34	-3
6.1	0.95	120	149	1.29	23.1	0.0975 ±0.0015	2.988 ±0.063	0.2223 ±0.0033	.703	1,294 ±17	1,577 ± 28	18
7.1	0.08	219	230	1.08	51.3	0.09767 ±0.00055	3.669 ±0.048	0.2724 ±0.0032	.904	1,553 ±16	1,580 ± 10	2
8.1	0.04	82	118	1.48	19.5	0.09918 ±0.00091	3.790 ±0.069	0.2772 ±0.0043	.862	1,577 ±22	1,609 ± 17	2
9.1	0.13	138	148	1.10	32.6	0.09750 ±0.00074	3.679 ±0.053	0.2737 ±0.0034	.851	1,559 ±17	1,577 ± 14	1
10.1	0.16	148	165	1.15	35.4	0.09740 ±0.00076	3.726 ±0.055	0.2775 ±0.0035	.849	1,579 ±17	1,575 ± 15	0
11.1	0.65	218	260	1.23	47.8	0.0985 ±0.0020	3.449 ±0.081	0.2539 ±0.0031	.516	1,459 ±16	1,596 ± 38	9
12.1	4.42	305	568	1.93	59.0	0.0980 ±0.0065	2.92 ±0.20	0.2157 ±0.0033	.225	1,259 ±18	1,587 ±120	21
13.1	1.14	156	166	1.10	33.3	0.0965 ±0.0019	3.269 ±0.076	0.2457 ±0.0031	.540	1,416 ±16	1,558 ± 37	9
13.2	0.14	79	70	0.91	19.1	0.0972 ±0.0011	3.769 ±0.065	0.2811 ±0.0037	.770	1,597 ±19	1,572 ± 21	-2
14.1	0.19	139	168	1.25	33.2	0.09811 ±0.00078	3.745 ±0.055	0.2768 ±0.0034	.841	1,575 ±17	1,589 ± 15	1
16.1	0.57	92	108	1.22	21.1	0.0955 ±0.0012	3.497 ±0.068	0.2656 ±0.0039	.747	1,518 ±20	1,537 ± 24	1
17.1	0.15	147	144	1.02	34.2	0.09790 ±0.00069	3.663 ±0.052	0.2714 ±0.0033	.866	1,548 ±17	1,584 ± 13	2
18.1	2.75	265	384	1.50	42.0	0.0983 ±0.0025	2.434 ±0.068	0.1796 ±0.0022	.438	1,065 ±12	1,592 ± 47	33
19.1	1.02	194	474	2.53	56.0	0.0972 ±0.0015	4.463 ±0.092	0.3330 ±0.0044	.637	1,853 ±21	1,571 ± 30	-18
20.1	0.49	212	310	1.51	45.4	0.09792 ±0.00087	3.341 ±0.050	0.2475 ±0.0029	.801	1,425 ±15	1,585 ± 17	10
21.1	1.40	215	365	1.76	45.8	0.0993 ±0.0010	3.345 ±0.053	0.2444 ±0.0029	.754	1,409 ±15	1,611 ± 19	12
22.1	0.32	186	180	1.00	44.8	0.09752 ±0.00065	3.765 ±0.056	0.2800 ±0.0037	.894	1,592 ±19	1,577 ± 13	-1
23.1	0.16	72	61	0.88	16.9	0.0976 ±0.0010	3.694 ±0.062	0.2746 ±0.0036	.787	1,564 ±18	1,578 ± 19	1

Errors are 1-sigma;  $\text{Pb}_c$  and  $\text{Pb}^*$  indicate the common and radiogenic portions, respectively.

Error in Standard calibration was 0.20% (not included in above errors).

(1) Common Pb corrected using measured  $^{204}\text{Pb}$ .

Sample R469578

Spot	% 206Pb <sub>c</sub>	ppm U	ppm Th	232Th /238U	ppm 206Pb*	(1) 207Pb* /206Pb*	(1) 207Pb* /235U	(1) 206Pb* /238U	err corr	(1) 206Pb /238U Age	(1) 207Pb /206Pb Age	% Dis- cor- dant
1.1	2.18	1271	909	0.74	214	0.09112 ±0.00098	2.405 ±0.045	0.1914 ±0.0029	.818	1,129 ±16	49 ±20	22
2.1	0.25	338	234	0.71	80.9	0.10376 ±0.00053	3.975 ±0.050	0.2778 ±0.0032	.914	1,580 ±16	92.5 ± 9.	7
3.1	0.21	389	191	0.51	92.0	0.09879 ±0.00046	3.747 ±0.049	0.2751 ±0.0034	.935	1,567 ±17	01.4 ± 8.	2
5.1	0.10	227	198	0.90	57.6	0.10275 ±0.00055	4.189 ±0.063	0.2957 ±0.0042	.935	1,670 ±21	74.4 ± 9.	0
5.2	0.07	206	69	0.34	55.2	0.10309 ±0.00054	4.417 ±0.057	0.3108 ±0.0037	.913	1,744 ±18	80.5 ± 9.	-4
12.1	0.10	238	191	0.83	57.7	0.09937 ±0.00060	3.863 ±0.051	0.2819 ±0.0033	.891	1,601 ±17	12 ±11	1
12.2	0.67	211	175	0.85	48.3	0.09917 ±0.00096	3.611 ±0.058	0.2641 ±0.0034	.796	1,511 ±17	09 ±18	6
13.1	0.22	255	285	1.16	61.8	0.09837 ±0.00060	3.822 ±0.050	0.2818 ±0.0033	.887	1,601 ±17	93 ±11	0
13.2	0.11	240	271	1.16	57.0	0.09941 ±0.00053	3.785 ±0.050	0.2761 ±0.0033	.914	1,572 ±17	13.1 ± 9.	3
14.1	0.31	450	122	0.28	107	0.10026 ±0.00049	3.813 ±0.047	0.2758 ±0.0031	.917	1,570 ±16	29.0 ± 9.	4
17.1	0.30	141	155	1.14	33.5	0.09915 ±0.00084	3.778 ±0.056	0.2763 ±0.0034	.821	1,573 ±17	08 ±16	2
17.2	0.10	107	131	1.26	25.7	0.09988 ±0.00084	3.848 ±0.068	0.2794 ±0.0043	.879	1,589 ±22	22 ±16	2
17.3	0.42	123	132	1.11	30.7	0.09756 ±0.00094	3.888 ±0.061	0.2891 ±0.0036	.793	1,637 ±18	78 ±18	-4
18.1	0.52	363	281	0.80	87.3	0.09960 ±0.00052	3.820 ±0.048	0.2782 ±0.0032	.909	1,582 ±16	16.5 ± 9.	2
20.1	0.81	228	99	0.45	53.1	0.0996 ±0.0011	3.686 ±0.060	0.2685 ±0.0031	.718	1,533 ±16	16 ±21	5

Errors are 1-sigma; Pb<sub>c</sub> and Pb\* indicate the common and radiogenic portions, respectively.

Error in Standard calibration was 0.20% (not included in above errors).

(1) Common Pb corrected using measured <sup>204</sup>Pb.



Sample R387446.

Grain spot	U (ppm)	Th (ppm)	Th/U (ppm)	Pb* (ppm)	<sup>204</sup> Pb/ <sup>206</sup> Pb	f <sub>206</sub> %	Radiogenic Ratios						Ages (in Ma)				Conc. %	
							<sup>206</sup> Pb/ <sup>238</sup> U	<sup>207</sup> Pb/ ±	<sup>207</sup> Pb/ <sup>235</sup> U	<sup>207</sup> Pb/ ±	<sup>207</sup> Pb/ <sup>206</sup> Pb	<sup>206</sup> Pb/ <sup>238</sup> U	<sup>207</sup> Pb/ ±	<sup>207</sup> Pb/ <sup>235</sup> U	<sup>207</sup> Pb/ <sup>206</sup> Pb			
							±	±	±	±	±	±	±	±	±			
1.1	66	47	0.71	18	0.000030	0.05	0.2908	0.0046	4.064	0.080	0.1014	0.0010	1645	23	1647	1649	#	100
2.1	101	78	0.77	27	0.000119	0.19	0.2899	0.0047	3.933	0.074	0.0984	0.0008	1641	23	1621	1594	#	103
3.1	86	66	0.77	24	0.000101	0.16	0.2957	0.0145	4.200	0.220	0.1030	0.0014	1670	73	1674	1679	#	100
4.1	61	46	0.75	16	0.000653	1.04	0.2848	0.0047	3.731	0.092	0.0950	0.0016	1616	24	1578	1528	#	106
5.1	232	131	0.57	61	0.000024	0.04	0.2947	0.0039	4.057	0.061	0.0999	0.0006	1665	19	1646	1621	#	103
6.1	46	32	0.69	12	0.000109	0.17	0.2941	0.0058	3.959	0.098	0.0976	0.0013	1662	29	1626	1579	#	105
7.1	83	61	0.72	23	-	<0.01	0.2954	0.0045	4.040	0.072	0.0992	0.0007	1669	22	1642	1609	#	104
8.1	214	122	0.57	56	-	<0.01	0.2941	0.0037	4.063	0.059	0.1002	0.0006	1662	19	1647	1628	#	102
9.1	307	188	0.61	80	0.000017	0.03	0.2902	0.0035	3.991	0.054	0.0997	0.0005	1643	18	1632	1619	9	102
10.1	177	100	0.56	46	0.000062	0.10	0.2949	0.0038	4.061	0.060	0.0999	0.0006	1666	19	1647	1622	#	103
11.1	174	97	0.56	46	0.000010	0.02	0.2965	0.0041	4.067	0.064	0.0995	0.0006	1674	20	1648	1614	#	104
12.1	60	42	0.70	16	-	<0.01	0.2888	0.0047	4.023	0.084	0.1010	0.0011	1636	24	1639	1643	#	100
13.1	63	44	0.70	17	-	<0.01	0.2951	0.0054	4.143	0.125	0.1018	0.0022	1667	27	1663	1657	#	101
14.1	32	19	0.59	8	0.000181	0.29	0.2920	0.0062	3.908	0.107	0.0971	0.0014	1651	31	1615	1569	#	105
14.2	88	49	0.56	23	0.000007	0.01	0.2914	0.0049	4.022	0.081	0.1001	0.0009	1648	25	1639	1626	#	101
15.1	294	160	0.54	77	0.000029	0.05	0.2947	0.0062	4.057	0.119	0.0999	0.0018	1665	31	1646	1622	#	103
16.1	72	39	0.55	19	0.000106	0.17	0.2957	0.0057	4.079	0.104	0.1001	0.0015	1670	29	1650	1625	#	103
17.1	58	41	0.71	16	-	<0.01	0.2926	0.0059	4.077	0.093	0.1011	0.0009	1655	29	1650	1644	#	101
18.1	50	37	0.73	14	0.000010	0.02	0.2958	0.0071	4.032	0.112	0.0989	0.0011	1670	36	1641	1603	#	104
19.1	49	32	0.65	13	0.000246	0.39	0.2863	0.0073	3.872	0.128	0.0981	0.0018	1623	37	1608	1588	#	102

Notes :

1. Uncertainties given at the one  $\sigma$  level.
2. f<sub>206</sub> % denotes the percentage of <sup>206</sup>Pb that is common Pb.
3. Correction for common Pb made using the measured <sup>204</sup>Pb/<sup>206</sup>Pb ratio.
4. For % Conc., 100% denotes a concordant analysis.

Sample R387444.

Grain spot	U (ppm)	Th (ppm)	Th/U	Pb* (ppm)	<sup>204</sup> Pb/ <sup>206</sup> Pb	f <sub>206</sub> %	Radiogenic Ratios					Ages (in Ma)					Conc. %	
							<sup>206</sup> Pb/ <sup>238</sup> U	<sup>207</sup> Pb/ <sup>235</sup> U		<sup>207</sup> Pb/ <sup>206</sup> Pb		<sup>206</sup> Pb/ <sup>238</sup> U	<sup>207</sup> Pb/ <sup>235</sup> U		<sup>207</sup> Pb/ <sup>206</sup> Pb			
							±	±	±	±	±	±	±	±	±			
1.1	1032	510	0.49	256	0.000205	0.33	0.2827	0.0033	3.813	0.049	0.0978	0.0004	1605	17	1596	1583	8	101
2.1	371	120	0.32	91	0.000029	0.05	0.2901	0.0033	4.148	0.055	0.1037	0.0006	1642	16	1664	1692	11	97
3.1	431	178	0.41	110	0.000018	0.03	0.2977	0.0038	4.280	0.062	0.1043	0.0006	1680	19	1689	1701	10	99
4.1	1083	205	0.19	233	0.000134	0.21	0.2667	0.0029	3.578	0.044	0.0973	0.0004	1524	15	1545	1573	8	97
4.2	1498	429	0.29	333	0.000091	0.15	0.2679	0.0028	3.540	0.040	0.0958	0.0003	1530	14	1536	1544	5	99
5.1	1625	549	0.34	309	0.008365	13.34	0.2267	0.0024	2.873	0.060	0.0919	0.0015	1317	13	1375	1466	32	90
6.1	186	124	0.67	50	0.000006	0.01	0.2928	0.0038	4.025	0.064	0.0997	0.0008	1655	19	1639	1619	15	102
7.1	170	158	0.93	46	0.000143	0.23	0.2763	0.0039	3.764	0.065	0.0988	0.0008	1573	20	1585	1602	16	98
7.2	1402	465	0.33	304	0.000657	1.05	0.2573	0.0028	3.441	0.046	0.0970	0.0007	1476	14	1514	1567	13	94
8.1	93	77	0.83	27	0.000038	0.06	0.3105	0.0051	4.377	0.081	0.1023	0.0007	1743	25	1708	1666	13	105
8.2	1566	713	0.46	356	0.000044	0.07	0.2614	0.0028	3.559	0.042	0.0988	0.0004	1497	14	1540	1601	7	94
9.1	3008	1746	0.58	838	-	<0.01	0.3113	0.0032	4.518	0.048	0.1053	0.0002	1747	16	1734	1719	3	102
10.1	285	558	1.95	93	0.000581	0.93	0.2734	0.0035	3.703	0.066	0.0982	0.0011	1558	18	1572	1591	20	98
11.1	331	208	0.63	80	0.001019	1.62	0.2698	0.0032	3.679	0.059	0.0989	0.0010	1540	16	1567	1603	18	96
12.1	1017	317	0.31	401	0.000010	0.01	0.4497	0.0048	9.798	0.109	0.1580	0.0003	2394	21	2416	2434	3	98
13.1	693	188	0.27	296	0.000003	<0.01	0.4894	0.0060	####	0.189	0.1653	0.0017	2568	26	2536	2510	17	102
14.1	711	296	0.42	184	-	<0.01	0.3007	0.0033	4.355	0.051	0.1051	0.0003	1695	16	1704	1715	5	99
15.1	87	113	1.30	26	-	<0.01	0.2822	0.0089	4.151	0.181	0.1067	0.0028	1602	45	1665	1744	49	92
16.1	273	102	0.38	66	0.000182	0.29	0.2791	0.0035	3.994	0.058	0.1038	0.0006	1587	18	1633	1693	11	94
17.1	991	547	0.55	246	0.000017	0.03	0.2793	0.0031	3.803	0.045	0.0988	0.0003	1588	15	1593	1601	6	99

Notes:

1. Uncertainties given at the one  $\sigma$  level.
2. f<sub>206</sub> % denotes the percentage of <sup>206</sup>Pb that is common Pb.
3. Correction for common Pb made using the measured <sup>204</sup>Pb/<sup>206</sup>Pb ratio.
4. For % Conc., 100% denotes a concordant analysis.

Sample R387442.

Grain. spot	U (ppm)	Th (ppm)	Th/U	Pb* (ppm)	<sup>204</sup> Pb/ <sup>206</sup> Pb	f <sub>206</sub> %	Radiogenic Ratios						Ages (in Ma)						Conc. %
							<sup>206</sup> Pb/ <sup>238</sup> U	±	<sup>207</sup> Pb/ <sup>235</sup> U	±	<sup>207</sup> Pb/ <sup>206</sup> Pb	±	<sup>206</sup> Pb/ <sup>238</sup> U	±	<sup>207</sup> Pb/ <sup>235</sup> U	<sup>207</sup> Pb/ <sup>206</sup> Pb	±		
1.1	208	152	0.73	71	0.000016	0.03	0.3030	0.0039	4.291	0.063	0.1027	0.0006	1706	19	1692	1674	10	102	
2.1	565	199	0.35	175	0.000004	0.01	0.2976	0.0032	4.254	0.049	0.1037	0.0003	1680	16	1684	1691	4	99	
3.1	198	130	0.66	67	0.000015	0.02	0.3041	0.0038	4.302	0.060	0.1026	0.0005	1712	19	1694	1672	8	102	
4.1	179	70	0.39	57	-	<0.01	0.3050	0.0036	4.348	0.060	0.1034	0.0006	1716	18	1703	1686	11	102	
5.1	176	70	0.40	55	-	<0.01	0.2971	0.0037	4.256	0.062	0.1039	0.0006	1677	19	1685	1695	11	99	
6.1	351	181	0.52	116	0.000040	0.06	0.3061	0.0038	4.331	0.060	0.1026	0.0005	1722	19	1699	1672	9	103	
7.1	507	143	0.28	151	0.000003	0.01	0.2934	0.0037	4.144	0.059	0.1024	0.0005	1658	18	1663	1669	10	99	
9.1	334	57	0.17	103	0.000020	0.03	0.3105	0.0037	4.426	0.057	0.1034	0.0004	1743	18	1717	1686	7	103	
10.1	179	84	0.47	57	0.000056	0.09	0.2962	0.0041	4.267	0.066	0.1045	0.0005	1673	21	1687	1705	9	98	
11.1	274	97	0.35	87	-	<0.01	0.3055	0.0036	4.355	0.059	0.1034	0.0005	1718	18	1704	1686	10	102	
12.1	297	1339	4.50	73	-	<0.01	0.1989	0.0030	2.850	0.046	0.1039	0.0005	1169	16	1369	1695	9	69	
13.1	297	112	0.38	93	0.000015	0.02	0.3015	0.0039	4.315	0.063	0.1038	0.0005	1699	20	1696	1693	9	100	
14.1	203	100	0.50	63	-	<0.01	0.2944	0.0037	4.198	0.057	0.1034	0.0004	1663	18	1674	1686	7	99	
15.1	385	97	0.25	114	0.000046	0.07	0.2924	0.0037	4.134	0.060	0.1026	0.0006	1654	19	1661	1671	10	99	
16.1	239	116	0.48	72	0.000105	0.17	0.2818	0.0038	3.959	0.065	0.1019	0.0008	1600	19	1626	1659	15	97	
17.1	750	340	0.45	179	0.000160	0.25	0.2295	0.0026	3.127	0.039	0.0988	0.0004	1332	14	1439	1602	7	83	
17.2	863	704	0.82	204	0.000325	0.51	0.2130	0.0023	2.776	0.036	0.0945	0.0005	1245	12	1349	1518	10	82	
18.1	410	50	0.12	120	0.000013	0.02	0.2994	0.0034	4.268	0.055	0.1034	0.0005	1688	17	1687	1686	9	100	
19.1	244	138	0.57	78	0.000011	0.02	0.2954	0.0036	4.177	0.059	0.1026	0.0006	1668	18	1670	1671	10	100	

Notes :

1. Uncertainties given at the one s level.
2. f<sub>206</sub> % denotes the percentage of <sup>206</sup>Pb that is common Pb.
3. Correction for common Pb made using the measured <sup>204</sup>Pb/<sup>206</sup>Pb ratio.
4. For % Conc., 100% denotes a concordant analysis.

# Munjeela Granite

## Results

Label	W%(Pb)	W%(Th	W%(U )	Age	1sig			Pb	W%(Th	W%(U )
GF gte mon1a	7309.774	88170	3365	2E-05	1580	29	1.942 0.001	0.73098	8.817	0.3365
GF gte mon1b	6871.817	87276	3429	1E-05	1500	29	1.843 0.001	0.68718	8.7276	0.3429
GF gte mon1c	7245.789	87791	3503	6E-07	1565	28	1.941 0.001	0.72458	8.7791	0.3503
GF gte mon2a	9657.476	94360	11507	3E-07	1545	22	3.157 0.002	0.96575	9.436	1.1507
GF gte mon2b	10120.74	95844	12063	2E-09	1576	22	3.379 0.002	1.01207	9.5844	1.2063
GF gte mon5	6814.378	84407	3221	1E-05	1541	29	1.801 0.001	0.68144	8.4407	0.3221
GF gte mon6a	5343.936	61836	1848	7E-06	1685	39	1.121 7E-04	0.53439	6.1836	0.1848
GF gte mon6b	4890.292	63127	2000	7E-06	1511	37	1.075 7E-04	0.48903	6.3127	0.2
GF gte mon7a	8192.551	89009	6258	4E-06	1591	26	2.319 0.001	0.81926	8.9009	0.6258
GF gte mon7b	7737.418	84461	5788	6E-06	1592	27	2.157 0.001	0.77374	8.4461	0.5788
GF gte mon9a	6844.74	84207	2969	2E-05	1564	30	1.747 0.001	0.68447	8.4207	0.2969
GF gte mon9b	6653.748	80446	2850	2E-05	1589	31	1.686 0.001	0.66537	8.0446	0.285
GF gte mon10a	6614.063	82716	3882	2E-05	1488	29	1.757 0.001	0.66141	8.2716	0.3882
GF gte mon10b	6806.449	83309	2899	2E-06	1574	30	1.743 0.001	0.68064	8.3309	0.2899
raw average				1564	13.03		1562 7.514 weighted average			
GF gte mon11	2464.406	36146	482	8E-07	1417	60	0.395 3E-04	0.24644	3.6146	0.0482
GF gte mon12a	3276.336	52183	1051	1E-05	1281	43	0.708 6E-04	0.32763	5.2183	0.1051
GF gte mon12b	3858.137	71329	727	3E-09	1145	34	0.978 9E-04	0.38581	7.1329	0.0727
				0.0001	1281	78.51	1234 24.35			